UNIVERSITÄT PADERBORN
Die Universität der Informationsgesellschaft

FAKULTÄT FÜR
ELEKTROTECHNIK,
INFORMATIK UND
MATHEMATIK

Analyse und Nachfragesteuerung (Demand Side Management) Ostafrikanischer ländlicher Mikronetze: Modellierung und experimentelle Studie

Von der Fakultät für Elektrotechnik, Informatik und Mathematik
der Universität Paderborn

zur Erlangung des akademischen Grades

Doktor der Ingenieurwissenschaften (Dr.-Ing.)

genehmigte Dissertation

von

Godiana Hagile Philipo, M.Sc.

Erster Gutachter:	Prof. Dr.-Ing. habil. Stefan Krauter
Zweiter Gutachter:	Prof. Dr.-Ing. Henning Meschede

Tag der mündlichen Prüfung: September 19, 2024

Paderborn 2024

Diss. EIM-E/382

UNIVERSITÄT PADERBORN
Die Universität der Informationsgesellschaft

FACULTY OF
ELECTRICAL ENGINEERING,
COMPUTER SCIENCE AND
MATHEMATICS

Analysis and Demand Side Management of East African Rural Microgrids: Modelling and Experimental Study

From the Faculty of Electrical Engineering, Computer Science and Mathematics
the University of Paderborn

for obtaining the academic degree

Doctor of Engineering (Dr.-Ing.)

approved dissertation

from

Godiana Hagile Philipo, M.Sc.

First reviewer:	Prof. Dr.-Ing. habil. Stefan Krauter
Second reviewer:	Prof. Dr.-Ing. Henning Meschede
Day of the oral exam:	September 19, 2024

Paderborn 2024

Diss. EIM-E/382

UNIVERSITÄT PADERBORN
Die Universität der Informationsgesellschaft

NEK
Sustainable Energy Concepts
Prof. Dr.-Ing. habil. Stefan Krauter

University of Paderborn

Faculty of Electrical Engineering, Computer Science, and Mathematics

Department of Electrical Energy Technology - Sustainable Energy Concepts

DOCTORATE THESIS

in Partial Fulfilment of the Requirements for the Degree of Doctor of Philosophy in Electrical Engineering

Analysis and Demand Side Management of East African Rural Microgrids: Modelling and Experimental Study

Author

Godiana Hagile Philipo (6956796)

Supervisor

Prof. Dr.-Ing. habil. Stefan Krauter

Date: 09th October 2024

DECLARATION

I, GODIANA HAGILE, do hereby declare to the Senate of the University of Paderborn that this dissertation is my original work and that it has neither been submitted nor concurrently submitted for a degree or similar award in any other Institution.

Godiana Hagile Philipo

G. Philipo _____ 09th October 2024

Name and signature of candidate **Date**

The above declaration is confirmed.

COPYRIGHT

CERTIFICATION

The undersigned certify that they have read and hereby recommend for acceptance by the University of Paderborn the dissertation entitled: "***Analysis and Demand Side Management of East African Rural Microgrids: Modelling and Experimental Study***" and recommend for examination in partial fulfilment of the requirements for the degree of Doctor of Philosophy in Electrical Engineering of Paderborn University.

ACKNOWLEDGEMENT

First and foremost, I would like to thank the Almighty God, the giver of life; without the Almighty God, there is no variation or shadow due to change; without him, I am puny and powerless.

I sincerely thank my supervisor, Prof. Dr.-Ing. habil. Stefan Krauter for his constant support. The freedom to explore and share opinions and ideas during the research period was excellent under his supervision. I would also like to thank all my NEK chair members, especially Mr. Jörg Bendfeld, for the full cooperation they have given me during this time. Their enthusiasm for research made a strong impression on me, and I hope to deliver the same in the future.

I pass my heartfelt gratitude to my mentor, Prof. Thomas Kivevele, for his role in joining Paderborn University and his encouragement; it is whole-heartedly appreciated that your great advice proved monumental towards the success of this work. Also, I extend my sincere acknowledgement to my friends Josephine Kakande, Geradius Deogratias, Ibrahim Mwamenywa, Paul Bogere, Mark Kagarura, Teddy Mangeni, Henry Asiimwe, Irene Ngoti, Donna Namuju, Henrietta Acqway, Cedrik Maturin, Mr and Mrs Frohn and many others. I wish to thank all the people whose assistance was a milestone in the culmination of the three years.

I wish to acknowledge my family's support and great love, especially my beloved husband, Ansifrid, for being with me throughout the doctorate program. Thank you for your love and care. My sincere appreciation goes to my dear father, Mr Philipo Lubasha; my brother, Dr Godfrey Philipo; my sisters, Godliver Philipo and Godbertha Philipo; and to all my lovely children (Marietha, Maria, Austin, Kenzo, Abigail and newborn Audrey). I also thank Lubasha and Lekundayo's family, who have supported me over the last several years.

Lastly, I sincerely thank my employer, the Nelson Mandela African Institution of Science and Technology, for granting me study leave and the African Research and Teaching for Development Grids (ART-D-Grids) for the funding. May God bless you far more abundantly than ever you can ask or think (Ephesians 3:20).

DEDICATION

I dedicate this work to my late mother, *mama* Marietha Andrea Masamaki and my lovely daughters, Abigail and Audrey Ansifrid Lekundayo.

TABLE OF CONTENTS

ABSTRACT

Energy access is essential in achieving healthy and productive households with a growing modern economy; however, more than 17% of the world's population lacks access to electricity. Sub-Saharan African countries present only about two-fifths of the population with access to electricity, the statistics being the lowest worldwide. East Africa region offers the highest solar photovoltaic potential of about 220 Petawatt and wind potential of about 170 Petawatt per year, compared to other African regions; however, poor electric access and cost of transmission, especially in rural areas with pronounced outages to connected customers, is still articulating.

Microgrid technologies seem promising; however, their sustainability has been questioned and doubted due to several challenges. The ever-increasing level of demand and its uncertainty pose technical challenges leading to pronounced unscheduled power outages and uneconomic operational ways of the microgrid (e.g., demand and the availability of solar and wind power are often not synchronised, thus requiring large storage capacities to bridge the temporal gap between supply and demand). Demand-side management (DSM) is an indispensable tool for addressing challenges. Several DSM techniques have been adopted; however, they do not guarantee global convergence as the studies are limited in developing countries. In addition, the lack of tailored demand-side management strategies that align with the region's socio-economic context makes it hard for the established microgrids to be sustainable.

This study investigates and optimises demand-side management (DSM) strategies within solar microgrids in East Africa. Three microgrids in Tanzania (Mpale), Uganda (Bunjako), and Kenya (Lwak) were used to detail the region's specific microgrid technical challenges and propose DSM strategies for optimising the microgrids. Results show that the incentive-based DSM strategy achieved a power reduction of 14% by providing incentives to maximise utility benefits. Also, the presence of deferrable loads has been considered to bring more flexible demand-side management with a reduction in peak demand and peak-to-average ratio of about 31.2% and 7.5%, respectively. Load shifting efficiently reduces energy consumption during the unavailability of the sun, hence promising more flexibility to customers.

A notable association was observed between refrigerator and freezer inefficiency and failure in temperature control. The findings underscore the significance of addressing energy efficiency in these appliances to enhance overall performance and reliability. Potential cost savings were evident, revealing that replacing only two refrigeration appliances could yield substantial financial benefits, estimated at USD 1325 in five years. The findings hold significant implications for the broader field of energy engineering, offering a tailored approach to microgrid design and operation in regions with similar energy landscapes.

KURZFASSUNG

Die Energieversorgung ist für die Gesundheit und Produktivität von Haushalten und für das Wachstum moderner Volkswirtschaften von entscheidender Bedeutung. Mehr als 17 % der Weltbevölkerung haben jedoch keinen Zugang zu Elektrizität und damit auch keinen Strom. In Afrika südlich der Sahara haben nur etwa zwei Fünftel der Bevölkerung Zugang zu Elektrizität, das ist der niedrigste Wert weltweit. Im Vergleich zu anderen afrikanischen Regionen verfügt Ostafrika über das größte Potenzial an Photovoltaik und Windenergie (220 bzw. 170 Petawattstunden pro Jahr). Der schlechte Zugang zu Elektrizität und die hohen Stromübertragungskosten, insbesondere in ländlichen Gebieten mit häufigen Stromausfällen, stellen jedoch nach wie vor ein Problem dar. Microgrid-Technologien erscheinen vielversprechend, aber ihre Nachhaltigkeit wird durch eine Reihe von Herausforderungen gefährdet. Die ständig steigende Nachfrage und deren Unsicherheit stellen technische Herausforderungen dar, die zu hohen ungeplanten Stromausfällen und einem unwirtschaftlichen Betrieb des Microgrids führen (z.B. sind Nachfrage und Verfügbarkeit von Solar- und Windenergie oft nicht synchron, so dass große Speicherkapazitäten erforderlich sind, um die zeitliche Lücke zwischen Angebot und Nachfrage zu überbrücken). Demand Side Management (DSM) ist ein unverzichtbares Instrument zur Bewältigung dieser Herausforderungen. Verschiedene DSM-Techniken wurden bereits eingesetzt, konnten jedoch keine umfassende Lösung bieten, da nur wenige Studien in Entwicklungsländern durchgeführt wurden. Darüber hinaus fehlt es an maßgeschneiderten Strategien zur Nachfragesteuerung, die auf den sozioökonomischen Kontext der Region abgestimmt sind. Diese Studie untersucht und optimiert Strategien zur Nachfragesteuerung (Demand Side Management, DSM) in solaren Mikrogrids in Ostafrika. Anhand von drei Mikrogrids in Tansania (Mpale), Uganda (Bunjako) und Kenia (Lwak) wurden die spezifischen technischen Herausforderungen der Region für Mikrogrids untersucht und DSM-Strategien zur Optimierung der Mikrogrids vorgeschlagen. Die Ergebnisse zeigen, dass die anreizbasierte DSM-Strategie eine Leistungsreduzierung von 14% erzielte, indem sie Anreize zur Maximierung des Nutzens für den Versorger bot. Darüber hinaus wird davon ausgegangen, dass das Vorhandensein von verschiebbaren Lasten ein flexibleres Nachfragemanagement mit einer Reduzierung der Spitzennachfrage und des Verhältnisses zwischen Spitzen- und Durchschnittsverbrauch um etwa 31,2% bzw. 7,5% ermöglicht. Lastverschiebung reduziert effizient den Energieverbrauch in Zeiten, in denen die Sonne nicht zur Verfügung steht, und bietet den Kunden mehr Flexibilität.

Ein bemerkenswerter Zusammenhang wurde zwischen der Ineffizienz von Kühl- und Gefriergeräten und dem Versagen der Temperaturregelung festgestellt. Die Ergebnisse unterstreichen, wie wichtig es ist, die Energieeffizienz dieser Geräte zu verbessern, um die Gesamtleistung und Zuverlässigkeit zu erhöhen. Potenzielle Kosteneinsparungen waren offensichtlich und zeigten, dass der Austausch von nur zwei Kühlgeräten erhebliche finanzielle Vorteile bringen könnte, die auf 1325 USD in fünf Jahren geschätzt werden. Die Ergebnisse haben relevance Auswirkungen auf den breiteren Bereich der Energietechnik und bieten einen maßgeschneiderten Ansatz für die Gestaltung und den Betrieb von Mikrogrids in Regionen mit ähnlichen Energielandschaften.

IKISIRI

Upatikanaji wa nishati ni muhimu katika kupata kaya zenye afya na zenye tija na uchumi unaokua wa kisasa; Hata hivyo, zaidi ya asilimia 17 ya watu duniani hawana umeme. Nchi za Afrika Kusini mwa Jangwa la Sahara zinawasilisha tu karibu theluthi mbili ya idadi ya watu walio na upatikanaji wa umeme, takwimu ambazo ni za chini zaidi ulimwenguni. Ikilinganishwa na mikoa mingine ya Afrika, Afrika Mashariki ina uwezo wa juu wa jua na upepo wa karibu 220 PWh na 170 PWh kwa mwaka, kwa mtiririko huo; Hata hivyo, upatikanaji duni wa umeme na gharama za usambazaji, hasa katika maeneo ya vijijini yenye kukatika kwingi kwa umeme kwa wateja waliounganishwa, bado ni tatizo kubwa.

Teknolojia ya microgrid inaonekana kuwa ya kuahidi; Hata hivyo, uendelevu wao umehojiwa na kutiliwa shaka kutokana na changamoto kadhaa. Kiwango cha kuongezeka kwa mahitaji na kutokuwa na uhakika wake husababisha changamoto za kiufundi zinazosababisha kukatika kwa umeme usio na mpangilio na njia zisizo za kiuchumi za microgrid (kwa mfano, mahitaji na upatikanaji wa nishati ya jua na upepo mara nyingi hazisawazishwi, na hivyo kuhitaji uwezo mkubwa wa kuhifadhi kuziba pengo la muda kati ya usambazaji na mahitaji). Usimamizi wa upande wa mahitaji (DSM) ni chombo muhimu cha kushughulikia changamoto. Mbinu kadhaa za DSM zimefanyika; hata hivyo, hazihakikishi ushirikiano wa kimataifa kwani masomo ni madogo katika nchi zinazoendelea. Kwa kuongezea, ukosefu wa mikakati ya usimamizi wa upande wa mahitaji ambayo inaendana na muktadha wa kijamii na kiuchumi wa kanda husika hufanya iwe vigumu kwa microgrids zilizoanzishwa kuwa endelevu.

Utafiti huu unachunguza na kuboresha mikakati ya usimamizi wa upande wa mahitaji (DSM) ndani ya microgrids za jua katika Afrika Mashariki. Mikrogrids tatu nchini Tanzania (Mpale), Uganda (Bunjako), na Kenya (Lwak) zilitumika kuelezea changamoto maalum za kiufundi za kanda hiyo na kupendekeza mikakati ya DSM ya kuboresha microgrids. Matokeo yanaonyesha kuwa mkakati wa DSM unaotegemea motisha ulifikia kupunguza matumizi ya nishati kwa 14% kwa kutoa motisha ya kuongeza faida za matumizi. Pia, mabadiliko ya utumiaji wa baadhi ya vifaa vya umeme muda ambapo watumiaji ni wengi zaidi hupunguza matumizi ya nishati wakati wa kutopatikana kwa jua.

Uhusiano kati ya ufanisi wa friji na kushindwa kudhibiti joto ufanisi wake unapokuwa mdogo ulionekana. Matokeo yanasisitiza umuhimu wa kushughulikia ufanisi wa nishati katika vifaa hivi ili kuongeza utendaji wa jumla. Uwezekano wa kuokoa gharama ulikuwa dhahiri, kwani kubadilisha vifaa viwili tu vya friji kunaweza kutoa faida kubwa za kifedha, makadirio ya $ 1,325 katika miaka mitano. Hii inasisitiza motisha ya kiuchumi ya kutekeleza hatua za ufanisi wa nishati katika vifaa vya nyumbani. Matokeo yana athari kubwa kwa uwanja mpana wa uhandisi wa nishati, kutoa njia iliyolengwa kwa muundo wa microgrid na uendeshaji wake katika maeneo yaliyo na mandhari sawa ya nishati na haya yaliyozungumziwa katika utafiti huu.

LAY SUMMARY / CONTRIBUTION

The overarching objective of this study is to make pioneering contributions to the optimization of East African microgrids, particularly addressing economic load dispatch, coordination of multiple generators, and the integration of shiftable appliances. Within the practical implementation context, a key focus is placed on temperature-based control for refrigeration appliances, with a unique emphasis on its effect on inefficient refrigerators. In the realm of economic load dispatch, this work seeks to introduce a context-aware incentive structure that aligns with the socio-economic dynamics of the region. By doing so, it not only optimizes energy distribution but also fosters increased compliance and efficiency.

Additionally, in addressing the coordination of multiple generators, the research focuses on developing a novel dispatch algorithm tailored to East African microgrids' diversity of power sources. This algorithm aims to maximize utilization and reliability by effectively coordinating the output of various generators, ensuring a seamless and optimized power supply. Moreover, this study delves into integrating shiftable appliances within the microgrid framework. This involves designing a dynamic load control algorithm that enhances grid efficiency and considers the specific energy usage patterns and appliance characteristics prevalent in East African households. Integrating shiftable appliances contributes to a more flexible and responsive energy system, aligning with the unique demands of the region. Through these multifaceted contributions, this research aspires to redefine the energy management landscape in East African microgrids, offering innovative solutions that bridge critical gaps in the existing literature. The ultimate aim is to guide the development of sustainable energy practices, making a significant and practical contribution to the field and fostering energy resilience in the region.

LIST OF TABLES

LIST OF FIGURES

LIST OF EQUATIONS

ABBREVIATIONS

DSM	Demand Side Management
PSO	Particle Swarm Optimisation
AC	Alternating Current
DC	Direct Current
DG	Distributed Energy
ESS	Energy Storage System
PCC	Point of common coupling
HVDC	High voltage direct current
VAC	Voltage Alternating Current
DR	Demand response
CPP	Critical Peak pricing
RTP	Real-time pricing
DLC	Direct load control
EDRP	Emergency demand response programs
EIA	Energy Information Administration
HVDC	High-Voltage Direct Current
ToU	Time of Use
PBDRS	Price-based demand response schemes
IBDRS	Incentive-based demand response scheme
RTP	Real-time pricing
EC	Energy conservation
DLC	Direct load control
EE	Energy efficiency
CPP	Critical peak pricing
ASMP	Ancillary service market programs
CMP	Capacity market programs

DBP	Demand-bidding programs
kWh	kilo Watt hour
LED	Light Emitting Diode
LMI	Linear matrix inequality
ISO	Independent system operator
CVIs	Clustering validity indexes
PV	Photo Voltaic
PR	Performance Ratio
SOC	State of Charge of Battery
RMS	Root mean-square voltage
THD	Total harmonic distortion
DOD	Depth of Discharge
MATLAB	Matrix Laboratory
ANN	Artificial Neural Network
EPRA	energy and petroleum Regulatory Authority
PAR	Peak to Average Ratio
NUTEK	National Utveckfing Foer Teknik (Sweden National Board for Industrial and Technical Development)
GA	Genetic Algorithm
RPU	Remote Power Unit

CHAPTER ONE

1. Introduction

1.1. Background Information

Advanced civilisation and better quality of life depend significantly on energy availability, accessibility, acceptability, and affordability (Schnitzer et al., 2014; Stevanato et al., 2019). Availability entails an element of absolute or geological/physical existence and infinite supply (Kruyt et al., 2009; Narula, 2014). Accessibility entails the supply concentration resulting from a large spatial discrepancy between consumption and production of resources with geopolitical implications for access acquisition (Kruyt et al., 2009). Acceptability refers to the environmental and societal elements of resource extraction and energy use. Switching away from a carbon-intensive fuel portfolio is a good indicator of acceptability (Narula, 2014). Affordability relates to the economic element that influences energy prices. Energy access is essential in achieving healthy and productive households with a growing modern economy, having a multiplier effect on education, health, water supply, agriculture, transport, and other sectors (Blimpo & Cosgrove-davies, 2020; Pachauri, 2011).

Despite the world's dilemma between satisfying the increasing demand and preventing climate change impacts by reducing carbon dioxide emissions, the need for energy demand is expected to double in the next 40 years, putting the developing and developed world under economic pressure (Gebreslassie & Khellaf, 2021). Although Africa is the most vulnerable, energy scarcity significantly impacts economic activities worldwide. Approximately 1.2 billion people (about 17% worldwide) have no access to electricity, with the vast majority in Africa, particularly sub-Saharan Africa (Chirambo, 2018). Sub-Saharan African countries present only about two-fifths of the population with access to electricity, the statistics being the lowest worldwide (Blimpo & Cosgrove-davies, 2020; Philipo et al., 2020).

In East Africa (consisting of the countries Tanzania, Kenya, Uganda, Rwanda, Burundi, Democratic Republic of Congo, and South Sudan), energy access is still critical as about 80% of the population have poor access to electricity, mostly people in rural areas (Williams et al., 2017). Rural area electrification in developing countries poses challenges in constructing power generation and transmission networks (Micangeli et al., 2018).

Several studies have shown that despite efforts to improve grid transmission and power generation, emphasis is more on urban and industrial areas due to the higher load demand and political relevance (Azurza et al., 2012). The electrification discrepancy can be achieved using microgrid technologies and meet the sustainable development goal 7: "affordable, reliable, sustainable, and modern energy for all by 2030". Microgrids offer potential alternatives to the challenging rural electrification framework due to their affordability (Stevanato et al., 2019; Takalani & Bekker, 2020; Williams et al., 2017).

Microgrids are an alternative to areas where grid extension is technically or economically infeasible. In addition, microgrids can meet the need for reliable and safe electricity through renewable energy sources (Stevanato et al., 2019; Takalani & Bekker, 2020; Williams et al., 2017). Several challenges are associated with deploying microgrids, such as the variability nature of renewables and unpredicted customer demand, especially during peak hours (Chauhan & Chauhan, 2018; Lazaroiu et al., 2016).

The commonly available solution to the challenges involves incorporating storage systems and adapting demand-side management schemes (Barton & Infield, 2004; Cecati et al., 2011; Philipo et al., 2020). Storage systems are practical yet very expensive technology; thus, economic viability has proven challenging, especially when microgrids are not optimised (Hartvigsson et al., 2015). Demand-side management uses techniques such as load shifting, direct load control, load filling, and energy efficiency appliances, where peak loads can be appropriately managed (Torriti, 2012; Warren, 2014). Several demand-side management programs have been implemented. However, not much attention is paid to the combination of classification and prioritisation of consumer demand, assessing their correlation, predicting their future demand, and studying their energy input and output to select proper demand-side management strategies while reducing the cost of storage. This study aims to find the best practice of a solar microgrid in East Africa through demand-side management, customer classification, and prioritisation.

1.2. Problem Statement

Despite the rapid expansion of microgrids in East Africa, blackouts, brownouts, and poor sustainability are still the most significant challenges for microgrids. The reasons can be attributed to the intermittent nature of solar power, over/under design, and limited access to reliable data for demand forecasting, leading to unpredicted or variable energy consumption patterns. In addition, over-dimensioned or poorly designed systems increase the microgrid systems' operation costs (Bui et al., 2018).

Higher operational costs increase electricity costs, affecting affordability for end users and resulting in customer attrition (Steyer et al., 2014). Due to the unreliability of most microgrid data, finding an optimal solution for microgrid operation has proven challenging. Furthermore, the lack of a tailored demand-side management solution that aligns with the socio-economic context of the region makes it hard for the established microgrids to sustain.

This study aims to investigate and optimise demand-side management strategies within solar microgrids in East Africa by addressing the challenges related to energy consumption, appliance usage behaviour, and system design. Estimating near-accurate forecasts of load profiles and microgrid data is essential for selecting proper energy management. Weather and seasonal changes play critical roles in demand variability and the probability of microgrid failures (Yazdkhasti & Diduch, 2020). The results of this study will act as an essential push factor to guarantee a feasible operation of microgrids in East Africa.

1.3. The Rationale of Study

Poor access to reliable electricity imposes significant constraints on modern economic activities, the provision of public services, the adoption of new technologies, and the quality of life. This study focuses on the critical need to improve the performance and sustainability of solar microgrids in East Africa. By investigating today's microgrids and addressing the challenges associated with demand-side management, we aim to contribute valuable insights that can inform utility companies and governments to develop tailored solutions and customers to adopt energy efficiency behaviours to save energy. The study is motivated by the potential to optimise energy consumption, improve system efficiency, and promote the widespread adoption of renewable energy to foster sustainable development in the region.

1.4. Objectives

1.4.1. General Objective

To optimise microgrid operations, including minimisation of storage requirement and cost through load profile analysis and demand side management measures to synchronize demand with supply (e.g., by PV).

1.4.2. Specific Objectives

a) To assess and analyse customer demand and other power quality parameters to establish a baseline for demand-side management measures.

b) To investigate the correlation of daily/seasonal consumption with statistics, tasks, weather, season, appliances, etc.
c) To optimise microgrid operations through a proper demand-side management scheme using modelling and simulation considering location context.
d) To promote energy efficiency of microgrids through practical load control and appliance demand data analysis.

1.5. Significance of the Study

This study's significance is rooted in its potential to catalyse positive transformations within East African communities through overcoming challenges related to solar microgrid operations. The study anticipates the following outcomes: energy savings, increased energy access, improved reliability, and reduced end-user costs by employing optimisation and demand-side management solutions. Furthermore, the findings can inform microgrid operators on proper design and possible solutions to impose to customers for mutual benefits; policymakers can use the acquired results for better policy decisions, and the results can also guide investment in sustainable energy infrastructure and contribute to the broader discourse on enhancing energy resilience in developing regions. The study's significance lies in its ability to promote environmentally consciousness and economically viable solutions for powering underserved communities.

1.6. Research Outline

This dissertation utilised data from three microgrids in the East African countries of Tanzania, Uganda, and Kenya. The data were used to analyse the operation of microgrids and develop a proper demand-side management scheme and recommendation that aligns with the communities visited. The dissertation comprises five chapters.

a) Chapter One introduces the study. It includes the background information, problem statement, study rationale, research objectives and expected outcomes, and research significance.
b) Chapter Two presents a critical and in-depth review of published literature.
c) Chapter Three contains the study's methodology, including data collection, technical data analysis, modelling, and simulation.
d) Chapter Four presents an analysis and discussion of the modelling and simulation.
e) Chapter Five presents the conclusions and recommendations that have been arrived at based on the results obtained from modelling and simulation.

CHAPTER TWO

2. Literature Review

This chapter reviews the literature on the analysis and demand side management of East African rural microgrids through optimising and reducing storage costs. The chapter is divided into six sub-sections. Section 2.1 details the renewable energy potential in Africa, section 2.2 introduces the concept of microgrids, and section 2.2.2 discusses the classification of microgrids and their advantages and disadvantages. Section 2.2.3 narrows the discussion to microgrids in East Africa, challenges experienced, and proposed solutions to mitigate the challenges; section 2.3 discusses the demand-side management categories and their methods, and chapter 2.4 summarises the literature review.

2.1. Renewable Energy Resources in Africa

Africa has a natural advantage in benefiting from various renewable energy resources such as solar, wind, biomass, and hydropower. Due to its geographical position, Africa has a solar radiation potential averaging 325 days of sunshine with an estimated 656,730 TWh solar photovoltaic potential per year. The available solar potential varies between normal direct and global horizontal solar irradiation. In East Africa, solar energy is abundant due to its proximity to the equator, which results in high levels of sunlight exposure (Figure 2-1). It is a clean, renewable energy source that can be harnessed using photovoltaic (PV) panels. Solar panels can be installed on rooftops or in small solar farms, making them suitable for decentralized rural electrification. However, initial investment costs can be high, and solar energy production depends on weather conditions (Gebreslassie & Khellaf, 2021).

Africa's wind potential, estimated at 656,000 TWh annually, is mainly concentrated along the coastal, Sahel, and highlands areas (Figure 2-2). In Africa, East and North have better wind potential than others (Gebreslassie & Khellaf, 2021). East Africa has more wind potential in the coastal regions and highlands, where wind turbines can be installed individually or in wind farms to harness wind power. Wind energy is purely renewable and clean, with low operating costs once infrastructure is in place, but it can be unpredictable due to production variability and wind speed dependence (Erdoğan et al., 2022a).

Hydropower generation, estimated at 10,240 MW, is Africa's leading renewable energy resource, covering more than 70% of overall electricity generation in the continent

(Abriendomundo, 2023). East Africa has plenty of water bodies with notable rivers, such as the Nile (the world's longest river), which runs along its borders and is suitable for hydroelectric power generation (Figure 2-3). Large hydroelectric dams provide a stable and reliable source of electricity to rural areas. While large-scale hydropower projects can cost-effectively improve electricity access, they can have significant environmental and social impacts, including habitat disruption and displacement of communities. Also, they can take a decade or more to plan and build.

Biomass energy uses organic materials such as wood, crop residues, and animal waste for cooking and electricity generation (Figure 2-4). It plays a crucial role in the African energy mix, which has the potential to ensure a future fuel supply (Balat & Ayar, 2005). Biomass power plants utilize dedicated energy crops or agricultural residues for electricity generation. 40% of Africa's waste resources and wood residues are concentrated in North Africa, with the central region having the lowest wood residue potential (Gebreslassie & Khellaf, 2021). In rural areas of East Africa, biomass is commonly used for cooking and heating. Although biomass is readily available and can act as a source of income in rural communities, there are environmental repercussions of using biomass as a fuel source, depending on the type of conversion technology. Inefficient combustion practices can lead to indoor air pollution and deforestation.

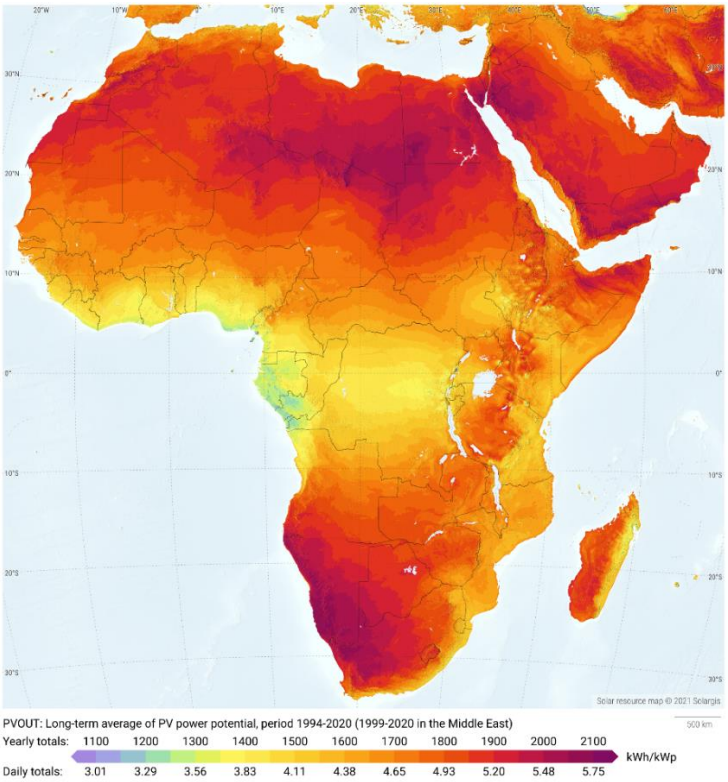

Figure 2-1: *Solar photovoltaic potential map of Africa (SolarGIS, 2021)*

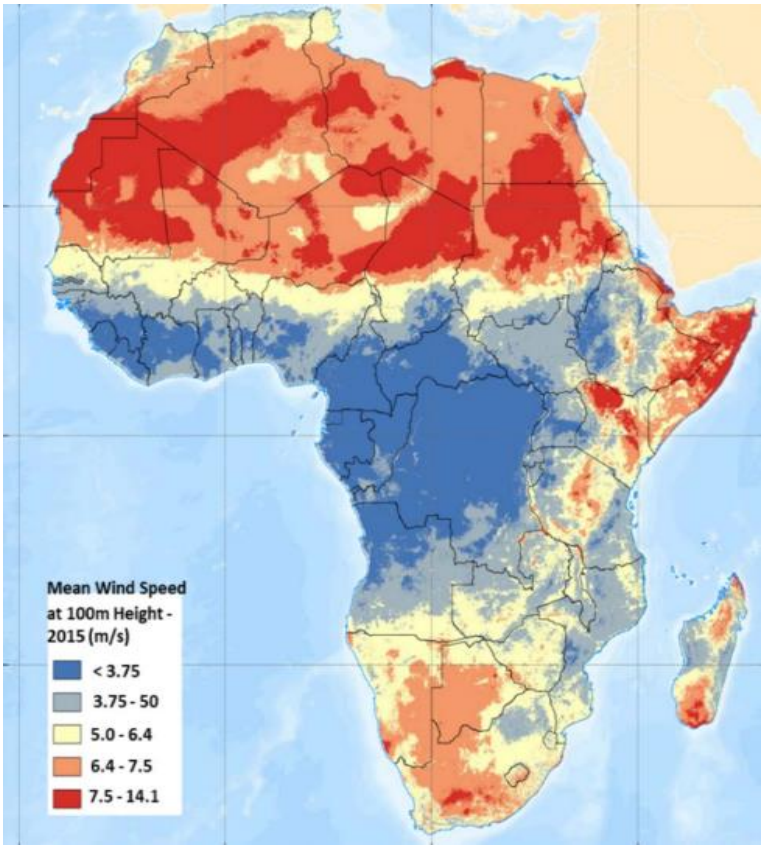

Figure 2-2: *Wind potential map of Africa* (Erdoğan et al., 2022b)

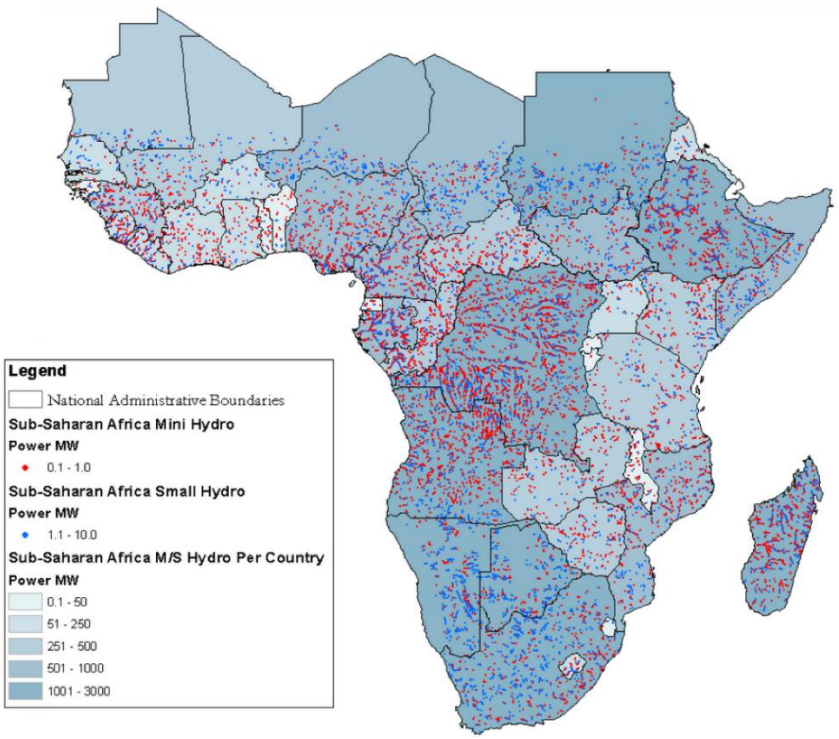

Figure 2-3: *Hydropower potential map of Africa* (Erdoğan et al., 2022b)

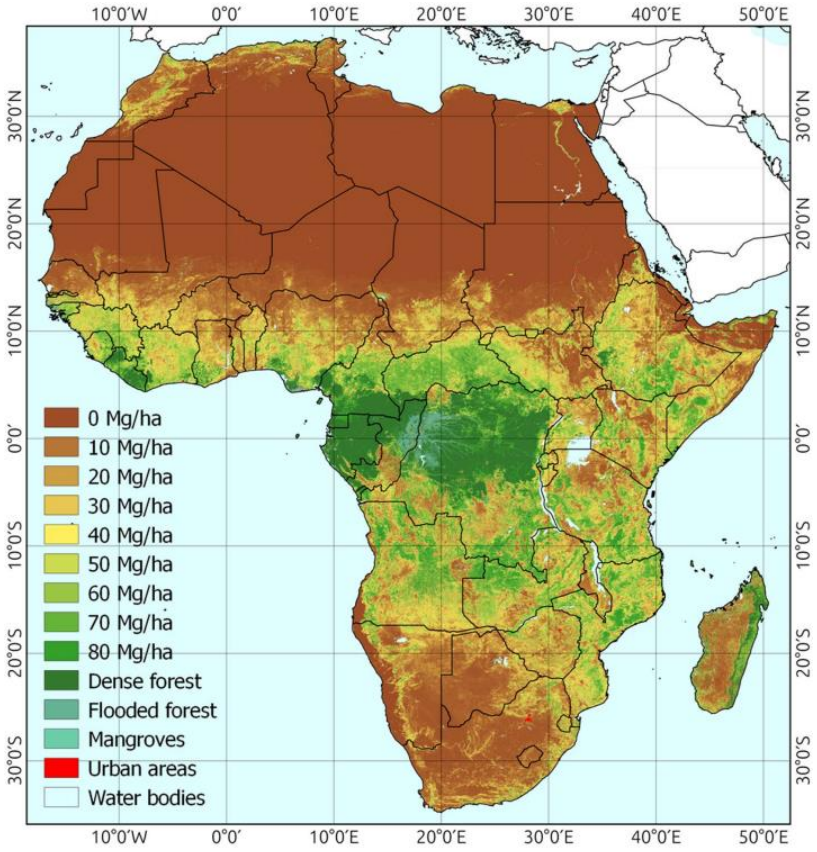

Figure 2-4: *Biomass potential map of Africa (Bouvet et al., 2018)*

Choosing the best energy source for rural electrification in East Africa should consider combining the available options considering the local conditions and needs. Areas with access to rivers and water bodies can make use of hydroelectric power to provide a stable source of electricity, and wind energy can act as a complement in regions with consistent wind patterns and with proper biomass management, it can be used as a supplementary source of electricity or for cooking and heating where appropriate. Generally, solar energy is often a suitable choice for decentralized electrification in remote areas with limited infrastructure. However, a diversified energy portfolio that harnesses the strengths of each energy source can enhance energy security and resilience in rural East Africa, and microgrids can help reach scattered rural settlements.

2.2. Microgrids

2.2.1. Introduction

Energy demands and electricity consumption worldwide are increasing daily due to technological advancements, population growth, and urbanisation. The primary source of energy consumed is from fossil fuel. The combustion of fossil fuels to generate power is one of the major causes of global warming (Greg Adams et al., 2016). Efforts to minimise

the effects of global warming require an alternative energy source which achieves green energy production while meeting rising energy demands.

Despite the rising energy demands, in Sub-Saharan Africa, large parts of the population lack access to electricity (Figure 2-5). The lack of access to electricity is due to poor coverage of the electricity grids, isolated areas such as islands, and remote regions where high investment costs are needed to extend the already built national grids. One of the reliable solutions for rural electrification is standalone power systems. Standalone power systems are off-the-grid, independent electricity systems for locations that lack an extensive utility-scale electricity distribution system. Microgrids are an example of such a system (Riahi et al., 2021).

Microgrids are electricity distribution systems containing loads and distributed energy resources such as distributed generators, storage devices, or controllable loads that can be controlled and coordinated while connected to the main power network or islanded. For rural electrification, microgrids are an exciting way to provide electricity to serve local needs and solve supply problems. They offer new ways to provide reliable and resilient electrical power. Coupled with the demand for alternative green energy, microgrids offer an alternative to fossil fuel energy in efforts to curb the effects of climate change (Riahi et al., 2021).

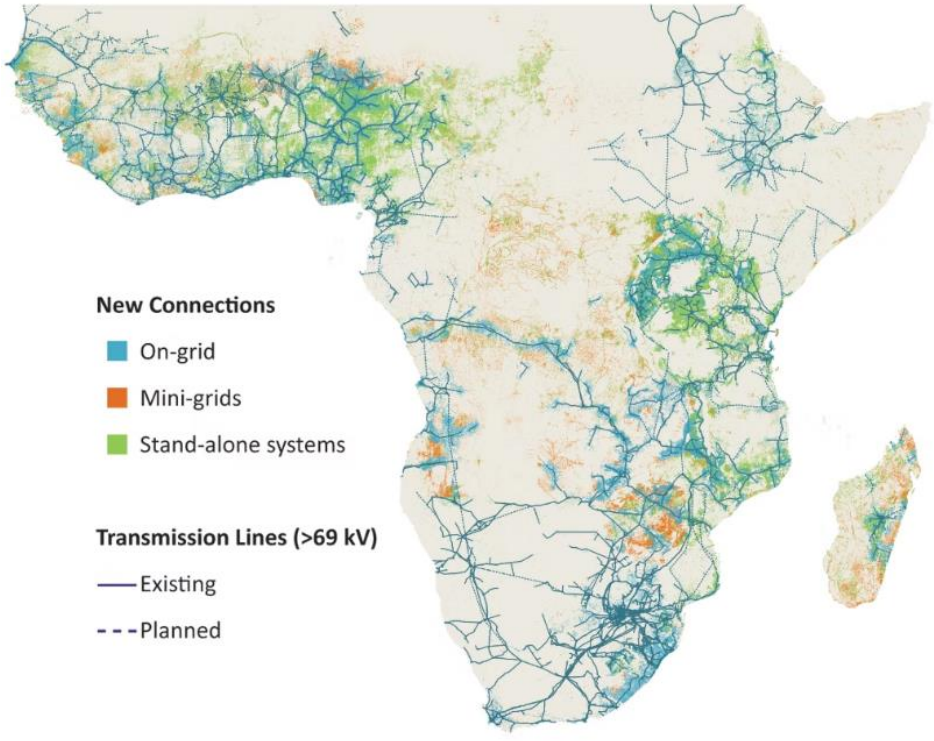

Figure 2-5: *The 2020 Electricity access map for sub-Saharan Africa (IRENA, 2003)*

With the advent of low-cost solar panels and the ability to generate, store and use direct current (DC) electrical energy locally, solar microgrids act as an ideal solution to transform energy infrastructure for rural communities to power households and local businesses. The implementation is affordable, safe, simple, flexible, and energy efficient. Various community-based working models can be implemented to operate and sustain these microgrids. Microgrids are expected to increase the power quality and bring multiple economic, environmental and technical benefits to consumers and electric providers, ensuring efficient systems (Thirunavukkarasu et al., 2022).

2.2.2. Classification of Microgrids

Microgrids can be categorized by their generation capacity, applications, system architecture, and customer type. The classifications of microgrids are outlined in Table 2-1. The categorisation of microgrids based on sizes is rarely accurate as functionality is the main difference between them. Minigrids and microgrids are similar based on their sizes. However, unlike microgrids, minigrid acts independently and cannot be connected to the main grid. Thus, it is best to categorise depending on their functionality and usage, such as customer type, application, generation capacity, and system architecture (Ogg, 2015).

2.2.2.1. By Customer Type

There are three categories available: true microgrids (μ-grids), milli-grids (m-grids), and remote microgrids (r-grids). True microgrids are microgrids in which the whole system is on a single site to a utility customer. Milli-grids are microgrids that involve a segment-regulated grid that allows distributed energy resources to be deployed and directed to critical infrastructure in emergencies. Remote microgrids are isolated and unable to operate in a grid-connected mode.

2.2.2.2. By Application

These are microgrids that are categorised based on the end user's application. Such microgrids include military microgrids, industrial microgrids, development microgrids for small commercial operations, hidden microgrids for those with generators on-site that they use to provide emergency power, microgrids for isolated vacation homes, and mobile microgrids for military and emergency power response in the event of disasters. In addition, mobile microgrids are often used for remote, strategic applications when electricity is immediately required, and there is no short-term potential to connect to the grid network (Roosa, 2021).

2.2.2.3. By Generation Capacity

There are six categories depending on the generation capacity, presented in Table 2-1, in addition to their characteristics and complexity.

Table 2-1: *Microgrid categories based on generation capacity, complexity, functionality and status on grid connection (Kempener et al., 2015; Ogg, 2015)*

Category	Size	Capability	Complexity	Function	Connection to Main Grid
Picogrid	0 – 1 kW	• Single controller • Single voltage (DC)	• DC systems • Serve single load	• Telemetry • Charging • Lighting	No
Nanogrid	0 – 5 kW	• Single voltage (DC) • Single price • Controllers negotiate with others across gateways to buy/sell power	• Both are grid-tied and remote systems • DC systems • Serving single load • Single administrator	• Telecom • Household	Off-grid
Microgrid	5 – 300 kW	• Manage local energy supply and demand • Provide a variety of voltages (AC/DC) • Provide a variety of quality and reliable power options	• Incorporate generation • Varying pricing possible	• Distributed	Possible

Category	Size	Capability	Complexity	Function	Connection to Main Grid
		• Optimise multiple-output energy systems			
Minigrid	5 – 300 kW	• Generation satisfying local demand • Transmission limited to 11 kV	• Interconnected customers	• Local	No
Macrogrid	> 300kW	• Transmission up to 400 kV • Single voltage (AC)	• It can be coupled to a microgrid	• Centralised	Yes
Supergrid	> 100MW	• Transmission up to 400 kV • AC/HVDC voltages	• It can be coupled to a microgrid	• Centralised	Yes

2.2.2.4. By System Architecture

2.2.2.4.1. AC Microgrid

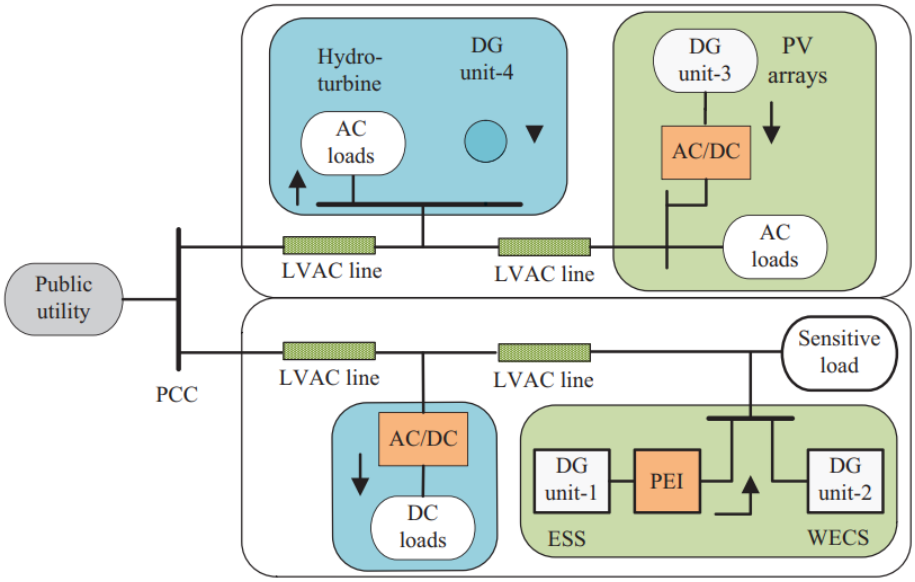

Figure 2-6: *Alternating current (AC) microgrid system layout (Ahmad et al., 2019)*

An AC microgrid system consists of distributed energy (DG) units (which can be from hydro under hydro turbines, photo voltaic (PV) or wind energy conversion system (WECS)) and Energy storage systems (ESS) connected at points within the distribution networks, forming a small, isolated AC electric power system (Figure 2-6). During normal operating conditions, the two networks are interconnected at the point of common coupling (PCC), while the loads are supplied from local sources. If the load demand power is less than the power produced by the DG units, excess energy can be exported to the utility (Ahmad et al., 2019).

2.2.2.4.2. AC/DC Microgrid

Microgrids have different types of sources, and loads are the type of AC/DC systems. The conceptual layout of the hybrid AC/DC microgrid is shown in Figure 2-7. The hybrid microgrids facilitate the benefits of integrating AC technology with DC technology through interlinking bidirectional converters. After staying on AC technology in the electric power supply, DC power joins it with increasing technology advancements in power conversion, generation, transmission, and consumption. However, challenges in DC technologies warrant the integration of algorithms in some or every step of the microgrid (Ahmad et al., 2019).

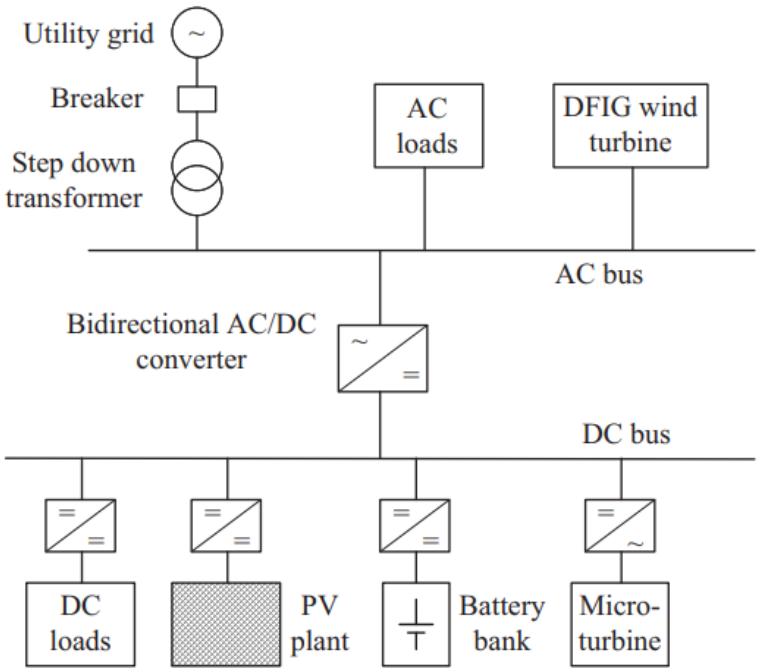

Figure 2-7: *The alternating current (AC) and direct current (DC) microgrid system layout (Ahmad et al., 2019)*

2.2.2.4.3. DC Microgrid

While traditional electric power system was designed to move the AC power via high-voltage AC transmission lines and lower voltage distribution lines to households and businesses, the DC power system has been used in industrial power distribution systems, telecommunication infrastructures, and point-to-point transmissions over long distances via sea cables and for interconnecting AC grids with different frequencies. Most consumer equipment and DG units are dominated by power electronics devices, which need DC power. However, all these DC devices require converting the available AC power into DC, and most of these conversion stages typically use inefficient rectifiers.

Thus, the DC-based DG units have been converted to AC to tie in with the existing AC electric network, only later to be converted to DC for many end users. However, the DC–AC–DC power conversion stages result in substantial energy losses. Using the positive experiences in the high-voltage DC (HVDC) operation and the advances in power electronics technology, interest in pursuing effective solutions has increased. Figure 2-8 shows the typical DC MG systems interconnected with the PCC's central systems: VAC networks from the conventional power plants or an HVDC transmission line connecting an offshore wind farm (Ahmad et al., 2019).

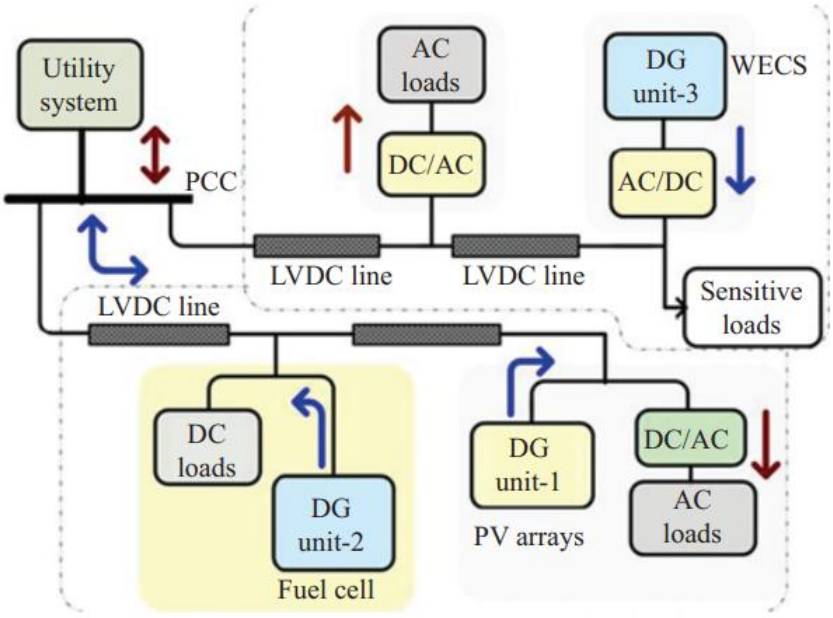

Figure 2-8: *Direct current (DC) microgrid system layout (Ahmad et al., 2019)*

2.2.2.5. Other Classifications

Further classifications of microgrids are available. Advanced microgrids can automatically interact with, connect to, and disconnect from another grid like many microgrids. They grant users the flexibility to securely manage the reliability and resiliency of the microgrid and connected loads while mitigating the economic impacts associated with power disruptions. A key feature of advanced microgrids is the ability to achieve plug-and-play interoperability within the sphere of the technologies used for electrical generation and compatible communication.

Some microgrids can be classified as virtual microgrids (v-grids). These include DERs located at multiple nonadjacent sites that are coordinated so that they can be presented to the grid as a single entity but operate virtually as a controlled island or coordinated numerous islands. Virtual microgrids are often loose aggregations of individual generation sources and loads that can be remotely controlled. In this case, they use the infrastructure of the host grid, and while unable to be decoupled physically, they are operated within the energy market as if independent. They can be configured based on software connectivity (cloud-based) (Ahmad et al., 2019).

2.2.2.6. Advantages and Disadvantages of Microgrids

There are advantages and disadvantages associated with the deployment of microgrids, as outlined in the following chapters.

2.2.2.6.1. Advantages of Microgrids

Microgrids generate and operate electricity from various electrical generation sources using multiple technologies. Microgrids have lower carbon footprints and emit less pollution when renewable energy sources are used.

Microgrids improve electrical system reliability, as the electricity is generated at or near the consumer loads, substantially reducing transmission costs and improving resiliency. Another advantage of microgrids is that they have lower repair costs as the line voltages are much lower than high voltage power transmission, and less transmission infrastructure is needed as energy is generated locally.

Microgrids can provide dispatchable power to critical loads, thus being available upon demand. Hydropower, biomass, tidal power, and geothermal energy can be designed to be dispatchable without energy storage. In addition, microgrid power can be stored in batteries or reservoirs to generate dispatchable electricity.

Microgrids can separate and operate in isolation (i.e., islanding) from the utility's distribution system. Islanding appeals to entities that experience high costs from electrical outages, as the microgrids offer an uninterrupted power supply. Furthermore, islanding ensures remote communities without connection to the electricity grid access to continuous electricity.

Microgrids have black-start capability due to multiple generation resources within the microgrid, allowing the system to restart independently. Black Start is restoring power to part of an electric grid without relying on external electric power transmission networks.

Utility companies install microgrids along the high-voltage electric grid to operate as command centres to coordinate response activities during massive area-wide outages. These microgrids can reduce investment costs to accommodate increased load, peak power requirements, or power quality issues. When a substation upgrade is required to address increased limitations or power quality, a microgrid with on-site generation could satisfy the need without a significant capital investment.

Microgrids allow the integration of multiple generation sources. Thus, decisions can be made about which type of fuel source is the least expensive at a given time. Microgrid management systems can be designed to reduce costs by incorporating peak-shaving capabilities and to regulate energy pricing differences profitably. Algorithms can be used to minimise risks and selectively energize loads during operations and extended outages.

Lastly, renewable generation inclusion in the microgrid eliminates the business risks associated with variable fossil fuel costs. Revenue can thus be generated by selling excess power to the grid if the microgrid is interconnected.

2.2.2.6.2. Disadvantages of microgrids

Development and maintenance costs can be expensive, especially when multiple electrical generation systems are included. If the microgrid is connected to grid power, increased charges for the interconnection equipment and storage system (i.e., batteries, compressed air, pumped storage hydropower, etc.) are incurred.

Economics and customer preferences are causing microgrids to integrate more significant amounts of non-dispatchable renewables, such as solar and wind power, from 50% to 100% of their capacity, which can present intermittency problems and system-balancing challenges.

The engineering expertise to develop and maintain microgrids may not be readily available, especially for remote microgrids. The maintenance and service costs at the remote location can be higher than anticipated.

Another disadvantage that prevents microgrid development involves imposed limitations by policymakers. Often, regulations concerning microgrid development are unclear or non-existent.

Lastly, existing electric utility companies often resist microgrid operations within their established service territories. Reluctance to embrace local renewable generation due to fears that the existing power grids cannot reliably integrate distributed energy generation has limited many microgrid projects to provide no more than 15% of peak power demands.

2.2.3. Microgrids in East Africa

Compared to other African regions, East Africa presents the highest solar photovoltaic and wind potential of about 220 PWh and 170 PWh, respectively (Figure 2-9). Among the East African countries, Kenya is leading in microgrid maturity and implementation with more than 40% of the total operational and under-construction microgrids (Duby et al., 2017).

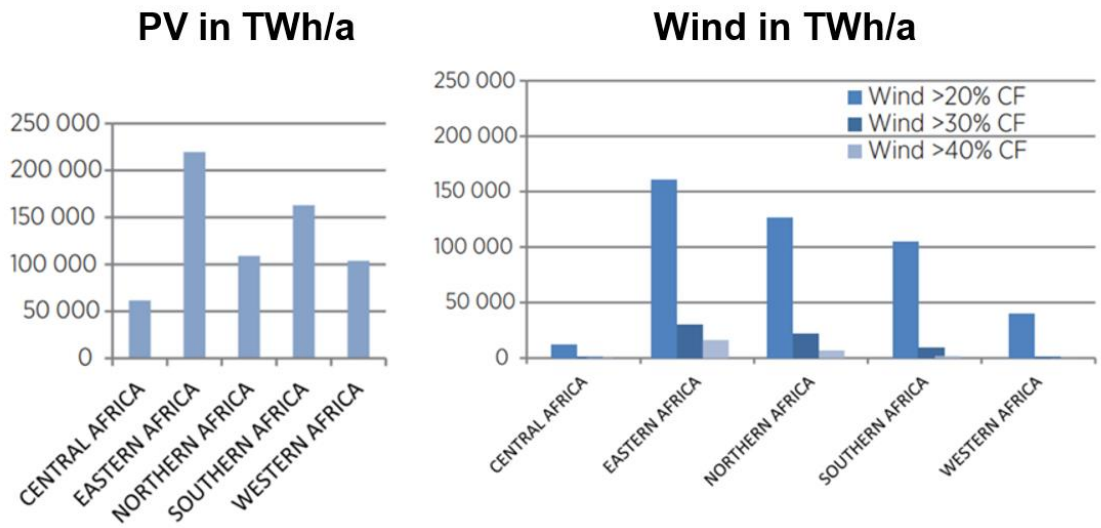

Figure 2-9: *The potential of solar photovoltaic and wind for African countries (IRENA, 2003)*

Despite the solar photovoltaic and wind potential, microgrid growth in the East Africa region is slowly increasing, and net addition is stunted due to several challenges (Kent, 2018). Some challenges are economic, ownership, environmental, policies or technical, which are discussed further in the next section. In addition, proposed solutions are also presented (Babayomi & Okharedia, 2019).

2.2.3.1. Challenges of Microgrids in East Africa

Investment risks in developing microgrid systems are high since microgrid projects are often funded by project finances based on projected future cash flows rather than physical assets or collateral. Thus, project developers must demonstrate to loan providers that the projects are financially secure throughout the loan tenure. Furthermore, the projects usually incorporate capital-intensive, especially renewable energy systems. Thus, the projects are expected to break even and generate profits. The financial expectations expose project owners to long-term risks that may lead to project failures before the recovery of initial capital investments (Williams et al., 2017).

Securing finance for microgrid projects is another challenge, especially in rural areas. Electrification projects are always seen as high risk by both debt and equity funders due to serving in developing countries. This frequently results in projects being unable to secure the capital required for implementation. Furthermore, upon obtaining money, the projects are compounded with unfavourable financial repayment terms such as high-interest rates and short debt tenors and damaging risk remedial measures such as grid encroachment,

unregulated competition, loss of operating subsidies, changes in regulated tariffs, and other sources of policy and regulatory uncertainty (Williams et al., 2017).

Unaffordable installation costs and electricity bills, especially for rural microgrid projects, pose challenges to microgrid growth. Rural microgrids often serve poor populations with limited means to pay for electricity services. As microgrid projects are usually expected to operate in a balance between risks and expected returns, the ability to pay for electricity services in rural communities is poor. Rural communities depend highly upon activities such as subsistence farming, with a small fraction of the population able to generate regular cash flow, thus resulting in seasonality of income. The inconsistent repayment of bills is costly to project owners and challenges revenue collection (Cross & Neumark, 2021).

Poor policies and an unfriendly regulatory environment for investment in microgrids. Microgrid policies for rural electrification have been unfavourable, especially in creating low electricity tariffs due to political pressure to maintain affordability. Unfortunately, these low tariffs have made the electricity sector in many countries unprofitable and unattractive to the private sector. In addition, policies and regulations that are frequently changing and poorly defined demoralise investors' confidence that the policies on which they build their business case will be respected. Institutional structures and regulatory processes are often complex and challenging to navigate as barriers to potential project developers and investors (Williams et al., 2017).

Furthermore, private investment in microgrids usually incurs roadblocks and is subject to state-owned monopolies in the electricity sector. There is no clearly defined relationship between the private and public sectors. Private sectors always succumb to bureaucratic red tape, increasing transaction costs, unnecessarily extending timelines, and discouraging investment (Williams et al., 2017).

Tampering of the microgrid systems, power theft, and theft of the microgrid systems elements affect microgrids' growth in East Africa.

A lack of local technical skills challenges the maintenance and operation of the system. Most microgrids are remotely located; thus, maintenance and repairs are challenging, with high costs and long lead times for the delivery of replacement parts, which may not be available in local markets.

Lack of prior demand data, especially in remote locations, renders demand forecasting ineffective, thus affecting the growth of microgrids. The demand forecast is essential for

proper microgrid design to guarantee sustainability (Yazdkhasti & Diduch, 2020; Yoder & Williams, 2020). The level of demand itself is highly uncertain as a direct measurement in a community that has never had access proves challenging. Methods such as surveys of current energy use or basing assumptions on other villages' experiences are usually used. Since the project profitability is highly dependent on the amount of electricity produced and sold, uncertainty in electricity demand poses a significant risk to investors. Should the demand fall short of expectations, the microgrid may be unprofitable. On the other hand, should the demand exceed expectations, the installed generation capacity may fall short, resulting in poor performance and customer satisfaction, jeopardising the project's sustainability.

Efforts to guarantee the sustainability of microgrids call for energy management schemes which can mitigate risks and improve microgrids' performance. Demand side management (DSM) is one of the management schemes that reduces the cost of energy acquisition by continuously monitoring energy use and managing appliance schedules (Bakare et al., 2023). DSM is used to lower peak loads, control time of service (TOU) levels of power demand, evaluate user profiles for electricity loads, lower carbon emissions, and provide consumers with a preferred energy source. This study will utilise demand-side management to achieve optimisation of rural microgrids.

2.3. Demand Side Management

2.3.1. Introduction

Demand-side management (DSM) is the planning and implementation of energy conservation strategies that seek to manage consumer demand for energy rather than supply it to produce desired changes in the utility's load shape. Customers are encouraged to willingly change load usage patterns without sacrificing their comfort and quality of service (Gyamfi et al., 2022). DSM is the best approach for supply-demand matching by which customer demand can be shaped to improve utilisation factors and load balance. In addition, DSM programs may defer capital investment in generation, transmission and distribution networks and storage and improve system load.

The initial concepts of DSM were defined by (Gellings, 1985) and can be visualized in Figure 2-10. The six mechanisms in Figure 2-10 can further be divided into three groups: Load reduction (Peak clipping and strategic conservation), load increase (valley filling and load growth) and Load shifting (Load shifting and flexible load shaping). Peak clipping aims to reduce demand during peak hours. Utilities achieve this control by incentivising

customers not to consume power during peak hours, directly controlling loads or setting higher prices. The method is helpful in cases where there is no possibility of setting up or installing new power plants. Valley filling focuses on raising usage during very low electricity profile periods to balance demand and supply, avoiding generators' start-up and ramp-up costs. Load growth is expected when using electric vehicles, where customers are encouraged to increase usage up to a certain threshold for grid stability. Load shifting gives consumers options to shift their usage pattern to off-peak hours based on cheap tariffs. It is the combination of load clipping and valley filling. Flexible load shaping is when consumers are flexible enough to shift their loads to different low-usage slots. Usually, customers willing to participate are identified and incentivized for their participation. Energy efficiency is when the overall load profile is lowered thought the day by using more energy-efficient devices or through cyclic operation.

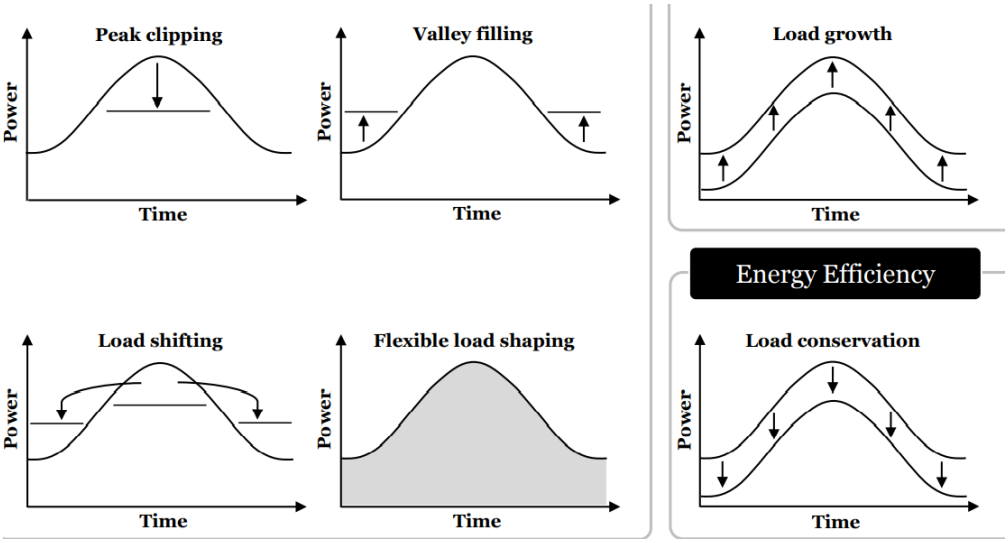

Figure 2-10: *Different demand-side management (DSM) techniques adapted from* (Lampropoulos, 2014).

2.3.2. Categories of Demand Side Management

DSM plays an essential role in power industry development and environmental protection by bringing the following advantages to the market: promoting and restraining efficient market operation and power; relieving demand congestion during peak hours; improving the reliability of power system; alleviating investment pressure on power generation, transmission, and distribution; and facilitate the creation of new prospects for realization of energy conservation and reduction of emissions. DSM can be further categorised into Demand Response and Energy Efficiency, Conservation, and Load Reduction (Figure 2-11).

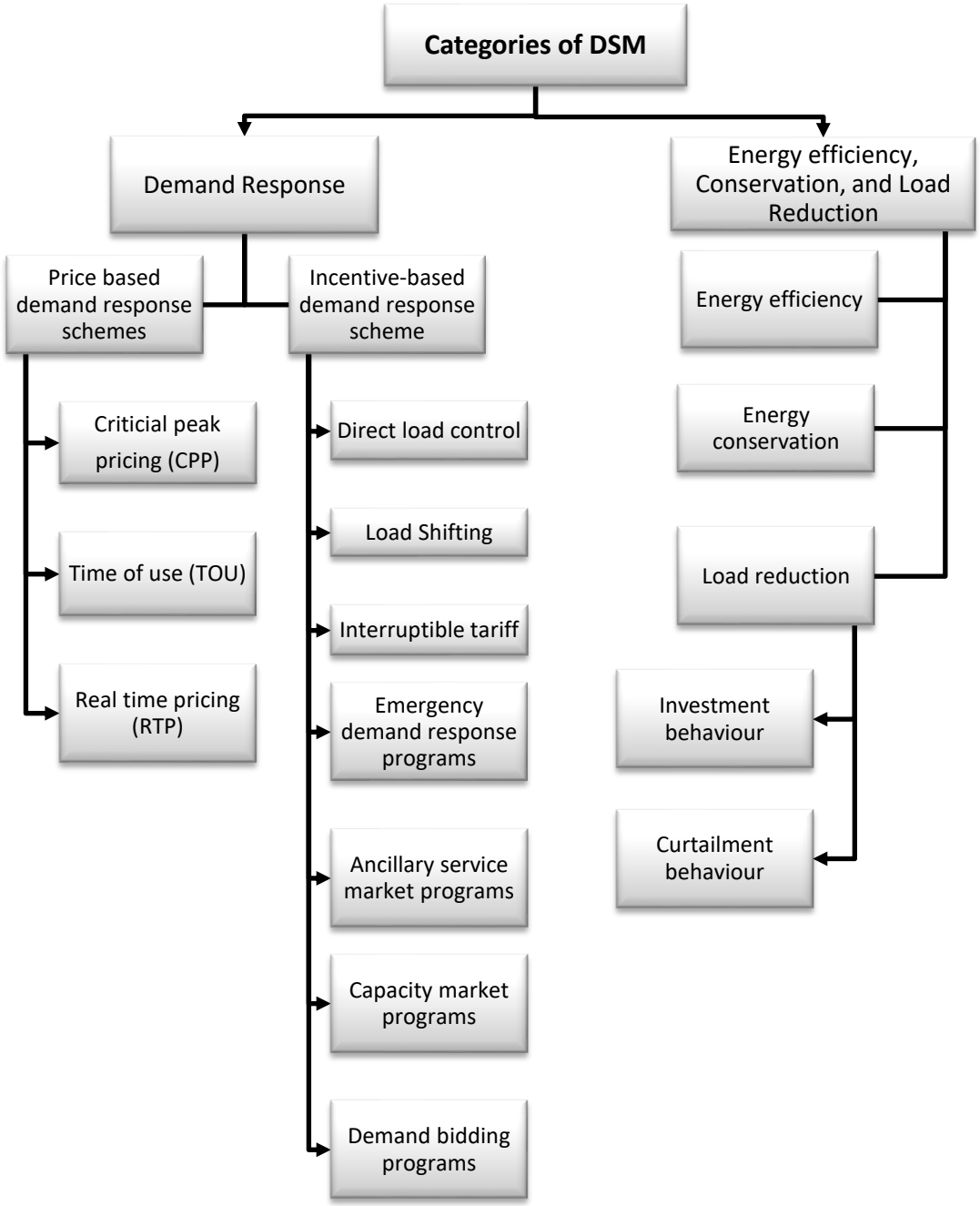

Figure 2-11: *Categories of demand side management (DSM) (Gyamfi et al., 2022)*

2.3.2.1. Demand Response

Demand Response (DR) is a strategy that minimises high-energy demand by influencing the consumption pattern of the end-users. DR is achieved by allowing consumers a more significant role in shifting their demand for electricity during the peak demand period (Gyamfi et al., 2022). DR strategies can be subdivided into price-based demand response schemes, energy-saving behaviours, and incentive-based demand response schemes (Figure 2-11).

a) Price-based demand response schemes (PBDRS)

i. Critical Peak Pricing (CPP)

In this strategy, an extreme peak demand period is picked out, during which a much higher electricity price per kWh is selected and designated as critical by the utility providers (Figure 2-12). Furthermore, two or three averaged price points are calculated to reflect different market conditions, and the consumer is informed of the periods for specific critical hours or days. Three types of pricing are usually considered: fixed-period critical peak pricing, variable critical peak pricing, and variable-period essential peak pricing. In a fixed-period critical peak pricing, a specific period during a day is selected, and a fixed high electricity price is set. The application period is specified for variable critical peak pricing, but the electricity price varies according to the current demand. In a variable-period critical peak pricing, the application period is not fixed, and the operation frequency and duration are limited. Utilities trigger the critical peak pricing based on predefined criteria (Gyamfi et al., 2022).

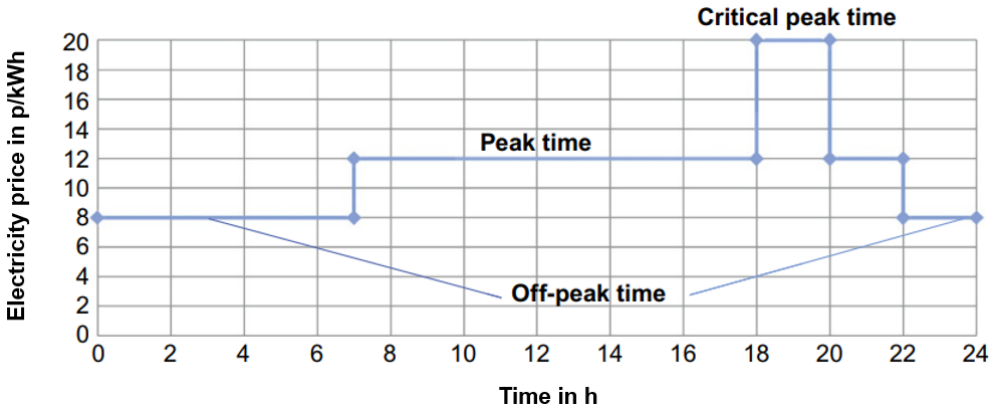

Figure 2-12: *Example of the profile showing the pricing of electricity at different usage periods with high prices at peak hours (Li et al., 2017)*

ii. Time of Use (ToU)

In the time-of-use strategy, a utility rate per kWh of electricity is higher during peak demand hours and lower during off-peak hours, which vary according to the time of the day, seasons, and day type, reducing the overall cost for both the utility and the consumers.

The prices differ in different time slots, with a flat fee applied to each slot. In this strategy, customers tend to shift their demand to a lower price period (Gyamfi et al., 2022).

iii. Real-Time Pricing (RTP)

In this strategy, the cost of power (per kWh) fluctuates frequently, usually by hours, based on the real-time electricity production cost at the end of the generation side (see Figure 2-13). Thus, retail electricity rates are higher during peak times than shoulder and off-peak times. Real-time pricing delivers efficient and effective utilization of power to adjust the power balance between supply and demand. This scheme is more acceptable to the industrial and commercial sectors than the residential ones. There are two main difficulties in applying for this scheme. Firstly, it relies on continuous real-time data exchange, which is unfavourable for customers. Secondly, large-scale data processing increases the complexity of the whole system (Li et al., 2017).

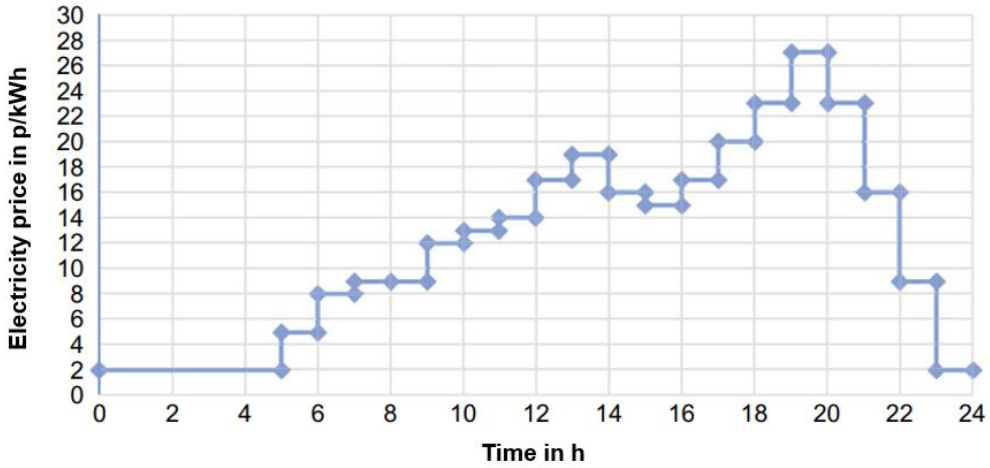

Figure 2-13: *Example of a profile showing real-time pricing in 30 min steps (Li et al., 2017)*

b) Incentive-based demand response scheme (IBDRS)

i. Direct Load Control (DLC)

In this strategy, as per advanced agreement between customers and utilities, the utilities can remotely control the operation of some equipment, such as air-conditioning systems and water heaters, during specific hours of the day and season. The notices for the procedure are typically announced a short time ahead. To participate in this method, customers must be equipped with a remote-control switch system so that utilities can reschedule, turn on, or turn off the appliances. This is usually achieved by incentivising consumers to minimize energy demand and stabilize the grid. The strategy is voluntary, and customers are not penalized for not curtailing their loads. Direct load control is primarily

applied to the residential or small-scale commercial sectors (Gyamfi et al., 2022).

ii. Load Shifting

Load shifting is a technique in which load demand is shifted from peak to off-peak hours, but the total consumption remains constant. Load shifting is beneficial as electricity market prices are dynamic depending on demand. An increase in total system demand increases the electricity bills and vice versa. Thus, industries and commercial businesses can optimise electricity consumption during night shifts when power demand is low relative to system supply.

iii. Interruptible Tariff

An interruptible tariff strategy is usually offered to residential and commercial customers based on a contractual agreement between the utility and the customer on the cost of electricity per unit. Consumers receive a rate or bill discount for agreeing to reduce their consumption when the system is congested. The energy consumed by the customer does not decrease but instead shifts to an off-peak period. This helps stabilise the grid or handle an emergency significantly when the demand is projected to increase. In this method, the operation frequency and the duration are limited; thus, if a customer fails to respond in the predefined period, they could receive a fine (Gyamfi et al., 2022).

iv. Emergency Demand Response Programs (EDRP)

The strategy is a voluntary emergency program that gives customers an incentive for a short-notice reduction in their energy consumption when there is a shortfall in supply reserves. There is no penalty if customers do not respond to curtail their loads (Li et al., 2017).

v. Ancillary Service Market Programs (ASMP)

Customers (usually independent system operators and regional transmission organizations) can bid on load curtailment in the spot market for energy balance maintenance, frequency and voltage regulation, voltage support, and constraint management in ancillary services market programs. After bid acceptance, the participating consumer is paid the market price for commitment (Li et al., 2017).

vi. Capacity Market Program (CMP)

CMP strategy is where a customer receives a guaranteed payment for committing to reducing consumption when there are contingencies in the

electric grid. These curtailments are treated as system capacity to replace the conventional generation and delivery resources. By proving their ability to curtail, customers can receive a reservation payment. And by providing the reduction, customers can receive an incentive. In contrast to the Emergency Demand Response Programs, customers can receive a penalty if they fail to deliver it (Li et al., 2017).

vii. Demand Bidding Programs (DBP)

In this strategy, consumers can bid on a specific load reduction based on their situation and the wholesale market. In this arrangement, utilities announce the total amount of electricity that must be curtailed based on the generation and demand situation. The bid is accepted if it is less than the market price. However, customers must curtail their loads by the amount specified in the terms; otherwise, they become liable for penalties. This method is also suitable for large-scale customers. Aggregators can integrate small-scale customers and be involved as a unit (Li et al., 2017).

2.3.2.2. Energy efficiency, Conservation, and Load Reduction

On the other hand, energy efficiency consists of using less energy, which reduces total energy consumption. This leads to reduced CO_2 emissions and the cost of utility bills. This category focuses on energy-saving behaviour or consumers' energy-use behaviour change. EE strategy requires little or no charge to implement and is divided into two, namely, investment behaviour and curtailment behaviour. Investment behaviour involves using monetary investment to improve energy-saving behaviour, while curtailment behaviour strategy requires little or no financial investment toward energy-saving (Gyamfi et al., 2022).

a) Energy Efficiency (EE)

EE reduces the overall demand for electricity while maintaining the same amount or quality of service output with less energy. For example, instead of lowering the temperature of a conventional furnace, you can install an energy-efficient furnace to keep your house at a specific temperature while consuming less energy than you would with a conventional one.

b) Energy Conservation (EC)

EC refers to the overall reduction of energy consumption or demand for electricity by adjusting behaviour. It involves a certain degree of sacrifice, such as using a

clothes dryer less often, turning down the heat in winter, turning off appliances when they are not in use, etc.

c) Load Reduction

   i. Investment behaviour

      This strategy involves motivating customers to reduce their electricity consumption by investing in compact fluorescent lamps and Light-emitting diodes (LED) rather than incandescent bulbs (Li et al., 2017).

   ii. Curtailment behaviour

      In this strategy, customers are motivated to save energy by being involved in user practices that promote load reduction, such as putting off electric loads that are not in use (Gyamfi et al., 2022).

In recent years, more efforts have been dedicated to improving the energy efficiency of home appliances worldwide (Sarfi et al., 2018). For major households in the developed world, using energy-efficient appliances has been enhanced due to several factors. In Canadian households' regulatory efforts, the imposition of standards for household appliances and technological advancement were considered critical factors. Research conducted in the United States (Golden Carrot program) and the work of NUTEK in Sweden show that energy labelling, procurement of energy-efficient appliances, enforcement of minimum energy efficiency standards, voluntary agreements and demand side management (DSM) are the reasons (Turiel, 1997). The last two methods contributed to significant reductions in residential and commercial sector electricity demand, highlighting the potential for reducing the number of new power plants through such programs.

2.3.3. Demand Side Management Methods

Demand-side management is vital for achieving sustainability of microgrids as it facilitates efficient use of resources and reduces electricity production waste and excessive storage capacities. Different demand-side generation methods are available, which help enhance microgrid stability and optimise renewable energy resources within the microgrid. The DSM methods include the multi-objective optimization method, the linear matrix inequality (LMI) approach, and the particle swarm method (Li et al., 2017).

2.3.3.1. Multi-objective Optimization Method

The multi-objective optimisation method considers several objectives and obtains an optimised decision without favouring any intent. A multi-objective artificial immune

system algorithm is used to find Pareto-optimal solutions. The multi-objective artificial immune system algorithm uses gene operation to maintain diversity. A solution is Pareto-dominated if other solutions can provide better performance for at least one objective without hurting other goals. First, a group of solutions are generated based on the predefined requirement. Then, the dominated solutions are gradually removed during the iteration while the nondominated solutions remain (Li et al., 2017).

The method has been used in multiple microgrid projects for a market operator and distribution network operator. Three participants are usually considered microgrids, a power grid, and an independent system operator (i.e., ISO). The power grid aims to maximize the net gain (in terms of energy and money) for providing power to microgrids. For microgrids, the aim is to maximize the net revenue for consuming power supplied by the power grid. For the ISO, in an emergency, the storage must be maintained around a standard level; the closer, the better. Therefore, the objective is to minimize the sum of differences between the current status and the average level.

From the above problem, a specific solution that can maximize the minimum improvement in all objectives is selected. Power demand is generally more significant than power generation. Storage systems are used to supply the imbalance between the demand and generation. An increase in renewable power generation can lead to a decrease in power generation by diesel generators. This multi-objective optimization method can be applied to other scenarios involving different objectives and constraints. Because this method is not based on a specific model, it represents a framework for searching for Pareto-optimal solutions to multi-objective problems.

2.3.3.2. Linear Matrix Inequality Method

The LMI approach has been used for many situations. Because of the convex property, the associated problem can be solved efficiently (Li et al., 2017). It has been used to design a storage system in intelligent grid networks (Li et al., 2017). The basic idea is to charge the batteries when the utility electricity price is lower than the threshold and discharge the batteries when the price is higher. Price signals, system uncertainties, and physical constraints are three critical factors that must be considered in this design.

2.3.3.3. Artificial Neural Network (ANN)

Artificial neural networks are a technology based on studies of the brain and nervous system simulating their electrical activity. The networks emulate a biological neural network

associated with a signal-processing system and information consisting of many simple processors called neurons (Walczak & Cerpa, 2003).

The neurons are interconnected by synapses, allowing distributed parallel processing to learn and establish precise, complex relationships between various numeric variables without imposing any preconceived model. ANNs are useful in systems where no mathematical model is available. Furthermore, ANNs can create nonlinear and traditional linear models, thus applicable across a broader range of problem types (both linear and nonlinear) (Devi & Ayswarya, 2015).

2.3.3.4. Genetic Algorithm (GA)

A genetic algorithm (GA) developed by John Holland and his collaborators in the 1960s and 1970s solves constrained and unconstrained optimisation problems based on Charles Darwin's theory of natural selection that mimics biological evolution (Yang, 2021). Genetic Algorithm involves encrypting an optimisation function as arrays of bits (mimicking chromosomes), manipulating strings by genetic operators, and selecting according to fitness to find an optimal solution to the problem. These genetic operators form an essential part of the genetic algorithm as a problem-solving strategy (Yang, 2021).

Genetic algorithms have several advantages over other optimisation algorithms. The two most notable are the ability to deal with various optimisations despite the objective function being stationary or non-stationary, linear or nonlinear, continuous or discontinuous, or with random noise. The other advantage is the ability to explore the search space in many directions simultaneously, making it ideal for parallelising the algorithms for implementation. Different parameters and even different groups of encoded strings can be manipulated at the same time.

2.3.3.5. Particle Swarm Optimisation (PSO) Method

The PSO method was introduced by James Kennedy and Russel C. Eberhart in 1995. It is based on the swarm intelligence paradigm and is motivated by the social behaviour of animals such as fish and birds, mimicking how they navigate or forage (Slowik, 2011). Birds fly in one direction, searching for food; if one bird sees the food, all other birds will follow in searching for the food. The swarm searches for food cooperatively, and each member learns from the experience and changes the search pattern to locate food. Thus, the best position is found when they move from one place to another.

The PSO method works under two principles: communication and learning. This study utilised the PSO as a demand-side management method to analyse the selected East African microgrids. Three power sources were considered: solar PV, battery, and backup generator. The aim was to minimize the conventional generator's fuel cost through provisional incentives. The basic idea is to encourage customers to cut-down loads or shift them from peak to off-peak hours to avoid consuming too much generator fuel when PV and batteries cannot cater for the peak load. The multi-objective function to be solved by the PSO involves minimising generator fuel costs and maximising utility benefits.

2.3.4. Particle Swarm Optimisation

The PSO algorithm shares principles with a search algorithm, as a large population of individuals (i.e., particles) aim to find the optimal solution in a given multi-dimensional search space (Menos-aikateriniadis et al., 2022). The particles represent possible solutions, and their location represents the value of the objective function that needs to be optimized (Roy et al., 2019). An optimal result is identified when the particles continue searching through hyperspace as they move towards a new location with an updated velocity (Eqn 2-1). After each iteration, the velocities are stochastically updated based on the historical optimal positions of individual particles and the historical global best position among all particles (Eqn 2-2). Figure 2-14 and Figure 2-15 describe the working mechanism and flow chart of the particle swarm optimisation method, respectively.

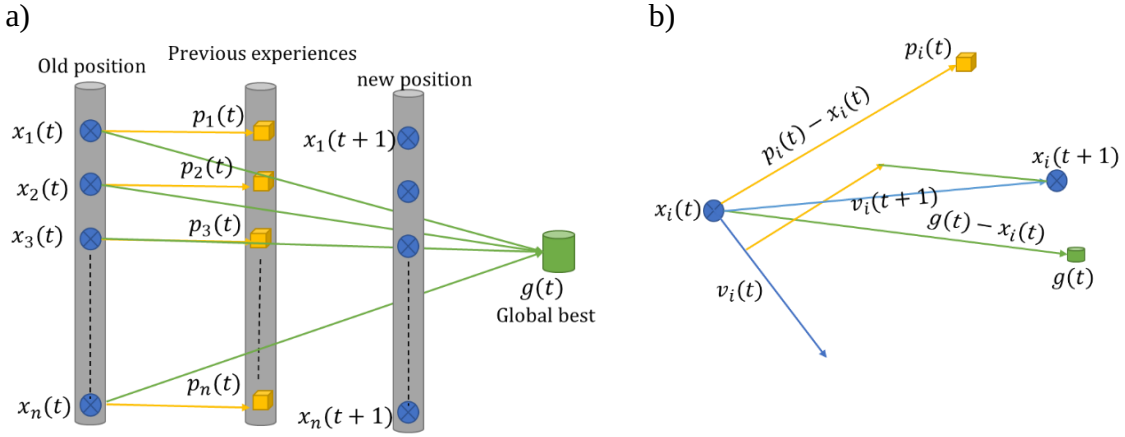

Figure 2-14: *a) Representation of particle swarm optimization algorithm (PSO) working mechanism b) Vectoral representation of particle movement in PSO method (own representation ideas borrowed from (Mirjalili et al., 2020).*

From the vectorial representation of PSO, new position and velocity can be calculated as;

$$x_i(t+1) = x_i(t) + v_i(t+1) \qquad \textit{Eqn 2-1}$$

$$v_i(t+1) = wv_i(t) + c_1[p_i(t) - x_i(t)] + c_2[g(t) - x_i(t)] \qquad \textit{Eqn 2-2}$$

The standard PSO equations for updating the velocity can be written as follows:

$$v_{ij}(t+1) = wv_{ij}(t) + r_1c_1[p_{ij}(t) - x_{ij}(t)] + r_2c_2[g_j(t) - x_{ij}(t)] \qquad \textit{Eqn 2-3}$$

$$x_{ij}(t+1) = x_{ij}(t) + v_{ij}(t+1) \qquad \textit{Eqn 2-4}$$

Where w and v are the inertia weight factors, r_1 and r_2 are random numbers uniformly distributed in the range of 0 to 1, c_1 and c_2 are acceleration coefficient, j is the jth component.

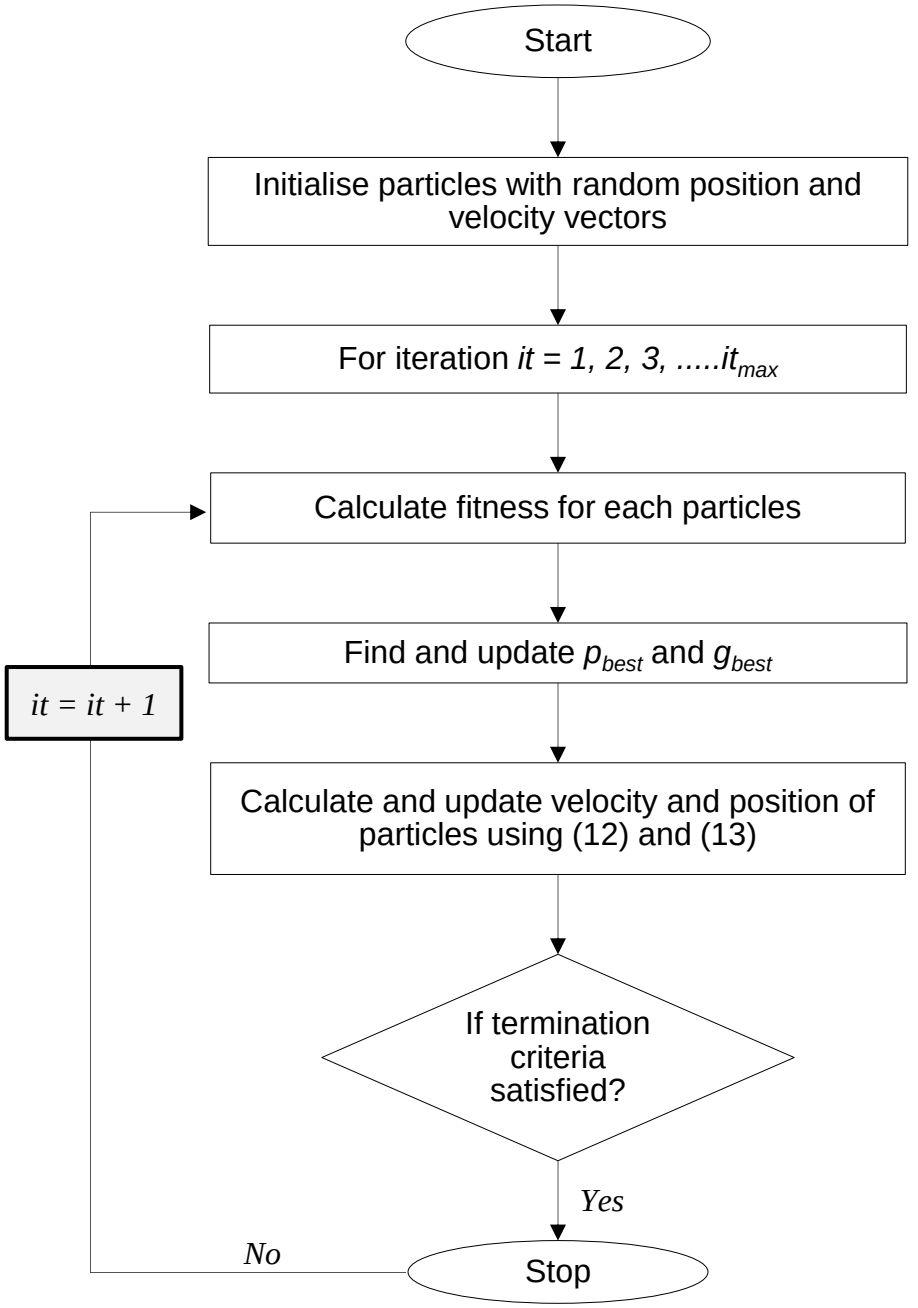

Figure 2-15: *Flow chart of particle swarm optimization algorithm (PSO) (Roy et al., 2019)*

The detailed algorithm of the PSO method can be described as follows;

Step 1) Input: A set of generation and load profiles, i.e., g_{t_c} and l_{t_1} regarding particle positions

Initialize the number of iterations and the number of population *n*.

Step 2) Output: An optimal set of design variables in terms of the position of the swarm

Step 3) *BEGIN ALGORITHM*

Step 4) */*Start iteration*/*

Step 5) *For it* = 1, 2, ..., it_{max}

Step 6) */*Generate random position of particles* x_i = [g_{t_c} l_{t_1}] *as designed variable*/*

Step 7) *For it* = 1, 2, ..., it_{max}

Step 8) For each particle, calculate the fitness. (Fitness refers to the objective function that the algorithm is optimizing. It quantifies the quality of a potential solution within the solution space. PSO uses fitness values to guide their movement through the search space, aiming to find the optimal solution)

Step 9) A particle with the best fitness is considered as p_{best}

Step 10) If (current fitness > p_{best})

Step 11) p_{best} = current fitness

Step 12) *else*

Step 13) p_{best} will retain its value

Step 14) *End If*

Step 15) The particle's overall previous best is known as g_{best}

Step 16) If (current fitness > g_{best})

Step 17) g_{best}= current fitness

Step 18) *else*

Step 19) g_{best} will retain its value

Step 20) Update the velocity and position of particles using (12) and (13), respectively.

Step 21) *End if*

Step 22) *If* ($it \geq it_{max}$)

Step 23) go to Step 27

Step 24) *else*

Step 25) go to step 8

Step 26) *End If*

Step 27) *End For*

Step 28) The individuals that generate the latest are the optimal design variables

Step 29) *END ALGORITHM*

2.3.4.1. Particle Swarm Optimisation Methods

PSO is selected over other methods due to its low computational needs, near-optimal solution identification, the small number of initialization parameters, and the lack of model training prior to implementation (Roy et al., 2019). Various methods employed within PSO are presented below.

a) Canonical/traditional
b) Multi-objective PSO
c) Bi-level PSO (BLPSO),
d) Binary PSO,
e) Gradient-based PSO,
f) Modified PSO,
g) Quadratic BPSO,
h) Cooperative PSO, such as stochastic attraction-repulsion of diversity (SARD) and stochastic repulsion,

2.3.4.2. Advantages of the Particle Swarm Optimisation Method

PSO has several advantages: it is a simple yet powerful algorithm, inexpensive in terms of memory and speed, can be easily implemented using computer programming, does not involve any probability distribution, and does not store any previous solution. PSO is the most widely used method compared to other optimization methods and has the following advantages;

a) Simple and easy to use,
b) Fast convergence and robustness, even in complex and highly constrained multi-dimensional search spaces,
c) High applicability as it can be used in numerous optimization problems and
d) High adjustability as it can be easily hybridized and modified to fit the purpose of each problem and improve its performance.

2.3.4.3. Disadvantages of the Particle Swarm Optimisation Method

Some of the potential drawbacks that can be encountered while using PSO are;

a) Risk of suboptimal solutions (local optima) due to either the problem formulation characteristics or a lack of diversity in particle movement that leads to premature convergence,
b) There is no guarantee that PSO will reach the global optimum solution since there is a risk of premature convergence to local optima and
c) Lack of interpretability given that the algorithm is not based on a strong mathematical theoretical basis (i.e., lack of mathematical proof of convergence).

It is worth noting that poor PSO performance can result from problem formulation, modelling inputs, and system constraints (Roy et al., 2019).

2.4. Summary

This chapter discussed the analysis and demand side management of East African rural microgrids through optimisation and reduction of storage costs.

Africa has a natural advantage in benefitting from various renewable energy resources such as solar, wind, biomass, and hydropower. Choosing the best energy source for rural electrification in East Africa should consider available renewable resources in context with the local conditions and needs. Generally, solar energy is often a suitable choice for decentralized electrification in remote areas with limited infrastructure. One of the reliable solutions for rural electrification employing solar energy is standalone power systems such as microgrids.

Different microgrids are categorised depending on the generation capacity, applications, system architecture, and customer type. The Microgrids face several challenges in their installation and application, such as investment risks in developing the microgrid systems, securing finance for microgrid projects, unaffordable installation costs and electricity bills once operational, poor policies and unfriendly regulatory environment for investment, tampering with the microgrid systems, power theft, theft of the microgrid systems elements, and lack of prior demand data, especially in remote locations. These challenges affect microgrids' growth in East Africa. Lack of local technical skills challenges the maintenance and operation of the system.

Efforts to curb these challenges and guarantee the sustainability of microgrids call for energy management schemes that can mitigate risks and improve microgrids' performance,

such as demand side management (DSM). Demand-side management (DSM) is the planning and implementation of energy conservation strategies that seek to manage consumer demand for energy rather than supply it to produce desired changes in the utility's load shape.

Different demand-side generation methods were implemented to help enhance microgrid stability and optimise renewable energy resources within the microgrid. However, not much attention was paid to the combination of classification and prioritisation of consumer demand, assessing their correlation, predicting their future demand, and studying their energy input and output to select proper demand-side management strategies while reducing the cost of storage. This study aims to find the best practice of a solar microgrid in East Africa through demand-side management, customer classification, and prioritisation. Thus, the above aspects provided the basis for further investigation, the details of which are presented in Chapter Three (3).

CHAPTER THREE

3. Methodology

3.1. Introduction

This chapter presented the methodology utilised in the research to achieve the general and specific objectives. Figure 3-1 presents the summary used.

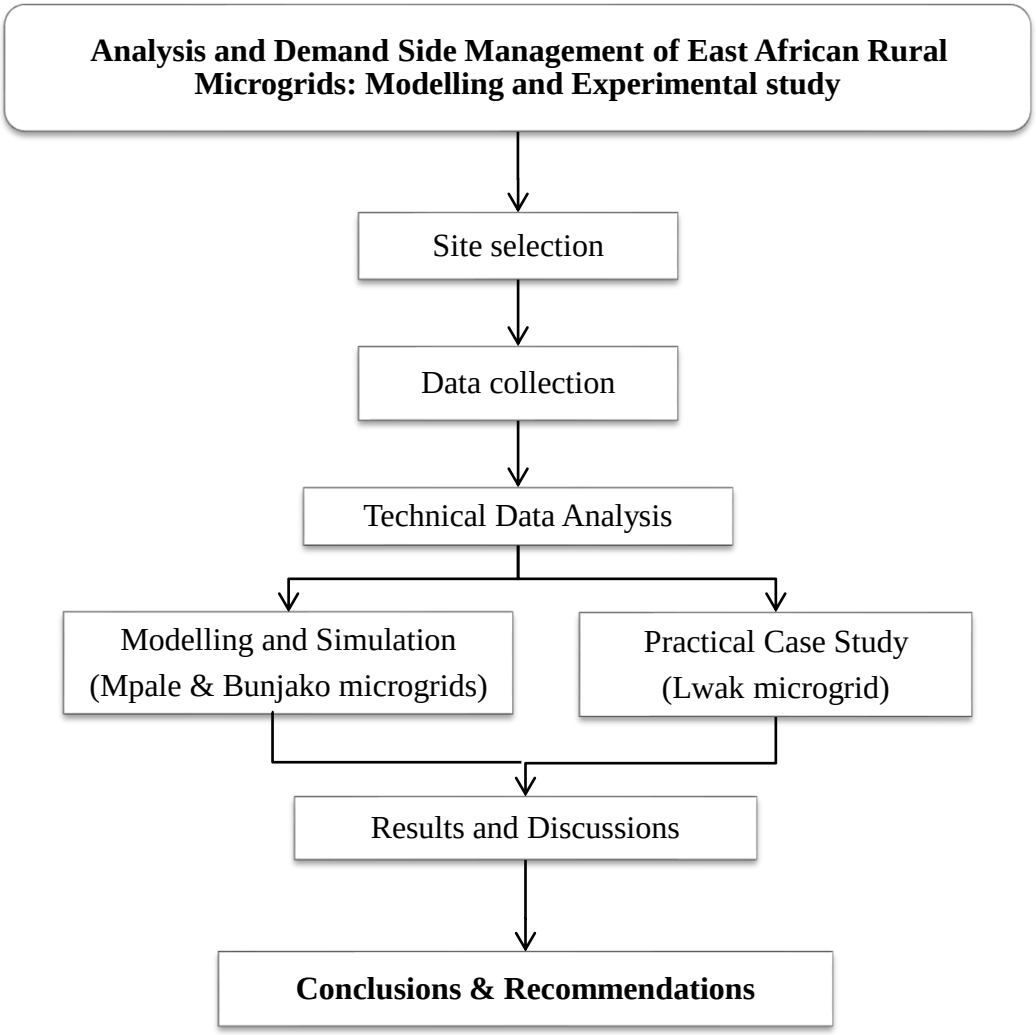

Figure 3-1: *Flow chart of the step-by-step activities involved in the modelling and experimental methodology.*

3.2. Site Selection and Data Collection

The study data was collected from three selected microgrids: Mpale, Lwak, and Bunjako microgrids in Tanzania, Kenya, and Uganda, respectively. Lwak microgrid was a new microgrid installed in July 2023, operated by ART-D Grids, and selected as a practical case study. Figure 3-2 presents the geographical location of the selected microgrids.

Figure 3-2: *Map showing the locations of the selected microgrids (Google Earth, 2023).*

Table 3-1: *Specifications and ratings of installed photovoltaic (PV) system for Mpale, Bunjako, and Lwak microgrids*

Name	**Unit**	**Specification**		
Microgrids		**Mpale**	**Bunjako 35kW**	**Lwak Convent**
PV generator (number of modules, type)				
Manufacture country		AMERISOLAR (China)	Jinko Solar	China
Model Name		AS-6P30-250 W	JKM375M-72-V	JA Solar modules
Type		Polycrystalline silicon	Polycrystalline silicon	Monocrystalline Silicon
Maximum power rating	W_p	250	400	415
Module efficiency	%	15.37	19.33	20.7
Number of modules		192	96	30
Battery				
Manufacturer Country		SUNLIGHT (Greece)	Hoppecke OPzV Sun/Power	Hoppecke / Germany
Model name		2 V-14 RES OPzS 2765	VR L 2-1700	Sun/Power VR M 12-105
Battery type		Lead–acid battery	Lead-acid battery	Lead–acid battery
Nominal Capacity (1 cell)	Ah	2769	1545	87 Ah C_{10} /101 Ah C_{100}
Nominal cell Voltage (1 cell)	V	1.85	2	2.25
Number of battery cells		48	48	36
Total storage capacity	kWh	246	148.32	36
Diesel Generator (AC Synchronous Generator)	kVA	MJB 200 SB4	None	(Cummins 40 kW generator)

3.2.1. Site Selection

3.2.1.1. Mpale microgrid

Mpale microgrid is located in Mpale ward, Korogwe district, Tanga region in Tanzania (Figure 3-3). Geographical coordinates of the Mpale microgrid are given as -4°59’58.2"S 38°28’4.44"E (-4.9995°,38.4679°). The microgrid is supplied only with solar energy and has battery storage. A diesel generator is available and switched on to charge the battery whenever there is an insufficient PV supply. The microgrid serves a community of about 700 inhabitants. The specifications and ratings of the installed PV system configurations are depicted in Table 3-1.

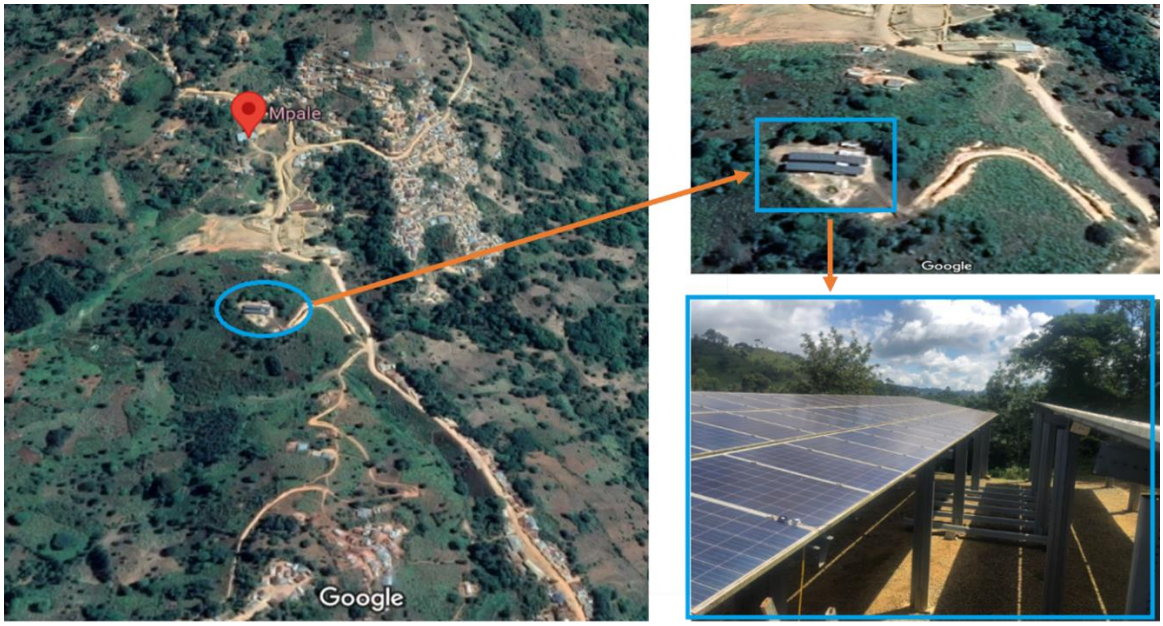

Figure 3-3: *Location of the Mpale Microgrid at Korogwe district in Tanga region, Tanzania (-4°59’58.2"S 38°28’4.44"E (-4.9995°,38.4679°))*

The microgrid was selected as a case study due to its customer variety, the magnitude of data (about three years of data in-store), which proved to be essential for the research, the nature of the demand, which fluctuates frequently, underutilisation of the grid, reports on blackouts assumed due to transients and reactive power, low generation during the rainy season prompting the use of an expensive backup generator, and non-agreeable tariff structure used.

Mpale microgrid offered several advantages: real-time data availability, plugging demand and weather instruments for measurements, and permission to interview connected customers. However, due to having many connected customers, accessibility to all appliances proved to be challenging.

3.2.1.2. Bunjako Microgrid

Bunjako microgrid is located on Bunjako island, Central region of Uganda (0°0’10" N, 32°8’4" E). The microgrid is an isolated microgrid supplied with solar PV coupled with battery storage.

The microgrids are in the form of containerized off-grid Remote Power Units (RPU), aiming to provide power and communications to schools, clinics, retail and commercial customers, and communities. The RPUs are designed to supply base load power ranging from 1 – 5 kW and peak loads from 6 up to 24 kW for 24 hours. Several versions of the RPUs are designed based on the solution’s real customer needs and scalability. Currently, up to 3 versions of the RPU have been developed (Table 3-2).

Bunjako microgrid has a total installed capacity of 114 kW with an inverter size of 174 kW and was aimed to power four (4) of eight villages on the island, targeting 500 connections. The specifications and ratings of the installed PV system configurations are depicted in Table 3-1.

Table 3-2: *Details of the Bunjako Remote Power Units (RPU) with their number of photovoltaic modules, capacity, storage, and energy supplied*

RPU version	No. PV modules	Nominal DC capacity (kW)	Energy supplied (kWh/day)	Battery pack (kWh)
RPU 7	24	7.92	34	32.7
RPU 17	54	17.82	76	74.2
RPU 30	96	31.68	135	148.3

3.2.1.3. Lwak Microgrid

Lwak microgrid is located in a convent at Siaya county in western Kenya at coordinates 0°8.4 S, 34°21.4E (Latitude: -0.1424748530737744; Longitude: 34.35782880740559) (Figure 3-4). The specifications and ratings of the installed PV system configurations are depicted in Table 3-1.

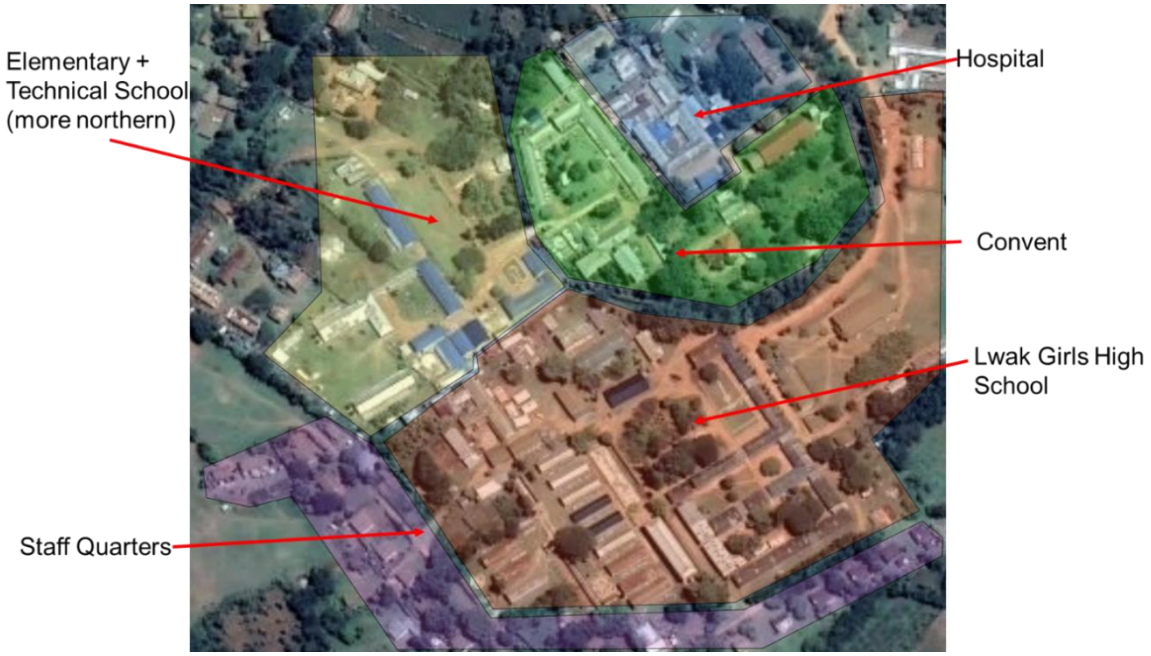

Figure 3-4: *Location of Lwak centre showing all the Lwak community composing of the convent, hospital, schools and staff quarters (Google Earth, 2023).*

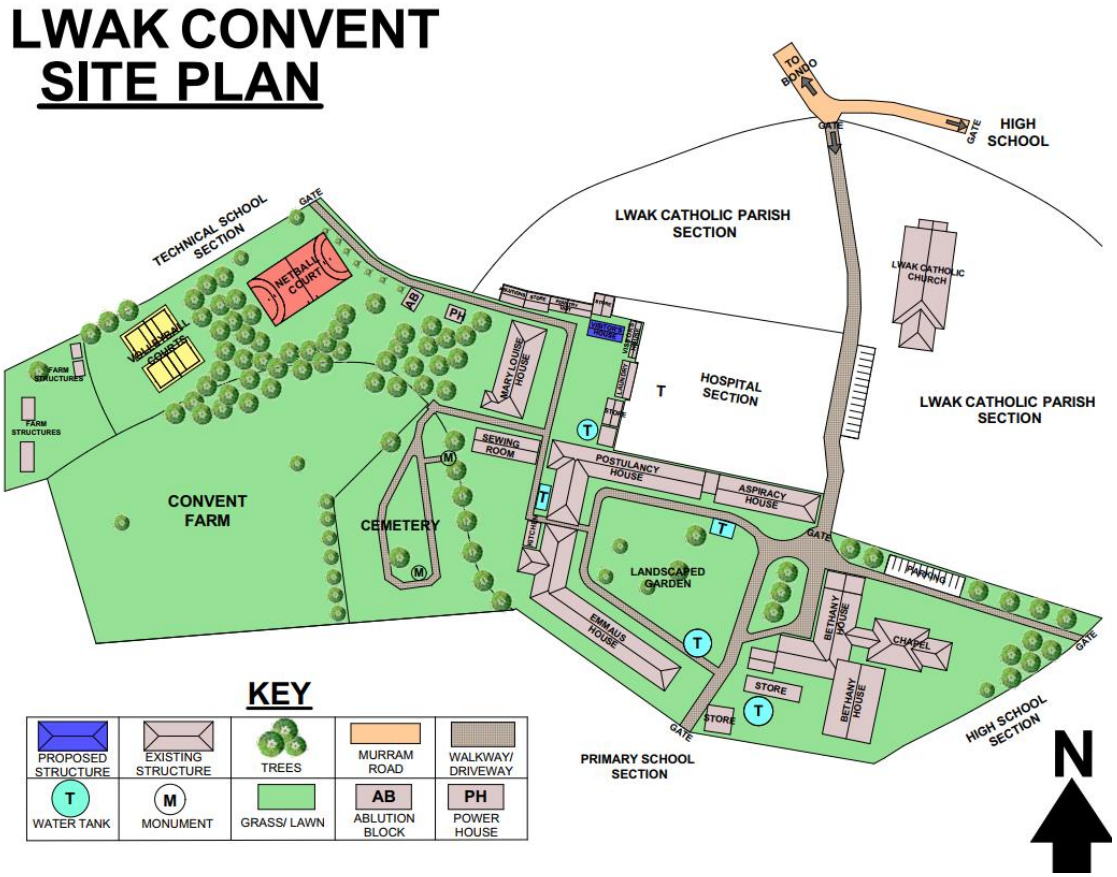

Figure 3-5: *Site plan of Lwak convent where the Lwak microgrid has been installed (Google Earth, 2023).*

Table 3-3: *List of appliances used in Lwak convent with power ratings and usage hours in a day (Acronyms B, E, and P represent Bethany, Emmaus, and Postulants houses, respectively)*

S/N	HOUSES	BETHANY	EMMAUS	POSTULANTS	CHAPEL	TOTAL	Hrs /day	RATING (W)
	LIGHTS							
1	Fluorescent Light (Long)	30	12	8	32	82	6	36 – 40 W
2	Fluorescent Light (Short)	56	20	13	–	89	6	18 – 20 W
3	Globe light	25	2	8 (2 in use)	–	27	2	5 – 15 W
4	Fluorescent bulbs	3	2	–	6	11	8	30 – 40 W
5	Energy server lights (coils)	1	2	2	–	5	8	7 W
6	Security lights	1	–	–	–	1	8	10 – 100 W
	COOLING/FREEZING APPLIANCES							
1	Fridges	Fridge 2 (Toshiba GR-EF 3)	Fridge 4 (Haier HRF-3674)	Fridge 6 (Goldstar GR-312S)	–	3	6	– E 80 W P 120 W
2	Freezers	Freezer 1 (Bruhm BCF- 398S)	Freezer 5 (ArmCoAF-C38S)	Freezer 7	–	3	6	B 106 W E 210 W –

S/N	HOUSES	BETHANY	EMMAUS	POSTULANTS	CHAPEL	TOTAL	Hrs /day	RATING (W)
		Freezer 3 (HTCF208A2)	–	Freezer 8 (Bruhm BCF-398SD)	–	2	6	B 94 W E 106 W
	OTHER APPLIANCES							
1	Kettles	–	1	–	–	1	1	2200 W
2	Irons	6	–	3	–	9	0.5	B 1000 W
3	Water Dispenser	1	2	–	–	3	4	B 530 W E 635 W
4	Laptops	8	–	–	–	8	5	50 – 150 W
5	Desktops	–	–	2	–	2	6	150 – 300 W
6	Televisions	1	2	1	–	4	4	40 W
7	Decoders	–	–	1	–	1	3	50 W
8	Blenders	–	1	–	–	1	0.5	300 – 700 W
9	Water Pumps	2	1	1	–	4	2	B 1700 W E&P 1210 W
10	Printer	–	–	2	–	2	2	–

The appliances' features (power ratings and usage time) were recorded per observation, and questionnaires were conducted at the site. The actual power consumption of targeted appliances (i.e., cooling appliances) was measured at the site and detailed in Chapter 3.6.

3.2.2. Data Acquisition

Two types of data were collected: primary and secondary. The primary data were qualitative data obtained via semi-structured interviews among electricity users, mini-grid operators, and local leaders. Secondary data, such as solar irradiance, demand data, and energy consumption, were collected from quantitative data to optimise microgrid performance.

3.2.2.1. Primary Data Collection

Mpale Village is divided into three localities, and qualitative data collection was done to capture a representation of all three divisions of the village (Figure 3-6). 75 interviews were conducted with 45 households, 18 businesses, eight (8) local leaders, and two (2) institutions (secondary school and dispensary).

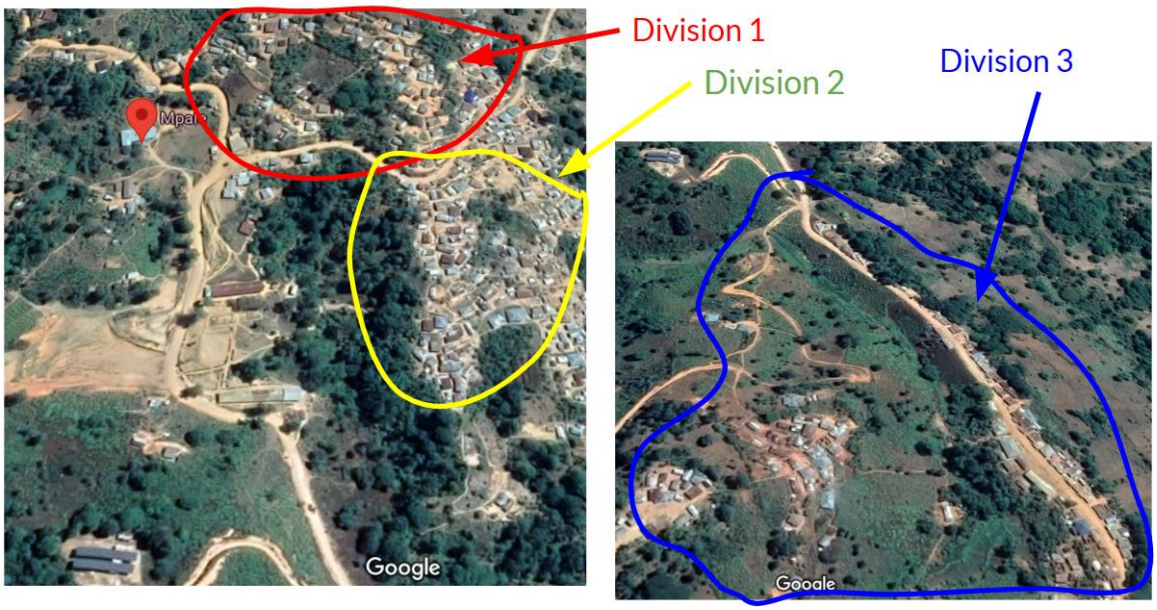

Figure 3-6: *Mpale microgrid divisions of customers for qualitative data collection*

3.2.2.2. Secondary Data Collection

The data acquisition process in the microgrids involved collecting and recording data related to solar generation, storage, and consumption (i.e., data from solar panels, batteries, inverters, and connected loads). The aim was to gather data on factors such as solar irradiance, battery state of charge, and energy consumption.

The recorded data was vital as it is crucial for optimizing the microgrid's performance, managing demand and supply, and ensuring microgrid efficiency and reliability. Furthermore, data collection enabled real-time monitoring and control, which helped make

informed decisions for sustainable and cost-effective energy management. The following tools were used in data collection.

a) MAVOWATT 270 Power Quality Analyser

MAVOWATT is a series of GOSSEN METRAWATT, a portable, hand-held, eight-channel power quality meter/monitor with a high-speed sampling board for capturing the details of high-speed transients. The MAVOWATT can simultaneously monitor, record, and display data on four voltage and current channels. It displays captured information in either graphic or textual form, including events and trends, voltage compliance and mini-reports. These include trended data and events generated from user-programmed triggers or thresholds.

Power quality and Energy information that can be generated and reported by MAVOWATT include voltage and current (rms, transients, sags, swells, unbalance, DC), flicker (voltage THD, current THD, short term, long term), frequency, phase, harmonics, power (active, reactive, apparent); power factor (true, displacement); energy (W-hrs, VA-hrs, var-hrs); demand (current, active power, apparent power, reactive power), predicted demand, peak demand (daily, weekly, monthly). It is a high-precision power quality and energy analyser with an impressive RMS accuracy of ± 0.1 % of reading ± 0.05 % of full-scale over 15 KHz bandwidth. ± 0.1 % of Reading for V > 60 Vrms, RMS Variations Accuracy: ± 0.2 % of reading (rdg). Transient Input Range: 50 - 2000 Vpeak Transient Accuracy: ± 10 % of rdg, ± 0.5 % Full Scale for Pulse widths > 10 μS. Frequency accuracy: ± 10 mHz of rdg. The recommended calibration interval for this unit is once every 12 months (Tiffany Sue Burgess, 2015).

b) Pyranometer/Irradiance sensor

A pyranometer is a solar irradiance sensor that measures solar radiation flux density (W/m^2) on a planar surface. It provides high-quality data for feasibility studies and monitoring the photovoltaic performance of established solar projects. This work uses a SPLite2 silicon pyranometer for solar radiation measurement. It creates a voltage output proportional to the incoming radiation that is done by a photodiode detector. It is uniquely designed so that its sensitivity is proportional to the cosine of the incoming radiation's angle of incidence, hence accurate and consistent measurements. The accuracy of the bubble level is less than 0.2°.

c) Temperature sensors

For temperature measurements, the SDL400 light meter or datalogger was used. It records data on an SD card in Excel format. The maximum range it can record is 10,000 Fc or 100 kLux. This was the limitation of the instruments as it was clipping the measurements above the maximum range. It utilizes a precision silicon photo diode and spectral response filter. Offset adjustment is used for zero function to make relative measurements adjustable data sampling rate. The meter can store 99 readings manually and 20 million readings via a 2 Gigabyte SD card. Table 3-4 shows details of the meter specifications, ranges, resolution, and accuracy.

Table 3-4: *Specifications, ranges, resolution, and basic accuracy of temperature sensor SDL400 light meter*

Specifications	Range	Resolution	Basic Accuracy
Fc Range	200, 2000, 10 kFc	0.1 Fc	± 4 %rdg
Lux Range	2000, 20 k, 100 kLux	1 Lux	± 4 %rdg
Type K Temperature	-148 to 2372°F (-100 to 1300°C)	0.1°	± (0.4 % +1.8°F/1°C)
Type J Temperature	-148 to 2192°F (-100 to 1200°C)	0.1°	± (0.4 % + 1.8°F/1°C)

d) Measurement setup

The microgrids taken as case studies are equipped with display, datalogger, monitoring and communication functionality. It has an Xtender system and a Remote control and programming unit (RCC) for configuration, display, and data logging. The remote control RCC-02/-03 offers a function that allows the system to record many electrical values over a long time. With this function, you can, for instance, follow the energy consumption and the battery voltage or see the power cuts, the state of the auxiliary relays, the input currents and voltages, the output powers, etc. The above configuration records all PV, battery, inverter, and load data. The data logging is done on the SD card at a 1-minute resolution.

Irradiation data was recorded at the site using an irradiation sensor (pyranometer) with a resolution of 10 seconds. The irradiation measured is the in-plane global irradiance since the pyranometer is placed on the module plane.

A temperature sensor was installed to record the panel's temperature (Figure 3-7). MAVOWATT 270® power quality analyser was also installed to measure different power quality parameters of the microgrid (Figure 3-8).

Figure 3-7: *The solar irradiance and temperature sensors installed on the plane of the module in the Mpale microgrid (Inclination of 10^{o} facing North-South direction)*

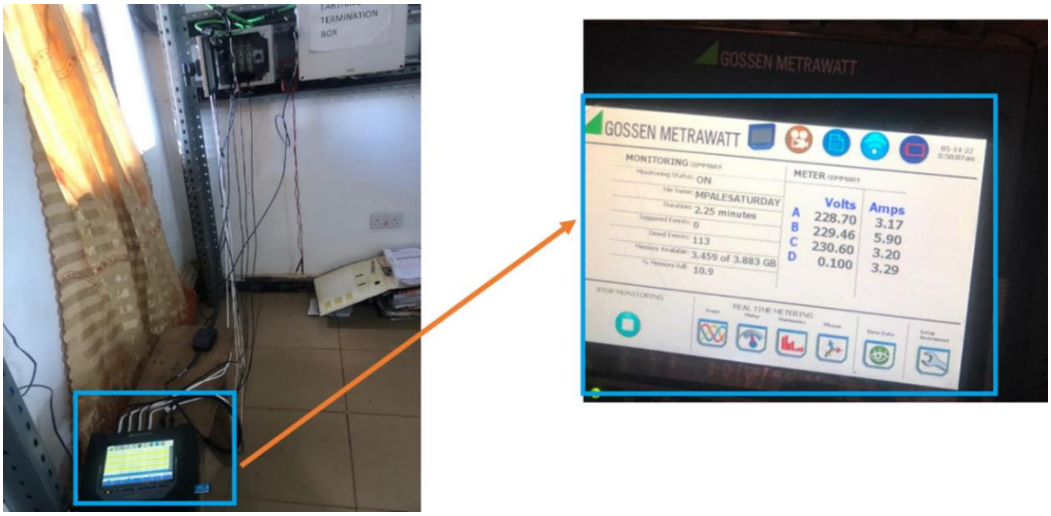

Figure 3-8: *Power Quality measurement and recording setup using MAVOWATT 270 Power Quality analyser in Mpale microgrid*

e) Measurement Setup: Lwak microgrid

Lwak microgrid comprises three convent houses and a chapel. Since measurements were taken on cooling appliances, only the chapel houses were prioritised as the chapel does not have cooling appliances. Houses Bethany and Postulants have two chest freezers and one fridge freezer. House Emmaus has one chest freezer and one fridge-freezer.

Apparatus and platforms used for measurement employed the Internet of Things (IoT), which was used to achieve temperature control for fridges and freezers and intelligent automation. This work uses a comprehensive technology stack to create a control and

monitoring system. Figure 3-10 presents an overall set-up of the IoT communication used in the Lwak microgrid.

i. **Docker** serves as our containerization platform, ensuring consistent deployment across various environments. It uses containerization technology to package an application and its dependencies into a standardized unit called a "container."

ii. **Node-RED** is a flow-based development platform which provides a user-friendly interface for creating automation flows. Leveraging its visual programming capabilities on an IoT lies in the users' ability to utilize its flow editor without extensive coding. Node-RED facilitates intuitive flow-based development, enhancing the efficiency of the system's design. It also supports MQTT and is commonly used in IoT applications for device-to-device communication.

iii. **MQTT, or Message Queuing Telemetry Transport,** is a server that receives and routes messages to the desired clients. It was employed for seamless communication. MQTT serves as a lightweight messaging protocol to facilitate communication between devices. It works as a publish-subscribe messaging protocol for the IoT, where Publishers send messages (publish) to specific topics, and subscribers receive messages from topics of interest. **Mosquitto,** as the MQTT broker, enables real-time data exchange and collaboration between components. The primary function of Eclipse Mosquitto is to facilitate communication between publishers and subscribers, essentially serving as a communication channel. MQTT enabled communication and data recording between shelly devices. A flow was created which receives MQTT messages from a Shelly device, processes the message, and sends control messages back to the device using MQTT.

iv. **The influxDB** database stores time-series data generated over time, offering optimal efficiency for the project's requirements.

v. The study utilized **Grafana** to visualise data, providing insightful dashboards and analytics. The synergy of Docker, Node-RED, MQTT, Mosquitto, InfluxDB, and Grafana forms the system's backbone, ensuring a cohesive and efficient architecture for the intended application.

vi. **Shelly Devices** known for their compact design and versatility, offer seamless integration with household appliances. By incorporating Shelly temperature sensors and smart switches into the fridge ecosystem, users gain real-time insights into

internal temperatures and the ability to control the appliance remotely. Implementation Steps

- Shelly smart sockets, together with their temperature sensor add-ons, were installed. Shelly temperature sensors were placed inside the fridge, connecting smart switches to control power.
- Node-RED Installation was done on a Raspberry Pi 4 as part of other docker elements like influxDB, graphana and mosquito.
- Node-RED Configuration: a flow within Node-RED was designed to monitor temperature data from shelly smart sockets (shelly plus 1 pm) Shelly sensors. The node-red flows are shown in the figure.
- Temperature Thresholds: Upper and lower temperature thresholds were defined according to the maximum and minimum temperatures a fridge or freezer is designed for. The specified temperature thresholds within the Node-RED flow aid in triggering actions.
- Automation Logic: an automatic control logic was created within Node-RED to switch OFF the fridge/freezer if it falls below the lower threshold temperatures and switch it back on when it exceeds the upper threshold.

This setup allows the development of a user interface within Node-RED or a separate application to enable users to customize temperature settings and view real-time data. Precise temperature control offers energy efficiency by ensuring optimal energy consumption, contributing to overall household energy efficiency. Users can remotely monitor and adjust fridge temperatures, providing flexibility and convenience. Also, customization allows users to set personalized temperature thresholds that align with specific storage needs.

By combining the capabilities of Shelly devices and Node-RED, this approach empowers users to take control of their fridge's temperature dynamics, fostering a more energy-efficient and tailored approach to appliance management.

The cooling appliances had 16 A, 110-240V AC smart sockets (shelly plus 1PMs) for power consumption measurement, monitoring, and control (Figure 3-9). The smart sockets can connect directly with temperature and humidity sensors, thus giving the advantage of monitoring other parameters simultaneously. Despite having several temperature and humidity add-ons, this study used a temperature sensor DS18B20 to monitor/measure the fridge/freezer's internal temperature.

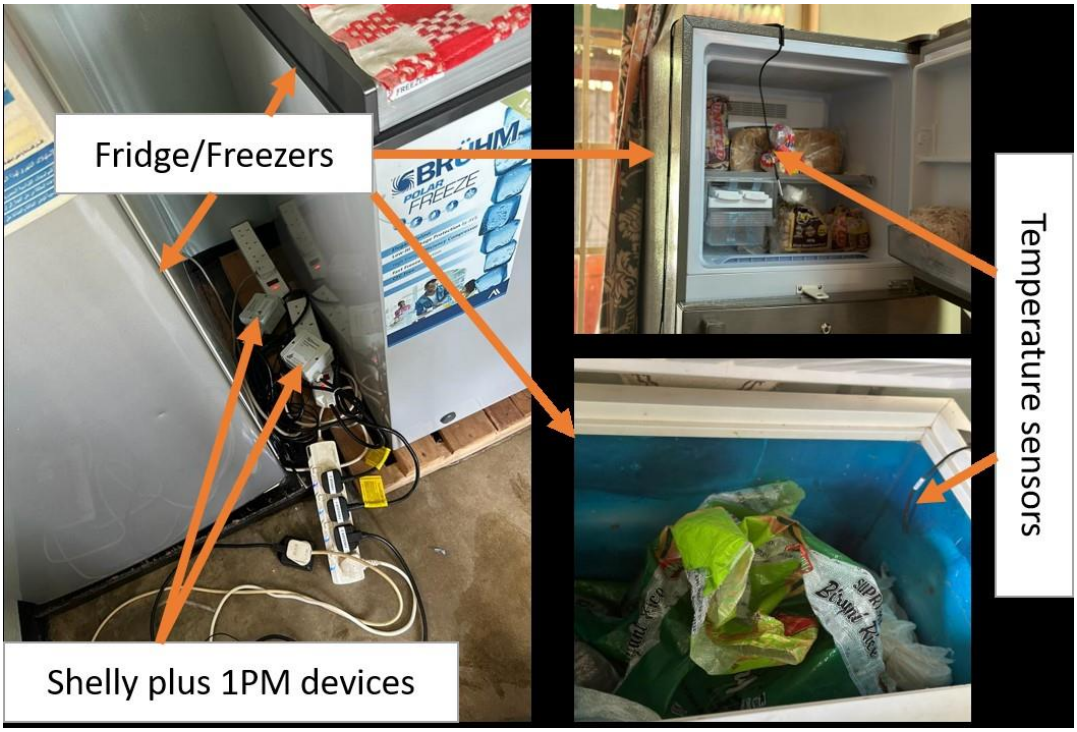

Figure 3-9: *Measurement setup for demand and temperature measurement at Lwak microgrid*

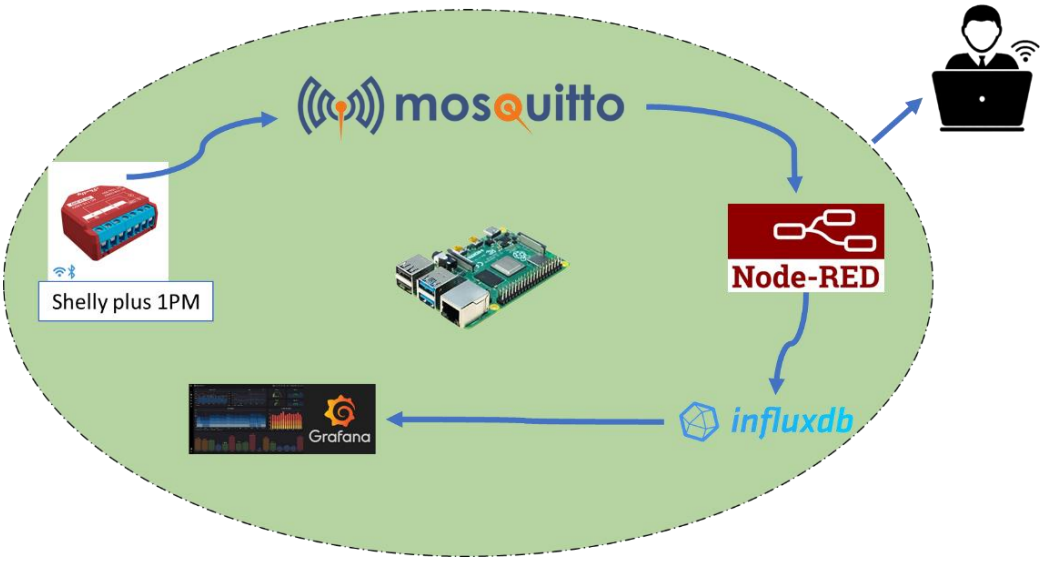

Figure 3-10: *Setup of the Internet of Things (IoT) communication system for data capturing, monitoring and control at Lwak microgrid*

A local network connection is essential for efficient communication in the IoT setup. Shelly devices, typically IoT devices, are designed for home automation and connect to local networks via Wi-Fi or Ethernet. The devices are then communicated with a router that acts as an internet gateway. Node-RED, a flow-based development tool, is often deployed on a local server within the network. It is an intermediary between the Shelly devices and

external services or applications. The local network connection facilitates seamless data exchange between these components, ensuring low latency, enhanced security, and reliable communication. Users can efficiently control and automate their Shelly devices by leveraging the local network. Figure 3-11 shows the overall local network for the setup at Lwak.

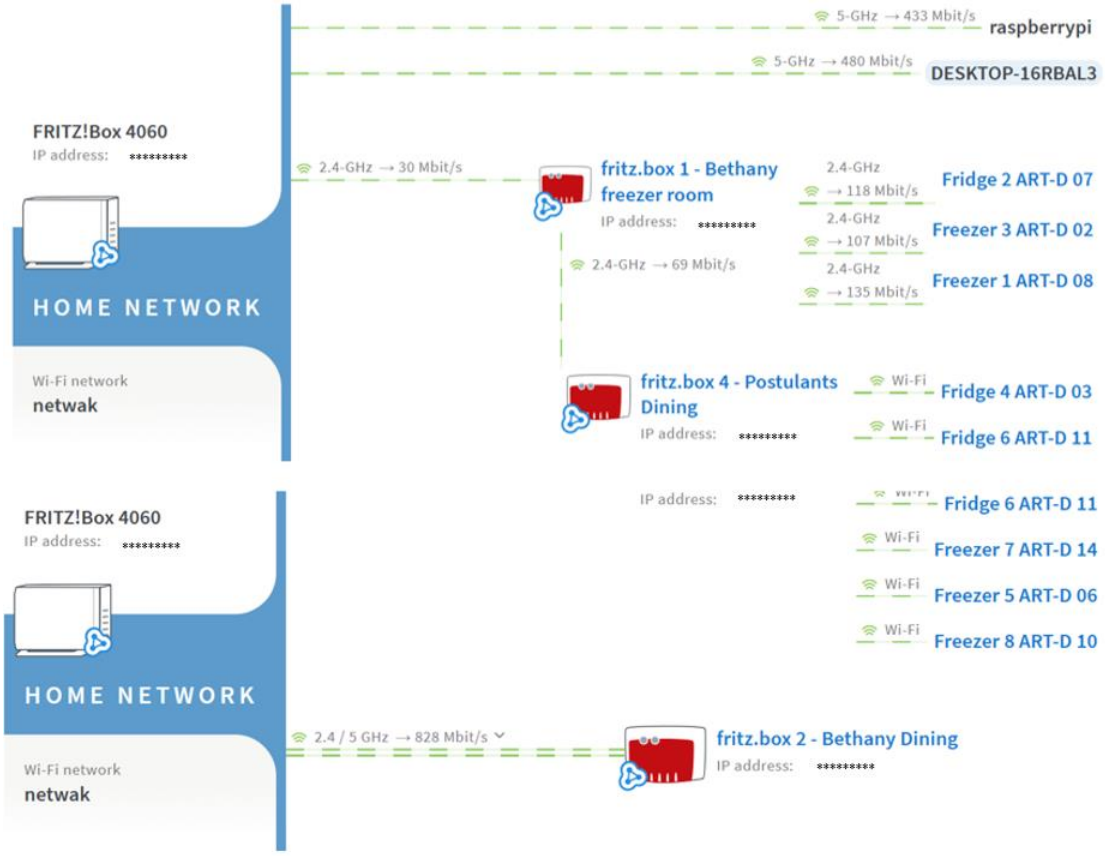

Figure 3-11: *Overall local network connecting routers and smart sockets placed at the cooling appliances at Lwak microgrid for data acquisition and control Lwak microgrid*

3.2.3. Data Pre-processing and Management

There is a high possibility of missing essential demand data from the measured data due to measurement, sensing errors, and communication failures. Predicting and reconstructing the data requires investigating correlation models among estimated data to recover the missing data. Generally, investigation of the correlation between different data, for example, voltage and power for houses connected to the same transformer, individual homes' voltage and frequency, and spatial and temporal power consumption for different places, proved effective in reconstructing and predicting missing and future data, respectively. Predicting future data is essential for real-time control and management (Huang & Zhu, 2016).

The usage pattern of all the connected customers in the microgrids will be identified to assess the current load profile of microgrids and their generation capacity. The household questionnaire analysis and field power measurement will determine the customer load characteristics. The effect of seasons, temperature and other demographic factors on customer power consumption will be investigated. The critical electric appliances, their usage period and seasonality will be identified. Customers will be grouped according to their usage from the meter data.

Both long-term and short-term load behaviour must be understood to design a financially stable microgrid. Long-term behaviour influences capacity expansion strategies, and short-term behaviour affects technology implementation and choice of energy sources. Figure 3-12 explains the step-by-step process of achieving load profile analysis.

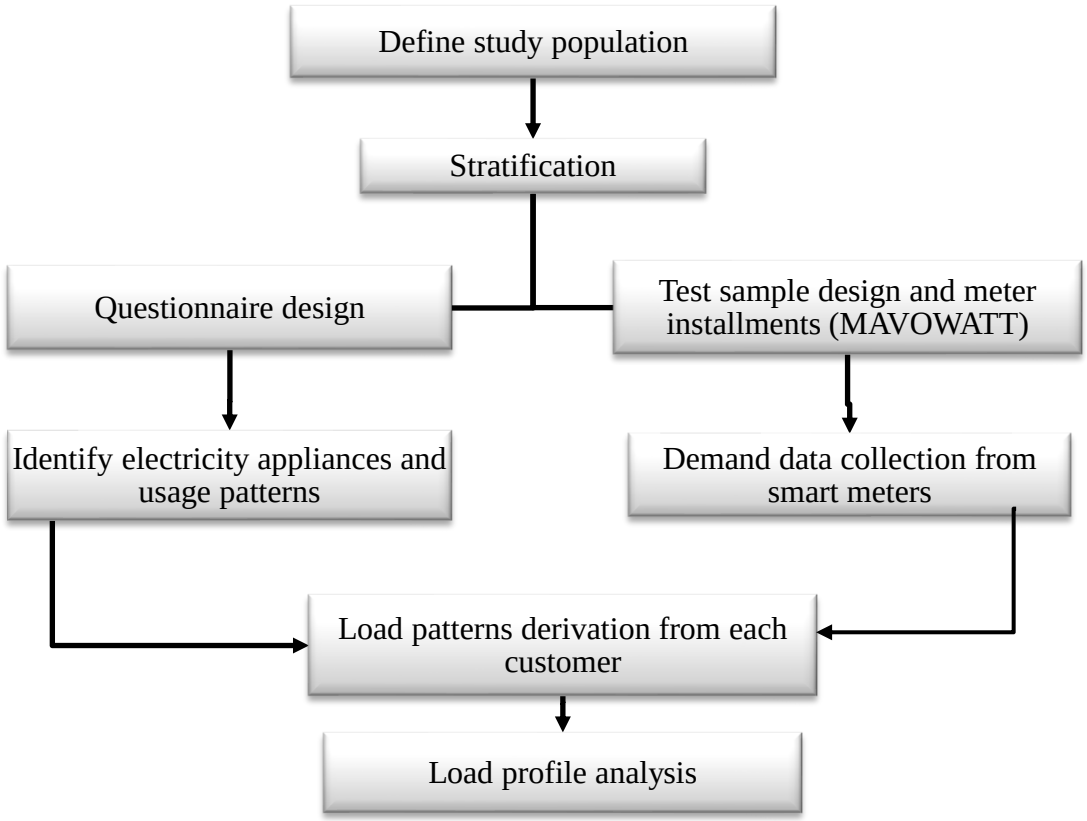

Figure 3-12: *Step-by-step process in achieving load profile analysis (Huang & Zhu, 2016)*

3.3. Technical Data Analysis

Technical data analysis presents the secondary data collected in Mpale, Bunjako, and Lwak microgrids prior to modelling and simulation.

3.3.1. Mpale Microgrid Data

3.3.1.1. Weather Data

Figure 3-13 shows the graph of measured global solar irradiance in the plane of modules from 10th May 2022 to 12th December 2022. The data were measured at intervals of 10 seconds. The measurements show that the maximum possible irradiance during that time interval is 1464.8 W/m^{2,} and the minimum is -0.4 W/m^2 with an average of 165.89 W/m^2. The irradiance values of the location show excellent potential for solar power production since the maximum is even more than the standard 1000 W/m^2. Table 3-5 shows that 25% of the data falls below 0.2 W/m^2, 50% falls below 2.5 W/m^2, and 75% falls below 237 W/m^2. The vast difference between the 25th and 75th percentile shows considerable variability in irradiance data, as shown in Figure 3-13.

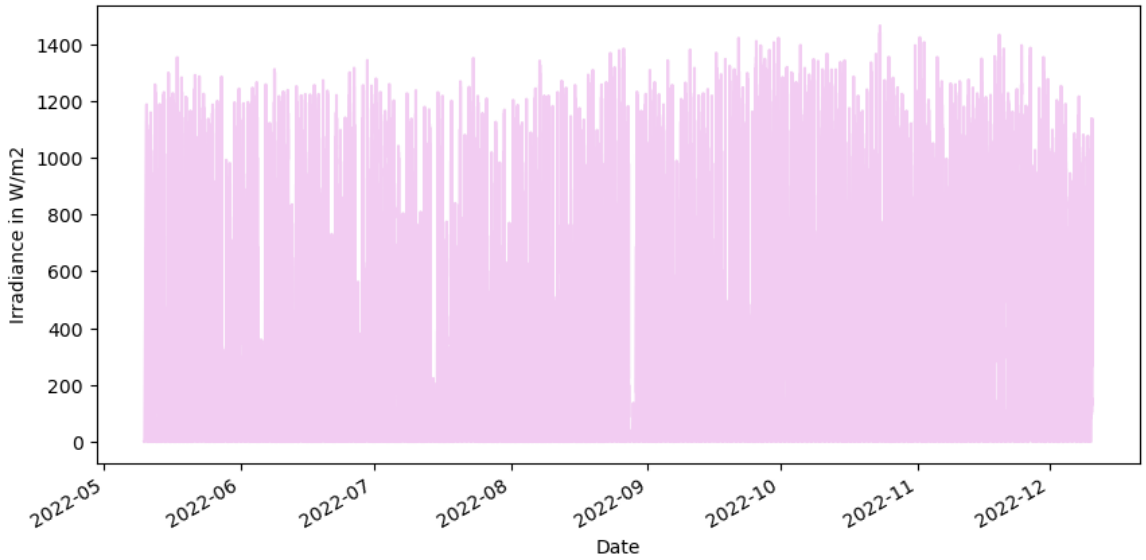

Figure 3-13: *Daily global solar irradiance in the plane of modules from 10th May 2022 to 12th December 2022 (measured by a calibrated pyranometer)*

Table 3-5: *Statistical summary of the measured irradiance data from 10th May 2022 to 12th December 2022*

Parameter	Irradiance quantity (W/m^2)
Count	$1.84\times10^{+6}$
Mean	166
Standard deviation	273
Minimum	0.0
25% (1st Quartile)	0.2
50% (2nd Quartile)	2.8

Parameter	Irradiance quantity (W/m^2)
75% (3rd Quartile)	238
Maximum	1460

Figure 3-14 shows a plot of hourly global solar irradiance with a dotted line representing the mean. The irradiance values peak around noon due to the fact that at solar noon, the sun is at its highest point, giving more direct sunlight on the surface of the earth and, hence, maximizing the solar irradiance received. There are lower irradiance values in the morning and evening hours since the sun's angle decreases, leading to a longer path for the sunlight to travel in the atmosphere. Figure 3-15 shows the same measured daily solar irradiance with a confidence interval band to convey the estimated value, in this case, the mean, and the level of uncertainty associated with it to understand the reliability of the data. The confidence band is narrow, indicating a more precise estimate.

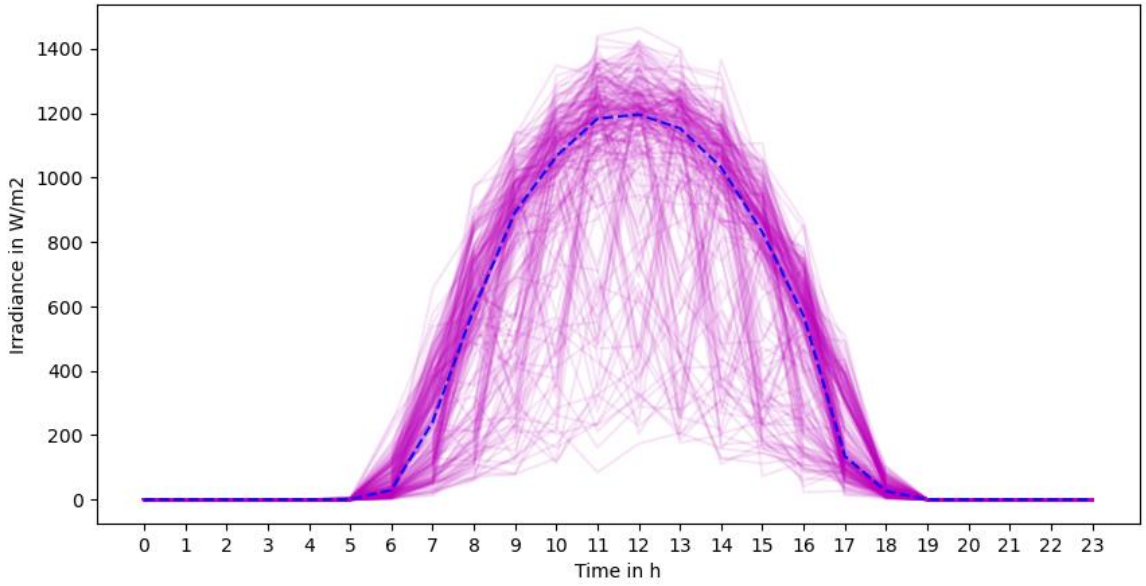

Figure 3-14: *Hourly global solar irradiance in the plane of modules from 10th May 2022 to 12th December 2022 (measured by a calibrated pyranometer with their mean representation in blue colour)*

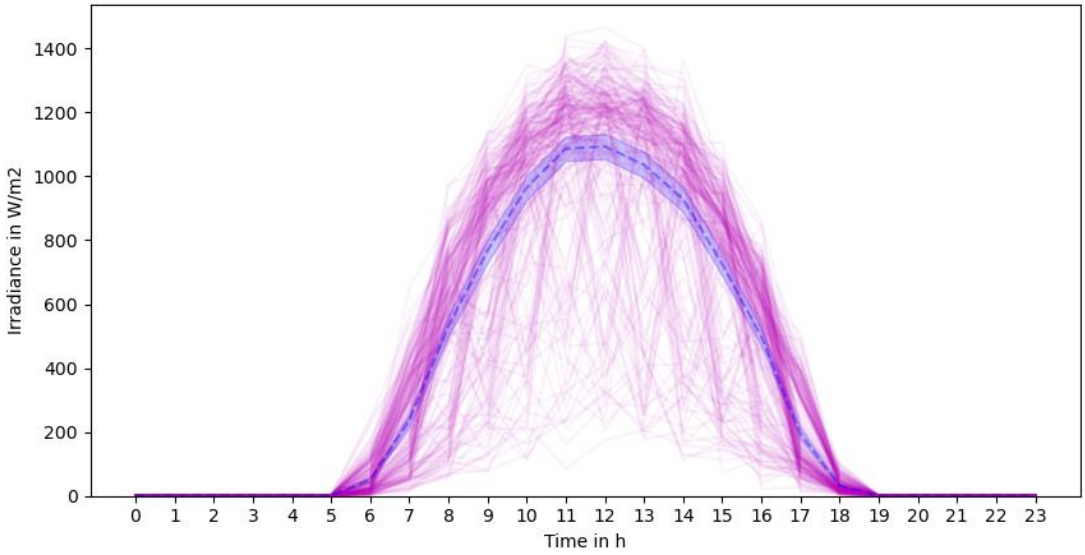

Figure 3-15: *Hourly global solar irradiance in the plane of modules from 10th May 2022 to 12th December 2022 (measured by a calibrated pyranometer with a 95% confidence band with dashed lines representing the mean values)*

Figure 3-16 and Figure 3-17 show the daily irradiance profile of the location as downloaded from the NASA website. The data trend looks similar, however, there are some differences which might be due to measurements location since the satellite data from NASA are based on satellite observations rather than ground-based measurements. Usually, the data derived from various NASA satellite missions are combined with weather models to provide global coverage and comprehensive datasets. Also, the location matters since on-site measurement might differ from satellite measurement as on-site measurements capture the temporal variabilities that are present. Resolution of measurement could be another reason.

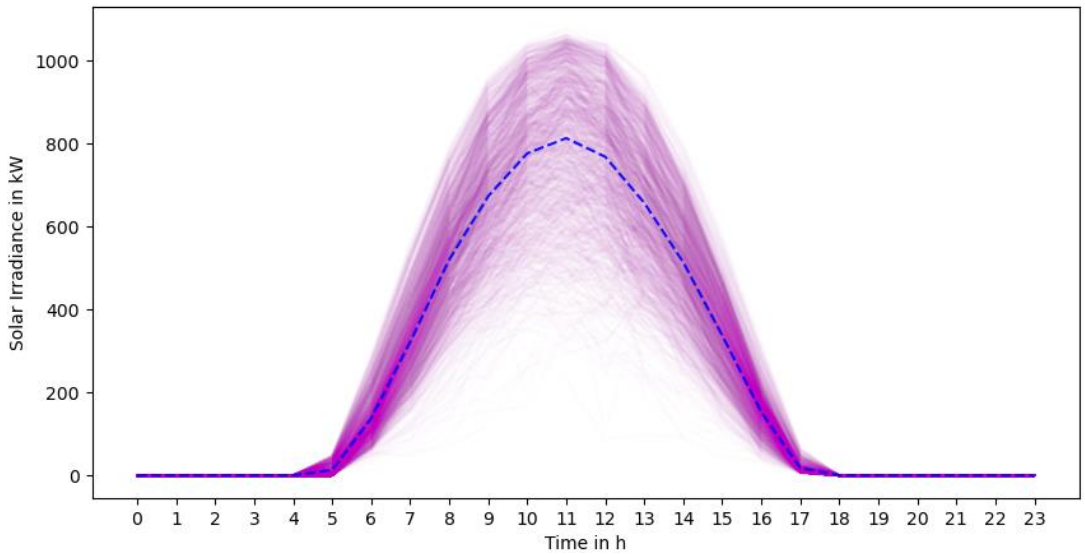

Figure 3-16: *Hourly global solar irradiance NASA satellite data from 10 May 2022 to 12 December 2022 with mean representation in blue colour (NASA, 2023)*

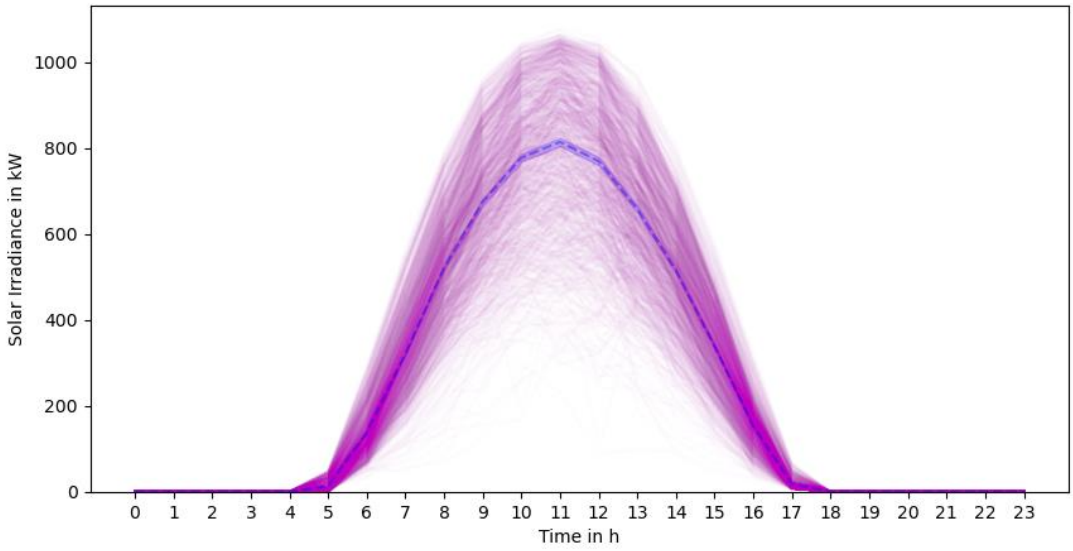

Figure 3-17: *Hourly global solar irradiance NASA satellite data from 10 May 2022 to 12 December 2022 with a 95% confidence band (NASA, 2023)*

Load demand relates to weather data such as temperature, wind speed, relative humidity, and cloud cover. These factors are vital in load forecasting and management. Temperature and relative humidity primarily affect demand during moderate weather. Load demand varies non-linearly with temperature, so load demand increases as the temperature reaches extreme points (high/low) (Aboul-Magd & Ahmed, 2001). Figure 3-18 compares irradiance data measured with a pyranometer and NASA satellite data from the 10th of May 2022 to the 12th of December 2022.

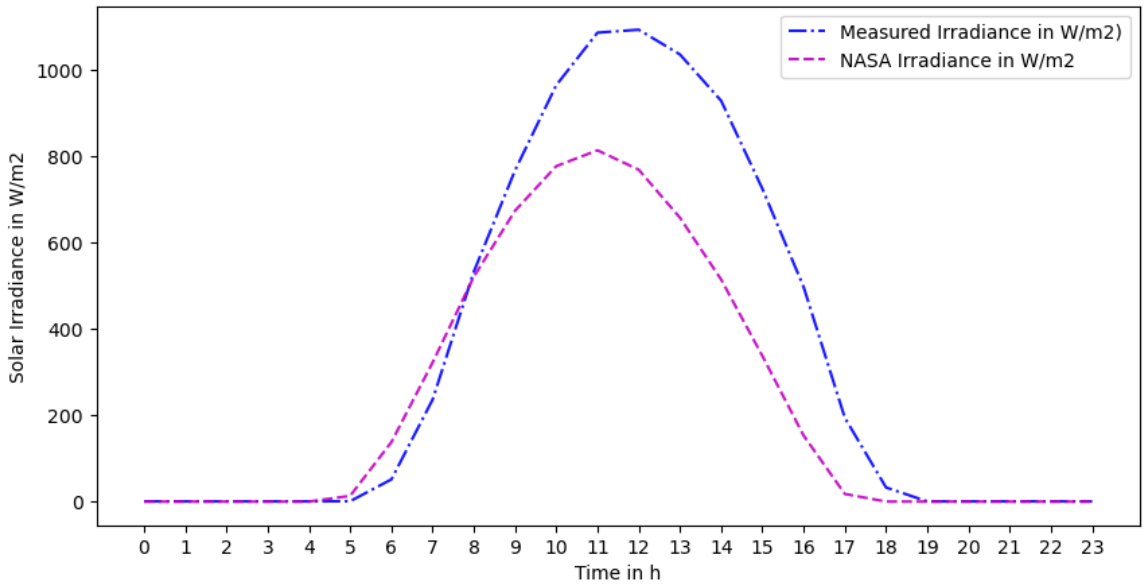

Figure 3-18: *Comparison between hourly average NASA satellite data and irradiance measured by a pyranometer from the 10th of May 2022 to the 12th of December 2022*

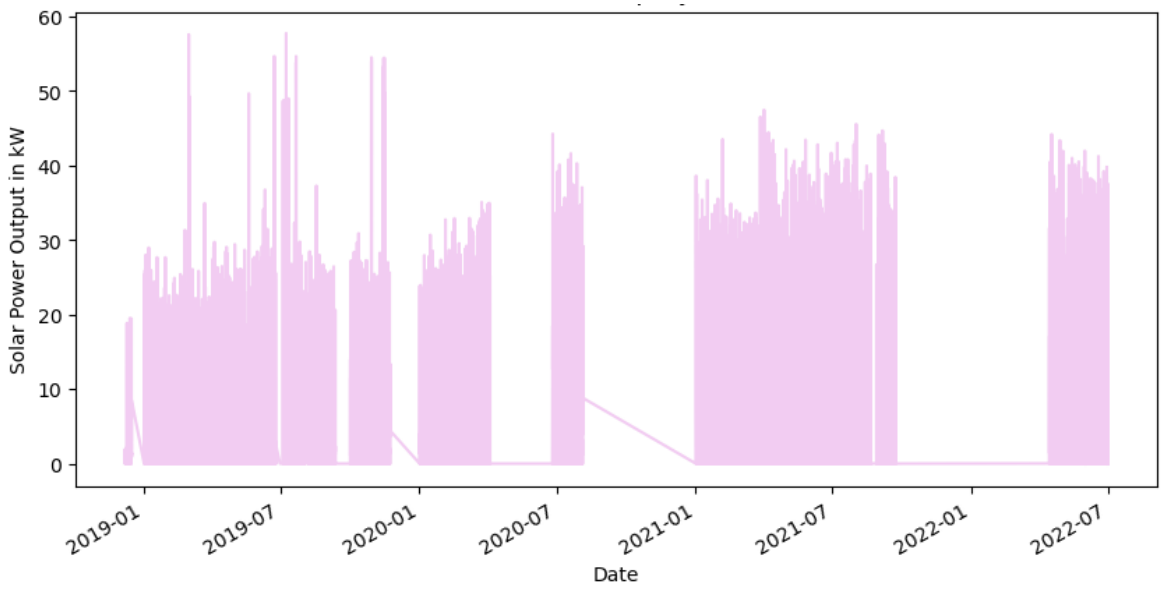

Figure 3-19: *Solar photovoltaic power output (kW) from January 2019 to July 2022 (measured and recorded by the solar system data manager in 1 – min intervals)*

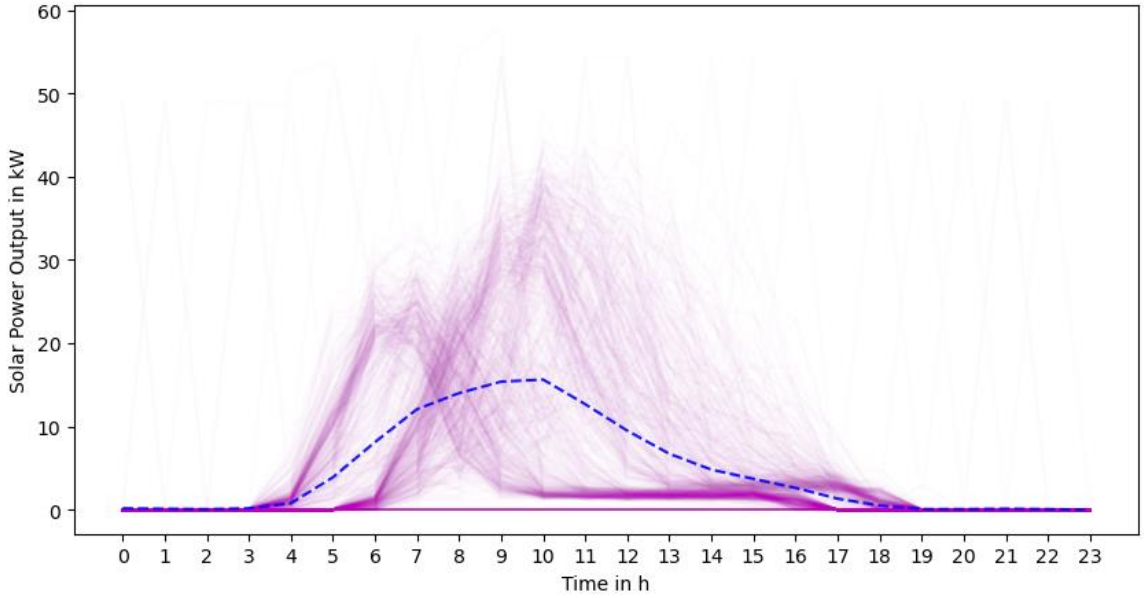

Figure 3-20: *Hourly solar photovoltaic power output (kW) from January 2019 to July 2022 sampled from the 1–minutes interval solar power output (with their mean representation in blue)*

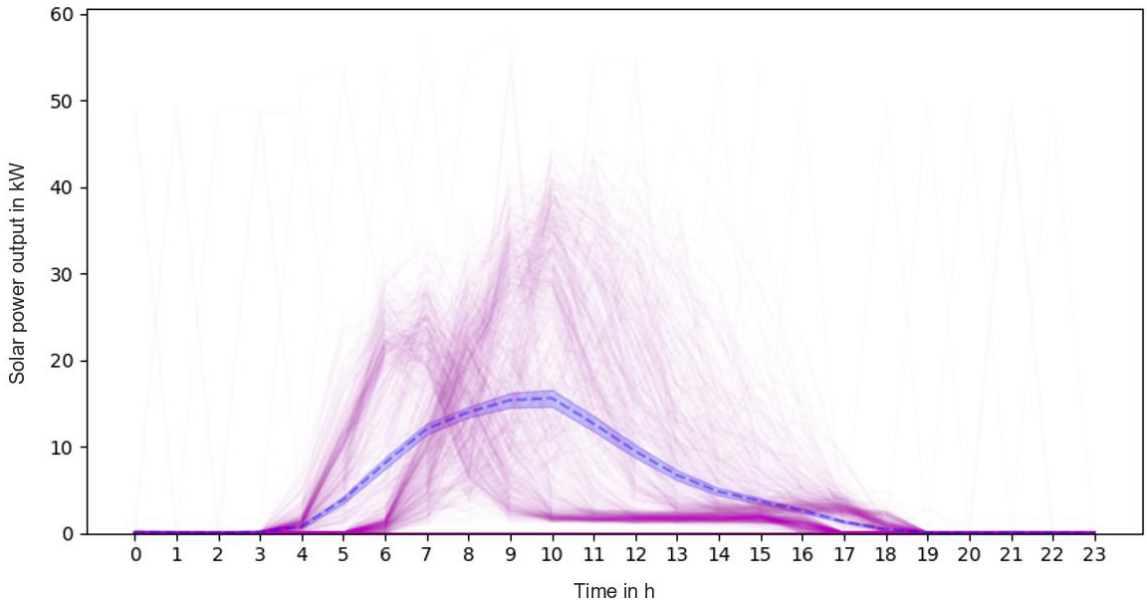

Figure 3-21: *Hourly solar photovoltaic power output (kW) from January 2019 to July 2022 sampled from the 1 – min interval solar power output (with 95% confidence band)*

Figure 3-19 shows the solar power output in kW measured from January 2019 to July 2022, while Figure 3-20 and Figure 3-21 show their sampled hourly solar power output without and with a confidence interval band, respectively. From Figure 3-20, the solar production of individual daily plots peaked at different times and values due to seasonal effects and the nature of the irradiation during the day. The maximum solar production on a typical day was around 11 am. The mean solar power output peaked at around 10 – 11 am, declining during waning hours and without irradiance.

Solar power output is calculated from the irradiation falling in a given square meter area, and its wattage value is provided by;

$$P_{PV} = A \times r \times I \times PR \qquad \textit{Eqn 3-1}$$

Where;

A = total area in meters squared of the solar panel (for Mpale microgrid area, the total area is 900 m^2),

r = percentage solar panel yield efficiency (i.e., 20.4%),

I = solar irradiance (in W/m^2), and

PR = performance ratio (0.75, default value) (Khalid et al., 2016).

The calculation compares expected and actual power generated from the analysis. Desired power is calculated using the actual irradiation falling on the panel on the basis that the solar panel converts all irradiation. Figure 3-22 shows the comparison between actual and

expected solar power generated. The actual solar power generated does not match the expected power attributed to solar panel efficiency, orientation, tracking system, and other weather-affecting parameters like temperature, wind, and cloud cover.

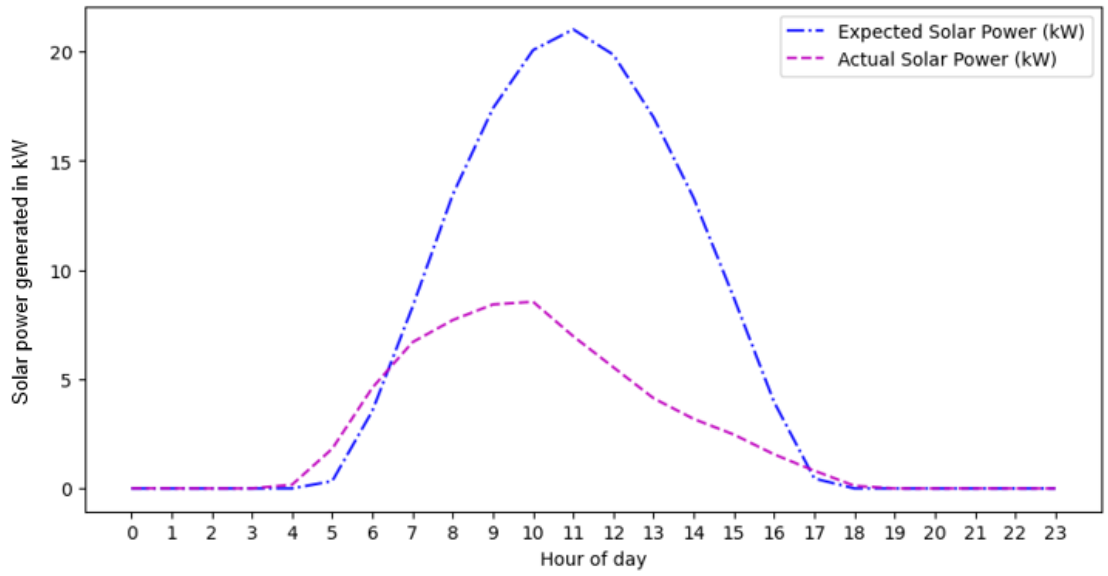

Figure 3-22: *Comparison between actual and expected average hourly solar photovoltaic power output (kW) from January 2019 to July 2022*

3.3.1.2. Historical Demand Data

Table 3-6: *Historical Demand Data for Mpale Microgrid over the five years showing their monthly mean, standard deviation, minimum and maximum values*

Solar Power Generated (kWh/m^2 per day)				
Months	**Mean**	**Minimum**	**Maximum**	**Standard deviation**
January	2.95	2.09	3.69	0.81
February	3.03	2.13	3.68	0.77
March	3.28	2.11	4.37	1.03
April	2.41	0.57	3.77	1.41
May	2.51	0.43	3.79	1.57
June	2.24	0.32	3.78	1.50
July	2.73	0.32	4.66	1.65
August	2.39	0.47	4.20	1.47
September	2.20	0.78	3.80	1.13
October	2.90	1.82	4.67	1.16
November	2.69	1.96	3.81	0.87
December	2.45	1.55	3.76	1.01

3.3.1.3. Yearly Solar Power Generation

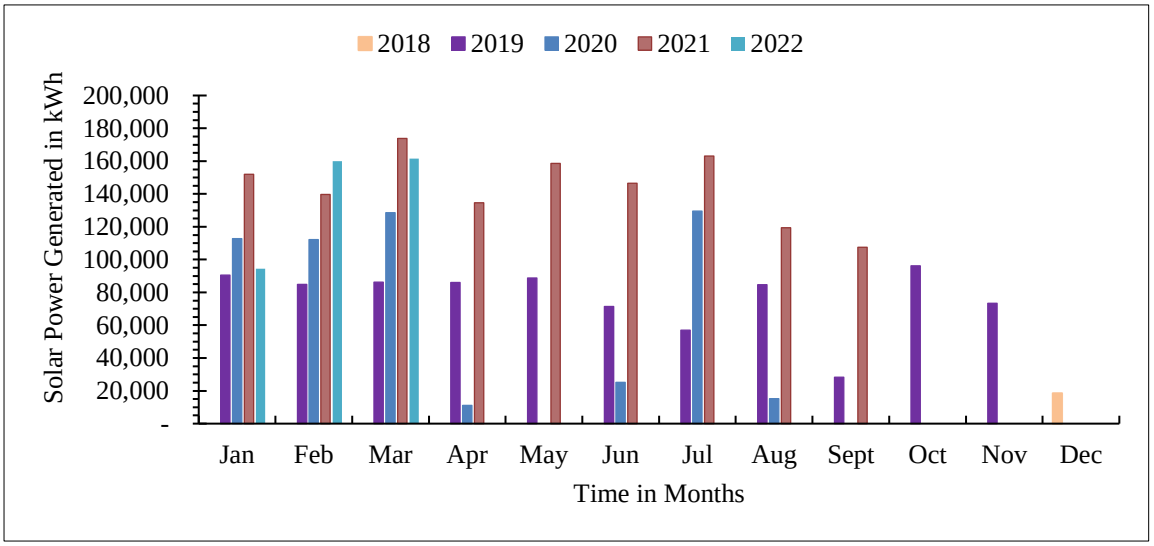

Figure 3-23: *Monthly solar power generated for five years with some months' data missing (2018 only December data, 2019: January -November 2020: January – August 2021: January – September 2022: January – March)*

Figure 3-23 shows the seasonal solar power produced from 2018 to 2022. An empty field means no data for such month in the respective year. Mpale microgrid experiences a rainy season from April to June, hence low power production. January to March is Tanga's hottest season, with the highest solar power production. They usually have spring seasons around September to December.

Figure 3-24 and Figure 3-25 show the cartesian and polar coordinates of the sun's position at Mpale village, respectively. The sun's position in a particular place is best described by its vertical angle (altitude) and horizontal angle (azimuth). These angles change throughout the day due to seasons and the earth's rotation. The azimuth angle, which indicates the sun's direction relative to the observer, is essential as it helps to know where solar panels should be positioned to receive maximum sunlight. For the Mpale location, with an azimuth angle of 71.02°, it suggests that the sun is slightly East of due North. The elevation angle (the angle between the horizon and the sun) measures or indicates how high the sun is in the sky. A higher elevation angle means the sun is more directly overhead; hence, solar panels should be placed to match that angle for optimal energy capture. An elevation angle of 41.44° observed at Mpale village signifies that the sun is relatively high in the sky, decreasing the sun's path through the atmosphere and allowing more direct sunlight to reach the solar panels with little scattering. Based on the angles, Mpale is a good location

for solar production if the panels are well placed to capture enough sunlight (slightly to the right of the north and with a tilt angle close to its latitude).

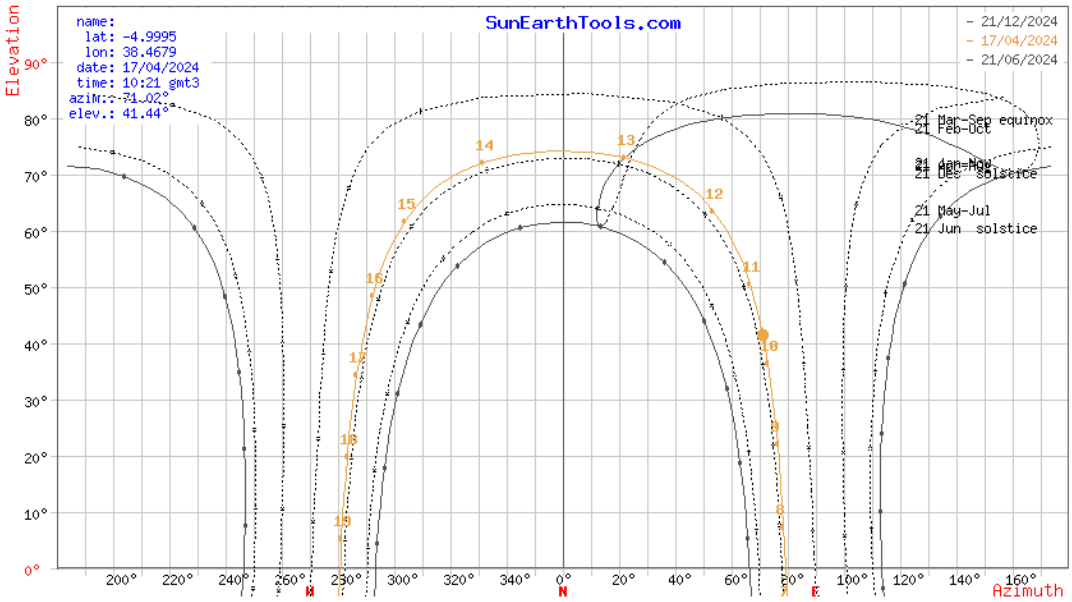

Figure 3-24: *Cartesian coordinate chart representation of the Sun's position over Mpale (-4.9995°, 38.4679) microgrid in Tanzania (SunEarthTools, 2023)*

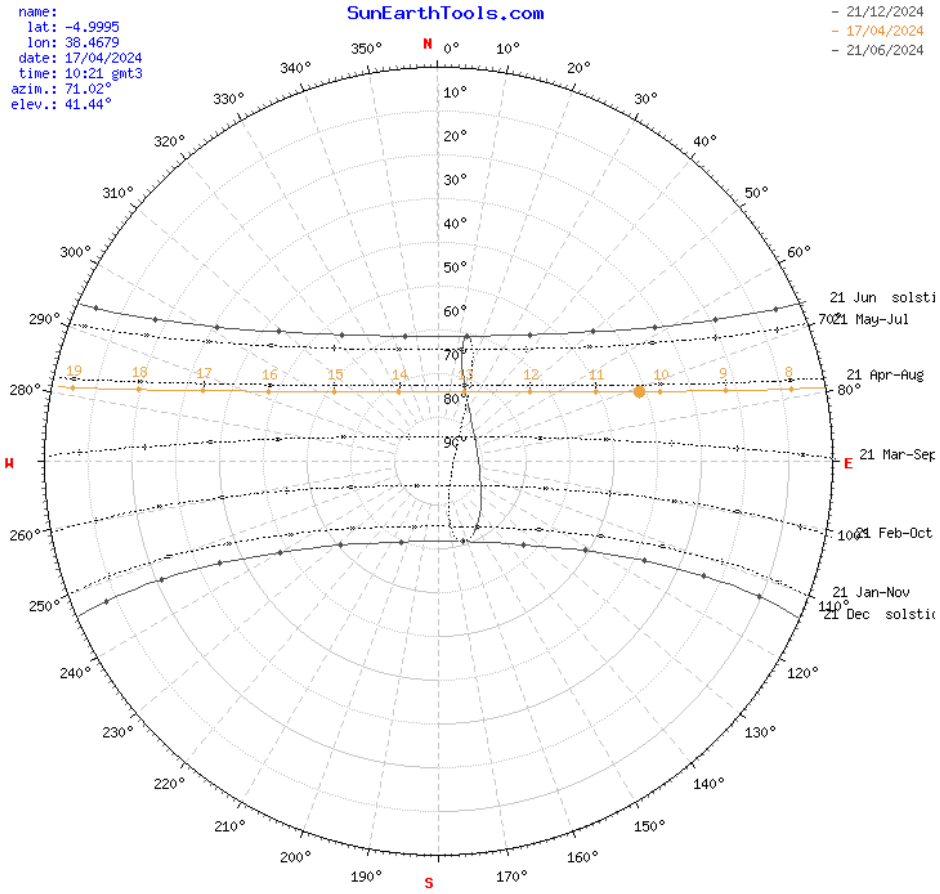

Figure 3-25: *Polar coordinate chart representation of the Sun's position over Mpale (-4.9995°, 38.4679) microgrid in Tanzania (SunEarthTools, 2023)*

Figure 3-26 shows the variation of irradiance values sampled at 10-minutes, 20-minutes, and 1-hour intervals, illustrating the irradiance trend expected at Mpale village. The differences between sampling rates are due to data resolution, averaging effect, and sampling frequency. The 20-minute and 1-hour intervals represent averages over long periods compared to the 10-minute interval, which provides a general view by smoothing the short-term variations.

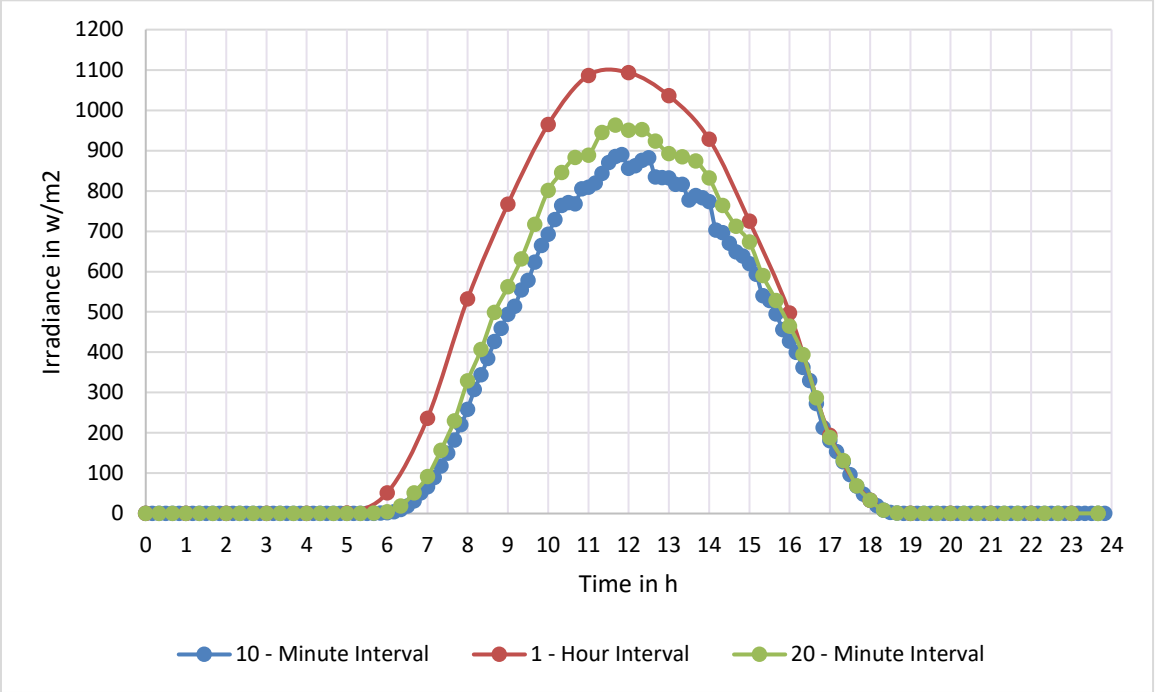

Figure 3-26: *Variations of minute and hourly mean values of global irradiance for the measured data at Mpale microgrid from 16th May 2022 to 16th December 2022*

3.3.1.4. Demand

The Mpale Microgrid system has four (4) inverters (two inverters share the load in phase two). From the type of data provided, as attached in the appendix, phase 2 is L2-2 plus L2-3. So, 1,2,3 are phases and 1,2,3,4 are inverters.

Figure 3-27 shows the average summation of total power consumed from 2018 to 2022. It is worth noting that the Mpale microgrid was constructed in 2016, commissioned in 2017, and data recording commenced in December 2018. It is clearly shown that there is a significant increase in energy usage each year. This can be attributed to buying new electrical appliances, new customers, and even starting new businesses due to electricity access. The increase will create significant demand in the future, so taking immediate measures to control the rise in demand is essential. This was validated by the survey

questionnaires, where the main load when the grid started was only lights and phones, but people kept adding more appliances.

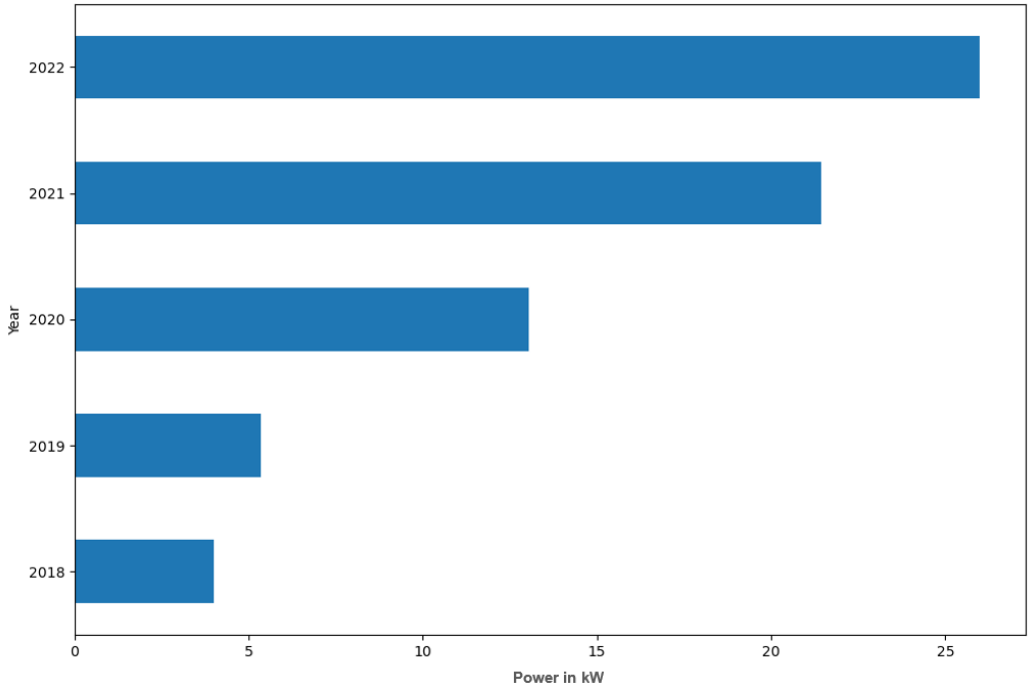

Figure 3-27: *Total average yearly electricity consumption for the years 2018-2022 at Mpale microgrid showing a trend of annual demand growth*

The four-year demand profile was prepared and sampled to a daily hourly profile (Figure 3-28). Peak load behaviour showed a typical load profile of households in the village with demands in the evening hours.

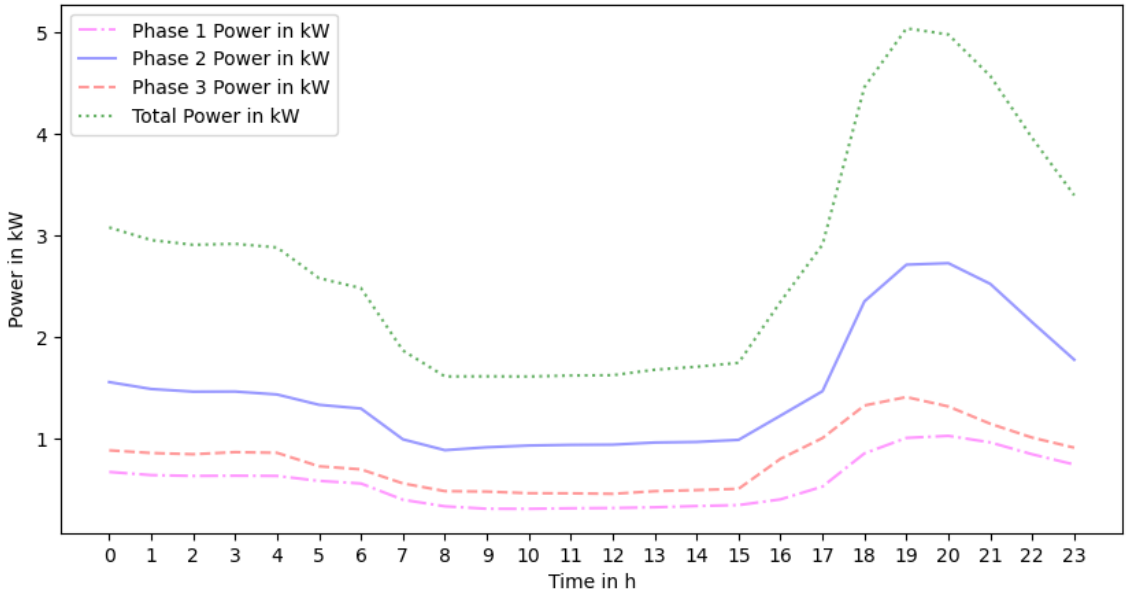

Figure 3-28: *Maximum power consumed in the three phases and their total power averaged from January 2019 to July 2022 sampled from the 1 – min interval power data*

The demand profile shows a spike in power consumption between 0500 and 0700, indicating that most inhabitants' activities were before work or school. Typically, from hours 7 to 18 on weekdays, less power was observed as inhabitants were involved in activities such as farming, which did not consume considerable power. From 1800 to 2200 hours, a spike in power consumption indicated that most inhabitants were back home performing activities that consume power, such as cooking and watching TV. The pie chart (Figure 3-29) represents the percentage of average power consumption for different days of the week, with Sunday being the highest in electric power consumption. The variations can be attributed to more people spending their time at home and using more power from staying at home**.**

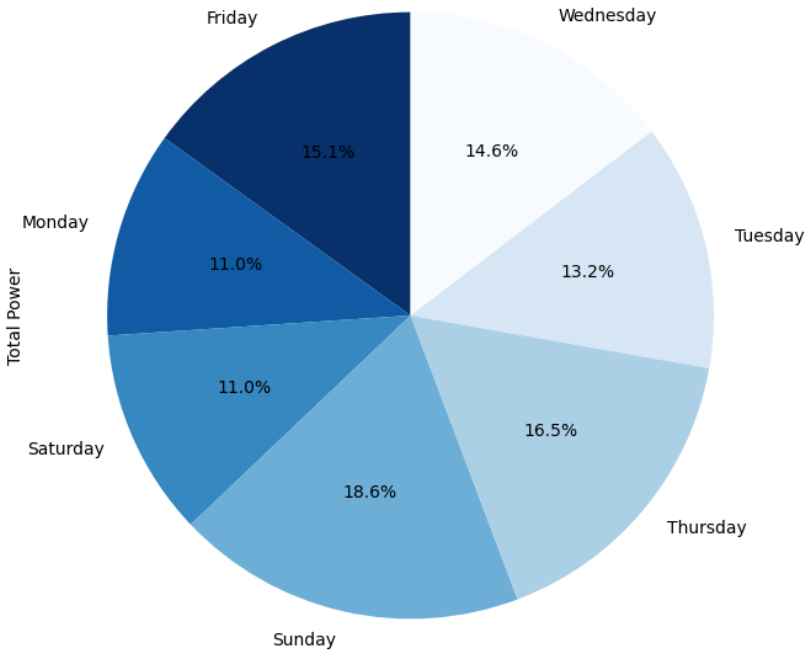

Figure 3-29: *Pie plot showing weekday and weekend demand of the percentage energy consumed at Mpale microgrid*

Figure 3-30 and Figure 3-31 show a plot of battery SOC and temperature. The plot shows that the battery SOC drops below 50% during morning hours due to higher power consumption. Also, the trend of decreasing SOC is observed in the evening hours. There is charging of the battery when the sun is available, meaning that at some point when there is not enough sunlight, batteries are not fully charged; hence, it brings us to the same importance of DSM. Also, Figure 3-31 shows the variation of battery temperature as the activity of the battery changes.

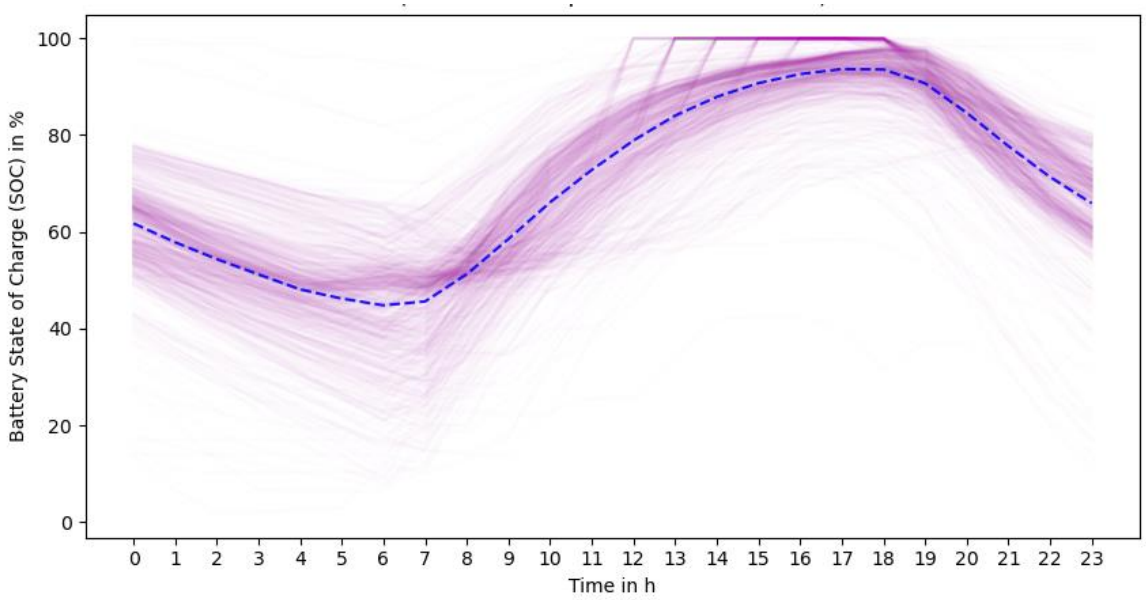

Figure 3-30: *Hourly Battery State of Charge (SOC) from January 2019 to July 2022 sampled from the 1–minutes interval battery state of charge data (with their mean representation in blue)*

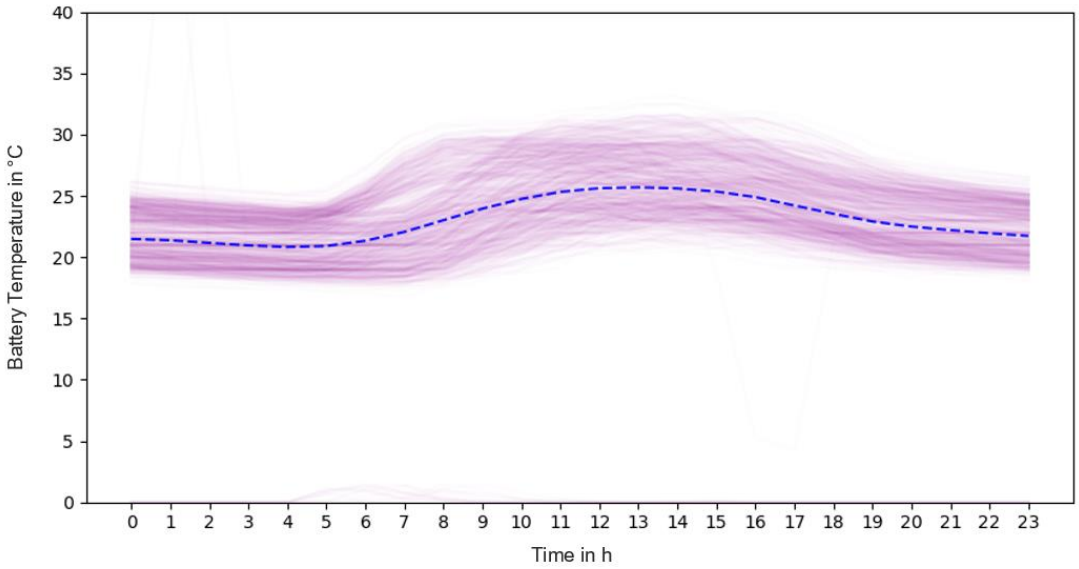

Figure 3-31: *Hourly Battery temperature from January 2019 to July 2022 sampled from the 1–minutes battery temperature data (with their mean representation in blue)*

Figure 3-32 shows the comparison of solar power produced and electricity usage. There is no proper correlation since people consume more when there is insufficient sunlight (morning and evening). Also, it should be noted that much power is wasted if it has already been used to charge the batteries. The idea of DSM through load shifting could make more sense in this way. Also, alternative storage, like electric vehicles, could help avoid power wastage.

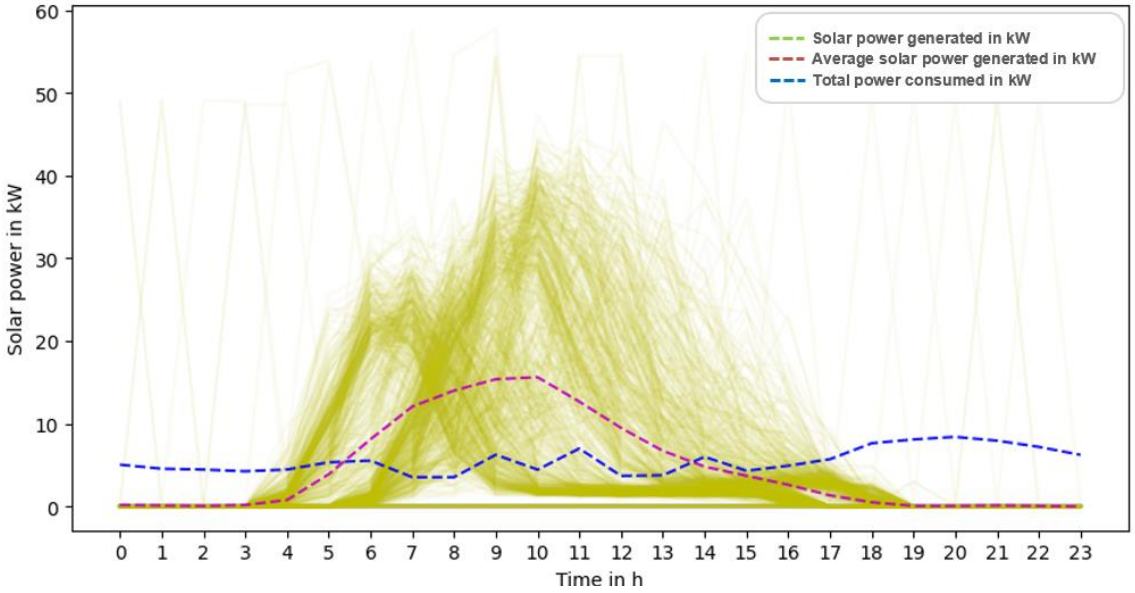

Figure 3-32: *Comparisons between average solar photovoltaic power generated and total energy consumed from January 2019 to July 2022 sampled from the 1–minutes solar power and demand data*

The generated solar power differs from the irradiation, possibly due to panel orientation, which prevents solar panels from capturing maximum sunlight. When solar panels are not correctly oriented, they can capture sunlight intensity earlier in the day than expected. Also, even a small amount of shading from nearby objects like buildings or trees could reduce solar output. Other reasons could be temperature effects and local weather patterns.

3.3.1.5. Power Quality results.

This section presents the power quality results measured by the MAVOWATT power quality analyser from 14/05/2022 to 12/06/2022. Figure 3-33 shows the voltage plots of the average and minimum rms values for the three phases. According to the Tanzania Bureau of Standards for Quality of Supply (TBS), voltage whose upper limit of nominal RMS value is 1 kV is termed as Low Voltage (LV), voltage ranging from 1 – 33 kV is medium voltage (MV), 33 – 220 kV is High Voltage (HV) and 33 – 400 kV Extra High Voltage (EHV) (Tanzania Bureau of Standards (TBS), 2011). This case study lies in the LV range. The standard AC voltage for customers supplied at LV shall be 400 V phase to phase and 230 V to neutral. However, it is observed that there are several voltage fluctuations and interruptions within the measurements, which will be further explained in the coming paragraphs. Reliability remains a serious concern with the poor access to electricity in most rural and urban areas in Sub-Saharan Africa. The system average interruption duration index (SAIDI) represents the average time (seconds) per year a customer's power is

interrupted (Paul et al., 2017). The SAIDI value for Nairobi in East Africa, viewed as standard reliability, is 216.3 hours (Muhihi & Paschal, 2022). According to the Tanzanian standard TZS 1374:201, the SAIDI value is supposed to be less than 650minutes (10.8 Hours) per customer per year; however, from 2012 to 2016, Tanzania had load-shedding of up to 20.3 hours; from June 2018 it had an unplanned outage of 1044 hours (Muhihi & Paschal, 2022). Reliability is crucial in electricity consumption for both productive and domestic use.

On 15 May 2022, a deviation from the standard voltage of 230 V was observed in phase A, as shown in Figure 3-33. Voltage swell refers to a sudden increase in voltage or simply overvoltage. The graphs show that the two phases, B and C, maintained the same voltage of 230 V, but phase A voltage increased to 266 V, which is almost 11.3% lower than the permissible voltage limit value of ±15% based on the TBS standards and the South African National Grid code (Eskom & Nersa, 2003). Also, on 28th May 2022, a voltage rise of almost 262.5 V was observed in phase A. Several factors are the reasons for voltage swell, including the sudden switching of large loads on or off could be the reason. Figure 3-34 shows the magnified phase A voltage rise to explain the event clearly.

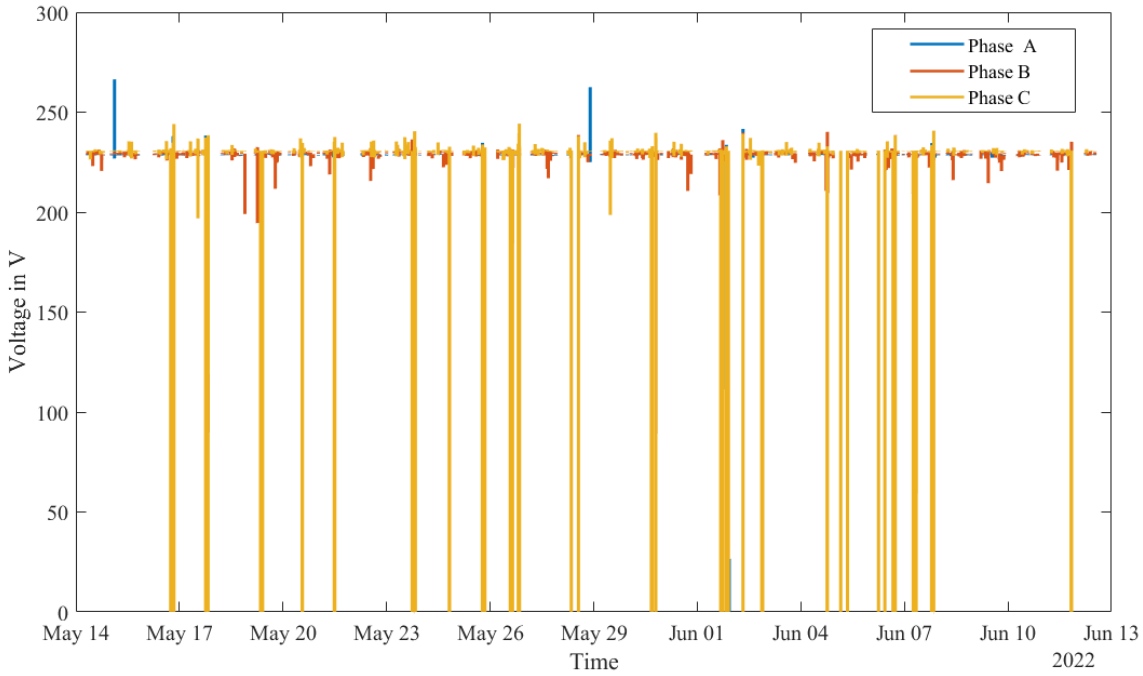

Figure 3-33: *MAVOWATT voltage plots for the three phases from 14th May 2022 to 12th June 2022*

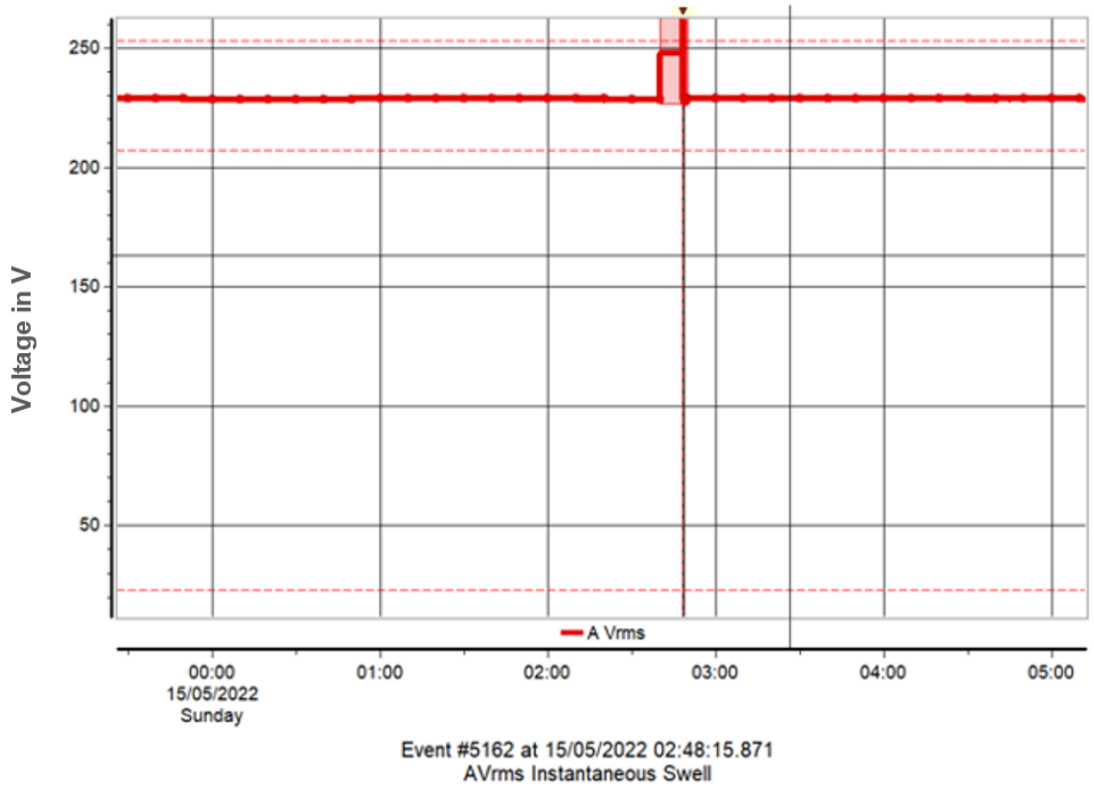

Figure 3-34: *The magnified voltage swell event observed on phase A on 15th May 2022 at 0248 hours*

When analysing voltage interruptions in the Mpale microgrid, Figure 3-35 shows the relationship between the total load profile and the voltage in the three phases. The observed pattern of interruptions, especially during evening hours, suggests potential challenges in maintaining a consistent and reliable power supply. These interruptions may stem from insufficient generation capacity, frequent equipment failures, or an overstrained grid during peak demand. Addressing these issues through enhanced capacity planning, infrastructure improvements, demand side management and proactive maintenance measures could significantly improve the microgrid's reliability and mitigate the impact of voltage interruptions on the community.

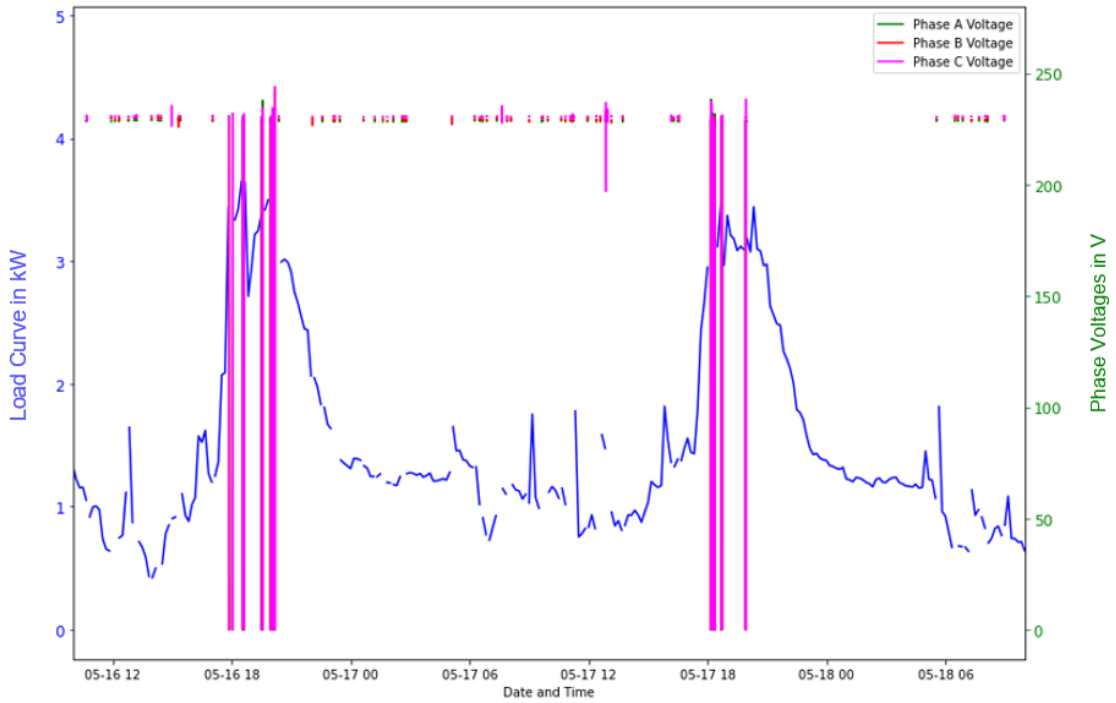

Figure 3-35: *Relationship between total load profile and voltage in the three phases from 14th May 2022 to 12th June 2022*

Harmonics or distortion in the waveforms was one of the other parameters measured. Figure 3-36 shows all the observed voltage harmonics in the time range of the measurements. They might have been caused by non-linear loads that draw non-linear currents in the system, introducing harmonics. Figure 3-37 shows the statistical distribution of the observed voltage and current harmonics in the three phases. For phases A and C, only 5% of the harmonic values are below 5 V and 1 A current, while most harmonics are between 15 and 20 V with a corresponding current of about 3.5 A. Phase B experiences the most harmonics values, with 5% reaching almost 7 V with 3.5 A and most harmonics being around 25 V and 9 A. According to the Tanzanian Bureau of Standards and the Kenyan Nation Distribution Grid Code, the THD of the supply voltage for the LV network shall not exceed 8% (ERPA, 2021; Tanzania Bureau of Standards (TBS), 2011). Phase B exceeded the set limit since it has almost 11% of the fundamental voltage, while phases A and C lie within the limit set.

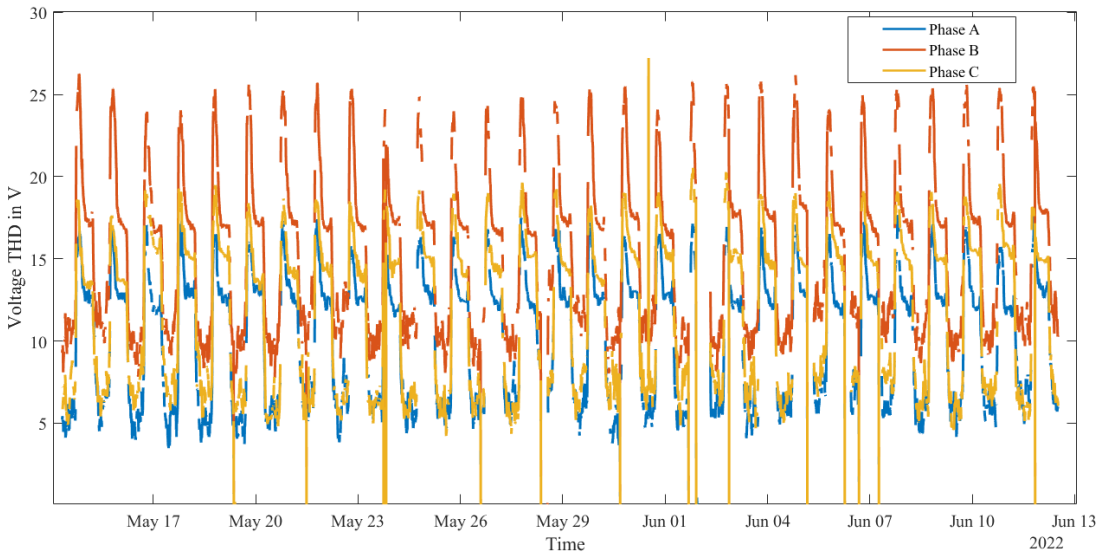

Figure 3-36: *Time plots for the voltage total harmonic distortion of the three phases measured from 14th May 2022 to 12th June 2022*

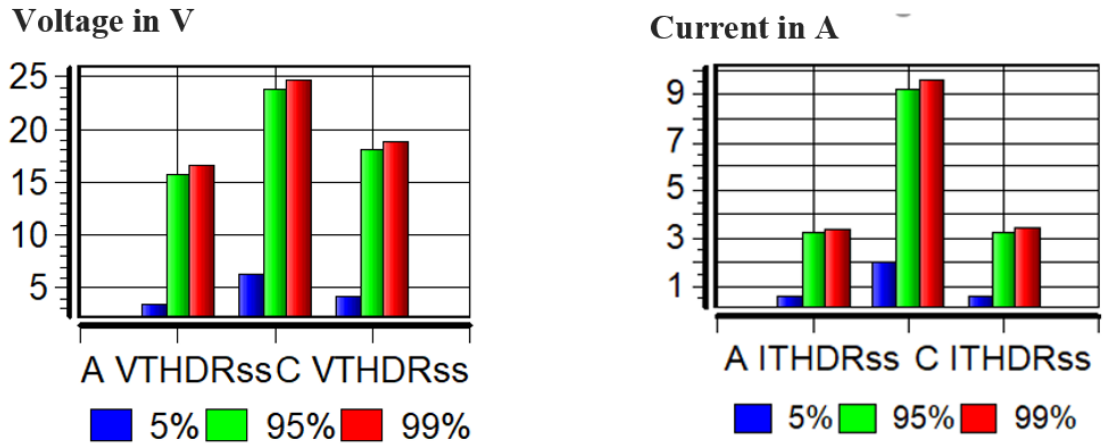

Figure 3-37: *Statistical distribution of the overall voltage and current harmonic distortion for the three phases from 14th May 2022 to 12th June 2022.*

Figure 3-38 and Figure 3-39 show a plot of the total frequency and total load curve with their respective zoomed versions to show the variations clearly. The observed variations provide valuable insights into the stability and performance of the microgrid. Significant fluctuations in frequency, especially during peak load periods, may indicate challenges in maintaining grid stability and proper frequency control. This could result from mismatches between generation and demand, insufficient grid inertia, or inadequate control mechanisms. According to the African national grid code, the allowable frequency limit for an islanded system is ± 5% (± 2,5 Hz) (Eskom & Nersa, 2003); however, for some of the periods, the limit is highly exceeded in this case.

Analysing the load curve with frequency variations helps identify periods of high demand and their impact on system stability. Implementing measures like demand-side management, energy storage, or optimizing generation capacity can contribute to a more stable frequency profile, enhancing the overall reliability of the microgrid.

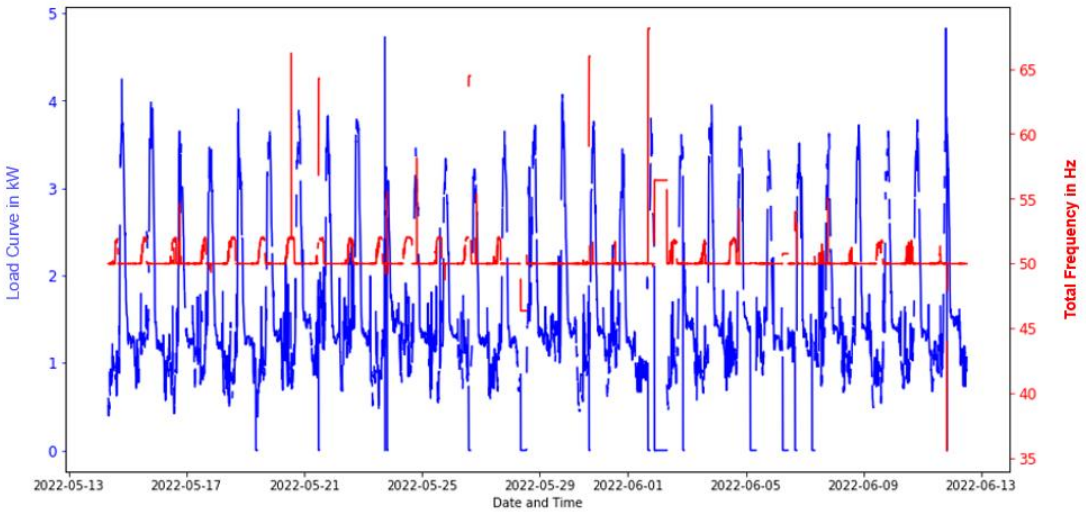

Figure 3-38: *A plot of total frequency versus total load curve for a period from 13 May 2022 to 12 June 2022*

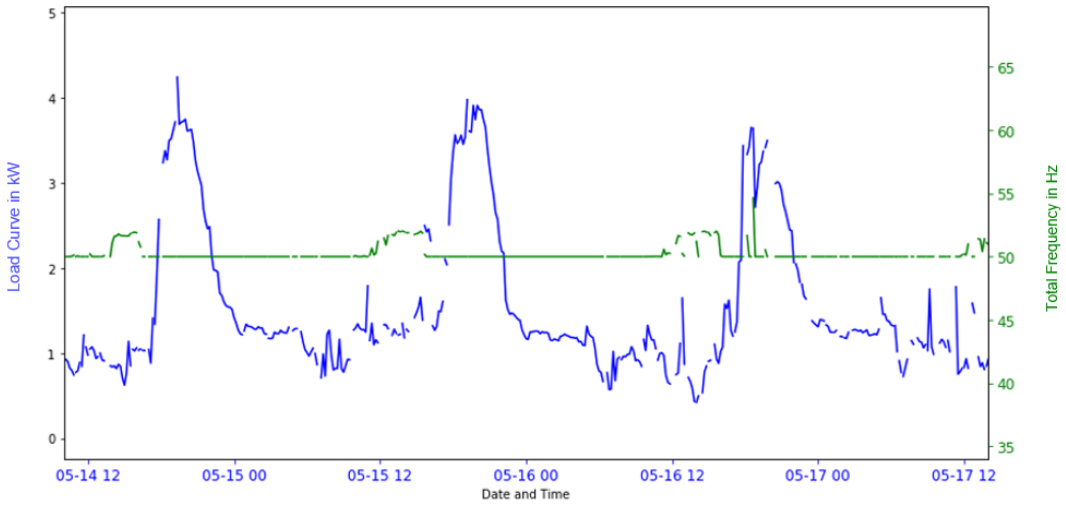

Figure 3-39: *A plot of total frequency versus total load curve for a period from 14 May 2022 to 17 May 2022*

Variations in load, both increases and decreases, can indeed lead to frequency variations in a power system. When the load on the microgrid increases, there's an immediate demand for more power. If the generation capacity cannot match this sudden surge in demand, it can decrease system frequency.

Conversely, when the load decreases, there is a surplus of generated power, leading to increased frequency. These frequency variations can affect the stability of the power system and the performance of connected devices. Figure 3-40 shows the mentioned effect for the measured data in the Mpale microgrid. Hence, proper load forecasting, efficient demand management, and a well-balanced generation mix are crucial to maintaining a stable frequency in a microgrid or any power system.

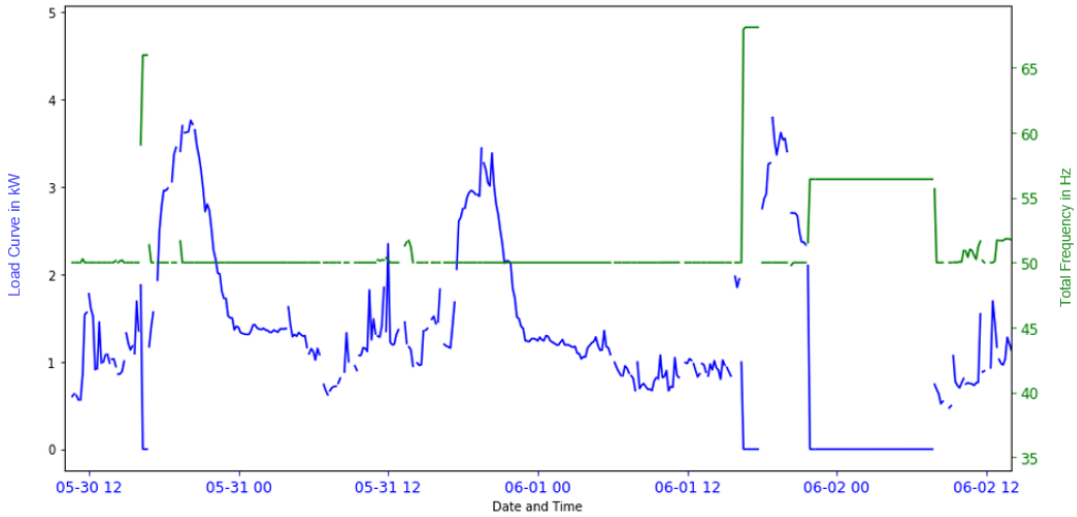

Figure 3-40: *A plot of total frequency versus total load showing the effect of increase and sudden decrease of the load on the frequency*

The quality of the power supply expressed as the percentage of voltage deviation from the nominal or rated voltage of 230 V was also examined. Figure 3-41 indicates the voltage distribution levels. For all three phases, most of the voltage recorded aligns with the nominal voltage of 230 V. Only 5% of the data set has voltages below 75 V. This can be due to events of interruption to the power system and blackouts.

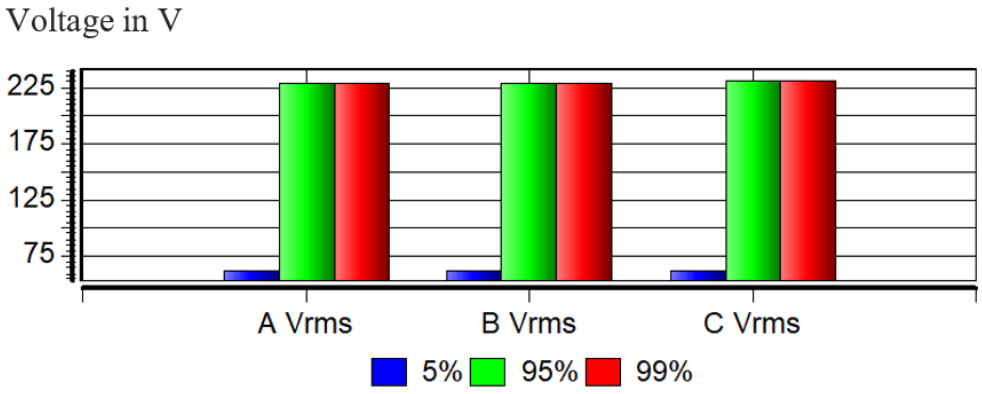

Figure 3-41: *Overall voltage distribution for three phases from 14th May - 12th June 2022*

Figure 3-42 represents the activities of voltage sags, swells, interruptions, and transients. They have been further explained in detail in

Table **3-7**. The simultaneous occurrence of dips, swells, interruptions, and transients in the system, with a concentration during evening hours, suggests a complex interplay of factors affecting the microgrid. The evening peak demand could contribute to dips and interruptions due to strained capacity. Swells may be linked to issues such as sudden load releases.

The presence of transients throughout the day may indicate external factors like lightning or switching events. A comprehensive analysis should consider upgrading infrastructure to handle peak loads, improving voltage regulation mechanisms, and implementing protective measures against transients. Balancing generation, load, and robust system protection becomes crucial for addressing these multifaceted challenges.

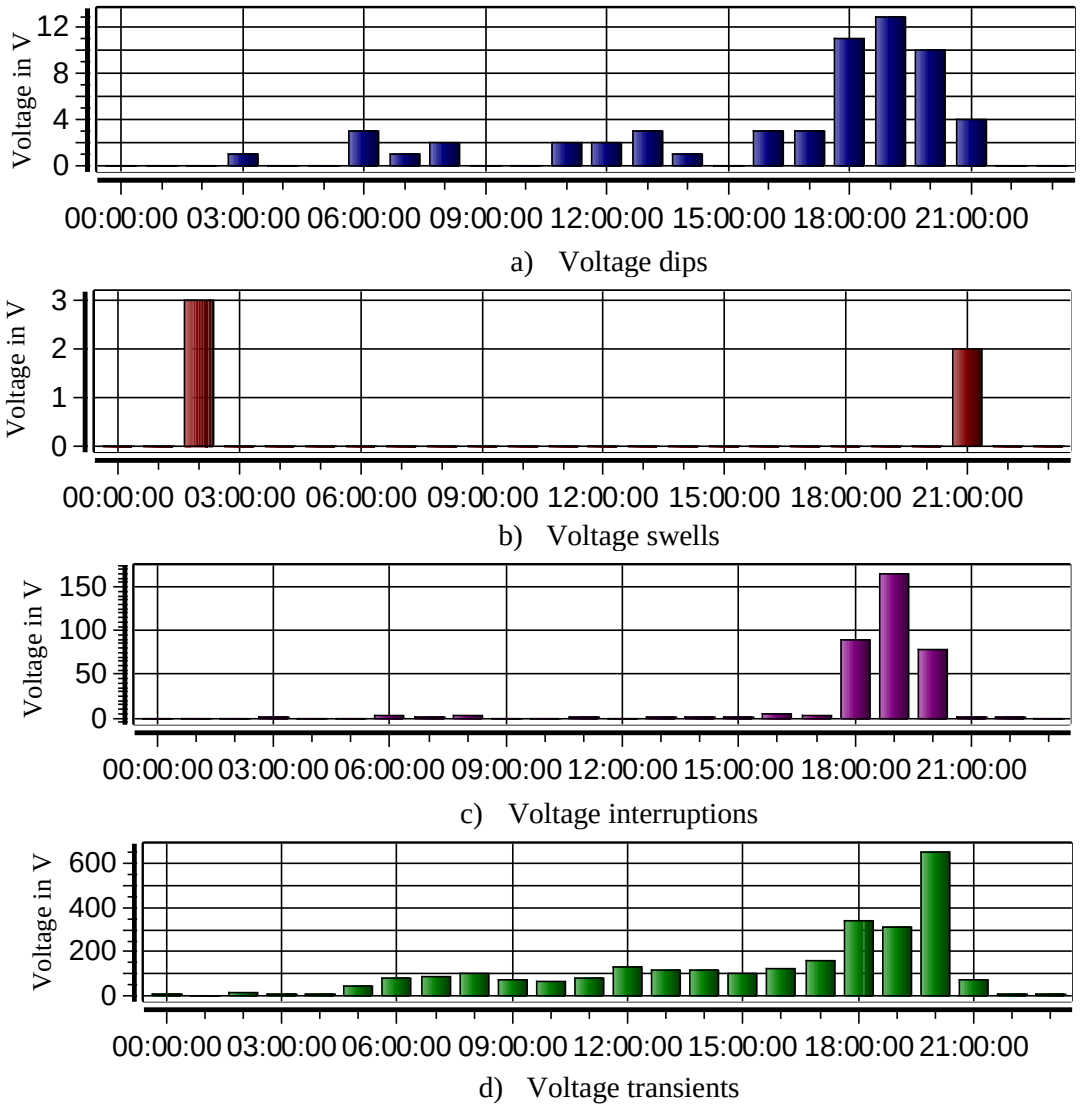

Figure 3-42: *Activity plots for the magnitude of voltage dips, swells, interruptions, and transients from 14th May 2022 to 12th June 2022*

Table 3-7: *Worst Case Summary of the magnitude and duration of the measured voltage dips, swells, interruptions, and transients measured from 14th May 2022 to 12th June 2022*

Out of 59 Total voltage dips				
Criteria	**Phase**	**Category**	**Data**	**Date Time**
Lowest Magnitude	C	SUSTAINED	0.1 V, 17.45 min.	11/06/2022 19:55:39.28
	C	SUSTAINED	0.1 V, 1.38 hrs.	01/06/2022 16:19:54.89
	C	SUSTAINED	0.1 V, 5.58 min.	07/06/2022 20:21:03.50
	C	SUSTAINED	0.1 V, 10.14 hrs.	01/06/2022 21:37:26.94
Longest Duration	A	SUSTAINED	0.1 V, 10.14 hrs.	01/06/2022 21:37:26.94
	A	SUSTAINED	0.1 V, 4.94 hrs.	28/05/2022 08:26:30.43
	A	SUSTAINED	0.1 V, 4.69 hrs.	05/06/2022 03:46:25.82
	A	SUSTAINED	0.1 V, 4.42 hrs.	06/06/2022 06:01:36.23
	A	SUSTAINED	0.1 V, 4.94 hrs.	28/05/2022 08:26:30.43
Out of 5 total VOLTAGE SWELLS				
Largest Magnitude	A	INSTANTANEOUS	266.4 V, 0.100 Sec.	15/05/2022 02:48:16.11
	A	INSTANTANEOUS	262.5 V, 0.040 Sec.	28/05/2022 21:33:26.11
	A	MOMENTARY	261.5 V, 1.460 Sec.	28/05/2022 21:33:26.61
	A	INSTANTANEOUS	261.4 V, 0.040 Sec.	15/05/2022 02:48:17.53
Longest Duration	A	MOMENTARY	261.5 V, 1.460 Sec.	28/05/2022 21:33:26.61
	A	INSTANTANEOUS	255.7 V, 0.130 Sec.	15/05/2022 02:48:15.87
	A	INSTANTANEOUS	266.4 V, 0.100 Sec.	15/05/2022 02:48:16.11
	A	INSTANTANEOUS	262.5 V, 0.040 Sec.	28/05/2022 21:33:26.11

Out of 354 total VOLTAGE INTERRUPTIONS				
Longest Duration	A	MOMENTARY	0.1 V, 9.57 hrs.	01/06/2022 22:11:31.56
	A	MOMENTARY	0.1 V, 17767.205 Sec.	28/05/2022 08:26:30.47
	A	MOMENTARY	0.1 V, 4.94 hrs.	05/06/2022 03:46:25.85
	A	MOMENTARY	0.1 V, 4.42 hrs.	06/06/2022 06:01:36.26
Out of 2733 total VOLTAGE TRANSIENTS				
Largest Magnitude	A		1314.8 V, 0.004 Sec.	04/06/2022 18:29:03.62
	C		1280.0 V, 0.003 Sec.	07/06/2022 20:26:48.64
	B		1278.0 V, 0.002 Sec.	06/06/2022 17:38:11.88
	B		1272.0 V, 0.004 Sec.	04/06/2022 18:29:03.62

Table 3-7 summarises all the recorded worst-case scenarios of measured voltage dips, swells, interruptions and transients from 14th May 2022 to 12th June 2022 with their duration and magnitude. From the observed results, phases A and C suffered more from prolonged time of voltage dip events. According to the TBS, voltage dips are generally caused by system or distribution network faults. Most voltage dips have a duration of less than 1s; however, voltage dips with greater depth and duration can occur infrequently. It also mentioned the causes of these dips, which could be switching loads in the network; however, it is impossible to set national compatibility levels of acceptable dips since the environment significantly impacts the frequency of faults that give rise to voltage dips. From the observed data, the two phases had a severe and prolonged dip, which led to a blackout. These were thought to be connecting large appliances, which consume more energy at the start-up. Only five voltage swells were observed, and none was sustained; they were instantaneous and momentarily, lasting less than two seconds. Voltage swells adhere to the TBS (measured following TZS 1382 standard), which states that a swell is defined to have a duration from 20 ms to 10 min with a voltage threshold of +15% of the standard voltage for the networks with voltage less than 500 V. although the most considerable swell magnitude of 266.4 V (15.82% of nominal voltage) exceeded the set threshold, its duration lasted only for 0.1 seconds.

Figure 3-43 and Figure 3-44 represent the total daily and weekly load profiles by their maximum, minimum, and average values. Analyzing the load profile with higher peaks in the evening reveals a pronounced demand pattern during those hours. This event likely indicates high energy consumption during peak hours when residents return home, businesses operate, and various activities intensify.

Strategies like demand-side management, energy storage deployment, or staggered operation of specific loads could be considered to address this. Implementing these measures can help flatten the load curve, ensuring a more balanced distribution of energy consumption throughout the day, thereby improving the overall efficiency and reliability of the microgrid.

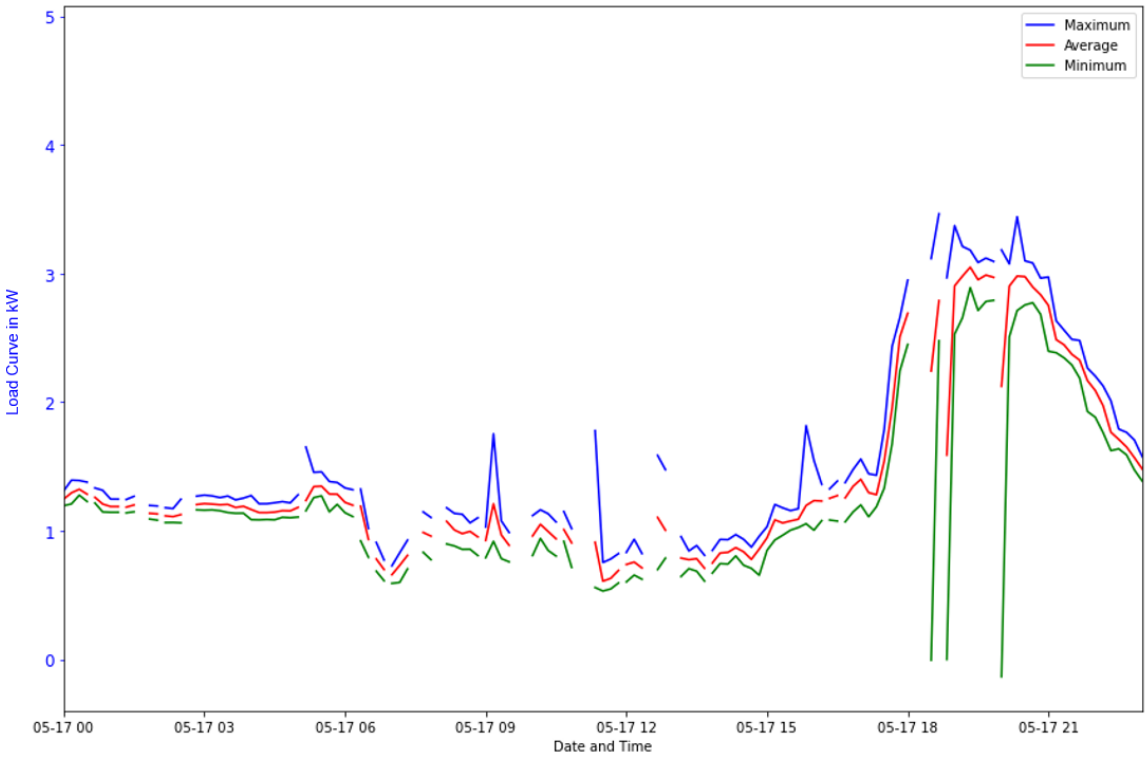

Figure 3-43: *Plots of total load profiles using maximum, average, and minimum values zoomed for a period from 2022-05-17 00:00 to 2022-05-17 23:00*

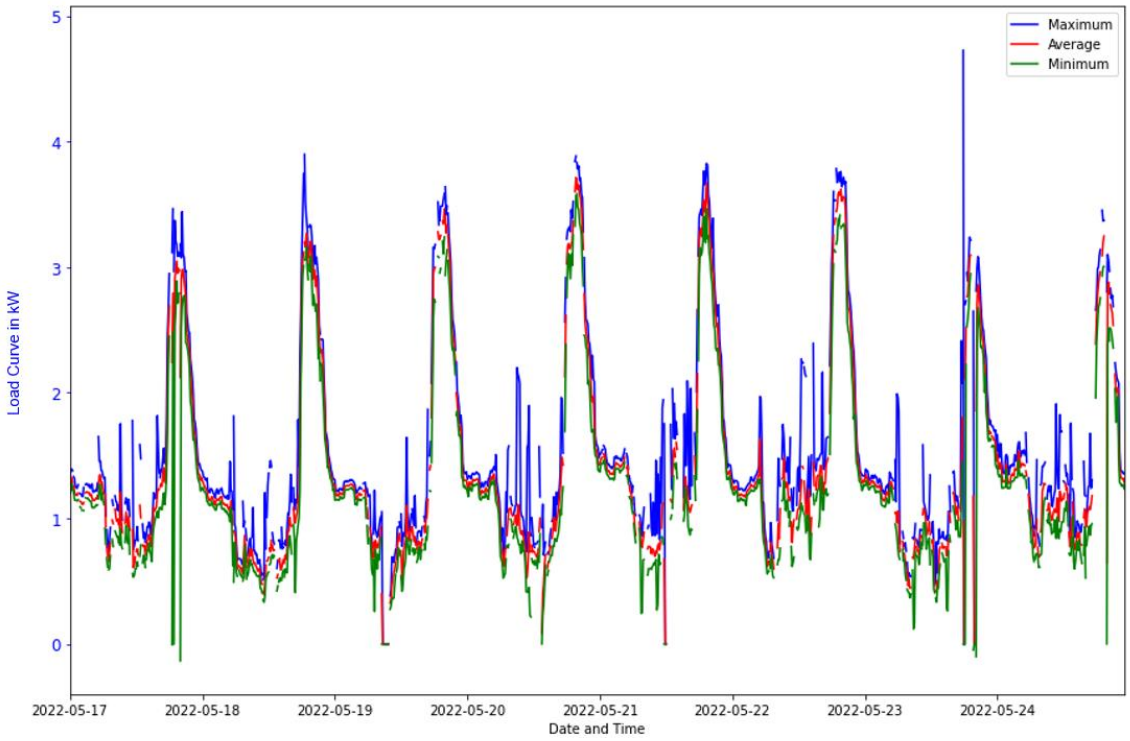

Figure 3-44: *Weekly total load profiles zoomed for a period from 2022-05-17 00:00 to 2022-05-24 23:00*

3.3.1.6. Reactive Power

Figure 3-45 shows how much reactive power is introduced into the system. A plot of the load curve and reactive power provides insights into the power factor and system efficiency. The presence of reactive power may indicate a power factor correction issue. Poor power factor can result in inefficient energy use and higher losses in the system. For this case study, the reason is customers' use of inductive loads, which is believed to be so since many connected customers in Mpale use the older cathode ray tube (CRT) televisions, which are considered inductive loads due to their technology, which relies on the movement of electrons facilitated by magnetic fields.

Addressing this could involve implementing power factor correction devices or optimizing the operation of existing equipment. A balanced load curve and improved power factor contribute to a more efficient and reliable power system, reducing energy losses and enhancing the overall performance of the microgrid.

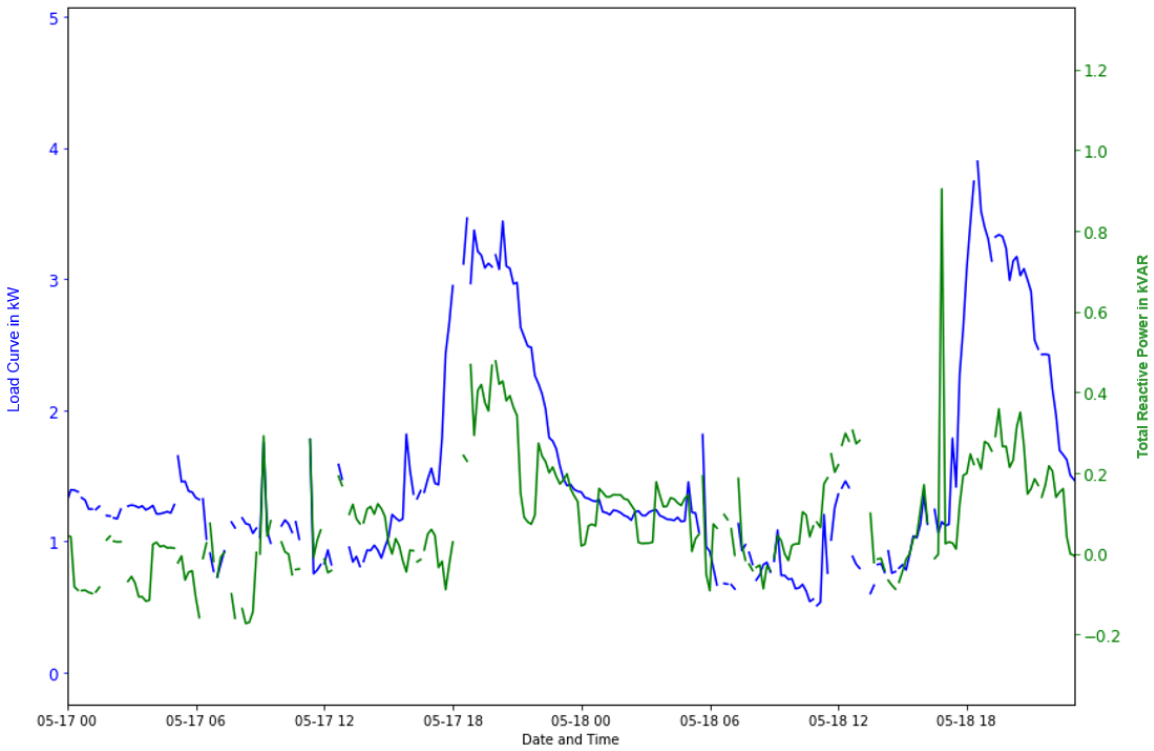

Figure 3-45: *A plot of the total load profile and its associated total reactive power generated in the system zoomed for a period from 2022-05-17 00:00 to 2022-05-18 23:00*

3.3.1.7. Correlation

For the first time, correlation and regression were defined as statistical parameters due to empirical and theoretical development by Sir Francis Galton in 1885, followed by Karl Pearson, who developed the coefficient a decade later (Rodgers & Nicewander, 1988). In 1904, psychologist Spearman Charles introduced the rank correlation coefficient called Spearman's coefficient (Zar, 1972). In 1955, the Kendall rank correlation coefficient was discovered, which evaluates the degree of similarity among two sets of ranks (Abdi, 2008). In literature, Pearson's correlation is widely used to analyse linear data by calculating its coefficient. Pearson's correlation tends to be one of the most representative methods for evaluating the correlation between two mutual variables with dissimilar physical quantities (Song et al., 2017). Pearson correlation is only sensitive to a linear relationship between two variables or even when one variable is a nonlinear function of the other. The coefficient talks about the direction and strength of correlation. The strength of the correlation is represented by the absolute value of the coefficient, in which the more significant the weight, the stronger the correlation. In order to minimise errors in estimating correlation, circumstances like the linearity and non-linearity of data needed to be carefully analysed. Pearson's correlation coefficient is calculated using Eqn 3-2.

$$r_{cc} = \frac{\sum_i^N (x_i - \overline{x})(y_i - \overline{y})}{\sum_i^N (x_i - \overline{x})^2 \sum_i^N (y_i - \overline{y})^2} \qquad \textit{Eqn 3-2}$$

Where, r_{cc} = Pearson's correlation coefficient; x_i, y_i = observations from populations x and y (where x is the independent variable, y is the dependent variable), respectively; $\overline{x}, \overline{y}$ = means of objects in the population.

The coefficient r_{cc} lies in the range of [-1,1], and different ranges in between signify various levels of relationship. A strong correlation is when the value is higher than 0.7.

Kendall and Spearman's correlation was more sensitive to nonlinear relationships.

Using a monotonic function, Spearman's rank coefficient assesses how well the relationship between two variables can be described. It is a nonparametric measure of statistical dependence between two variables. Spearman's rank coefficient assumes independent pairs of observation whereby the two variables should be measured on an ordinal, interval or ratio scale. Also, it assumes a monotonic relationship between the two variables. The formula by which Spearman's coefficient is calculated is as follows:

$$\rho = \frac{\sum_i^N (R(x_i) - \overline{R(x)})(R(y_i) - R(\overline{y}))}{\sum_i^N (R(x_i) - R(\overline{x}))^2 \sum_i^N (R(y_i) - R(\overline{y}))^2} = 1 - \frac{6 \sum_{i=1}^n (R(x_i) - R(y_i))^2}{n(n^2 - 1)} \qquad \textit{Eqn 3-3}$$

where $R(x_i)$ represents the rank of x_i, while $R(y_i)$ represents the rank of y_i, $R(\overline{x})$ is the mean rank of x_i, $R(\overline{y})$ is the mean rank of y_i , n is the number of pairs (Selami Shaqiri et al., 2023).

Kendall correlation is a lesser-used correlation method, represented by its coefficient Tau (τ). Kendall's tau is a correlation coefficient that can be used for data in the form of ranks as an alternative to Spearman's rho. It is a simple function of the minimum number of neighbour swaps needed to produce one order from another (Iljazi, 2021). The formula to calculate Kendall's Tau is as follows:

$$\tau = \frac{C - D}{\frac{1}{2} n(n-1)} \qquad \textit{Eqn 3-4}$$

Where C is the sum of the number of the most significant values of y (number of concordant pairs), D is the sum of the number of the smallest values of y (number of discordant pairs), n is the number of pairs. The sums C and D represent the pairs' incompatible and irreconcilable numbers. Table 3-8 describes the different correlation values in detail.

Table 3-8: *Interpretation of Pearson's, Spearman's and Kendall's correlation coefficients*

r_{cc}	**Description**
$\|r_{cc}\| > 0.9$	Very strong correlation
$0.9 \geq \|r_{cc}\| > 0.7$	Strong correlation
$0.7 \geq \|r_{cc}\| > 0.4$	Relatively strong correlation
$0.4 \geq \|r_{cc}\| > 0.1$	Moderate correlation
$0.1 \geq \|r_{cc}\| > 0$	Weak correlation
$\|r_{cc}\| = 0$	No correlation
$\|r_{cc}\| = 1$	Identical/linearly related
$\|r_{cc}\| = -1$	Strict anti-correlation
$\|r_{cc}\| = 0$	Anti-correlated
$\|r_{cc}\|$ = -ve values	Negative correlation
$\|r_{cc}\|$ = +ve values	Positive correlation

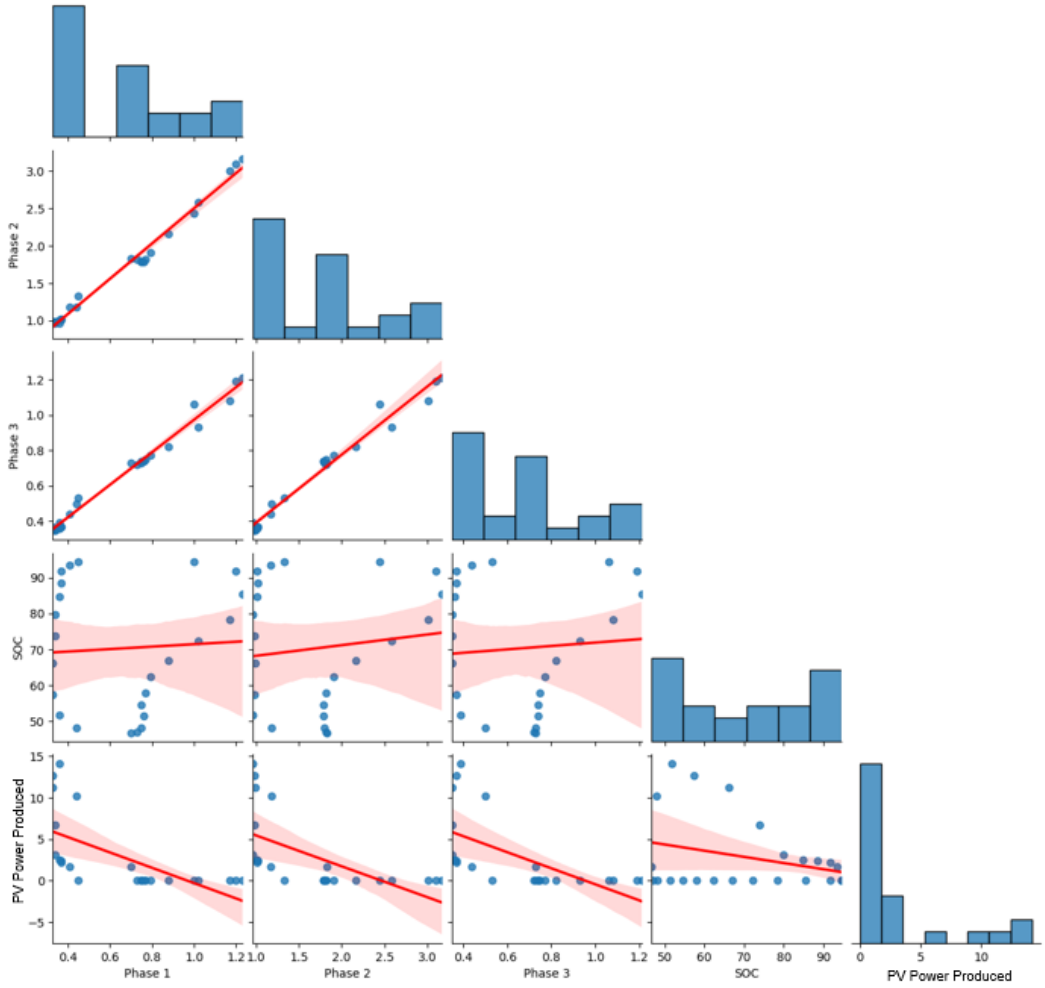

Figure 3-46: *Pearson's correlation scatter plots for solar photovoltaic power produced, power consumed in the three phases and SOC (The correlation red line represents the relationship between the two variables, and the shaded area around it indicates the*

confidence interval showing the range within which true correlation is likely to fall. Bar graphs represent the strength or direction of the correlation, which provides a visual summary of the relationship between observed data).

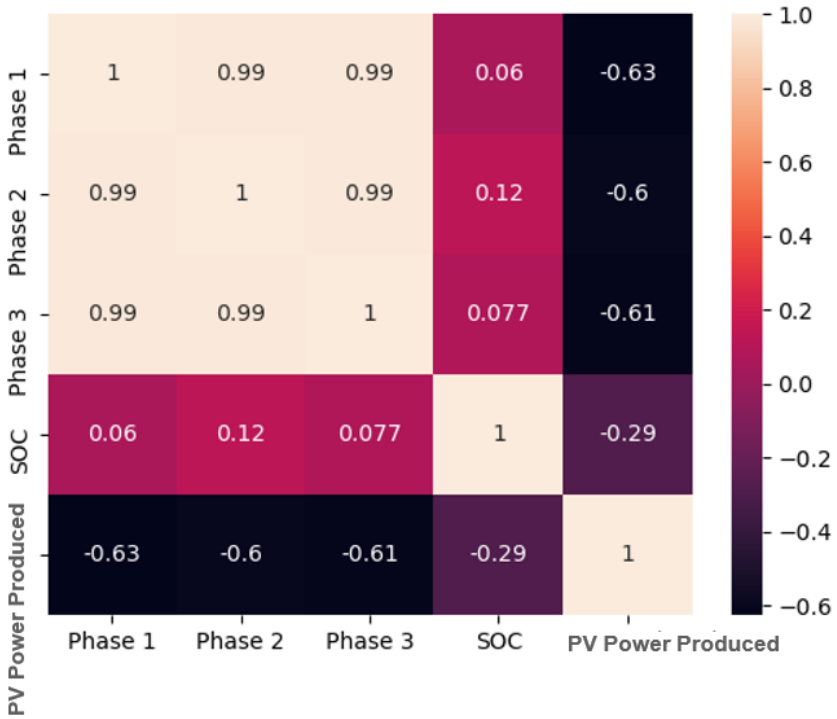

Figure 3-47: *The heat map plots of Pearson's correlation for solar photovoltaic power produced, power consumed in the three phases and SOC*

Table 3-9: *Spearman's correlation table for the power in the three phases, solar photovoltaic power produced and battery state of charge*

	Phase 1	Phase 2	Phase 3	Battery SOC	PV Power produced
Phase 1	1	0.96	0.98	0.09	-0.88
Phase 2	0.96	1	0.95	0.06	-0.84
Phase 3	0.98	0.95	1	0.03	-0.83
SOC	0.09	0.06	0.03	1	-0.09
PV Power Produced	-0.88	-0.84	-0.83	-0.09	1

Table 3-10: *Kendall Correlation table for the power in the three phases, solar photovoltaic power produced and battery state of charge*

	Phase 1	Phase 2	Phase 3	Battery SOC	PV Power produced
Phase 1	1	0.87	0.93	0.16	-0.74

	Phase 1	Phase 2	Phase 3	Battery SOC	PV Power produced
Phase 2	0.87	1	0.85	0.09	-0.70
Phase 3	0.93	0.85	1	0.11	-0.66
SOC	0.16	0.09	0.11	1	-0.12
PV Power Produced	-0.74	-0.70	-0.66	-0.12	1

Figure 3-46 and Figure 3-47 present Pearson's correlation scatter and heat plots between demand, supply and storage, respectively. All three phases show a strong correlation, an indicator that the trend of energy usage is similar. The lack of correlation of demand between sites is essential to determine potential investment deferment in generation and possibilities of new connections required to utilise the lack of correlation. Phase 1 has households connected; Phase 2 supplies families and businesses; Phase 3 is connected to homes. The almost similar correlation value may imply that the three phases only differ in the amount of power used, but the trend is the same.

The negative correlation between demand in the phases and solar power produced means that solar generation cannot meet demand, especially during peak hours. Solar PV, in effect, shaves demand in the middle of the day while most peak demand occurs later in the evening and early morning. This suggests that solar power requires supplementing with energy storage to meet peak demand (if demand cannot be shifted to the midday hours). The state of charge of a battery shows a moderate and weak correlation with demand in all three phases and the solar electricity power produced. The negative sign of its correlation with solar electricity power produced may signify the charging of the battery, which, as a result, decreases solar power when battery SOC is increasing (e.g., in the late afternoon hours).
Table 3-9 and Table 3-10 show the same correlation coefficients using Spearman's and Kendall's correlation coefficients, respectively.

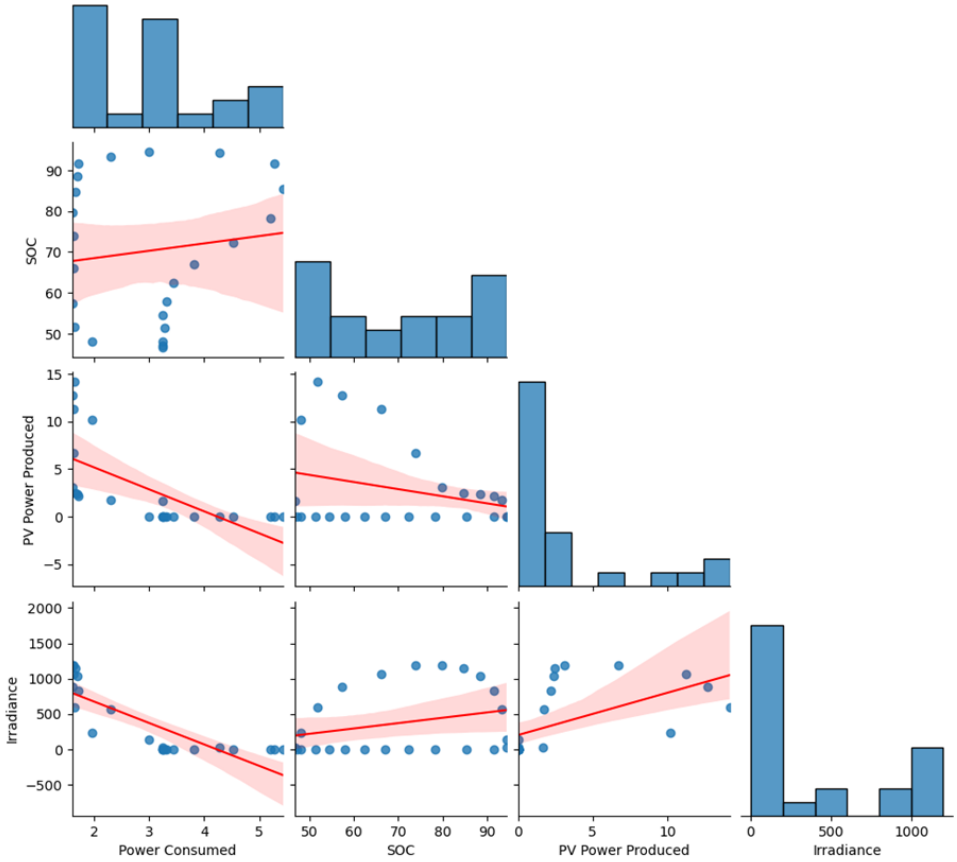

Figure 3-48: *Pearson's correlation scatter plots for irradiance, solar photovoltaic power produced, total power consumption and SOC*

Figure 3-49: *The heat map plots of Pearson's correlation for irradiance, solar photovoltaic power produced, the total power consumed and SOC*

Figure 3-48 and Figure 3-49 represent Pearson's correlation scatter and heat map plots showing correlation coefficients for irradiance, solar power produced, total power consumed and SOC. It is observed that the correlation between irradiance and solar power produced is around 0.6. This value suggests a moderate correlation between the two, i.e., solar power is produced as irradiance increases. The two do not show a perfect correlation since other factors influence power production, such as solar panel efficiency, panel temperature, orientation, dust on the panel, etc.

A strong negative correlation between irradiance and total power consumed signifies more irradiance with low power consumption and vice versa. This may be because more power is consumed during morning hours and late evening when there is insufficient irradiance. Also, one may argue that higher irradiance coincides with sunnier conditions, reducing the need for artificial lighting, which is the most power consuming unit in the villages. The same reason explains the negative correlation between solar power produced and consumed. A weak correlation between SOC and other parameters indicates a weak relationship since other factors are behind the overall dynamics, such as charging/discharging efficiency. Also, A weak negative correlation value of -0.29 between battery State of Charge (SOC) and solar power generation might imply that the battery SOC tends to decrease slightly as solar power generation increases. The negative correlation could indicate factors such as energy consumption exceeding solar generation during specific periods, leading to reduced battery SOC. It doesn't necessarily mean the battery is full, but rather, a modest inverse relationship exists between solar power generation and the battery's state of charge.

3.3.1.8. Clustering of Data

Clustering is one of the methods for determining intrinsic patterns in data sets. The main goal of clustering is to group data according to their similarities into clusters, e.g., to determine inherent patterns in data sets (Rajabi et al., 2020). With clustering, items in the same cluster are more similar than those in different clusters. Therefore, high intra-cluster and low inter-cluster similarities are achieved. Clustering of data was done using the following steps:

a) Demand data collection

   Data on electricity consumption from customers' smart meters was collected. They pre-process the gathered data to cater for incomplete (missing), insufficient, and corrupted data due to uncommon situations like unexpected failures. Different

techniques like regression can be used to repair the data. Data abnormalities can also be handled uniquely as one of the clustering stages (Rajabi et al., 2020).

b) Clustering stage

The selection of accurate parameters and a proper clustering algorithm is performed in this stage. The type of clustering technique depends on various factors such as the type and size of the dataset, user preferences, computational facilities and the final clustering goal. More than one clustering technique may be applied to the demand profiles and final results compared to achieve the best results. Furthermore, the author proved that different clustering techniques could be combined to obtain better results or speed up the process (Kwac et al., 2014).

c) Clustering performance assessment

Although assessing the quality of the clusters obtained is not clear due to an unsupervised process of the clustering algorithm, a suitable clustering method should ensure the compactness of each cluster and wide separation of different clusters (Wang et al., 2015). Clustering validity indexes (CVIs) are used to evaluate the clustering results.

d) Formation of customer classes

This stage can be termed postprocessing of the resulting clusters to match real-world scenarios. For example, depending on whether the final goal for clustering is tariff design or demand response, the number of clusters can be in a specific allowable range. The ultimate user (DR personnel or operator) should specify the number of customer segments. In this stage, consolidation of clusters with similar patterns is possible (Smith et al., 2012).

Electricity consumption data of the Mpale microgrid were considered, whereby the K-means clustering algorithm was performed using the Scikit-Learn Python package (Barupal & Fiehn, 2019). Clustering was done to identify the typical usage patterns of the customers and group them into respective clusters depending on their electricity usage trends. Knowing the respective clusters is essential to achieve a more flexible DSM, especially in deciding suitable candidates for DSM and designing incentives in case of incentive-based DSM (Philipo et al., 2021). Figure 3-50 shows the optimal number of clusters using the elbow method. The elbow method decides the optimal cluster numbers K by the turning

point of the graph that gives the slightest decrease in the error sum. From Figure 3-50, the optimal K value obtained in this case is three; hence, three clusters will be identified.

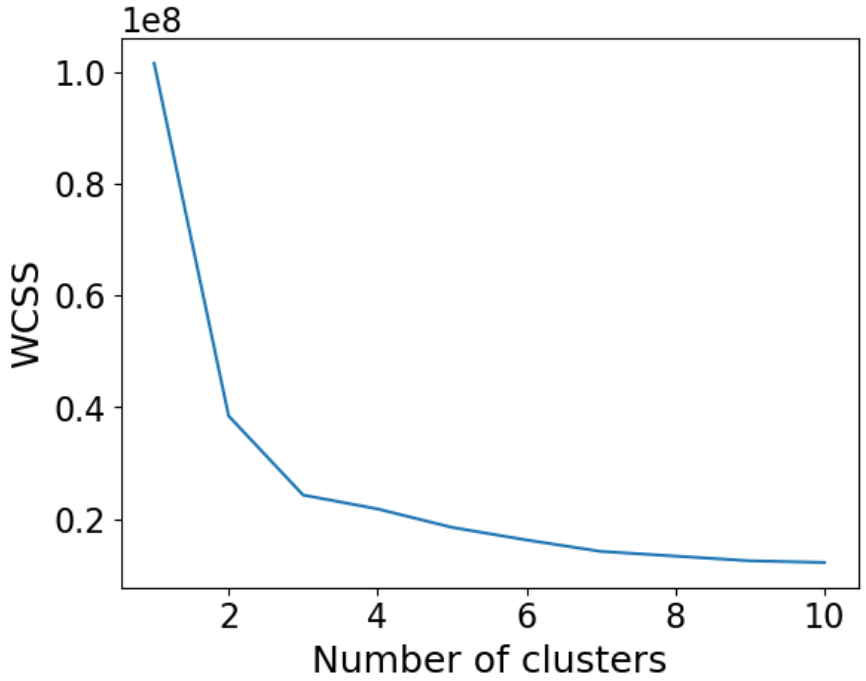

Figure 3-50: *A graph of the elbow method used to determine the optimal value of K in clusters*

Figure 3-51 shows distinct patterns in electricity demand throughout the day in the village, comprising households and businesses. Cluster 2, the highest power consumption, peaks around 7-10 PM, likely representing peak evening usage when villagers return home from work or school. Activities such as cooking dinner, watching TV, using electric appliances, and lighting up homes contribute to increased electricity demand during this time. The 7 – 10 PM peak aligns with the typical residential consumption patterns, suggesting that cluster 2 comprises mainly households.

Clusters 1 and 3 represent medium usage trends with peak demand around 4-7 PM. These clusters may correspond to the early evening and late afternoon periods when villagers are still active but perhaps not yet engaged in peak household activities. The clusters reflect the combination of early household and business operational activities since most businesses are active at that particular hour. Also, the presence of two separate clusters within this time frame could indicate variations in the timing of activities among different households or businesses within the village. For example, some households may start their evening routines earlier than others.

The clustering analysis reveals distinct usage patterns that align with daily routines and activities within the village. Understanding these patterns can help electricity providers optimize resource allocation, plan for infrastructure upgrades, and implement targeted energy efficiency initiatives.

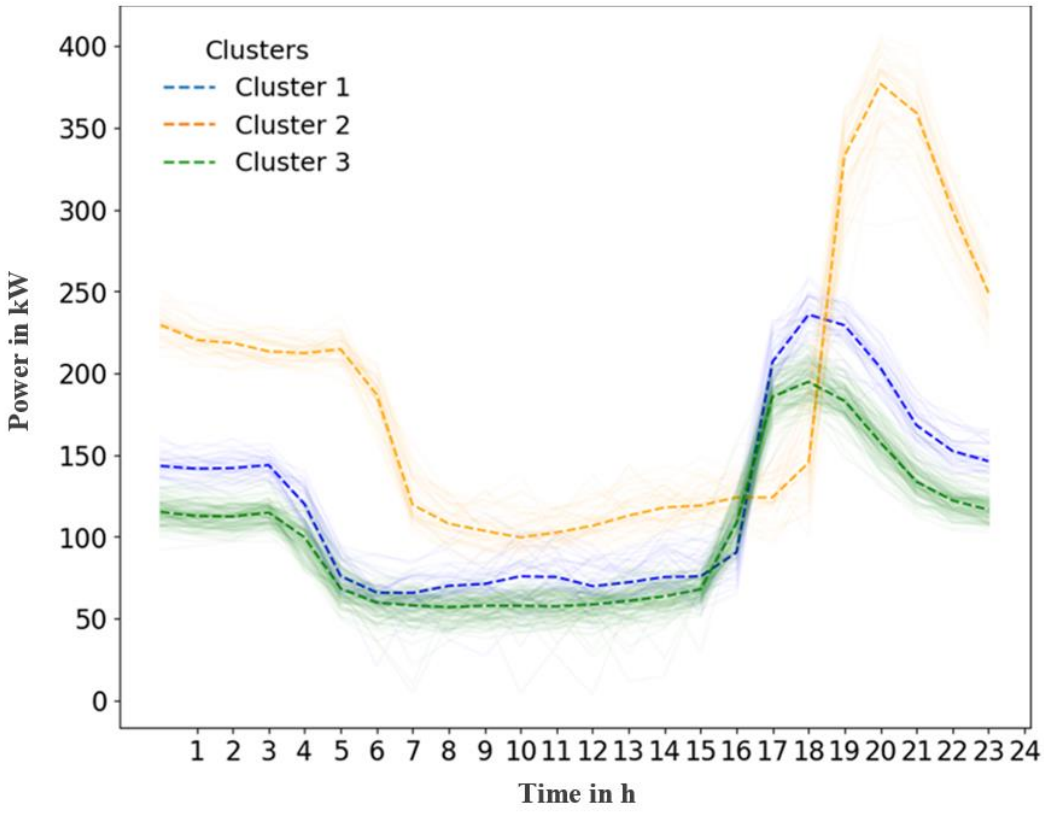

Figure 3-51: *Clusters obtained after applying the K-Means clustering algorithm to the demand data of Mpale microgrid*

3.3.2. Bunjako Microgrid Data

3.3.2.1. Weather Data

Figure 3-52 shows the measured irradiance using irradiation sensors for a week in February 2022, sampled in a daily profile, as shown in Figure 3-53. The aim was to see the trend and the fitting between the load profiles and irradiation, generating solar power. Figure 3-54 shows the measured power consumed for the same period from 22–28 February 2022.

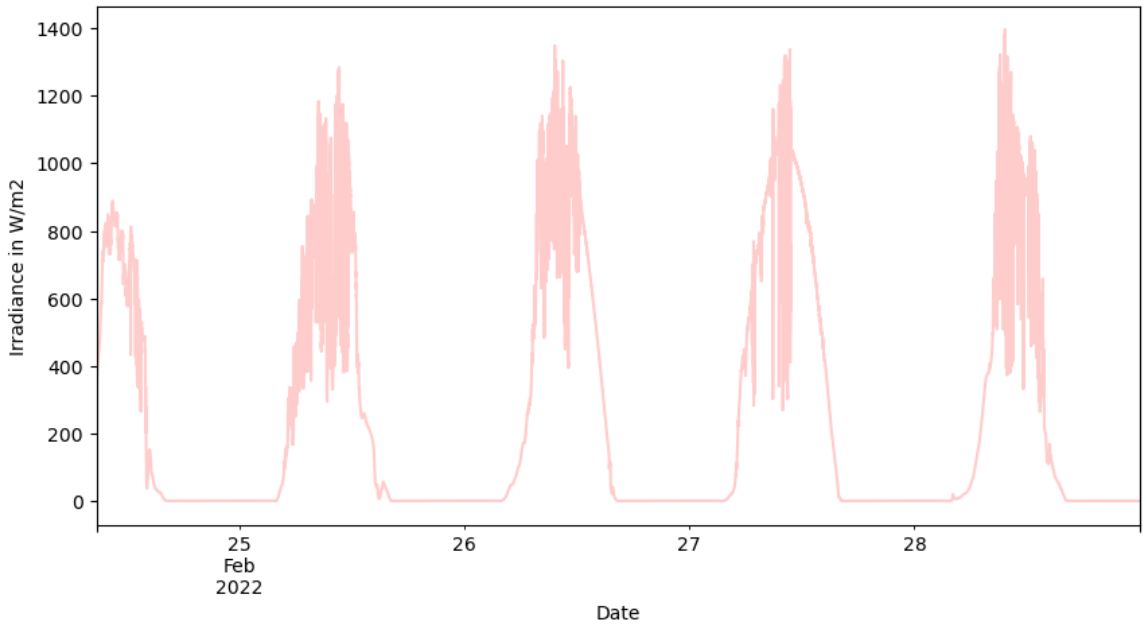

Figure 3-52: *Measured Solar Irradiance in the plane of the modules for the Bunjako Microgrid for the period from 24 February to 28 February 2022*

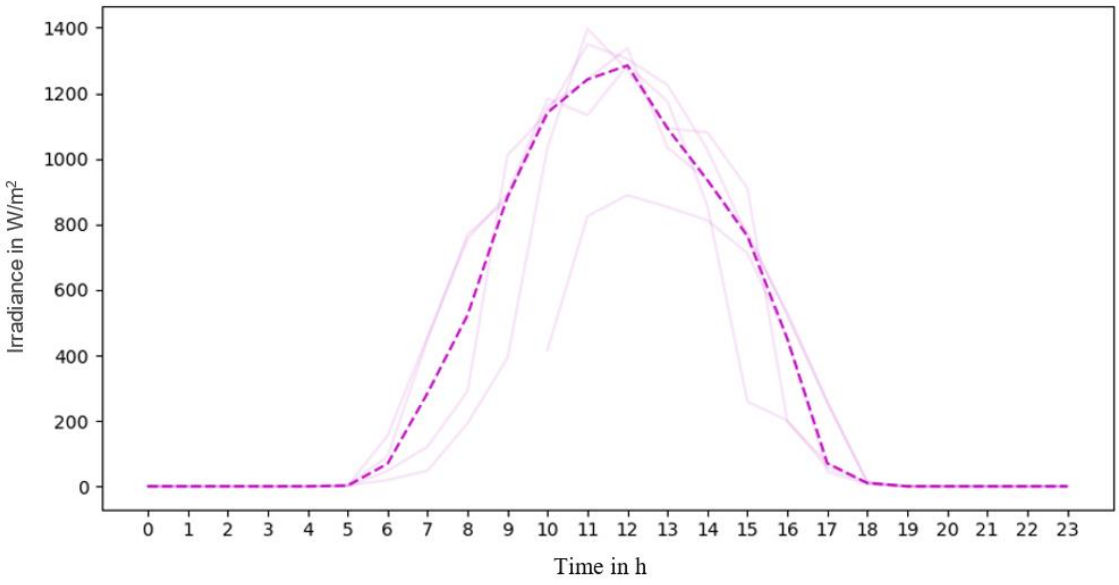

Figure 3-53: *Hourly irradiance sampled from the Measured Solar Irradiance in the plane of the modules for the Bunjako Microgrid for the period from 24 February to 28 February 2022*

3.3.2.2. Demand Data

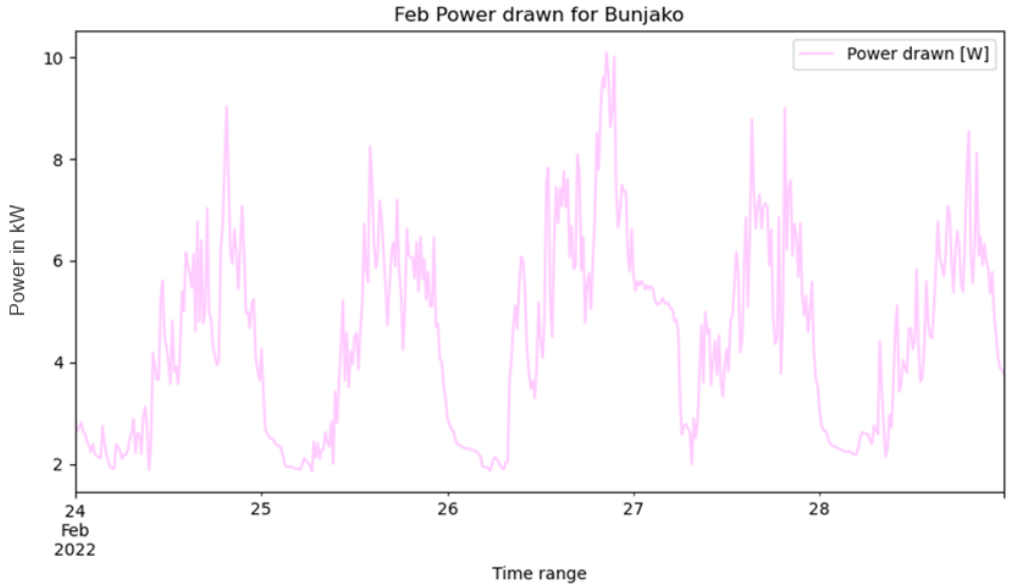

Figure 3-54: *Total measured power demand for Bunjako Microgrid from 22 February to 28 February 2022.*

Figure 3-55 shows the customers' total daily power consumption profiles connected to one of the Bunjako microgrids sampled into a daily load profile from July 2021 to September 2021. Peak demand of about 5 kW was observed between 1800 h and 2200 h, implying that most customers are back home and have switched on various electric appliances, such as lights, fans, and televisions. Demand–response strategies and control were not considered or implemented. Figure 3-56 shows the total daily power consumption profile with a 95% confidence interval.

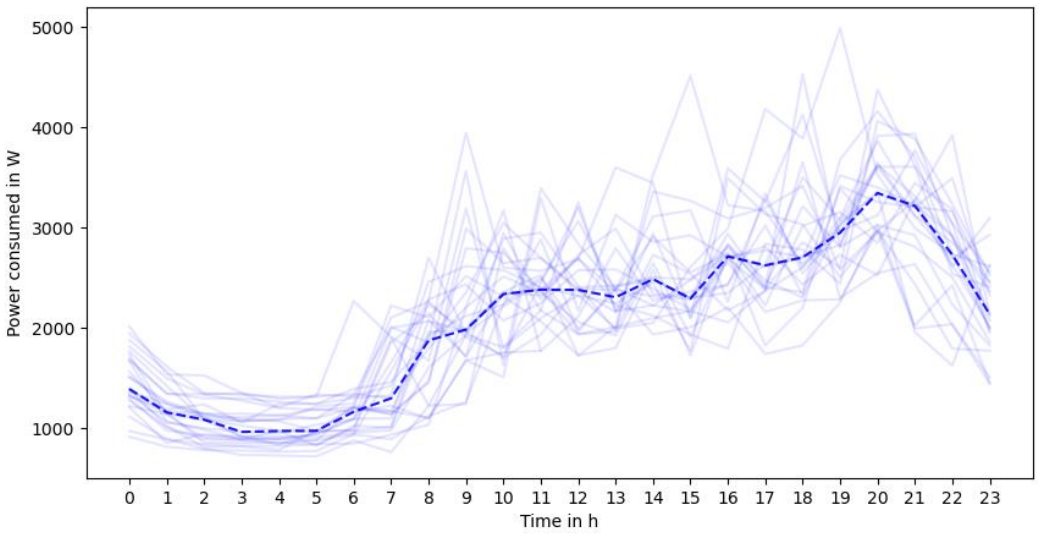

Figure 3-55: *Power demand sampled from the measured demand data for the Bunjako Microgrid for the period from 26 July to 31 August*

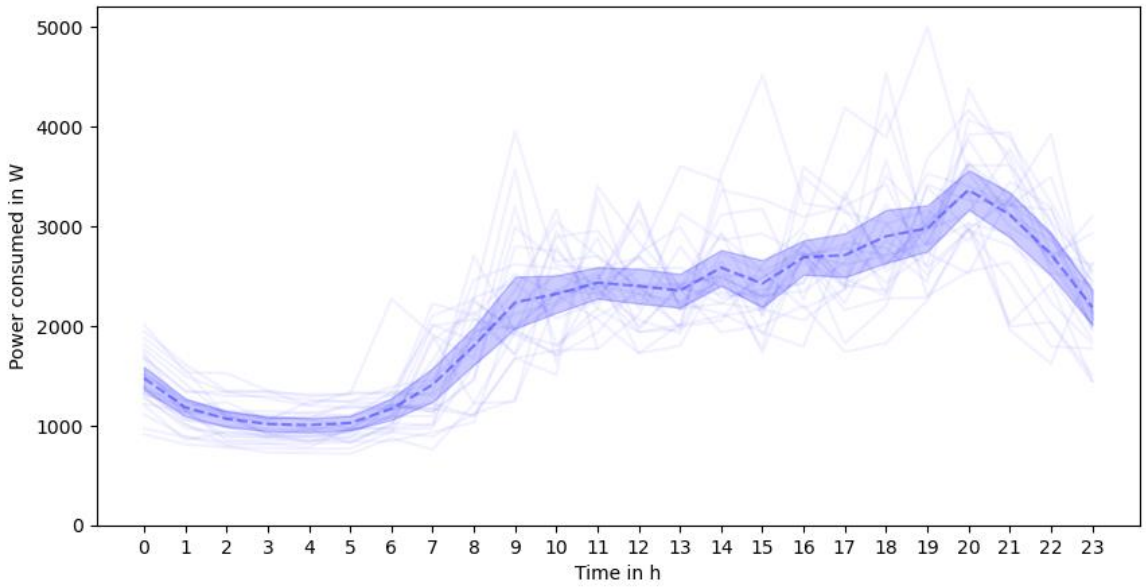

Figure 3-56: *Power demand sampled from the Measured demand data for the Bunjako Microgrid for the period from 26 July to 31 August with a 95% Confidence interval*

Figure 3-57 shows the median, average, maximum and minimum power consumed from the grid in a 24-hour time horizon. The average electricity demand of the data samples ranges from 1000 W to 2000 W, with a total range from a minimum of about 750 W to a maximum of 5000 W. The median and average values are closely related, and all the profiles peak in the evening, a typical load profile for users in the village.

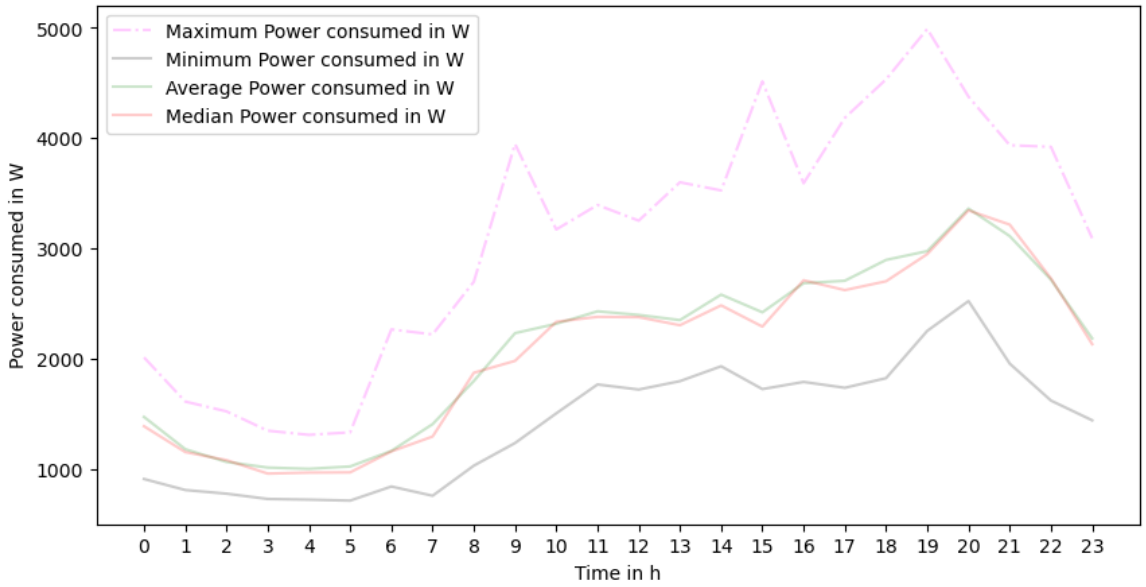

Figure 3-57: *Maximum, minimum, and average daily power sampled from the Measured demand data for the Bunjako Microgrid for the period from 26 July to 31 August*

Electricity consumption significantly depends on the day, whether weekend or weekday and the activities taking place. It may further depend on several factors, such as whether people stay at home most of the time, the kinds of people present in the households, e.g., students, and the nature of economic activities. The box plot in Figure 3-58 shows the variation in power consumed for different days of the week. The central line on each box plot represents the median value, and the dots are the outliers.

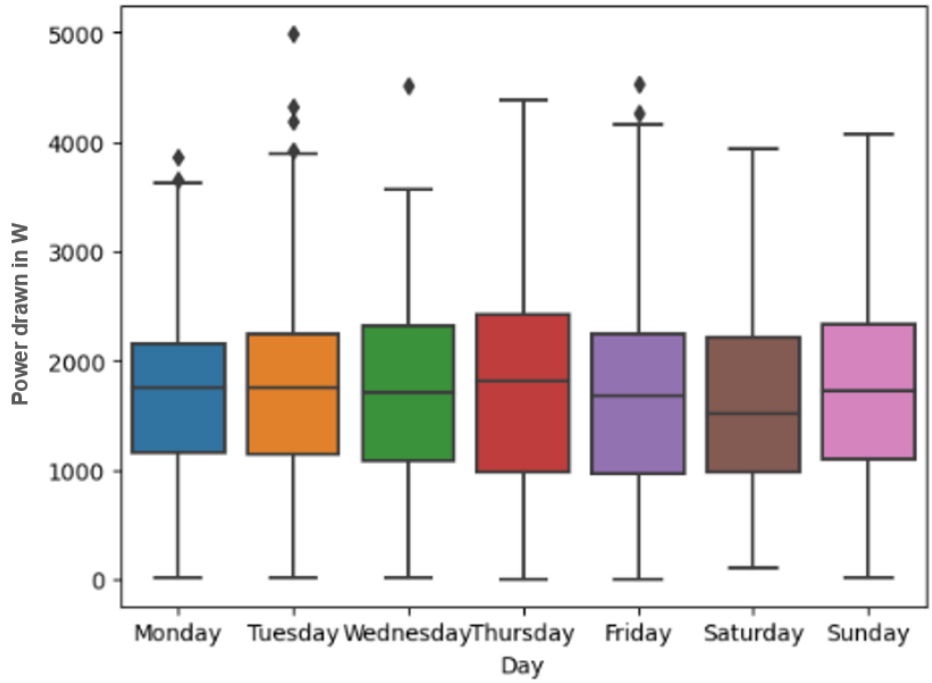

Figure 3-58: *Box plots of the power demand distribution for the days of the week sampled from measured demand data of Bunjako microgrid for the period from 26 July to 31 August*

3.3.2.3. Power Quality Data

3.3.2.3.1. Voltage and Current magnitude

Figure 3-59 shows the values of the measured voltage time plots from 24th February 2022 to 4th March 2022. The East African power quality standards consider the low voltage system to be less than 1000 V, which is the case for the Bunjako microgrid (ERPA, 2021; Tanzania Bureau of Standards (TBS), 2011). The standard phase voltage for such a system is 230 V. However, substantial voltage fluctuations were observed, with phase B being the most affected line. On 26th February 2022, phase B experienced an instantaneous low voltage of about 152.4 V, which might have resulted from sudden significant load changes in current time plots. Figure 3-60 clearly shows events of a sudden increase in loads, represented by a sudden increase in current, which is proportional to the sudden drop in voltage.

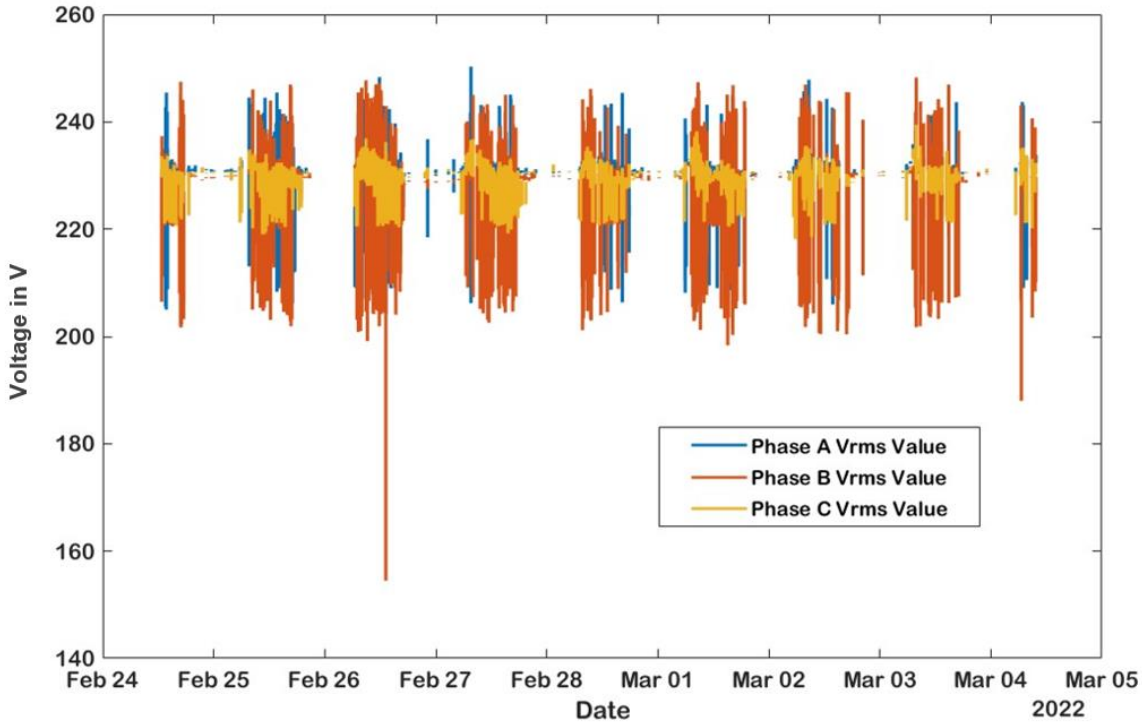

Figure 3-59: *Voltage time plots measured from 24th February 2022 12:43:14.0 to 4th March 2022 10:05:00.0*

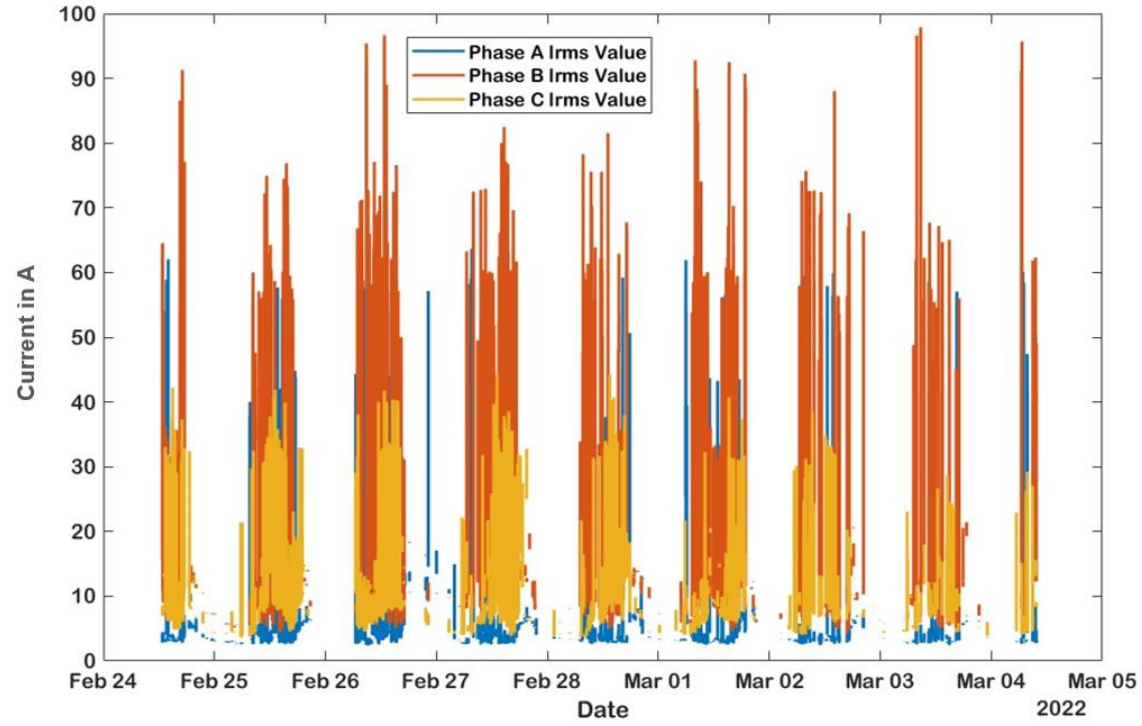

Figure 3-60: *Current time plots measured from 24th February 2022 12:43:14.0 to 4th March 2022 10:05:00.0*

3.3.2.3.2. Current and Voltage Harmonic Distortion Time Plots

Harmonics, an integer multiple of the fundamental frequency in the electrical signal, was measured and analysed within a time frame from 24 February 2022 to 4 February 2022. The presence of harmonics in the power system leads to distortion of the current and voltage waveforms. Figure 3-61, Figure 3-62 and Figure 3-63 show the current harmonic distortion waveforms for phases A, B and C, respectively, while Figure 3-64, Figure 3-65, and Figure 3-66 show their respective voltage waveforms.

Phase A, being the highest, had a total harmonic distortion of around 7.32 A, with odd harmonics of 7.34 A and even harmonics of 0.14 A. Phase B experienced odd and even current harmonics of 5.3 A and 0.2 A, respectively, with total harmonic distortion of 5.29 A. Phase C had a total harmonic distortion of 4.24 A with odd harmonics 4.25 A and even harmonics of 0.14 A which was the phase with minimal current harmonics.

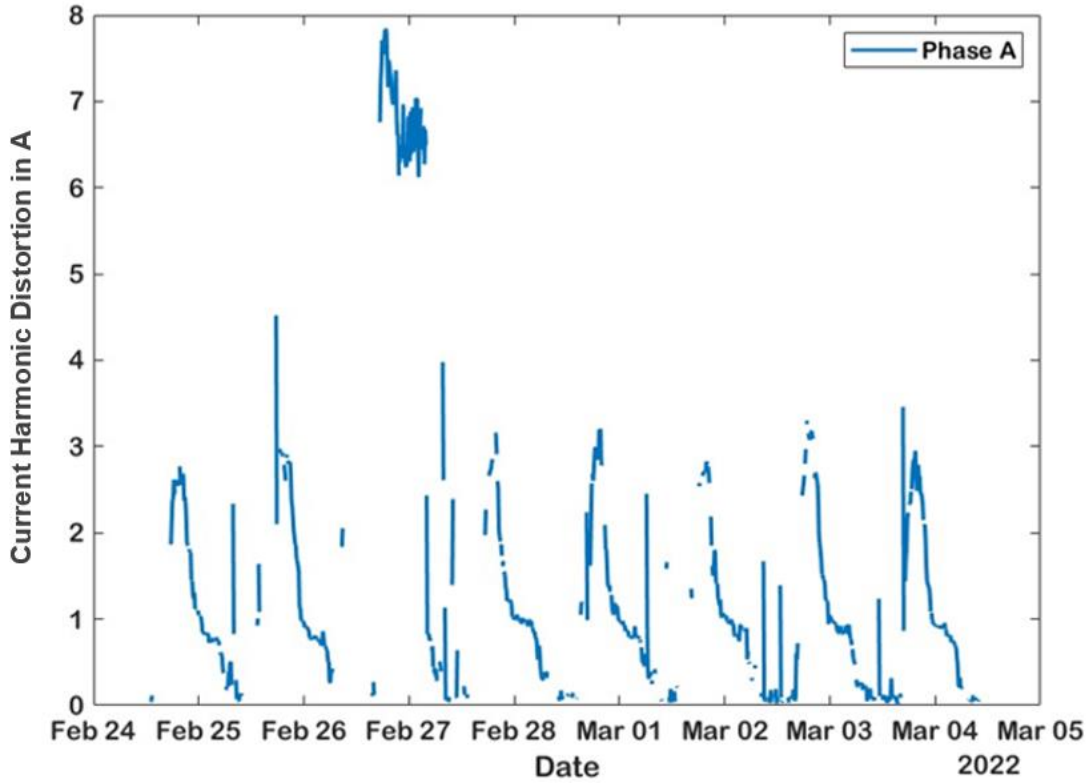

Figure 3-61: *Current harmonics of phase A time plot measured from 24th February 2022 12:43:14.0 to 04th March 2022 10:05:00.0*

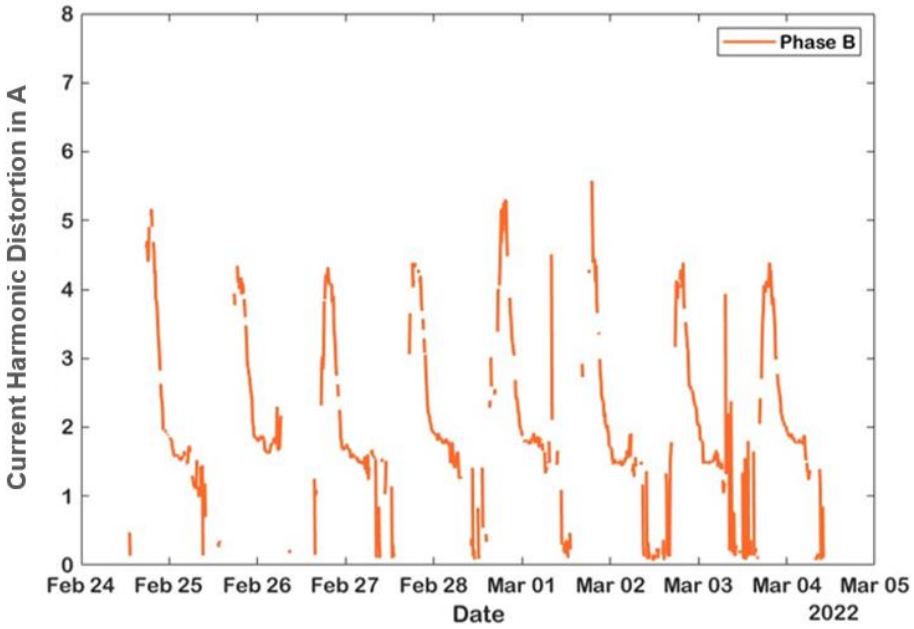

Figure 3-62: *Current harmonics of phase B time plot measured from 24th February 2022 12:43:14.0 to 04th March 2022 10:05:00.0*

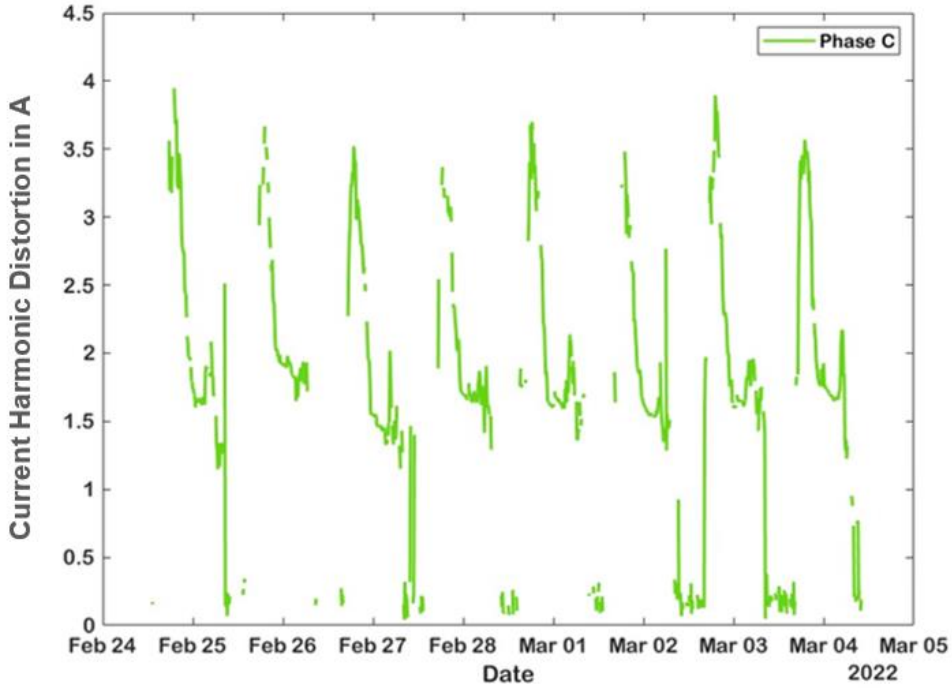

Figure 3-63: *Current harmonics of phase C time plot measured from 24th February 2022 12:43:14.0 to 04th March 2022 10:05:00.0*

For the voltage harmonics distortion, Figure 3-64, Figure 3-65, and Figure 3-66 represent their time plots for phases A, B and C. Phase A had the highest total harmonic distortion of almost 29 V, Phase B had 20.43 V total harmonics distortion (1.15 V even, 20.87 V odd) and phase C experienced a total harmonic distortion of 17.07 V (0.74 V even, 17.32 odd).

According to the East African standards, which follow the IEEE Standard 519, harmonic limits on THD should be 8% of the fundamental voltage; however, the limit can be relaxed for special loads like converters (ERPA, 2021; Tanzania Bureau of Standards (TBS), 2011). Phases A and B exceeded the set harmonic limit since they have almost 12.6% and 9% of the fundamental voltage, respectively. Phase C has 7.4%, which is within the limit.

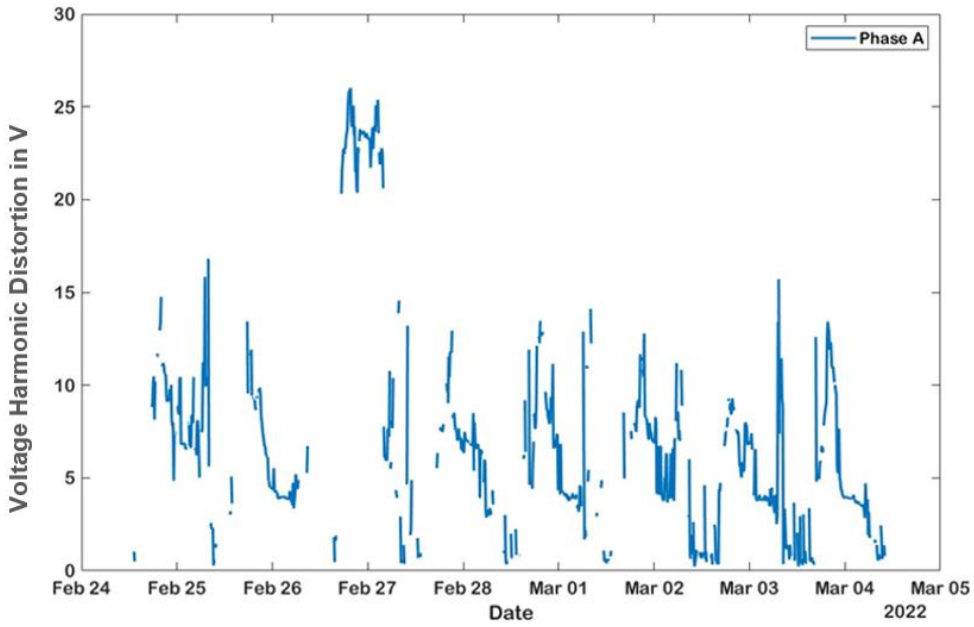

Figure 3-64: *Voltage harmonics of phase A time plot measured from 24th February 2022 12:43:14.0 to 04th March 2022 10:05:00.0*

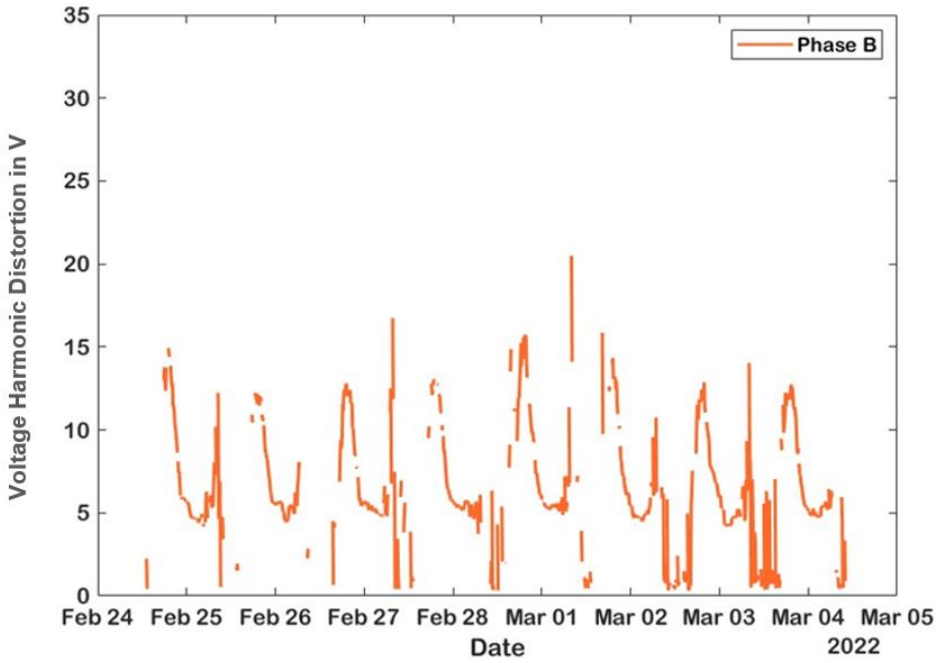

Figure 3-65: *Voltage harmonics of phase B time plot measured from 24th February 2022 12:43:14.0 to 04th March 2022 10:05:00.0*

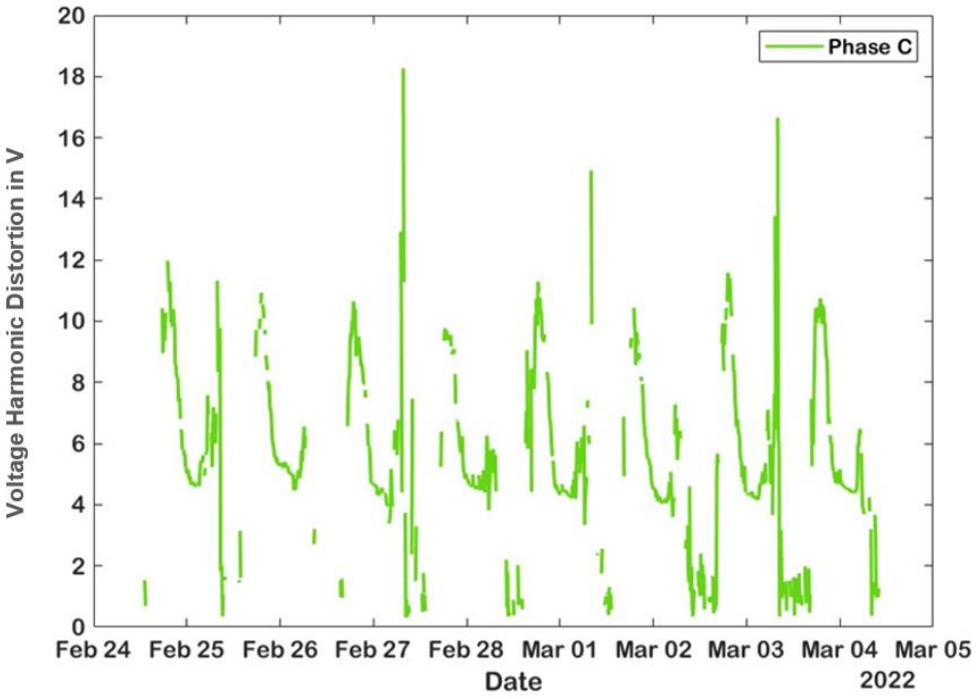

Figure 3-66: *Voltage harmonics of phase C time plot measured from 24th February 2022 12:43:14.0 to 04th March 2022 10:05:00.0*

Figure 3-67 shows the percentage composition of voltage and current harmonics for the three phases. It clearly indicates that phase A has the highest voltage THD values, most of which lie between 20 to 25 V, followed by phase B with most values ranging from 15 to 20 V. Phase C has the least values between 10 to 15 V.

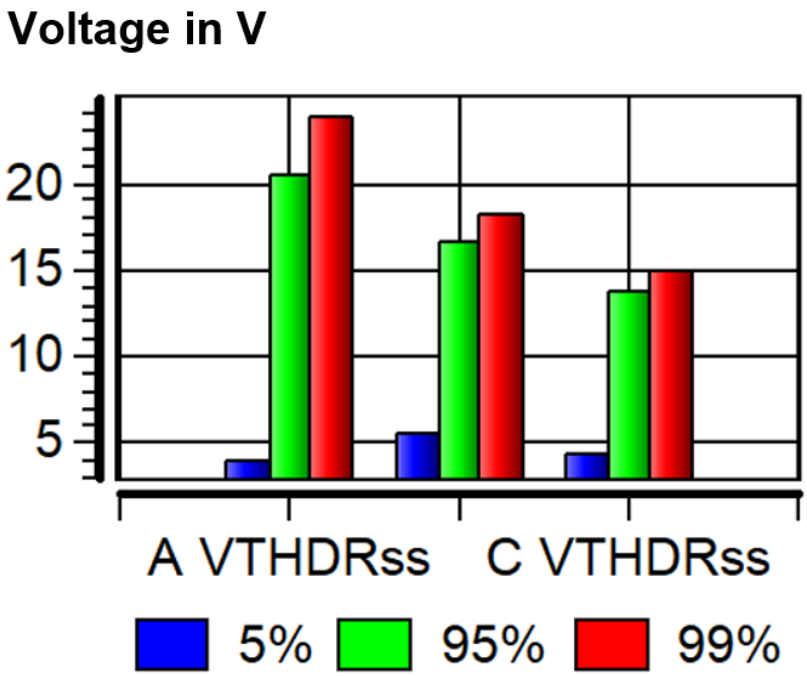

Figure 3-67: *Total voltage and current harmonics percentage composition for each phase*

3.3.2.3.3. Voltage Frequency Plots

Figure 3-68 shows the total average voltage frequency plots, and Figure 3-69 shows the average, minimum and maximum voltage frequency plots measured for a period spanning from 24th February 2022 to 4th March 2022. There is an observance of frequency variations between 49 Hz and 52 Hz, which can be attributed to fluctuations in supply and demand, sudden load changes or grid disturbances. A minimum voltage of around 49.7 Hz is observed, and the maximum frequency is almost 51.75 Hz. According to the quality of supply standards, frequency excursions outside the range of 51.5 Hz and 48.5 Hz is not within the permitted limit of the generation unit to be connected to the supply unit to avoid damage (ERPA, 2021). Therefore, the higher frequency value observed was more than the permitted value.

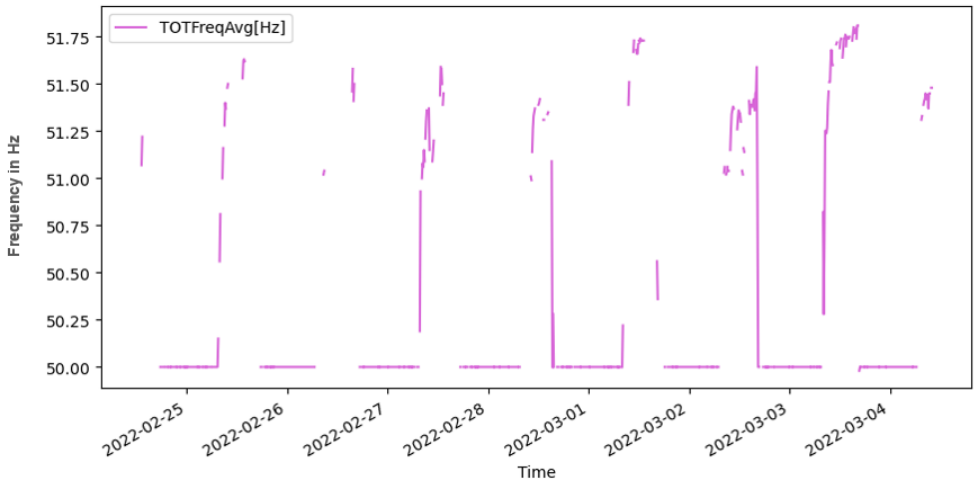

Figure 3-68: *Total average Voltage frequency plots measured from 24th February 2022 12:43:14.0 to 4th March 2022 10:05:00.0*

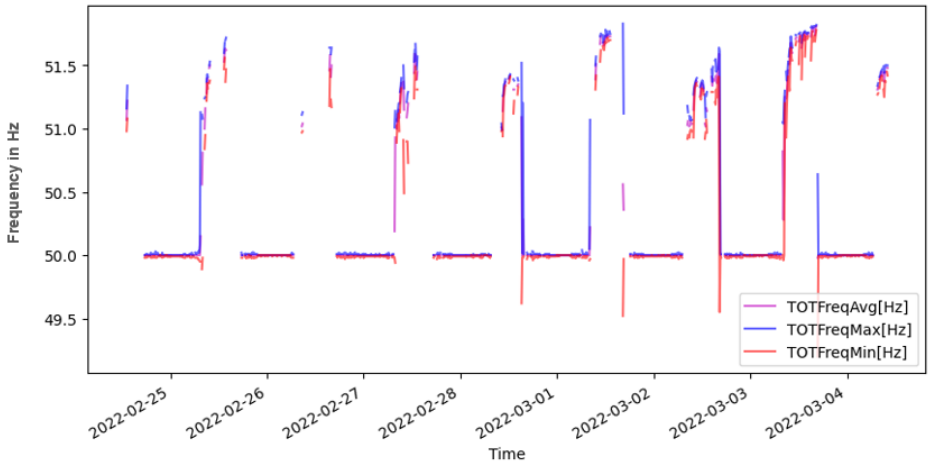

Figure 3-69: *Average, Maximum and Minimum Voltage frequency plots measured from 24th February 2022 12:43:14.0 to 4th March 2022 10:05:00.0*

3.3.2.3.4. Quality of Supply

The quality of the power supply expressed as the percentage of voltage deviation from the nominal or rated voltage of 230 V was also examined. Figure 3-70 indicates the voltage distribution levels. For all three phases, most of the voltage recorded ranges between 229 V and 233 V, which aligns with the nominal voltage of 230 V. Even the few percentages of under or overvoltage do not cross the rated voltage to a significant number, which indicates a good quality of supply compared to the Mpale microgrid in Tanzania.

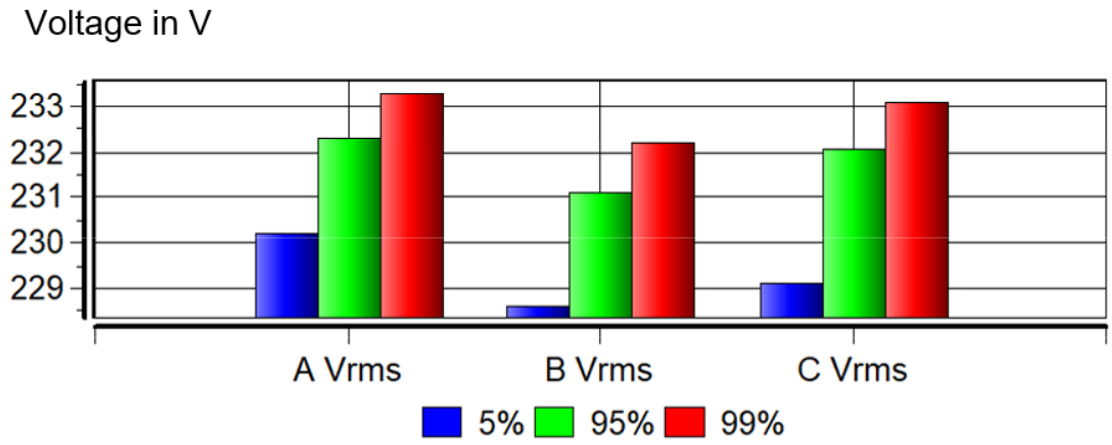

Figure 3-70: *Quality of supply represented as a percentage of voltage deviation from the rated voltage of 230 V for the three phases*

3.3.2.4. Activity Plots

Figure 3-71 and Figure 3-72 represent all the observed voltage dips and voltage transients at Bunjako Microgrid for the measured period (24th February 2022 to 4th March 2022). Unlike the Mpale microgrid in Tanzania, the voltage dips are higher between 07:00 am and 4:00 pm, the reason being most of the connected customers in phase B, which is the line with more customers composed of businesses which work or consume power within that stipulated time. The same applies to transients in Figure 3-72, which might be because most types of equipment prone to causing transients are operated in the said time range.

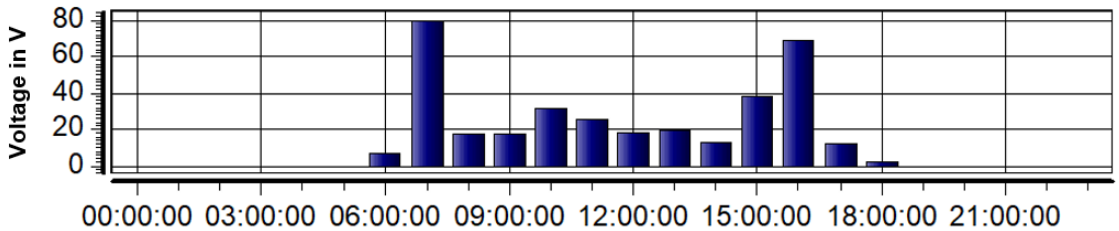

Figure 3-71: *Voltage dip events observed at Bunjako microgrid for a period from 24th February 2022 12:43:14.0 to 4th March 2022 10:05:00.0*

From Figure 3-71, no voltage swells or interruptions were found.

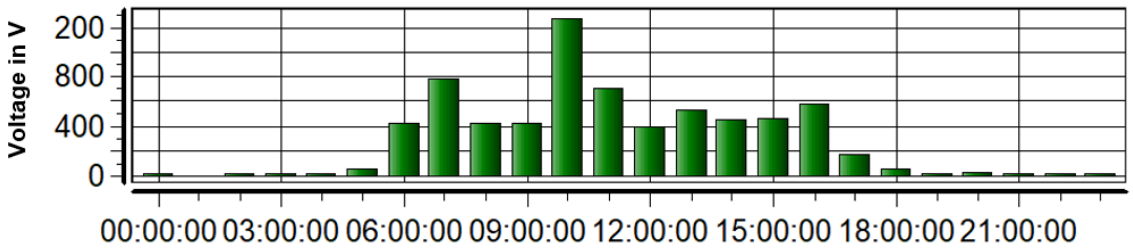

Figure 3-72: *Transients measured at Bunjako microgrid for a period from 24th February 2022 12:43:14.0 to 4th March 2022 10:05:00.0*

Table 3-11 summarizes the worst-case scenarios of all the events that occurred within the period of measurements with their respective magnitude, duration and how long they lasted. Out of all 349 voltage dip events, only phase B had the worst case, with the lowest magnitude of 154.5 V, which lasted for half a second. For the case of voltage transients, phase B had the most significant magnitude of 720.8 V, lasting for 0.002 seconds, followed by phase A with a magnitude of 711.6 V for 0.001 Sec. Phase C had no report of the worst case. No worst-case voltage interruptions and voltage swells were observed.

Table 3-11: *Worst-case scenario for activity plots showing the lowest magnitude and duration of all the observed events for a period from 24th February 2022 12:43:14.0 to 4th March 2022 10:05:00.0*

Out of 349 Total voltage dips				
Criteria	**Phase**	**Category**	**Data**	**Date Time**
Lowest Magnitude	B	INSTANTANEOUS	154.5 V, 0.519 Sec.	26/02/2022 13:10:42.80
	B	INSTANTANEOUS	188.0 V, 0.350 Sec.	04/03/2022 06:36:03.29
	B	INSTANTANEOUS	198.4 V, 0.029 Sec.	01/03/2022 15:07:10.30
	B	INSTANTANEOUS	199.1 V, 0.029 Sec.	26/02/2022 09:13:19.31
Longest Duration	B	INSTANTANEOUS	154.5 V, 0.519 Sec.	26/02/2022 13:10:42.80
	B	INSTANTANEOUS	188.0 V, 0.350 Sec.	04/03/2022 06:36:03.29
	B	INSTANTANEOUS	203.3 V, 0.040 Sec.	01/03/2022 07:57:34.07
	B	INSTANTANEOUS	205.5 V, 0.040 Sec.	02/03/2022 07:02:40.32
0 total VOLTAGE SWELLS				
0 total VOLTAGE INTERRUPTIONS				
Out of 6782 total VOLTAGE TRANSIENTS				
Largest Magnitude	B		720.8 V, 0.002 Sec.	01/03/2022 16:17:59.73
	B		716.0 V, 0.000 Sec.	04/03/2022 06:31:14.03

	A		711.6 V, 0.001 Sec.	25/02/2022 10:52:18.82
	B		711.0 V, 0.000 Sec.	04/03/2022 08:56:46.88

3.3.3. Lwak Microgrid Data

3.3.3.1. Demand Data

Demand data were also measured for the consumers in the Lwak microgrid in Kenya, as represented by Figure 3-73, Figure 3-74, Figure 3-75 and Figure 3-76. In analysing the recorded demand power for three phases representing distinct houses in Lwak, Kenya, it becomes evident that there are notable disparities in maximum power consumption across the phases. Phase 1 exhibits the highest maximum power demand at 3576 watts, followed by Phase 3 at 2300 watts, with Phase 2 displaying the lowest maximum power requirement at 1499 watts. These variations in maximum power consumption may be attributed to various factors, including differences in household size, usage patterns, and appliance types among the residences. Phase 1, potentially housing an enormous household or featuring more energy-intensive appliances, demonstrates the highest power demand.

In contrast, Phase 2 may represent a smaller household with fewer appliances, resulting in lower power consumption. Phase 3 falls between these extremes, suggesting a moderate power usage level. Understanding these distinctions provides valuable insights into household energy consumption patterns within the studied location, facilitating informed decision-making for energy management strategies and infrastructure planning. Table 3-12 shows power in the three phases plus their respective summation. Together, they consume maximum power of around 6 kW, as represented by Figure 3-77.

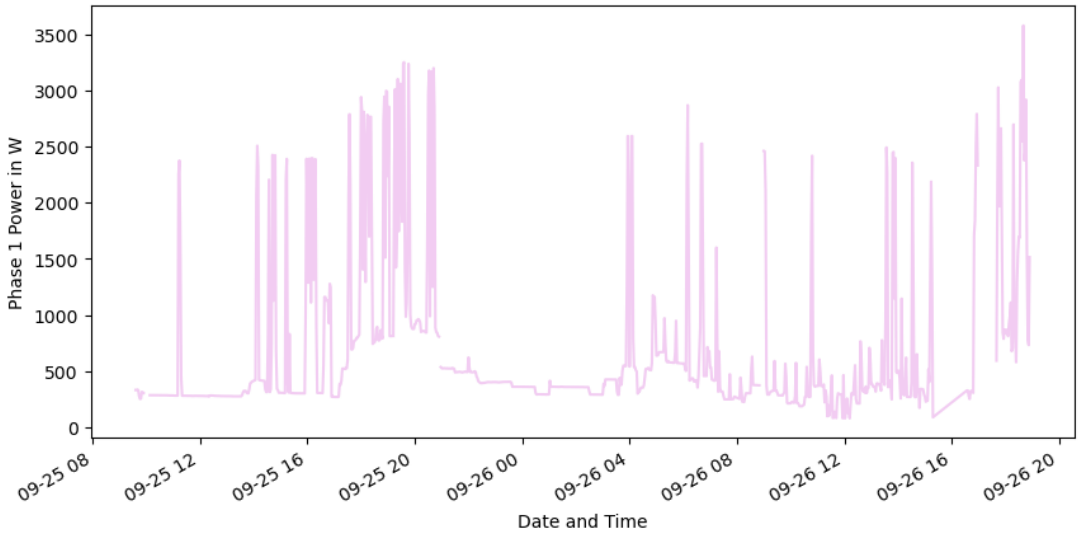

Figure 3-73: *Total power consumption at Lwak microgrid for Phase 1 for the period from 25th September 2023 and 26th September 2023*

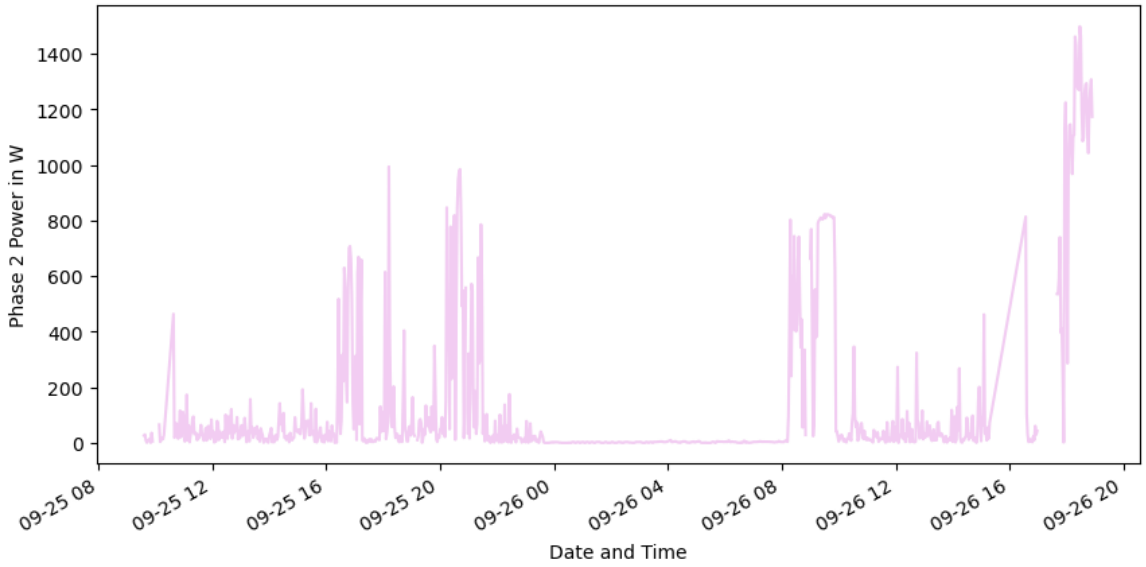

Figure 3-74: *Total power consumption at Lwak microgrid for Phase 2 for the period from 25th September 2023 and 26th September 2023*

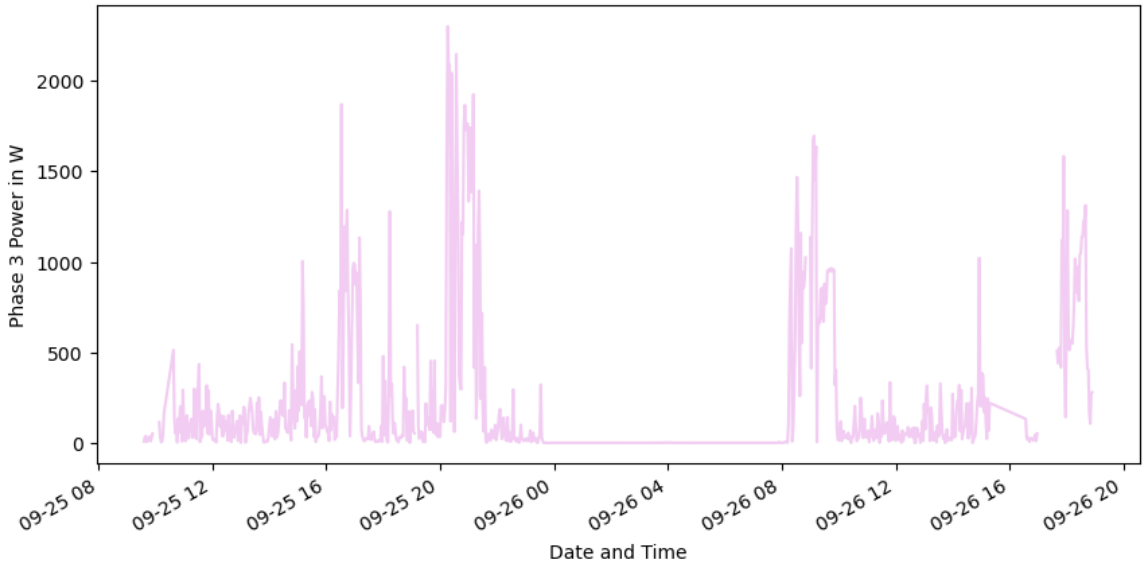

Figure 3-75: *Total power consumption at Lwak microgrid for Phase 3 for the period from 25th September 2023 to 26th September 2023*

Table 3-12: *Summary of demand power for all three phases (W) at Lwak microgrid for the period from 25th September 2023 to 26th September 2023*

	Maximum	Average	Minimum
Phase 1	3576.00	676.20	81.10
Phase 2	1499.00	125.02	0.00
Phase 3	2300.00	199.37	0.00
Total	6178.00	1000.59	102.15

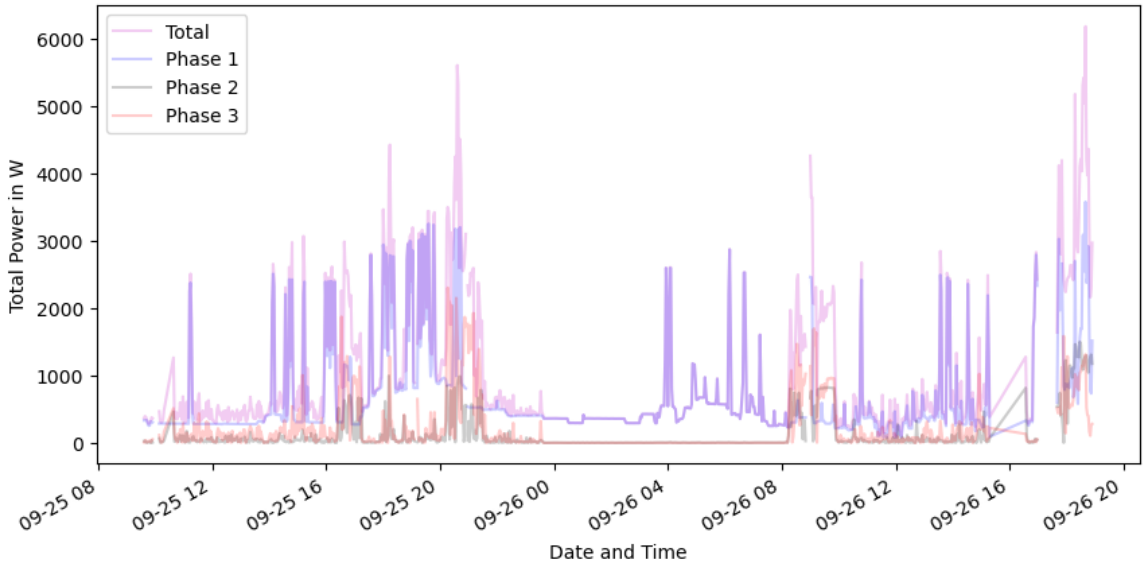

Figure 3-76: *Total Power consumption at Lwak microgrid for all three phases with their total for the period from 25th September 2023 to 26th September 2023*

Figure 3-77 and Figure 3-78 show the average per phase and total power consumed for the Lwak microgrid measured in two days. There are two prominent daily consumption peaks, 7 am - 9 am and 6 pm - 9 pm. The maximum measured power is considered as peak values are better for solar system and battery sizing applications.

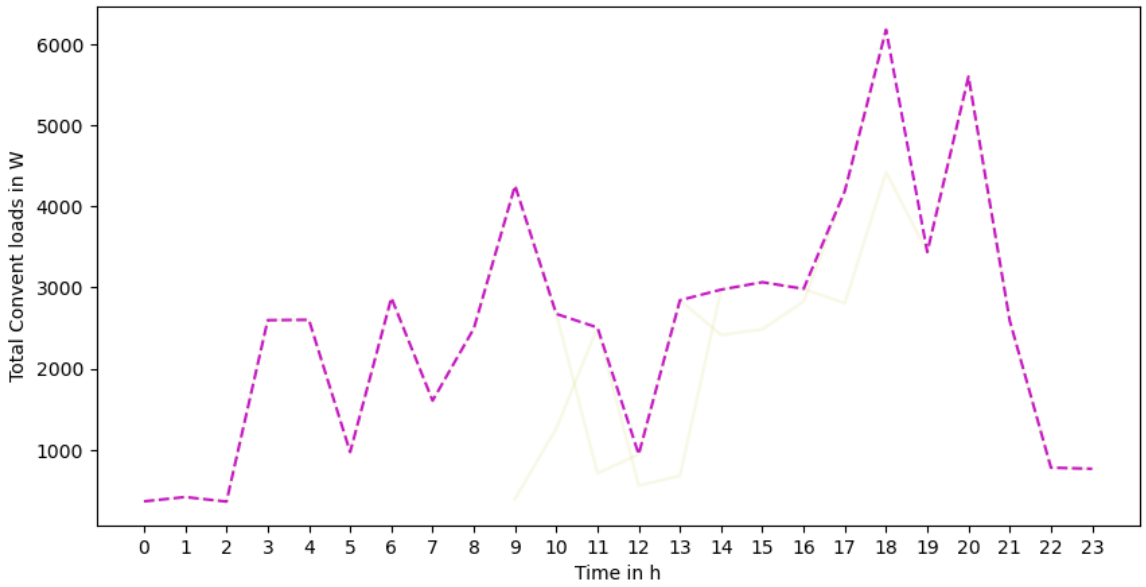

Figure 3-77: *Daily total convent power for the Lwak convent for the period from 25th September 2023 to 26th September 2023*

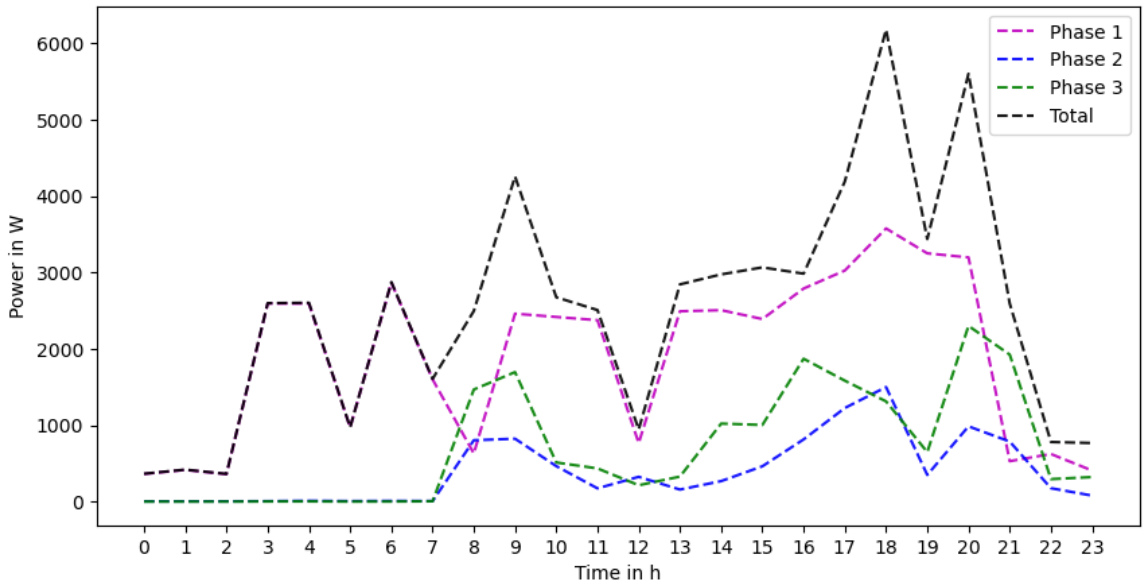

Figure 3-78: *Daily average power consumed for all three phases and their respective summation of all consumption at Lwak microgrid for the period from 25th September 2023 to 26th September 2023*

3.3.4. General observation from all the three microgrids

From the intensive data analysis for the selected microgrids, here are some of the problems generally facing the microgrids, which motivates the need for optimization and practical approach to take place as core of this study as it will further be explained in the following chapter of modelling and valuable case study.

a) Intermittent Power Supply:

   Due to unreliable electricity, there is a trend of frequent occurrence of power outages or intermittent power supply in the microgrid, negatively impacting daily life, businesses, and essential services. The unreliable power gave rise to reliance on Diesel Generators as a primary source of power in off-grid or weak-grid areas, which has the economic and environmental implications of relying on non-renewable and often costly fuel sources.

b) Variable Renewable Resource Utilization:

   The utilization of variable renewable energy resources like solar, in which its availability is widely affected by weather conditions, affects energy production and, subsequently, the microgrid's reliability.

c) Inefficiencies in Energy Dispatch:

The microgrids face challenges in meeting the demand during peak periods. Also, there are inefficiencies in the dispatch and scheduling of energy generation sources. For example, certain generators are underutilized.

d) Lack of appliance/ load control mechanisms: No initiatives of load control mechanisms or appliance scheduling based on their internal conditions to facilitate shifting usage to more energy production hours.

e) Inefficiency appliances used: Substantial energy wastage or suboptimal performance in many connected appliances due to a lack of knowledge of the importance of efficiency measures.

f) Costs and Affordability: The operators being forced to operate at a high price, e.g., using diesel generators when batteries could not support the system, gave rise to the economic burden of high energy costs on consumers.

3.4. Modelling and Simulation: Mpale Microgrid

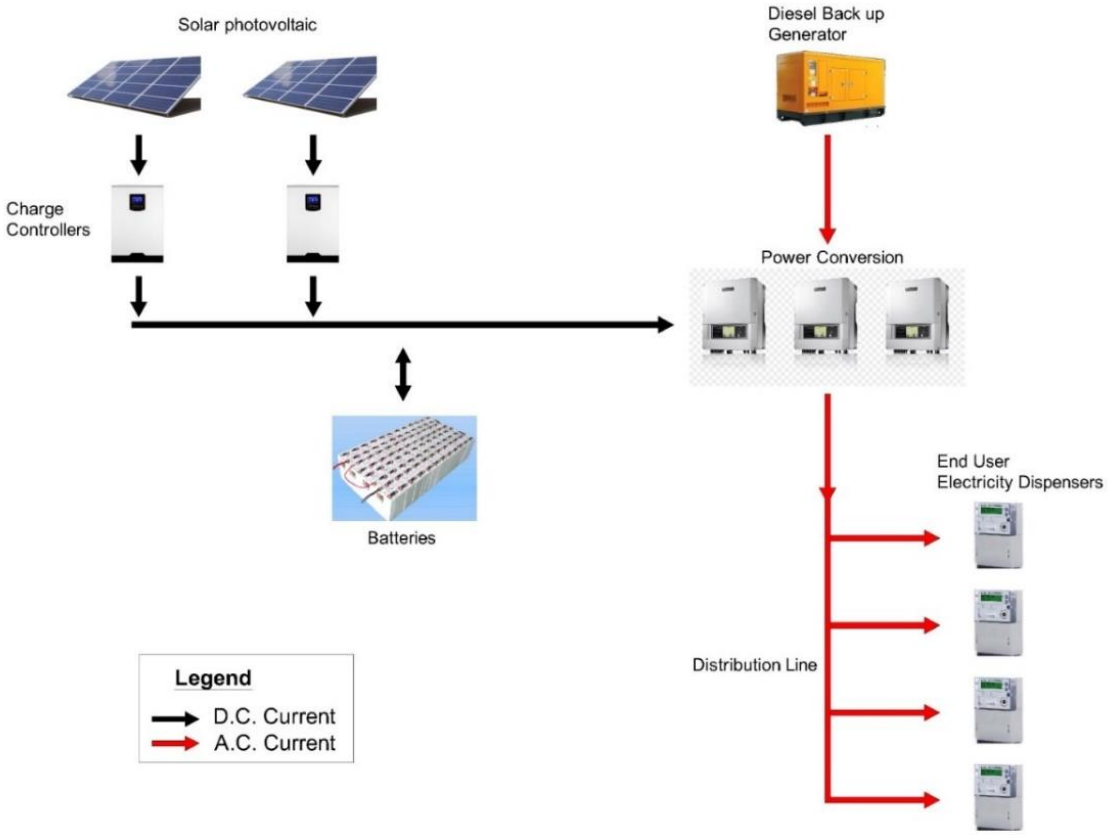

Figure 3-79: *Schematic layout of Mpale microgrid (Source: own diagram modified from Mpale microgrid diagram).*

3.4.1. Case 1: Minimising fuel cost through incentive provision

Figure 3-79 presents a schematic layout of the Mpale microgrid system. Eqn 3-5 provides the hourly electrical energy output of the PV (Tazvinga et al., 2014).

$$S_{PVt} = \eta_{PV} A_C I_{PVt} \qquad \textit{Eqn 3-5}$$

Where, η_{PV} = is the nominal STC efficiency of the solar panel used, A_C = front surface area, I_{PVt} = the hourly solar irradiance in kWh/hm^2 and S_{PVt} = Estimated (maximum) solar power from the solar generator in kW.

In this case, the objective was to minimise the conventional diesel generator's fuel cost by including an incentive-based demand response program.

$$F_1(t) = \sum_{t=1}^{T} \left(P_G(t)\right) \times C \qquad \textit{Eqn 3-6}$$

Where; $F_1(t)$ = Objective function in \$/kWh, t = Time, C = Cost in \$, and $P_G(t)$ = Generator power. The equation is subject to:

a) Power balance, i.e., total supply, should be able to meet demand.

$$P_D(t) - \sum_{n=0}^{N} X(t) = P_{SPV}(t) + P_B(t) + P_G(t) \qquad \textit{Eqn 3-7}$$

b) Generator limits

$$0 \leq P_G(t) \leq P_{GMax}(t) \qquad \textit{Eqn 3-8}$$

$$DR_G \leq P_G(t+1) - P_G(t) \leq UR_G \qquad \textit{Eqn 3-9}$$

Where, $P_D(t)$ = Demand power, $P_{SPV}(t)$ = Solar power produced, S_{PVt} = Maximum solar power generated, $P_B(t)$ = Battery power, $P_{GMax}(t)$ = Maximum generator power, DR_G = Minimum generator ramp–up rate and UR_G = Maximum generator ramp-up rate.

c) Power generated by the solar generator at any time t should not be negative or exceed the maximum estimated PV power.

$$0 \leq P_{SPV}(t) \leq S_{PVt} \qquad \textit{Eqn 3-10}$$

d) The battery's energy must always be between the minimum and maximum levels. Also, there should be a maintained energy balance for the start and end of the storage time.

$$E_{Bmin} \leq E_B(t) \leq E_{Bmax} \qquad \textit{Eqn 3-11}$$

$$E_{Bmin} = (1 - DOD) \times E_{Bmax} \qquad \textit{Eqn 3-12}$$

$$SOC_{Min} \leq SOC \leq SOC_{Max} \qquad \textit{Eqn 3-13}$$

Where, E_{Bmax} = Maximum battery energy, E_{Bmin} = Minimum battery energy, SOC = State of charge of battery, SOC_{Max} = Maximum State of charge of battery and SOC_{Min} = Minimum state of battery charge.

Therefore, the demand side model for minimisation of the conventional generator's fuel cost by including an incentive-based demand response program can be formulated using the following steps.

Let, $C(n, x)$ be the cost of customer n who shifted or switched off load by power x W and receives an incentive of y in monetary values, i.e. \$/kWh. The benefit to the customer will be;

$$F_2(\theta, x, y) = y - C(\theta, x) \qquad \textit{Eqn 3-14}$$

The utility function will be as follows;

$$F_3(\theta, x, y) = \rho x - y \qquad \textit{Eqn 3-15}$$

Where, ρ = saved cost of not supplying power when load x has been shifted or cut off.

The customer aims to reduce its electricity bills, and the utility seeks to maximize its benefit. Thus, Eqn 3-15 should be maximised using the following equation.

The cost of customers can be calculated as follows: (Alvarado & Fahriog, 2000)

$$C(\theta, x) = a_1 x^2 + a_2 x - a_2 x\theta \qquad \textit{Eqn 3-16}$$

Where, $a_1$and a_2 = cost coefficients, and θ = customer readiness to switch off loads during peak hours/customer preference parameter (It is a kind of probability/likelihood function).

The term $a_2 x\theta$ sorts customers by way of θ such that different θ results in different marginal costs ($\frac{dC}{dx}$). $a_1$and a_2 are assumed to be $1/2$ and 1, respectively. θ ranges between 0 and 1, with more θ value the less the cost of the customer (Alvarado & Fahriog, 2000).

For a customer to participate in a demand response program, they need to see the benefit of the load curtailment. Thus, it is necessary that:

$$F_3(\theta, x, y) \geq 0 \qquad \textit{Eqn 3-17}$$

$$F_3(\theta, x, y) = \sum_{t=1}^{T} \sum_{n=1}^{N} \rho x(n,t) - y(n,t) \qquad \textit{Eqn 3-18}$$

T is the total time period, and N is the total number of customers.

Eqn 3-17 and Eqn 3-18 constraints are such that:

a) At any time, the total incentive given to all customers should not exceed the budget set by the utility/utility budget (UB).

$$\sum_{t=1}^{T} \sum_{n=1}^{N} y(n,t) \leq UB \qquad \textit{Eqn 3-19}$$

b) The load to be shifted or curtailed by the individual customer within the time horizon should be within the limit of the loads that can be shifted at that particular time. x ≤ acceptable non-critical loads and SL=Shiftable loads.

$$\sum_{t=1}^{T} X(n,t) \leq SL(n) \qquad \textit{Eqn 3-20}$$

or

$$P_{SPV}(t) + P_B(t) + P_G(t) \geq Baseline \qquad \textit{Eqn 3-21}$$

There are two objective functions involved in this case, one being the minimization of generator fuel costs $F_1(t)$ and the second one is the maximization of the utility's benefit $F_3(\theta, x, y)$.

Therefore, the overall demand side equation for case 1 becomes:

$$Min\ w \sum_{t=1}^{T} \big(P_G(t)\big) \times C + (1-w) \sum_{t=1}^{T} \sum_{n=1}^{N} \rho x(n,t) - y(n,t) \qquad \textit{Eqn 3-22}$$

Where w is the objective function weight.

3.4.2. Case 2: Economic and emission dispatch of a microgrid with multiple diesel generators

Economic and emission load dispatch intend to operate online generation units economically at minimal emission levels while satisfying power demand and operational constraints (Trivedi et al., 2018). The combined economic and emission problem was formulated as a single optimisation problem (Eqn 3-23).

$$\text{Min F} = \sum_{\text{i}=1}^{\text{N}} (\text{F}_\text{i}(\text{P}_\text{i}), \text{E}_\text{i}(\text{P}_\text{i})) \qquad \textit{Eqn 3-23}$$

The generator fuel cost is defined as a quadratic function (Eqn 3-24).

$$F_1 = \sum_{i=1}^{N} \left(x_i {P_i}^2 + y_i P_i + z_i\right) \qquad \textit{Eqn 3-24}$$

Where, F_1 = Total fuel cost in $\$/h$, N = is the number of generators, P_i = Active power generation of the *i*-th generator, x_i = Cost coefficient of *i*-th generator in $\$/MW^2h$, y_i = Cost coefficient of *i*-th generator in $\$/MWh$, and z_i= Cost coefficient of *i*-th generator in $\$/h$ (independent of power or energy delivered).

Operating diesel generators results in the emission of various pollutants, such as carbon dioxide (CO_2), nitrogen oxide (NO), and Sulphur dioxide (SO_2) (S Krishnamurthy & Tzoneva, 2012; Palanichamy & Babu, 2008). Thus, the emission minimisation function is added to the optimisation problem to achieve clean energy's universal goal (Elattar, 2018).

$$F_2 = \sum_{i=1}^{N} \left(a_i {P_i}^2 + b_i P_i + c_i\right) \qquad \textit{Eqn 3-25}$$

Where, F_2 = Total Emission value in kg/h, N is the number of generators, P_i = Active power generation of the ith generator, a_i = Emission coefficient of ith generator in kg/MW^2h, b_i = Emission coefficient of ith generator in kg/MWh, and c_i= Emission coefficient of ith generator in kg/h.

The emission equation is subject to power balance (i.e., total supply should be able to meet demand). The equation is also used to calculate the deficit that the generators should supply. The power balance of the Mpale microgrid indicates that when the demand exceeds the energy generated by the PV system plus the energy stored in the ESS for an hour, the dispatchable generators supply the deficit power.

$$P_D(t) = P_{SPV}(t) + P_B(t) + \sum P_i(t) \qquad \textit{Eqn 3-26}$$

Where, $P_D(t)$ = Total demand at any time t; in kW, $P_{SPV}(t)$ = Total solar power generated at time t and $P_{SPV}(t)$ = Total battery power supplied at time t.

Generator limits:

$$P_{iMin}(t) \leq P_i(t) \leq P_{iMax}(t) \qquad \textit{Eqn 3-27}$$

Where, $P_{iMin}(t)$ = Minimum value of real power allowed at generator *i and* $P_{iMax}(t)$ = Maximum value of real power allowed at generator *i.*

Power generated in kW by the solar generator at any time t should not be negative or exceed the maximum forecasted PV power.

$$0 \leq P_{SPV}(t) \leq S_{PVt} \qquad \textit{Eqn 3-28}$$

The energy and power of the battery must always be between the minimum and maximum levels. Also, there should be a maintained energy balance at the start and end of storage time.

$$E_{Bmin} \leq E_B(t) \leq E_{Bmax} \qquad \textit{Eqn 3-29}$$

$$SOC_{Min} \leq SOC \leq SOC_{Max} \qquad \textit{Eqn 3-30}$$

The overall objective function combines economic and emission problems, which are correlated using the penalty factor w_i in $\$/kg$. The penalty factors used include Max – Max, Min – Max, Min – Min, average, and common (Senthil Krishnamurthy & Tzoneva, 2011; Thakur et al., 2006). The Min – Max price penalty has been proven to yield a minimum cost of the combined function (Eqn 3-31) and thus was adopted in this study (S Krishnamurthy & Tzoneva, 2012).

$$w_i = \frac{\left(x_i {P_{i,min}}^2 + y_i P_{i,min} + z_i\right)}{\left(a_i {P_{i,max}}^2 + b_i P_{i,max} + c_i\right)} \qquad \textit{Eqn 3-31}$$

Table 3-13 provides the generator's cost and emission coefficients of the system components, which are borrowed from Jakhrani et al., (2012) and Nwulu & Xia, (2017). All the generators' minimum power limits start at zero.

The overall multi-objective function F becomes;

$$F = \sum_{i=1}^{N} (F_1 + w_i F_2) \qquad \textit{Eqn 3-32}$$

Where, F_1 = Total fuel cost in $\$/h$, penalty factor w_i in $\$/kg$, and F_2= Total Emission value in kg/h.

Table 3-13: *Generator cost and emission coefficients of the selected generators with their maximum power (Traoré et al., 2018)*

i	Emission coefficients			$P_{i,Max}$	Cost coefficients		
	x_i	y_i	z_i		a_i	b_i	c_i
1	0	0.511	0.1298	2	0	1.22	0.32
2	0	0.569	0.155	3	0	1.46	0.383
3	0	0.694	0.181	4	0	1.70	0.446
4	0	0.791	0.206	5	0	1.94	0.509
5	0.04	0.3	0	9	0.04	3.43	0.60

3.5. Modelling and Simulation: Bunjako microgrid

A MATLAB/Simulink-based model was implemented to simulate the Bunjako microgrid. A microgrid model with possible shiftable loads was simulated for 24 hours, starting from midnight and running for the next 24 hours.

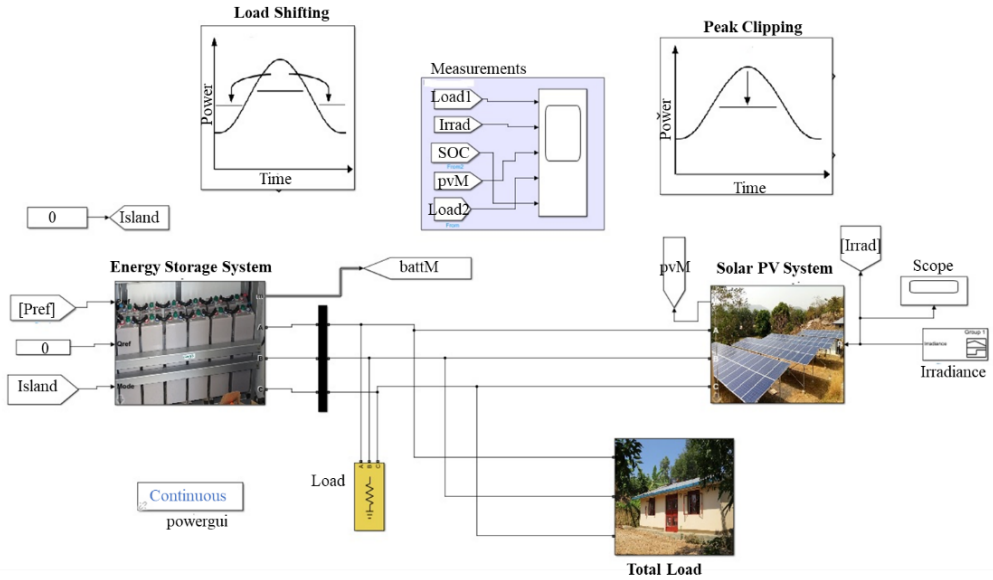

Figure 3-80: *Simulink model of the Bunjako microgrid showing all sources and loads with their control strategies (load shifting and peak clipping) [Images: (Weetch, 2021)]*

Figure 3-80 shows the block diagram of the model in Simulink, in which a three-phase system is connected to a battery and solar PV with consumer loads. The irradiation measurement and battery state of charge measurements were also linked. In the Bunjako microgrid, load shifting and peak clipping used two demand-side management subsystems.

Bunjako's total loads were divided into deferable and non-deferable loads to enhance switching on/off loads during peak and off-peak hours. Table 3-14 represents household appliance categories described by Nawaz et al., (2020). Based on a study conducted in Bangladesh, the related on-and off-times were noted to have characteristics similar to those in Africa. Thus, the on and off times were used for the simulation in the Bunjako microgrid to decide the rating of deferrable loads to be either switched on/off or shifted.

It is noted that the load profiles will not be the same as no two appliances with the same rating can be used for the same program all the time (Degefa et al., 2018). In addition, Denholm et al., (2012) estimated shiftable demand by subtracting base demand from its peak for the days of almost similar characteristics. This background gave the basis for evaluating the deferable load profile in this study.

Table 3-14: *Household appliances categories, ratings and hours of operation (Nawaz et al., 2020; Panda et al., 2022)*

Appliance Category	**Appliance Name**	**Power rating (kW)**	**Hours of operation/day (h)**
Shiftable interruptible	Personal computer	0.03	4
	Microwave	1.5	0.5
	Pump (41m/75LPM)	0.9	4
	Blender	0.3	4
Shiftable non-interruptible	Iron	1	2
	Washing machine	0.5	2
Consistency	Refrigerator	0.3	6
	Fan	0.05	8
	Water Purifier	0.5	9

Figure 3-81 represents the simulation of the two load categories in Simulink. Some loads can be shifted only for a certain amount of time, e.g., freezers. The duration of possible shifting depends on the actual state of the freezer (temperature of goods).

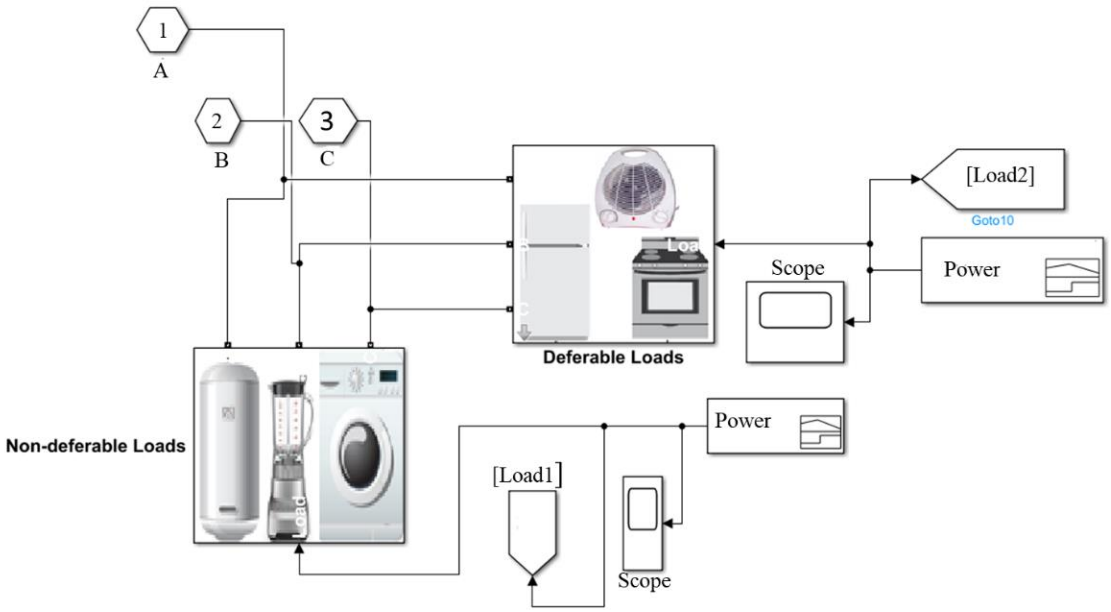

Figure 3-81: *Simulink model of deferable and non-deferable loads [Images: (Lundstrom et al., 2018)]*

Figure 3-82 shows the energy inlet and outlet from the microgrid, including the battery's state of charge (SOC).

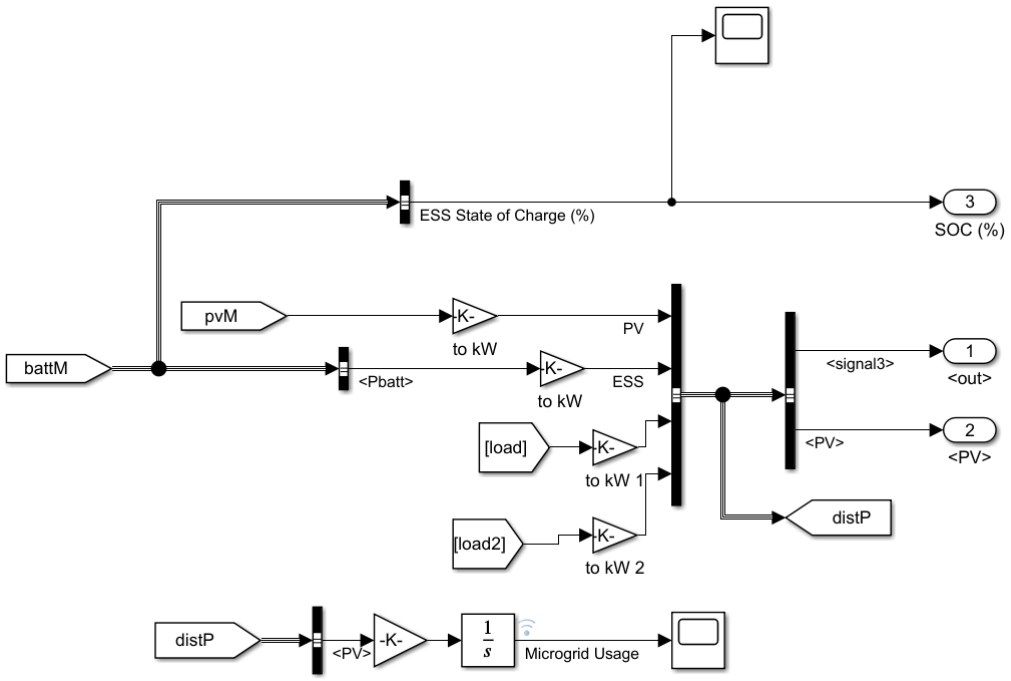

Figure 3-82: *Block diagram of energy inlets and outlets to and from the microgrid*

From Figure 3-83 and Figure 3-84, the two DSM strategies (load shifting and peak clipping) are simulated. The approaches make use of ANN to achieve the results. The use of switches allows control of the on and off time of the shiftable loads.

The input data provided to the ANN control scheme are the consumer usage and time horizon of the day (24 hours). The overall horizon is 24 hours. Based on this, the ANN returns generated signal pre-defined deferable loads to either switch off/on or shift to another time of the day, depending on the solar power generated. This is in the case of peak clipping and load shifting, respectively. Philipo et al., (2022) further explain the ANN approach.

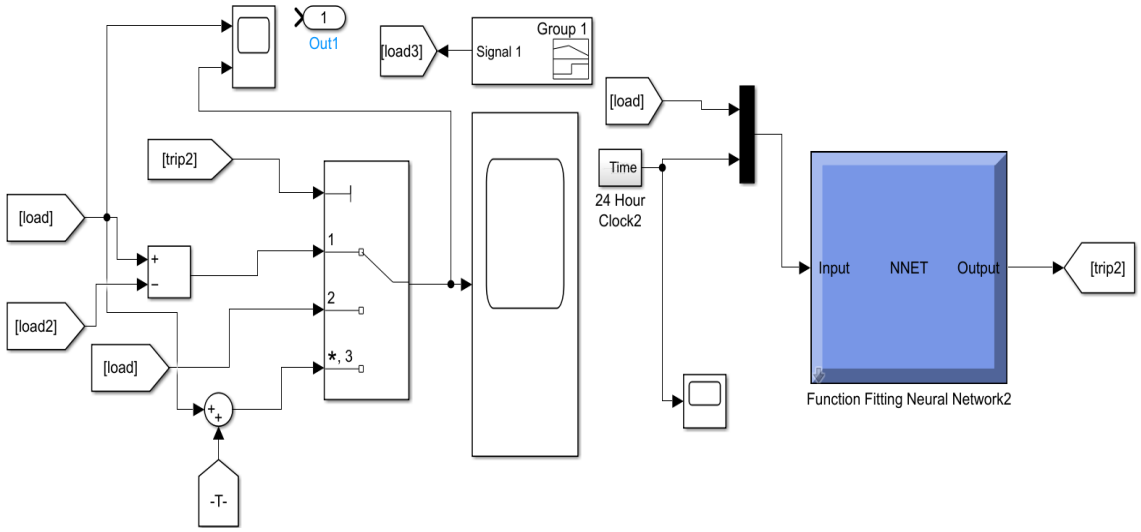

Figure 3-83: *Simulink energy management model through Load Shifting (LS) using a neural network*

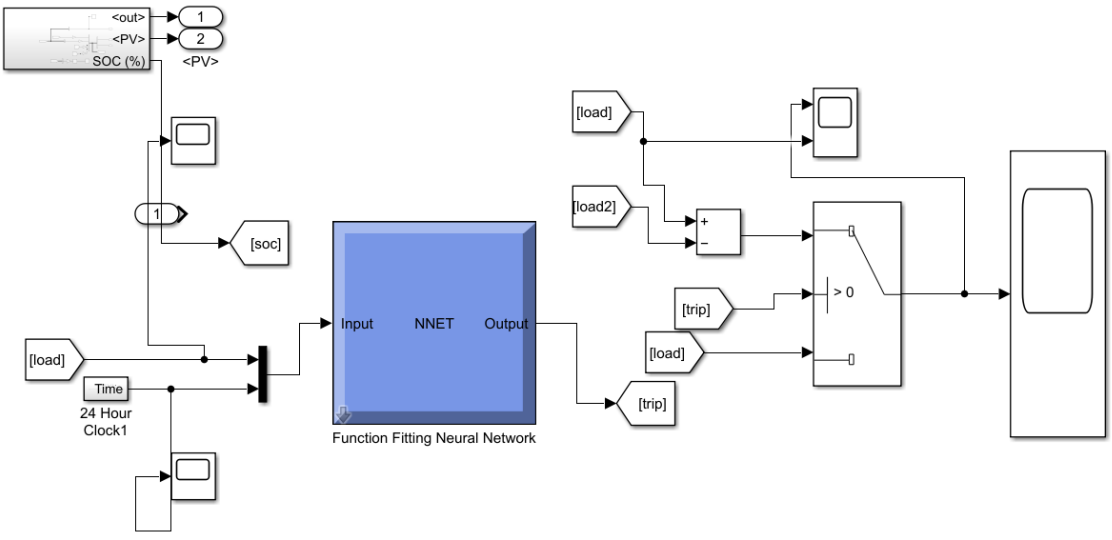

Figure 3-84: *Simulink energy management model through Peak Clipping (PC) using a neural network*

3.6. Practical case study (Lwak Microgrid)

Based on the modelling and simulation of Mpale and Bunjako microgrids, it was deduced that most East African microgrids have similar attributes in electricity consumption. Most microgrids in rural areas consist of medium home appliances such as fridges, freezers, and water pumps. In addition, most inhabitants use inefficient appliances (i.e., Mpale microgrid appliances). Thus, the Lwak microgrid was selected to be a practical case study for several reasons:

a) Ease accessibility to the site as part of the Art-D project. Thus, measurement can be easily conducted,
b) Different practical improvements can be achieved to the microgrid,
c) The grid has a good relativeness as the microgrid is composed of both shiftable and non-shiftable loads; thus, demand-side management is possible.

Demand side management of the Lwak microgrid was conducted to achieve the following:

a) Appliances' control of usage time and temperature-based control
b) Energy efficiency demand-side management analysis due to implications on the power quality of the microgrid.

3.6.1. Motivation for Energy Efficiency Demand side management

Improved energy efficiency in home appliances is vital for guaranteeing sustainable and clean energy usage. The study aimed to analyse and explore energy efficiency for home appliances in the Lwak microgrid. The adaptation of energy-saving appliances was an essential strategy for achieving energy efficiency.

The study delved into an energy audit of the inhabitants by observing their consumption profile and appliances, particularly the cooling appliances, to introduce a model for assessing energy efficiency possibilities. Furthermore, efficient and non-efficient devices were also observed to analyse potential savings achievable through the adaptation of energy-saving appliances. Finally, based on the results, the microgrid best practices were recommended, promoting economic savings.

3.6.2. Current Electricity Usage

A list of all appliances used in the Lwak convent has been presented (Table 3-3). Power consumption in percentage for all appliances was prepared and is shown in Figure 3-85.

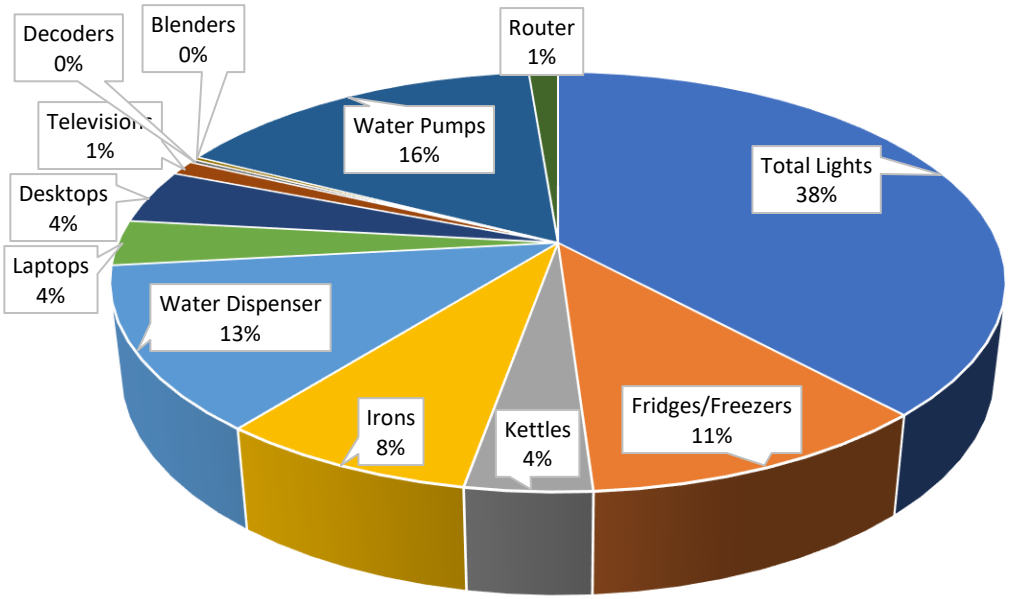

Figure 3-85: *A pie chart showing the hourly load composition of appliances in Lwak*

Lightning recorded the highest power consumption. Apart from water pumps, cooling appliances (i.e., fridges and freezers) consume a reasonable percentage of power. Thus, attention was given to fridges and freezers as their consumption is continuous compared to water pumps and dispensers. Water pumps' power consumption behaviour proved an excellent candidate for load-shifting demand-side management. In addition, PV pump applications are relatively resilient to power outages due to the use of a sufficient water tank, as long as they do not last extremely long. Demand side management also appears advantageous due to the water tank, where pumped water can be easily stored, especially for load-shifting applications.

3.6.3. Fridge/Freezer temperature control with Shelly Devices and Node-RED

3.6.3.1. Assumptions

Several assumptions were considered in the study;

a) All fridges and freezers kept the same type and quantity of food, thus having similar specific heat capacities. All three houses are inhabited by nuns who conform to similar lifestyles, i.e., cooking and eating the same food.
b) The effect of door openings has been neglected.
c) The ambient temperature effects were not considered.

3.6.3.2. Temperature threshold set

After data collection, the temperature inside fridges and freezers was monitored and analysed to observe their minimum and maximum operating temperatures before initiating control. The minimum and maximum temperature thresholds were set depending on the operating temperature to avoid food spoilage.

From the literature, the recommended fridge temperature to prevent food spoilage is 1.1℃ to 4.4℃ (Kakande et al., 2023), while a temperature of 2℃ to 4℃ is recommended for ready-to-eat foods (He et al., 2017). Other sources reported 5℃ to 8℃ as refrigerator temperature thresholds (Refrigeration, 2019). For freezers, Postnikov et al., (2019) recommended temperature as below -12℃, while Tran et al., (2015) stated the temperature to be below -18℃. Table 3-15 shows the temperature of all the fridges and freezers plus their set temperature thresholds.

It is worth noting that consumption may increase with increasing external temperature; thus, placing a fridge/freezer in a cooler environment may result in lower energy consumption. In addition, it is recommended that consumers not store their refrigerators or freezers in areas that will experience temperatures below 55°F or above 90°F (Tiffany Sue Burgess, 2015).

Figure 3-86 shows a flow chart of load control using shelly devices. After the fridge/freezer connection to the intelligent socket, instant temperatures are monitored using the IoT arrangements and compared with the thresholds set. When the temperature lies below the threshold minimum, the fridge will be turned OFF, and when the temperature increases to above or equal to the threshold maximum, the fridge/freezers are switched back ON to avoid food spoilage.

Table 3-15: *Minimum and maximum recorded temperatures for fridges and freezers with their respective minimum and maximum thresholds for temperature control*

	Temperatures /℃			
	Minimum	Room Temp	Threshold Minimum	Threshold Maximum
Freezer 1	-16	28.4	-15	-12
Fridge 2	-15.9	29.1	-15	-12
Freezer 3	-14.4	25.9	-14	-12
Fridge 4	-23.8	29.7	-18	-12
Freezer 5	-14.2	36.2	-14	-12

	Temperatures /°C			
	Minimum	Room Temp	Threshold Minimum	Threshold Maximum
Fridge 6	-16.1	30.4	-15	-12
Freezer 7	-14.4	32.4	-14	-12
Freezer 8	-25.2	28.6	-18	-12

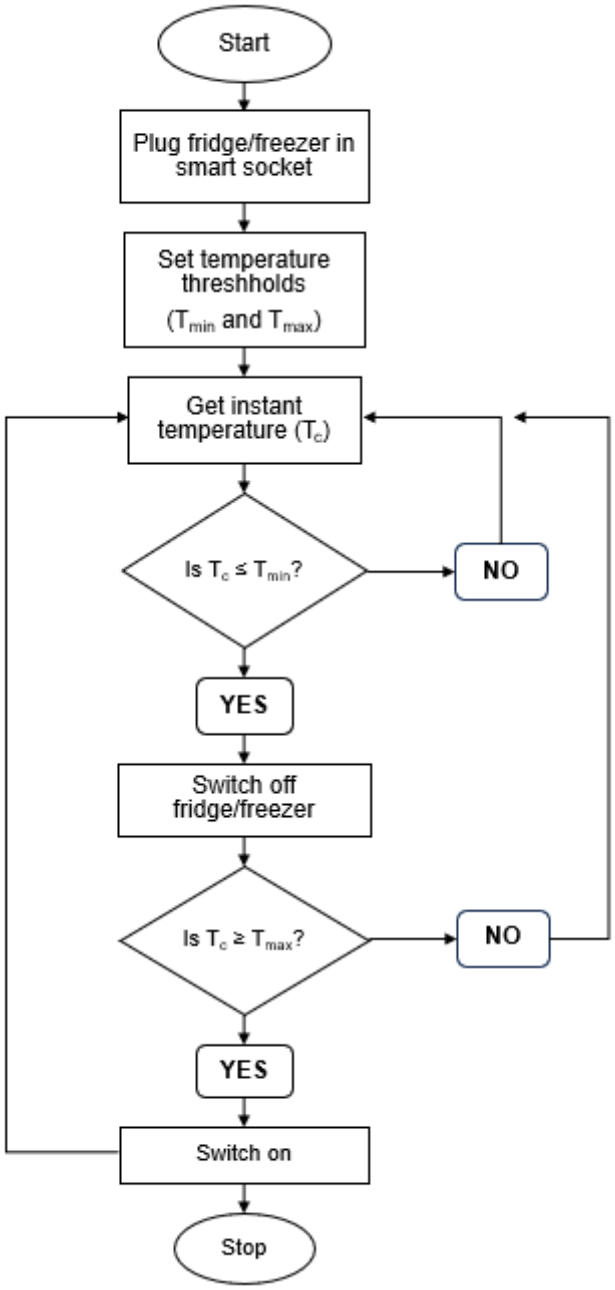

Figure 3-86: *Flow chart of the cooling appliances control mechanism of switching ON and OFF appliances based on temperature*

CHAPTER FOUR

4. Results and Analysis

4.1. Results and Analysis (Mpale Microgrid)

4.1.1. Case 1: Minimising fuel cost through incentive provision

With reference to Figure 3-28, medium peaks were observed between 00:00 and 05:00 hrs as most residents switched on storage appliances (i.e., fridges and freezers) as per the survey. Morning peaks were not significant considering the lifestyle in the village, where most engage in farming activities early in the morning. Highest peaks observed from 18:00 to 22:00 hours were attributed to consumption by many appliances (TV, cooking, fans) switched as household members were at home. Gradually, the peaks decline towards 24:00 hours up to 07:00 hours, where only light bulbs and fans remain on. Phase 2 recorded the maximum power consumption through the 24-hour interval, attributed to the type of customers connected (i.e., households and businesses).

Figure 4-1 shows the average daily demand and maximum potential solar power based on measured irradiance. The mismatch between the demand and solar power produced signifies that solar generation cannot meet demand growth, especially during peak hours. Solar PV shaves demand in the middle of the day, while most peak demand occurs later in the evening and early morning. This suggests that solar power requires supplementing with energy storage and backup generation to meet the peak demand.

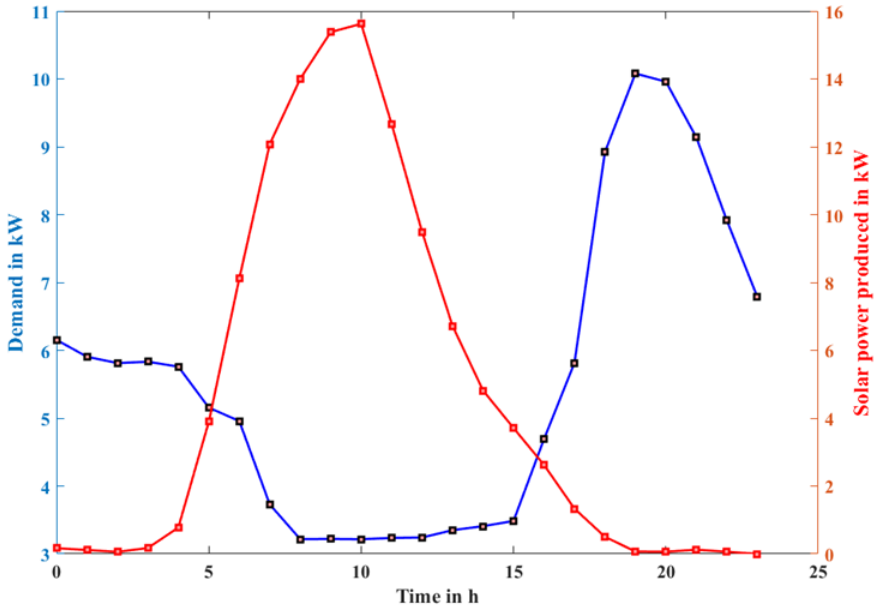

Figure 4-1: *Total average daily demand vs maximum daily solar power produced at Mpale microgrid*

Figure 4-2 summarizes the optimal power curtailed by each customer group. More curtailment is observed during peak hours and less in the afternoon when there is enough solar production. The amount of power curtailed is proportional to the incentive received, as Table 4-1 illustrates. Power curtailment may be achieved by scheduling responsive loads from the customer end. Results agree with Jasim et al., (2022), where optimal dispatch was achieved based on appliance scheduling. Furthermore, customers connected to phase two present more power reduction since most are suitable candidates for DSM.

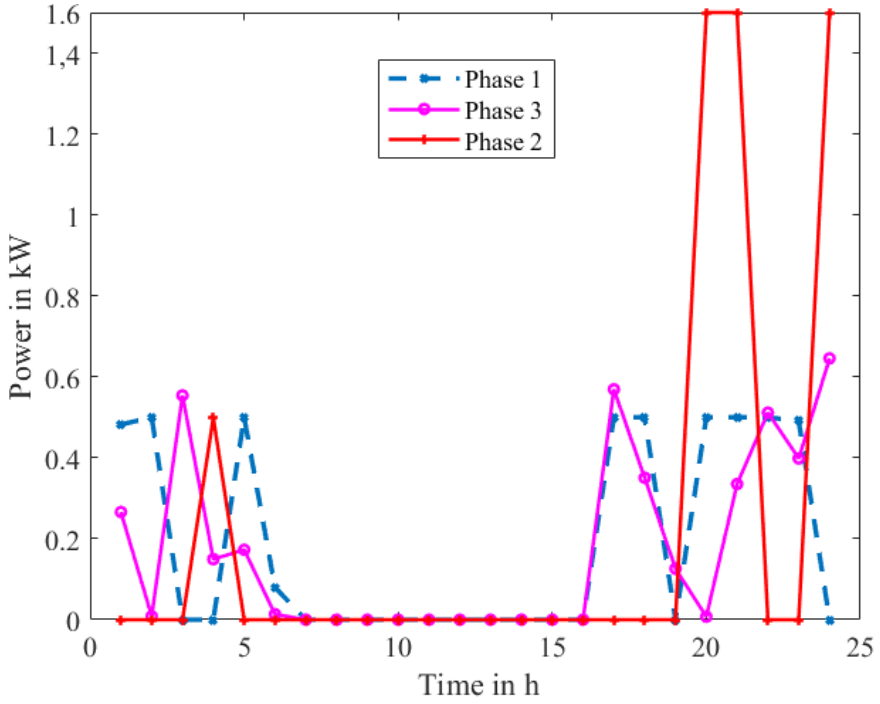

Figure 4-2: *A plot showing total daily customer power curtailed after receiving incentives*

Table 4-1: *Total daily energy curtailed and incentive received in US dollars (1 USD = 2515 Tanzania shillings)*

	Energy curtailed (kWh/day)	**Incentive received ($/day)**
Customers in Phase 1	3.94	3.40
Customers in Phase 2	10.62	4.95
Customers in Phase 3	4.07	3.75
Total	**18.63**	**12.10**

Figure 4-3 results provide a viewpoint on the microgrid operation. Throughout the 24-hour interval, the solar generator operates with a conventional generator and battery support. Conventional generators and batteries reduce their power output when solar generators begin to work. During the peak period, the battery works in the discharge state supported by the generator. The battery is charged or out of operation in the valley periods. The

charging and discharging modes of the battery depend on its state of charge (SOC) value (Xu et al., 2020).

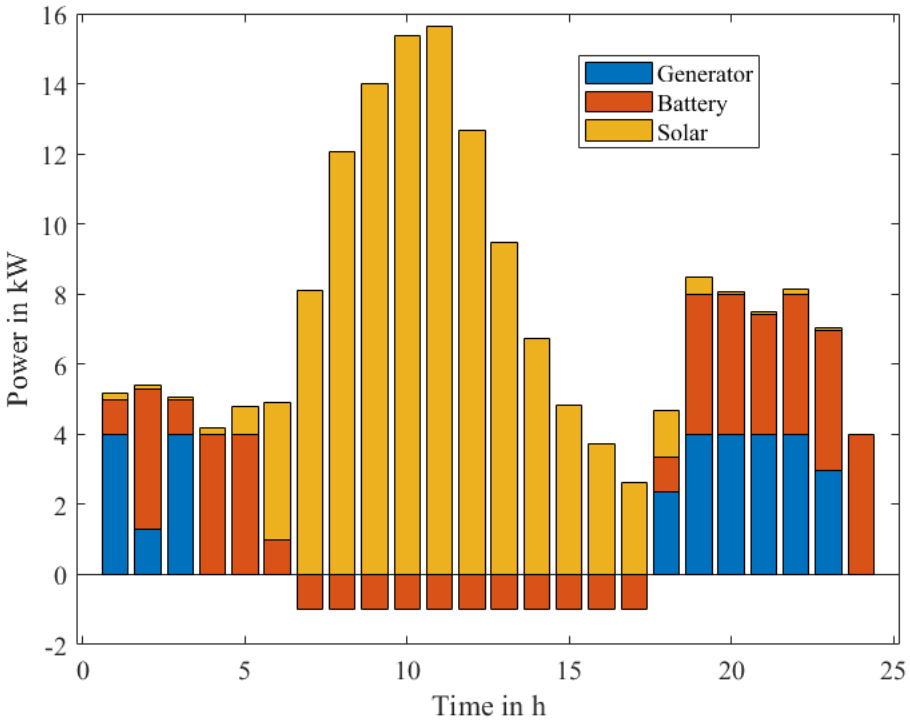

Figure 4-3: *Average daily output power from a solar generator, diesel generator and battery averaged from data measured for a period of 5 years at Mpale microgrid*

Figure 4-4 shows the load profile before and after DSM. Customers can curtail some loads during peak hours through incentives, resulting in peak reduction. It is observed that during the evening peak, a significant amount of power curtailment is possible with higher incentive values. Summing up per hour daily demand before and after the proposed strategy gives an overall saving of around 11.02%. Higher incentives resulted in a higher willingness to save. However, it should be noted that without proper incentive selection, the utility may suffer revenue loss (Philipo et al., 2020). Hence, mutual benefit among all microgrid actors should be considered for a successful DSM approach (Pacheco & Foreman, 2017).

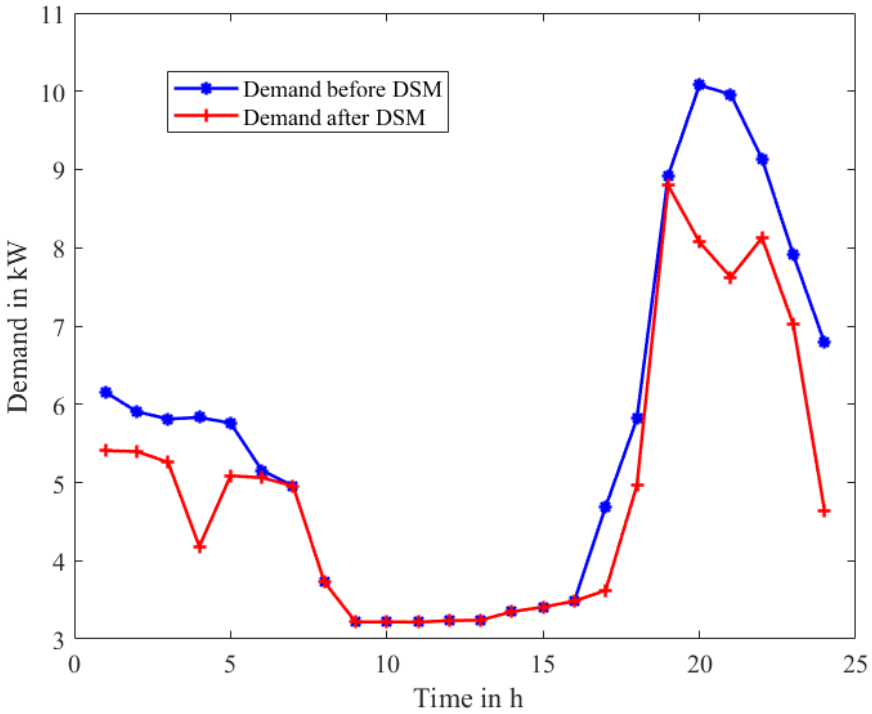

Figure 4-4: *Load profile before and after demand side management*

4.1.1.1. Sensitivity Analysis

The base case is assumed when the operator assigns equal weights to the two objective functions (Tazvinga et al., 2014). However, in any multi-objective optimisation, studying and analysing the impact of different weight preferences on the objective function and how they influence the optimal solution is crucial. The weight w varies from 0 to 1. In this case, the study when w = 0 implies that the objective is to maximise the operator's benefit without minimising fuel cost. When w = 1, more attention is paid to minimising fuel cost rather than maximising utility benefit. Table 4-2 explains the sensitivity of the operator decision to objective function preference. Utility incurs more cost of paying incentives to the customer at less power curtailment when they focus only on neglecting the concept of demand response. Also, less power is saved when no attention is paid to minimising the generator fuel cost. The best microgrid operation is achieved when equal weight is given to both demand response and generator fuel minimisation. This observation is also supported by Figure 4-5.

Table 4-2: *Effect of objective function weights (w) on different parameters of the microgrid*

	w = **0.00**	w = **0.50**	w = **1.00**
Total energy curtailed (kWh)	19.48	18.63	15.77
Total incentive received ($)	16.10	12.10	13.03

	w = **0.00**	w = **0.50**	w = **1.00**
Total energy from generator (kWh)	24.66	24.08	28.85
Total energy supplied by a battery (kWh)	49.82	52.68	49.98

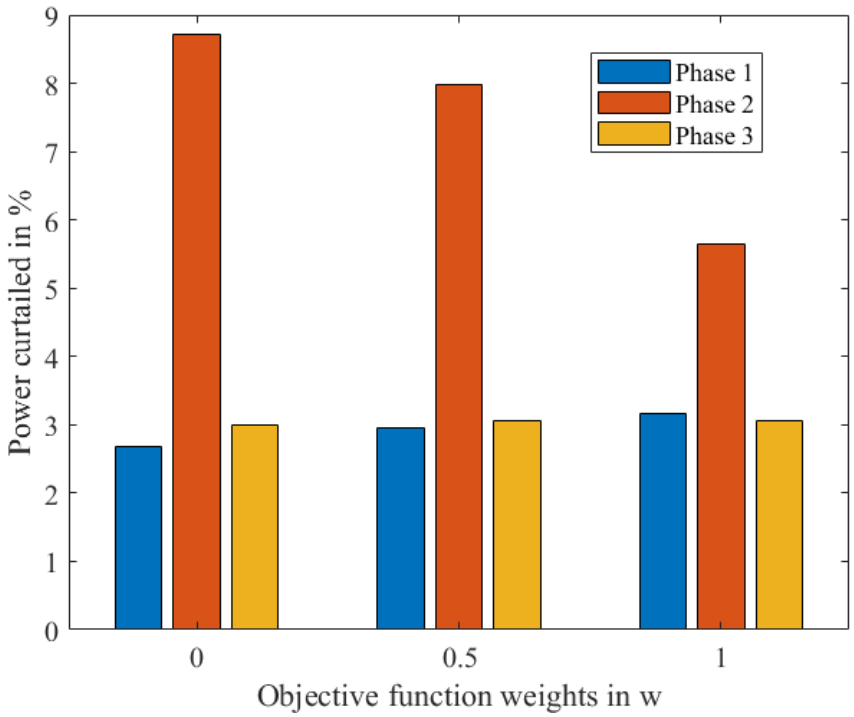

Figure 4-5: *Percentage of power curtailed at different weight values*

4.1.2. Case 2: Economic and emission dispatch of a microgrid with multiple diesel generators

The per-hour daily load profile, presented in Figure 4-6, determines power supply requirements. The profile is characterised by morning peaks (02:00 – 06:00) and evening peaks (20:00 – 23:00) hrs. These can be attributed to people's daily routines, which demand more energy in the morning when they wake up and late evening when they return home. Figure 4-7 shows the overall power balance in the microgrid. The negative power of the battery implies charging, which takes place more in the afternoon when solar power is abundant with minimal load. Battery discharges to supply loads when solar is not available.

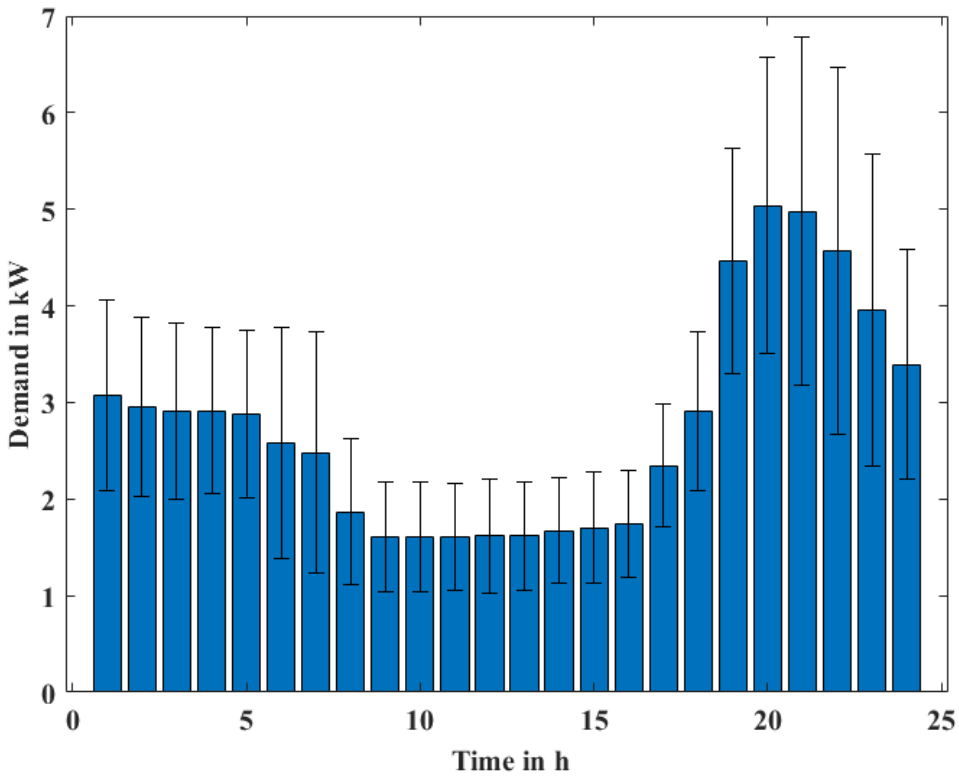

Figure 4-6: *Per-hour average daily load demand profile of Mpale microgrid averaged from data recorded over 5 years period*

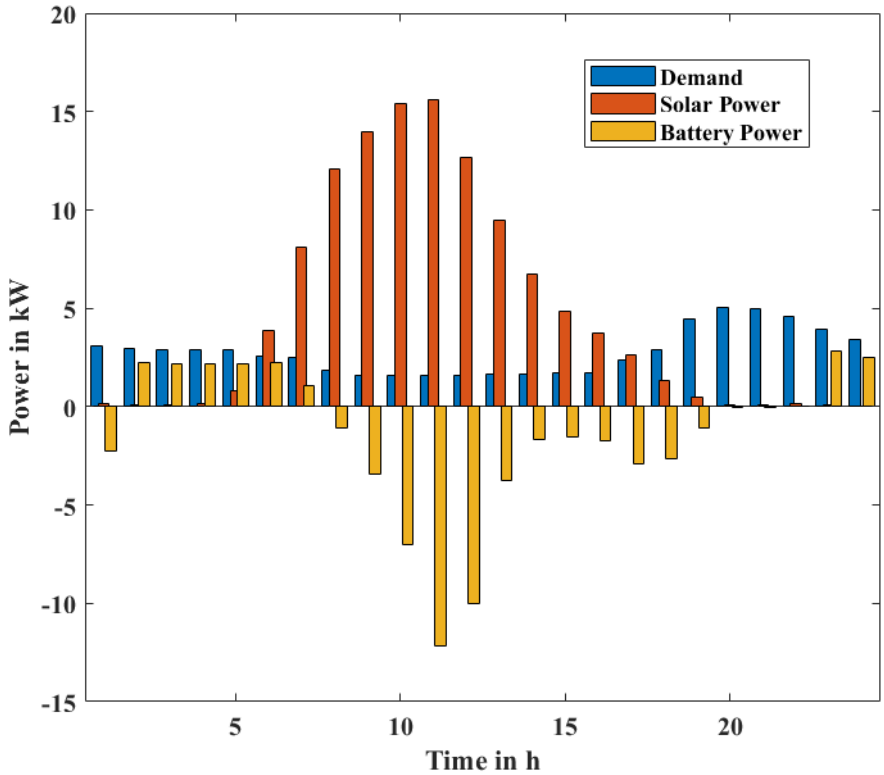

Figure 4-7: *Average power produced by solar photovoltaic and battery storage to meet power demand of Mpale microgrid (Power balance of the system)*

Different arrangements of five generators were used as dispatchable sources. GA and PSO algorithms were used to optimise the selection of generators in various system configurations, i.e., which generators or generators should be ON to minimise cost during peak demand. The results of different generator selections were analysed. The proposed study optimised five generators considering morning and evening peaks. GA gives the lowest cost of 28.06 $/day, and power sharing among the generators is shown.

Figure 4-8 and Figure 4-9 shows the energy shared among the generators for the two optimisation algorithms. The optimisation results indicate that three diesel generators (G1, G2, and G5) are the most prioritised to allow the optimum performance of the diesel generators, minimising fuel consumption and emissions.

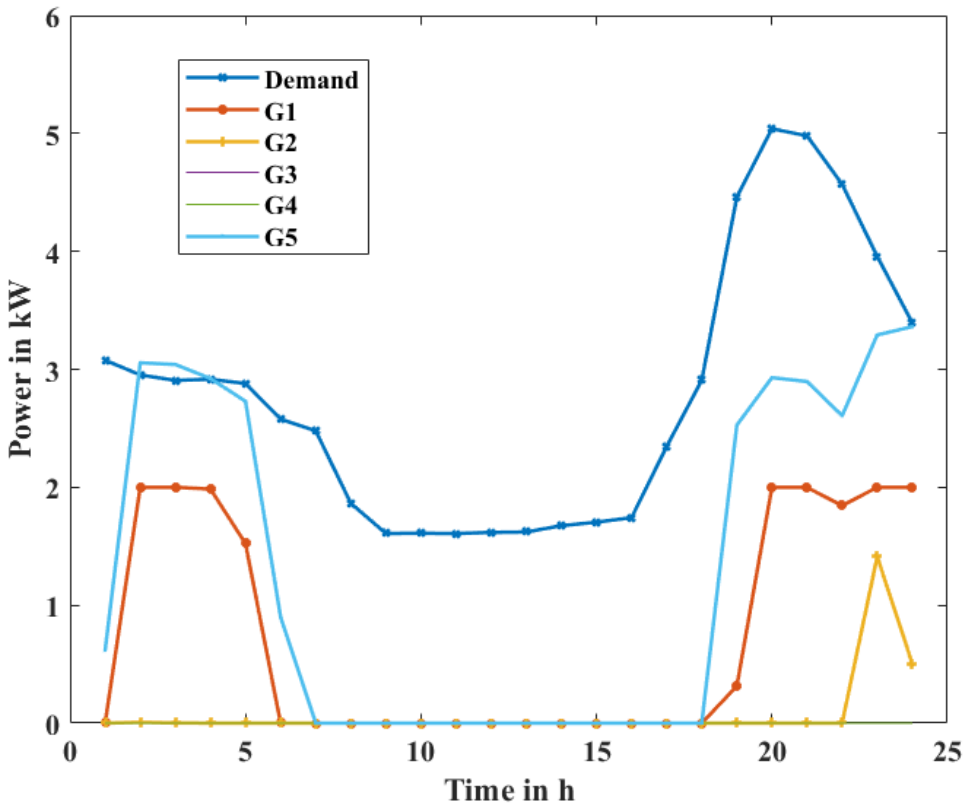

Figure 4-8: *Optimal generator arrangements selected to provide backup power to the load out of the five diesel generators using genetic algorithm (GA)*

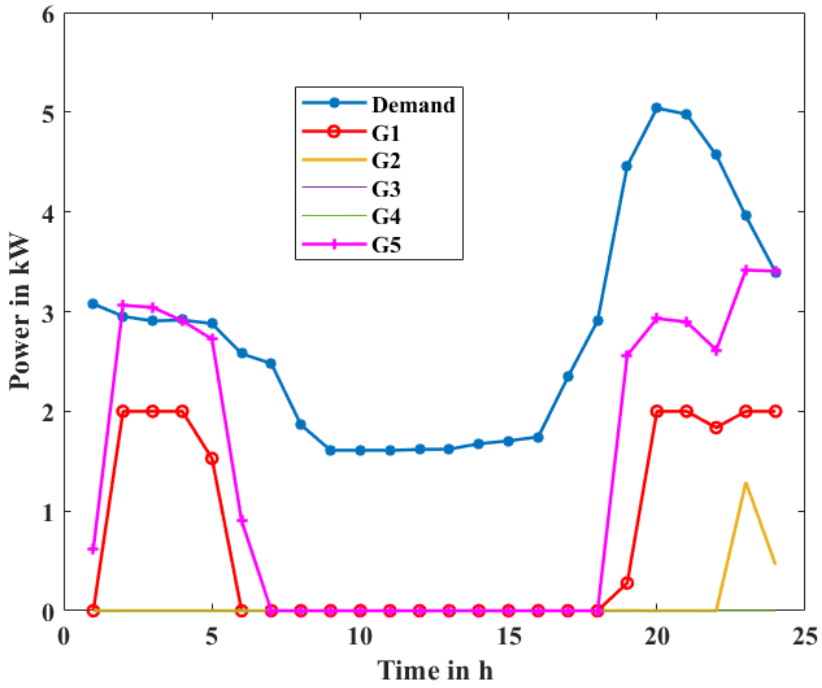

Figure 4-9: *Optimal generator arrangements selected to provide backup power to the load out of the five diesel generators using PSO*

On the other hand, only one diesel generator is required for the minimum cost of all the algorithms, as shown in Figure 4-10. This observation aligns with Rangel et al., (2023), who simulated different hybrid configurations and observed that one generator system promises minimum costs if a battery is included.

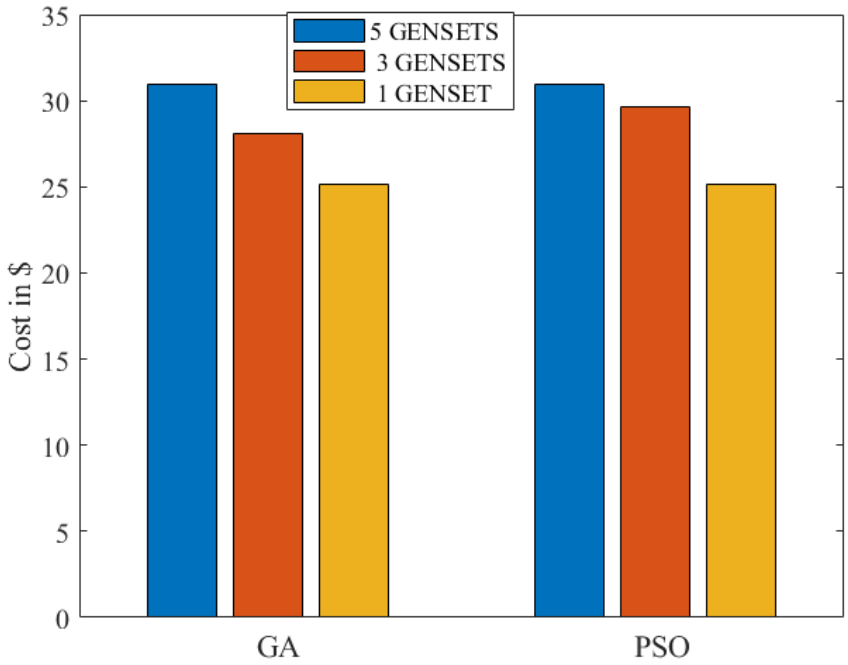

Figure 4-10: *Overall cost of fuel and emissions incurred per day for different diesel generator configurations using genetic and particle swarm optimization algorithms*

Figure 4-10 shows the optimisation costs for the two algorithms (GA and PSO) at different generator arrangements. GA and PSO yield almost the same results for the cases of five and one generators. For the case of three generators, GA gives the most optimal results compared to PSO. However, the computational run time of GA for all the scenarios is more than that of PSO.

However, it is crucial to assess the specific situation, including load requirements, fuel efficiency, emissions, and other factors, since choosing between one big diesel generator and multiple small diesel generators to minimize emissions and fuel costs depends on several factors, as explained. For a significantly fluctuating power demand, having two smaller diesel generators that can be turned on and off as needed might be more efficient to avoid running a single large diesel generator at partial load, which can be less fuel-efficient and produce more emissions.

Also, it is essential to consider the maintenance and reliability requirements of the generators. Smaller diesel generators may have shorter maintenance intervals but can be more easily replaced if one fails. Large diesel generators might require less frequent maintenance but can be costlier to repair. A comparison between the fuel efficiencies of the specific diesel generators should be made since smaller diesel generators are often more fuel-efficient at partial loads. In contrast, some modern large diesel generators are designed to be efficient across various loads. Other things to consider are scalability and initial costs; a single larger diesel generator might be more scalable for future power growth.

4.2. Results and Analysis (Bunjako Microgrid)

Figure 4-11 compares the average hourly power consumed and minimum irradiance measured at the Bunjako microgrid (0°0’10" N, 32°8’4" E). As is typical, average irradiation peaks around 11 am and, after that, declines, while the power consumption displays an increasing trend during the hours of waning and no irradiance (Akmam Naamandadin et al., 2018).

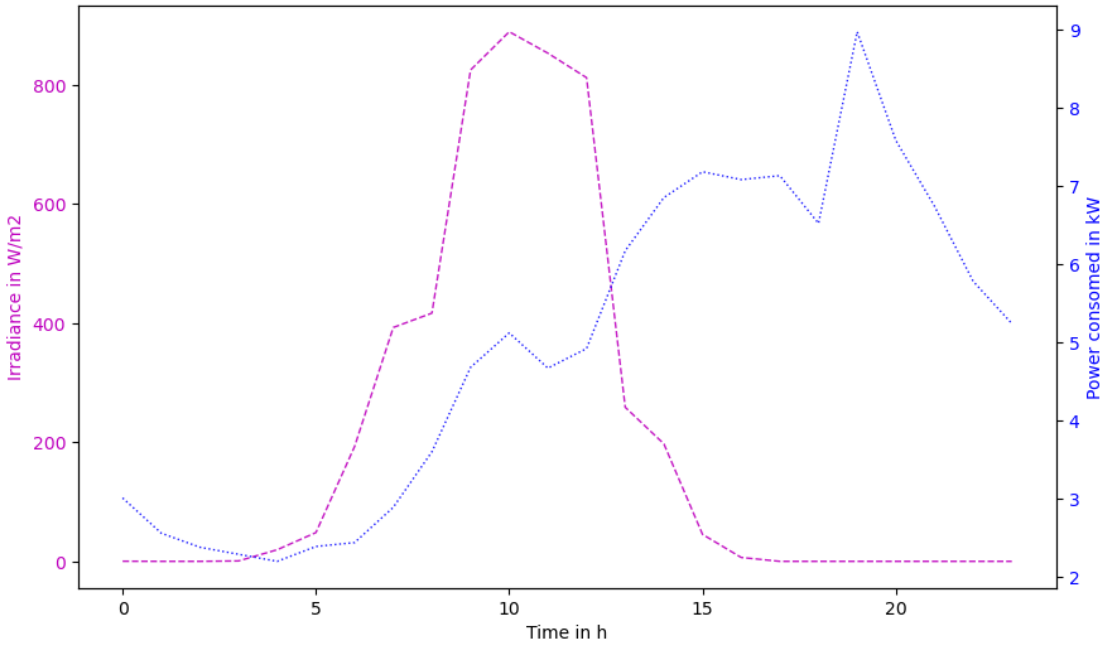

Figure 4-11: *Comparisons between hourly average power consumed (in kW) and minimum daily irradiance (in W/m^2) measured at Bunjako (22nd to 28th of February 2022)*

Figure 4-12 represents measurements of the microgrid model before DSM. The model takes irradiance and demand data from the measurements, and accordingly, the profile of deferable loads is decided based on the peak and base load profile.

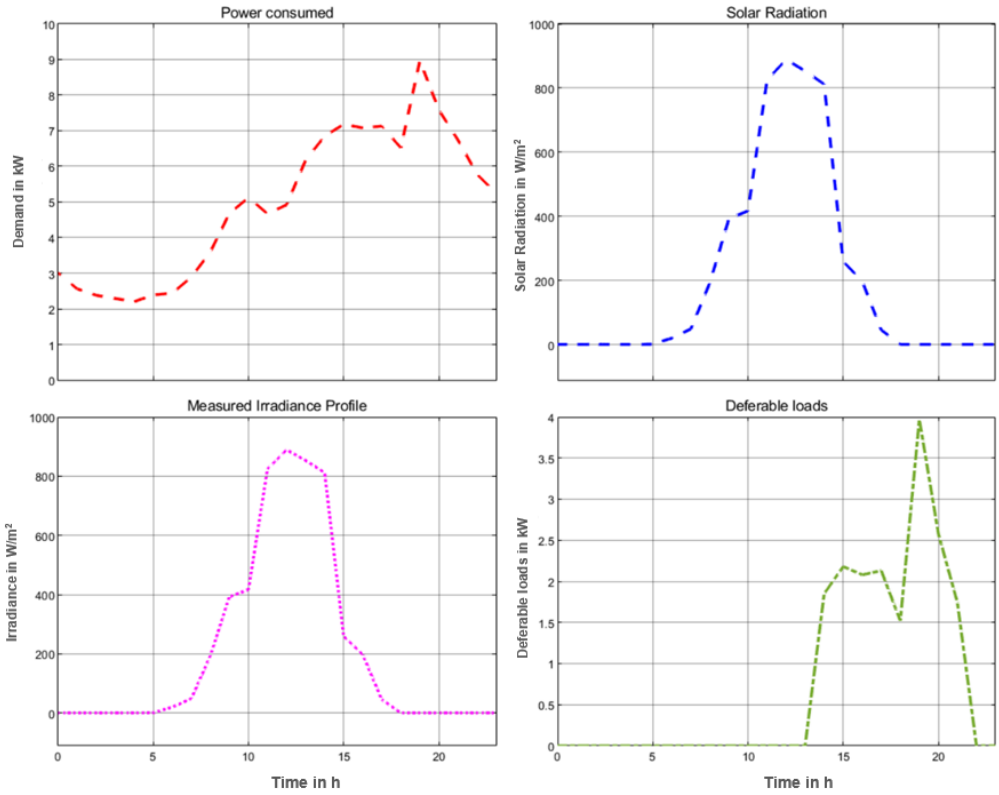

Figure 4-12: *Simulink measurement results before the application of DSM*

4.2.1. Effect of Peak Clipping

Peak clipping is achieved using an energy controller or switches. The energy consumption trend is monitored; the controller switches deferable loads off if it approaches unwanted levels. Examples of deferable loads that can be switched off are washing machines, pumps, water purifiers, etc. In this work, the loads to be shut down are decided based on consumer priority and grouped as deferable and non-deferable loads.

Figure 4-13 represents power usage reduction through DSM using a peak clipping strategy. A significant improvement in the load profile is observed, with a decrease of about 31.2% in peak demand. This method shows a more substantial improvement in the PAR of the system, as shown in Table 4-3. However, there is a question regarding customer comfort regarding the importance of considering priority from both utility and customer points of view (Moghaddam et al., 2011; Philipo et al., 2020).

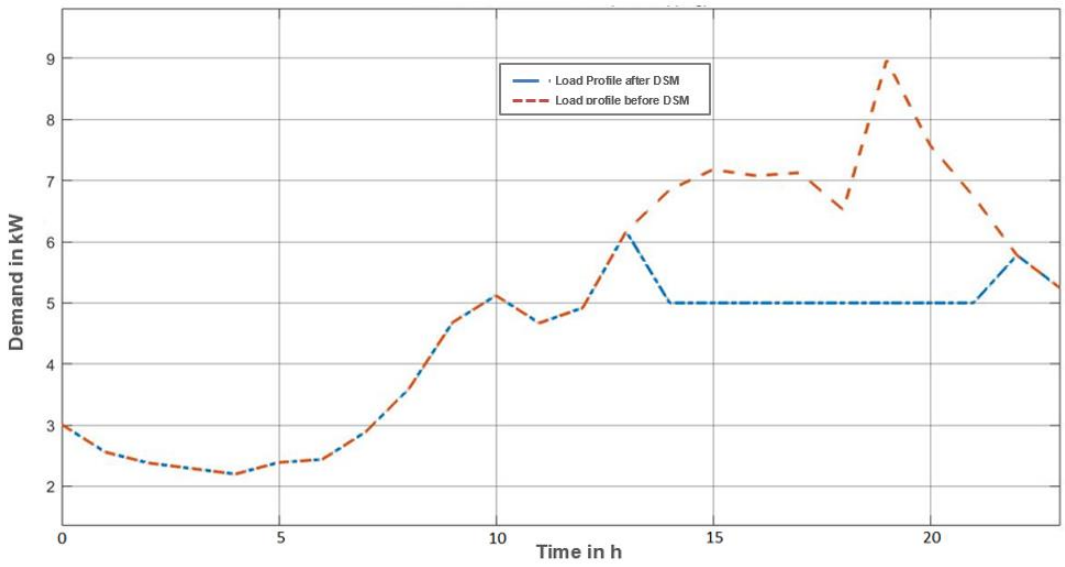

Figure 4-13: *Load profile before and after DSM through Peak Clipping*

4.2.2. Effect of Load Shifting

Figure 4-14 represents DSM through load shifting. A close look at the simulation results shows that deferable load operation is being shifted during the 24 hrs of a day. Most of the operation is taken towards hours, during which solar irradiance is used to reduce storage.

Shifting most of the usage pattern towards hours of more generation gives a window for most critical loads whose operation cannot be stopped to be supplied even during peak hours, as shown in the results from around (1800 – 1900) hrs. Critical loads such as security systems and fridges have strict energy necessities, and once their operation is initiated, it becomes hard to reschedule (Diyan et al., 2020). However, adaptable and manageable

appliances can be rescheduled from peak hours to off-peak if the demand for these devices cannot be satisfied (Lu et al., 2019).

During peak hours, the clipping scheme lowers energy consumption and discomfort by switching off excess loads. Load shifting allows the rescheduling of appliances to off-peak hours with less energy consumption reduction, as shown in Figure 4-15. The results are comparable to Diyan's (Diyan et al., 2020).

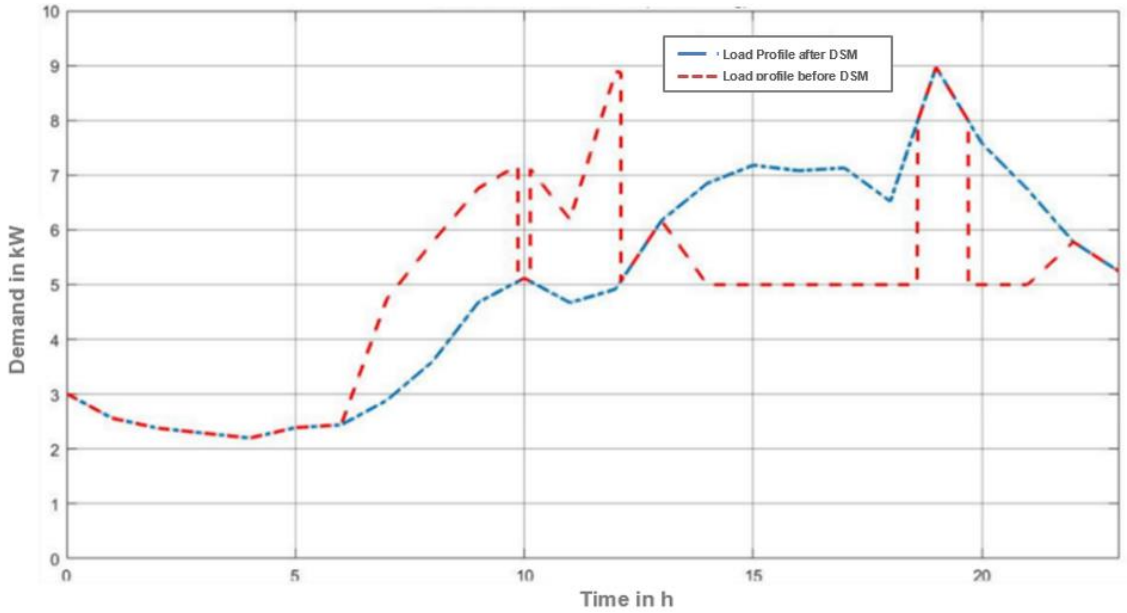

Figure 4-14: *Load profile before and after DSM through Load Shifting*

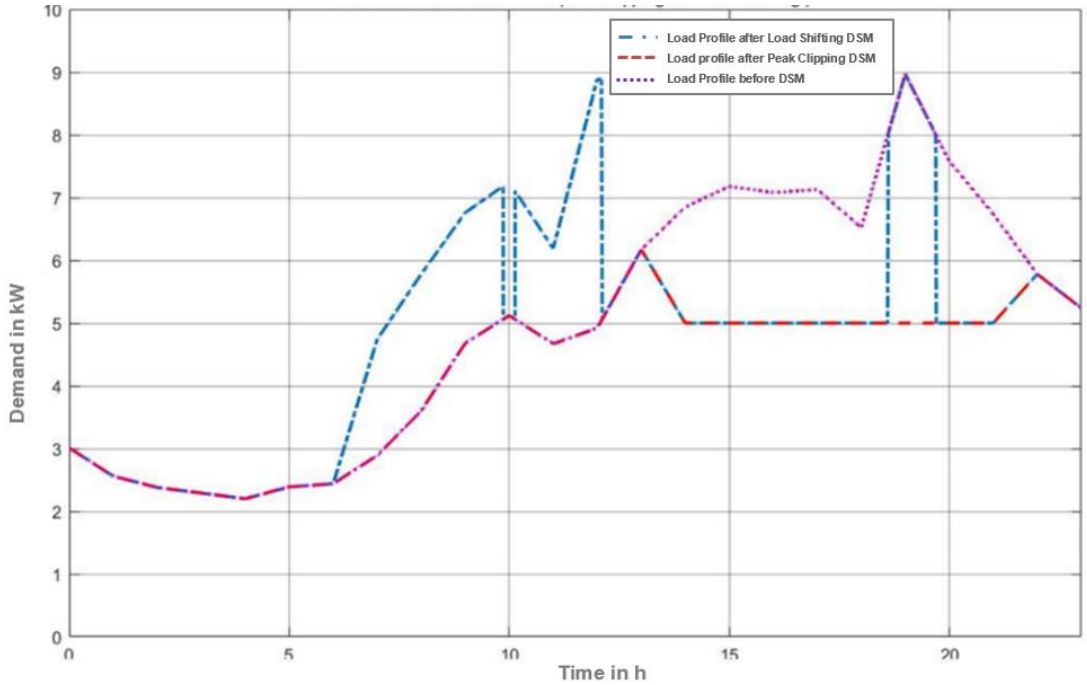

Figure 4-15: *Load profile before and after demand side management through both Peak Clipping and Load Shifting*

Table 4-3: *Statistical parameters of profiles before and after demand side management*

Statistical value	Original Profile	Load shifting	Peak clipping
Maximum	8.970	8.970	6.170
Minimum	2.200	2.200	2.200
Peak to Peak	6.770	6.770	3.970
Mean	4.899	4.773	3.645
Median	4.989	5.000	2.899
RMS	5.289	5.085	3.873
Maximum Hour	19	19	13
Minimum Hour	4	4	4
PAR	1.831	1.879	1.693
% Peak reduction	**0.000%**	**0.000%**	**31.215%**

4.2.3. Peak to Average Ratio (PAR)

Peak to Average Ratio (PAR) is a measure of how an electric system's reliability and efficiency are affected by peak electricity consumption. It is measured as the ratio of the peak to time-averaged power level. Customers' power consumption behaviour directly affects the system's peak consumption. Through maintaining a balance between supply and demand, PAR can be minimized, which benefits both utility and consumer. One of the primary goals of DSM is PAR minimization, hence maintaining the reliability and stability of the grid. PAR is given as follows,

$$PAR = \frac{Max\ (Power)}{1/24\ (\sum_{t=1}^{24} Power)} \qquad \textit{Eqn 4-1}$$

The plotted histogram of the comparisons of PAR of demand profiles before and after DSM using the two approaches is shown in Figure 4-16. Profile before DSM has a PAR of 1.831, whereas LS DSM and PC DSM have PAR of 1.693 and 1.879, respectively. High PAR in load shifting resulted from the generated peak power consumption (see Figure 4-14) after the loads were shifted. It can be seen clearly from the results that peak clipping performs better in minimising PAR, which is comparable to results with load shifting.

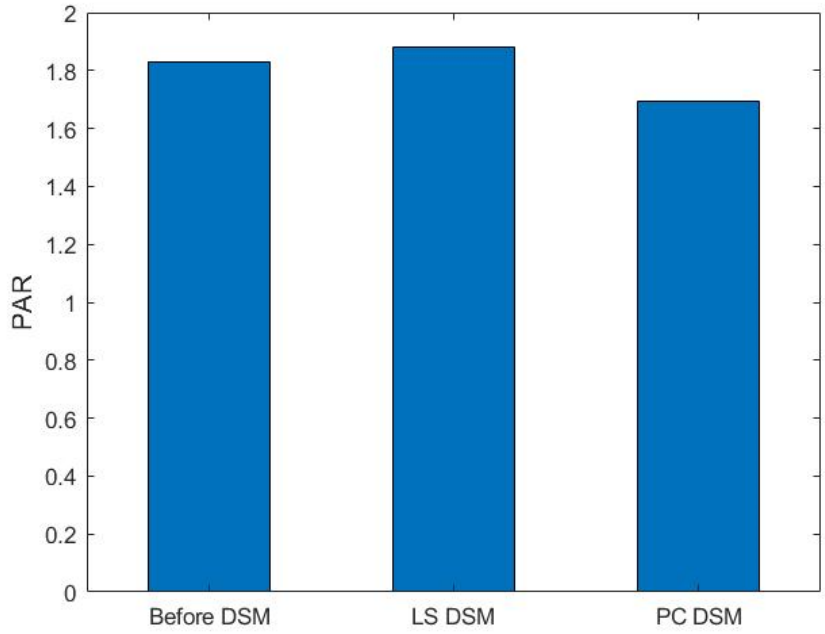

Figure 4-16: *Peak-to-average ratio values for load shifting and peak clipping for the case of Bunjako Island July-September 2021*

4.3. Results and Analysis (Lwak Microgrid)

4.3.1. Current Energy consumption analysis

This section measured the daily profile of cooling appliances in the locality (Fridges and Freezers) using the installed smart sockets. The results of the measurements are represented by Figure 4-17 to Figure 4-22.

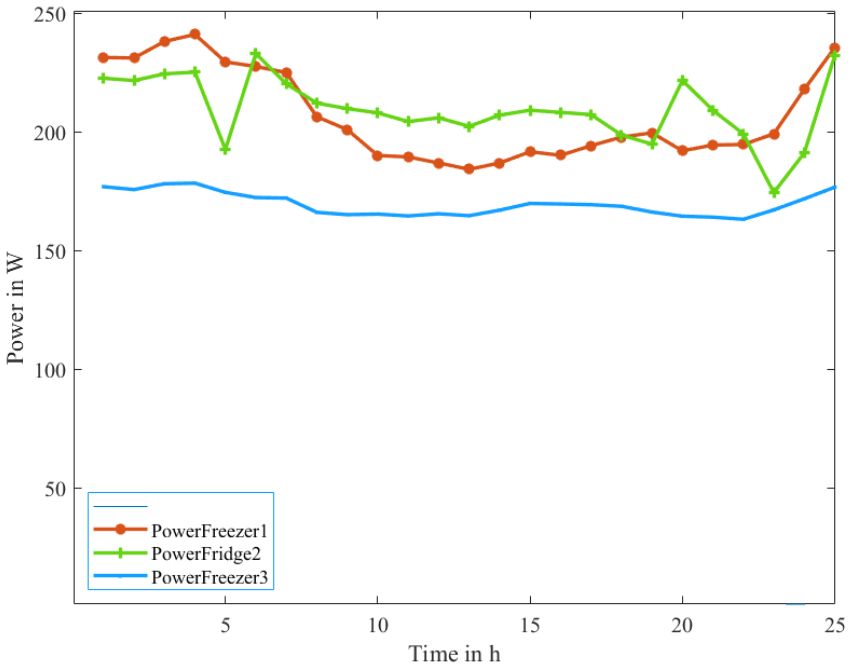

Figure 4-17: *Daily measured power consumption of cooling appliances for the Bethany house at Lwak microgrid*

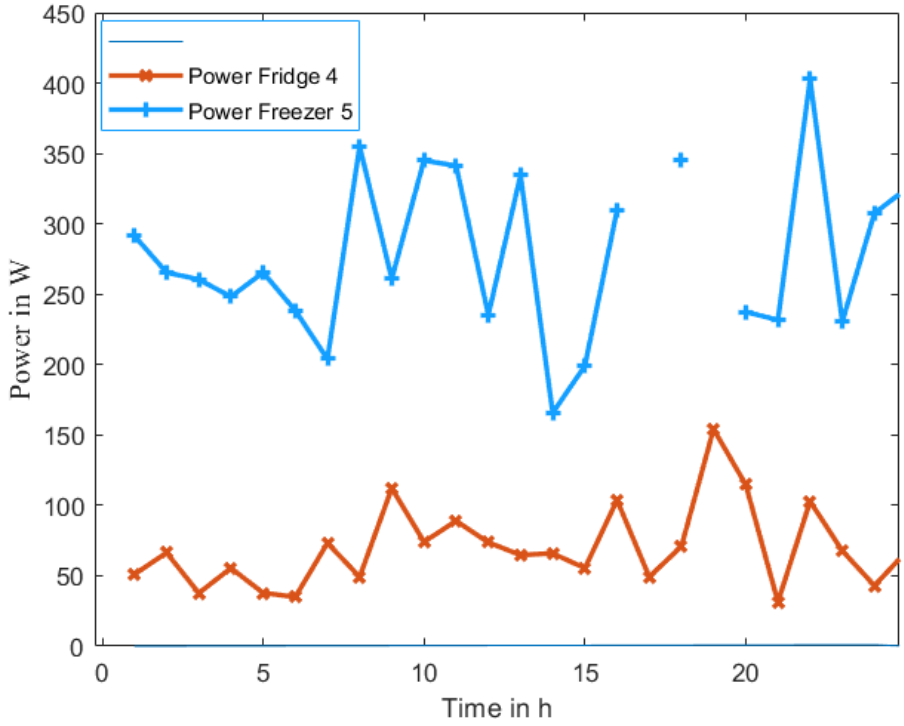

Figure 4-18: *Daily measured power consumption of cooling appliances for the Emmaus house at Lwak microgrid*

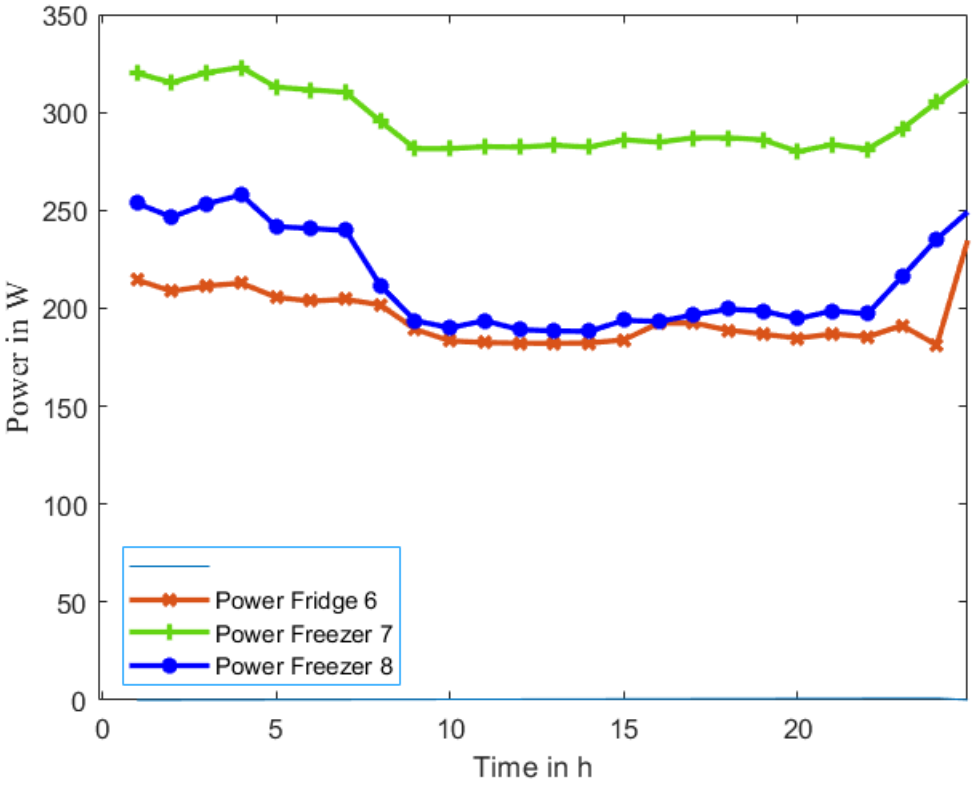

Figure 4-19: *Daily measured power consumption of cooling appliances for the Postulancy house at Lwak microgrid*

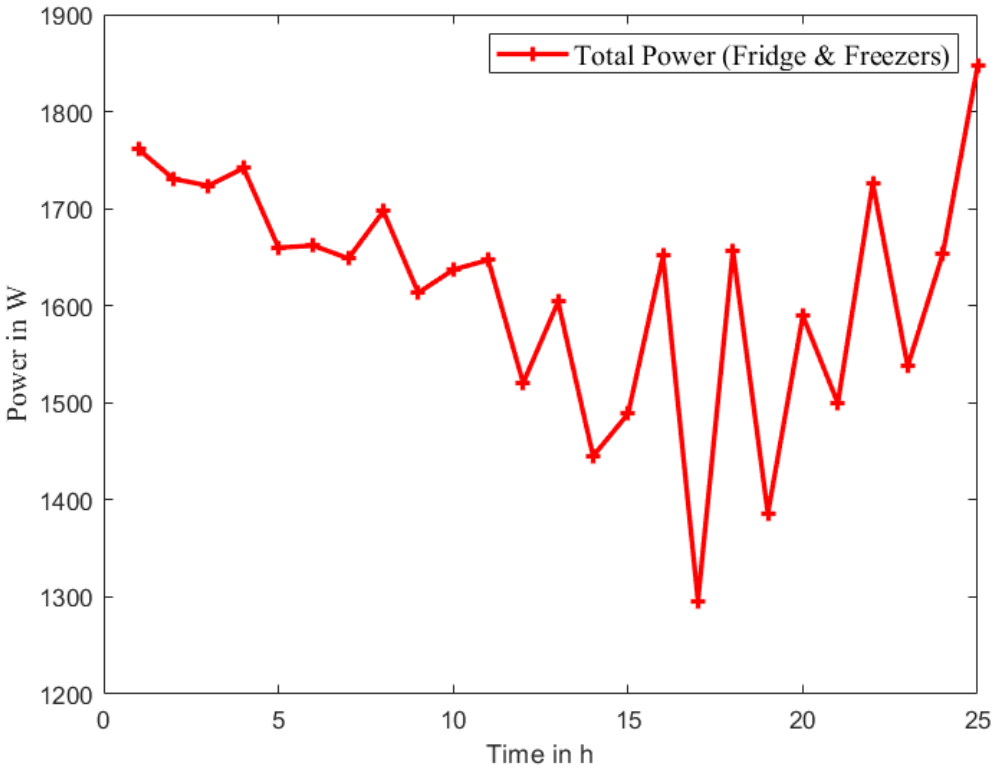

Figure 4-20: *Total daily measured power consumption of cooling appliances for all three houses (Postulancy, Bethany and Emmaus) at Lwak microgrid*

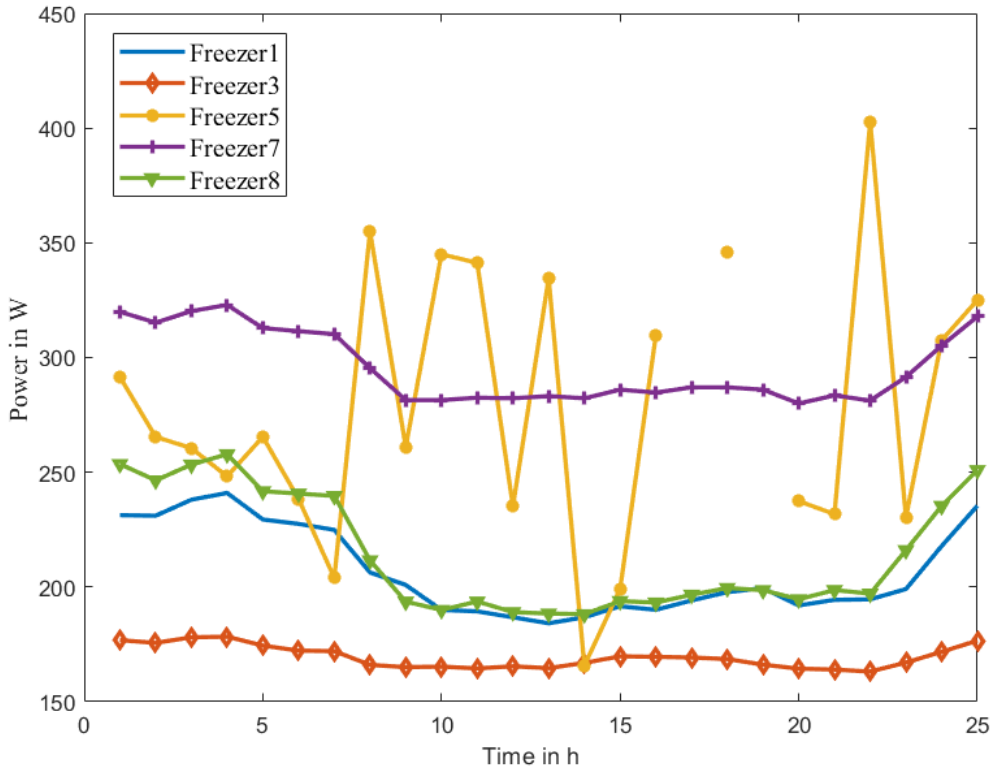

Figure 4-21: *Daily measured power consumption of freezers of all the houses at Lwak microgrid*

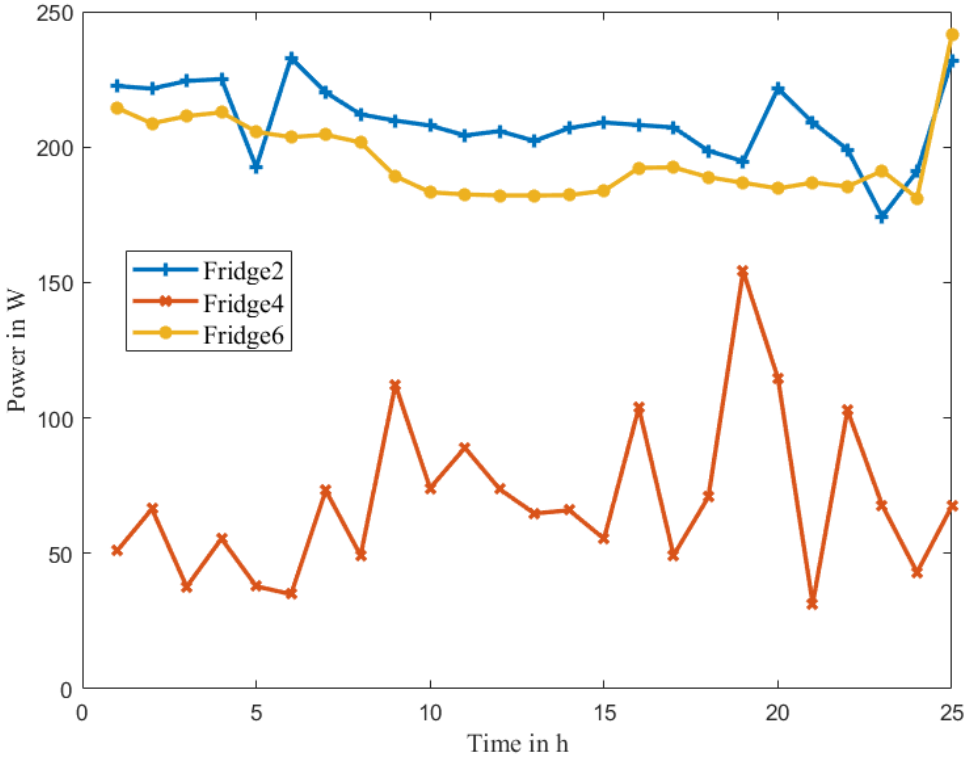

Figure 4-22: *Daily measured power consumption of fridges of all the houses at Lwak microgrid*

Figure 4-20 represents the total daily power consumption from all three houses. It is noticeable that the maximum consumption curve does not occur in the early afternoon, which would have been expected given the outside temperatures, but in the evening hours. This was presumably due to opening, removing, or exchanging refrigerated goods when the sisters prepared food.

Figure 4-21 and Figure 4-22 represent the separate hourly power plots of freezers and fridges. Figure 4-21 represents five freezers and their hourly power pattern within a day. The figure indicates that freezer three draws the least power due to its low-rated power capacity of 94 W compared to the other freezers, as shown in the table. Freezers one and eight show the second least power consumption, and the two freezers show almost a similar trend and values because they are the same brand of freezers with the same rated values. The minor discrepancies might be due to different foods in the fridges and different times of opening and closing of doors for the freezers. Freezer five shows a more varied profile with some gaps due to missing data during recording. This might be due to interference with human activities at the location. Freezer seven, which holds almost the maximum power usage, was found to be the most energy-drawing freezer, and due to its being too old, its model and power rating description could not be found, as shown in the table. It

might be too old due to its high power consumption; hence, replacing it with a more energy-efficient one is better.

Moreover, looking closely at the figure and comparing it to the table of rated values shows that the freezers operate more than their rated capacity at particular points. From the research point of view, this can be attributed to the following factors;

a) Overloading of freezers

   It is noted that putting over the recommended amount of food in the fridge forces the fridge to operate more than its rated power to cool the foods, drawing more current.

b) Dusts and Debris

   When the condenser accumulates dust or debris, it reduces efficiency and works inefficiently by drawing more power.

c) Age and wear

   The older the compressor, the less efficient it becomes; hence, it draws more power than required. A good example is freezer 5, rated at 210W, but through the operation, it was going beyond that due to its age. (Biglia et al., 2018) and (Evans et al., 2018) confirmed that appliances use more energy as they age. Their tests revealed that appliances under two years used approximately one-third of the energy they used over 11 years.

d) Refrigerant problems and thermostat issues

   A malfunctioning thermostat and leakage problems of the refrigerant may affect the freezers' cooling mechanism, causing them to work harder to draw more power.

e) Poor seals

   Ineffective door seals allow hot air to affect cooling and force the compressor to compensate by drawing more power. According to the literature, testing of proper sealing can be done using an 80 gsm A4 sheet of paper. If the paper can be pulled out easily or where the paper was not gripped, the seals are rated as poor or awful, which might need replacing (Evans et al., 2018). Also, opening and closing freezer doors can influence how they should be handled.

Likewise, from Figure 4-18, fridge four has the least energy consumption pattern. The reason might be that it is a new and energy–efficient fridge labelled with the Energy Star

certification by the Kenyan Energy and Petroleum Regulatory Authority (EPRA), and one of its responsibilities is labelling appliances. It currently uses a five-star to more or the highest energy-efficient appliances and one for the lowest (Figure 4-23).

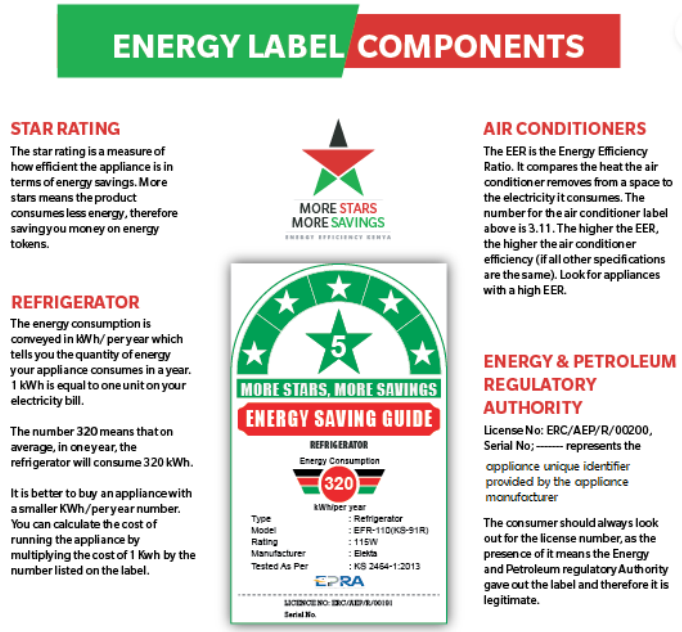

Figure 4-23: *Components of energy labels for cooling appliances labelled with the Energy Star certification by the Kenyan Energy and Petroleum Regulatory Authority (EPRA)*

After analysing the cooling appliances, we suggested that the star-labelled appliances should be kept and the remaining old appliances replaced.

4.3.2. Identification of energy inefficiency: Rebound Effect

In this case, the rebound effect is calculated as a temperature and correlation coefficient ratio. The temperature coefficient describes the relative change in power consumption associated with a given per-unit change in temperature. It provides the quantified direct impact of temperature on power consumption. The correlation coefficient is a numerical value varying from -1 to 1 that measures the strength and direction of the linear relationship between power consumed and temperature. Through correlation, we can get an insight into how the temperature explains variations in power consumption. The ratio of the two gives a normalized relationship between temperature coefficient and strength, which helps better interpret the impact of temperature on energy usage.

$$Temperature\ coefficient = T_c = \frac{\sum_i^N (x_i - \overline{x})(y_i - \overline{y})}{\sum_i^N (x_i - \overline{x})^2} \qquad Eqn\ 4\text{-}2$$

$$Correlation\ Coefficient = r_{cc} = \frac{\sum_i^N (x_i - \overline{x})(y_i - \overline{y})}{\sum_i^N (x_i - \overline{x})^2 \sum_i^N (y_i - \overline{y})^2} \qquad Eqn\ 4\text{-}3$$

$$Rebound\ effect = T_c / r_{cc} \qquad Eqn\ 4\text{-}4$$

Where, T_c = temperature coefficient t, r_{cc} = correlation coefficient, x = independent variable (temperature), y = dependent variable (power consumed), $\overline{x}\ and\ \overline{y}$ = means of the variables, and N = a number of data points.

Correlation analysis used the linear regression model of the fridge's internal temperature and daily power consumption (Figure 4-24). Rebound effect was calculated to decide which fridge/freezer was efficient or inefficient; hence, decision on replacement was made. Relationship between temperature changes and energy consumption was established. Sudden temperature drop in temperature leads to an increase in power consumption, thus, more pronounced increase in power consumption due to temperature changes suggests higher inefficiency in of the fridges/freezers as fridges/freezers work harder to maintain lower temperatures. An absolute value of the rebound effect represents this scenario. The higher the absolute value of the rebound effect, the more inefficiency of the appliance.

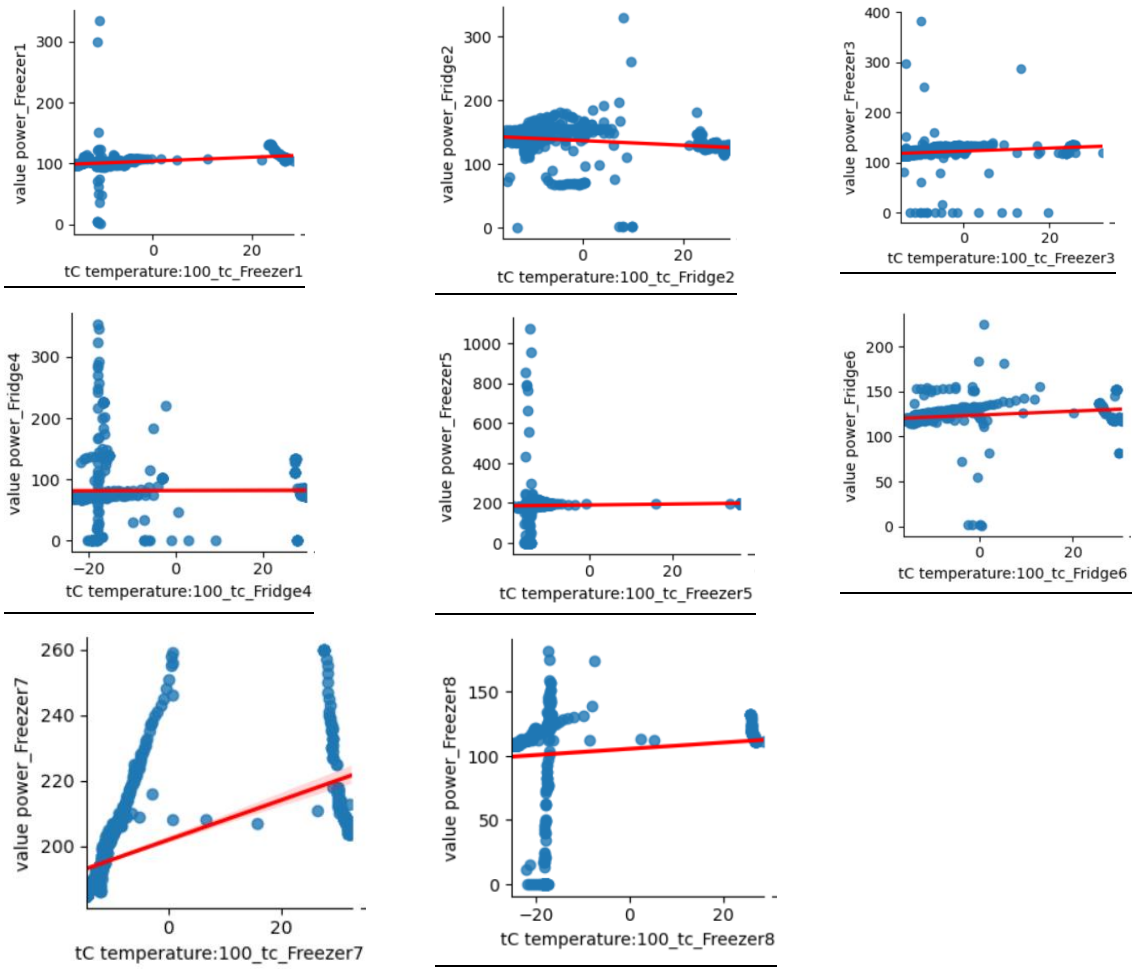

Figure 4-24: *Correlation scatter plots scatter plots for fridge and freezer power consumption and their temperature.*

	Freezer 1	Fridge 2	Freezer 3	Fridge 4	Freezer 5	Fridge 6	Freezer 7	Freezer 8
Temperature 1	0.274 -1.148							
Temperature 2		-0.232 -1.394						
Temperature 3			0.151 -1.741					
Temperature 4				0.006 -4.239				
Temperature 5					0.051 -3.764			
Temperature 6						0.254 -0.943		
Temperature 7							0.621 -1.007	
Temperature 8								0.135 -1.867

Figure 4-25: *Rebound and correlation (Top values = correlation, downward values = rebound value)*

Figure 4-25 shows the correlation coefficient and rebound values. Rebound values represent the change in power consumption associated with a unit temperature change. A more negative value reflects a more significant increase in power consumption due to temperature change, hence a potentially inefficient appliance.

Based on the observed results, the cooling appliances were classified into three main grades (A, B, C) based on their rebound effect values. Table 4-4 and

Table **4-5** represent the categories. Grade C represents relatively inefficient appliances that should be considered for replacement first. Freezer 5 and fridge 4 were found to have higher rebound values, representing their higher inefficiency. This observation suggests that freezer 5 and fridge 4 cannot maintain stable internal temperature properly. This observation is supported by our previous work that measured the average ON state power, and it was found that their instantaneous power and consumption values exceeded the rated values, suggesting inefficiency.

In this study, fridge 4 and freezer 5 should be replaced first, and the target efficiency should be grade A (More efficient). Group B represents medium inefficient fridges, which should be considered for replacement; however, considering the income or nature of the people in the villages where microgrids are common, the work suggested slow improvement to avoid straining their income. In that case, fridge 4 and freezer 5 will be replaced. Since freezer 5 has almost the same measured/average ON state Power (W) as freezer 1, freezer 1 was considered a replacement since it is found in group A (highly efficient group). Fridge 4 was suggested to be replaced with a new fridge of the same rating since there were no fridges

of the same rating on site. The study has considered replacing existing, more efficient fridge/freezer models; however, the replacement should be done with more energy-efficient fridges to achieve more energy savings. Table 4-6 shows the current model of fridge 4 and freezer 5 in use with their energy efficient alternatives available on market. The suggested replacement guarantee to reduce not only electricity usage but also lowers the overall energy profile of the microgrid contributing to a more sustainable energy profile.

Table 4-4: *Fridge-rated power and rebound values with their respective classes based on efficiency*

Appliances	Rating (W)	Absolute Rebound	Class
Fridge 2	_	**-1.394**	B
Fridge 4	_	**-4.239**	C
Fridge 6	120	**-0.943**	A

Table 4-5: *Freezer-rated power and rebound values with their respective classes based on efficiency*

Appliances	Rating (W)	Absolute Rebound	Class
Freezer 1	_	-1.148	A
Freezer 3	94	-1.741	B
Freezer 5	210	-3.764	C
Freezer 7	_	-1.007	A
Freezer 8	106	-1.867	B

Table 4-6: *Refrigeration appliances details and their replacement model with market price*

Appliance type	Model	Rating	Replaced to	Market Price
Fridge 4	Haier HRF-3674	80 W	Haier HRF-3674	417.99
Freezer 5	ArmCoAF-C38S	210 W	Bruhm BCF- 398S	269.07
TOTAL COST				687.06

Figure 4-26 and Table 4-7 show energy savings before and after replacing fridge 4 and freezer 5. The comparison between the load profiles before and after the replacement of the appliances clearly demonstrates the effectiveness of the intervention with about 15%

energy and cost savings per year. Prior to replacement, the energy consumption profile was notably higher, reflecting the inefficiency of older models. After the replacement, the energy profile shows a marked reduction, highlighting the impact of using energy-efficient fridges/freezers available on the market. This outcome underscores the importance of upgrading appliances to energy-efficient models, which offer both economic and environmental benefits.

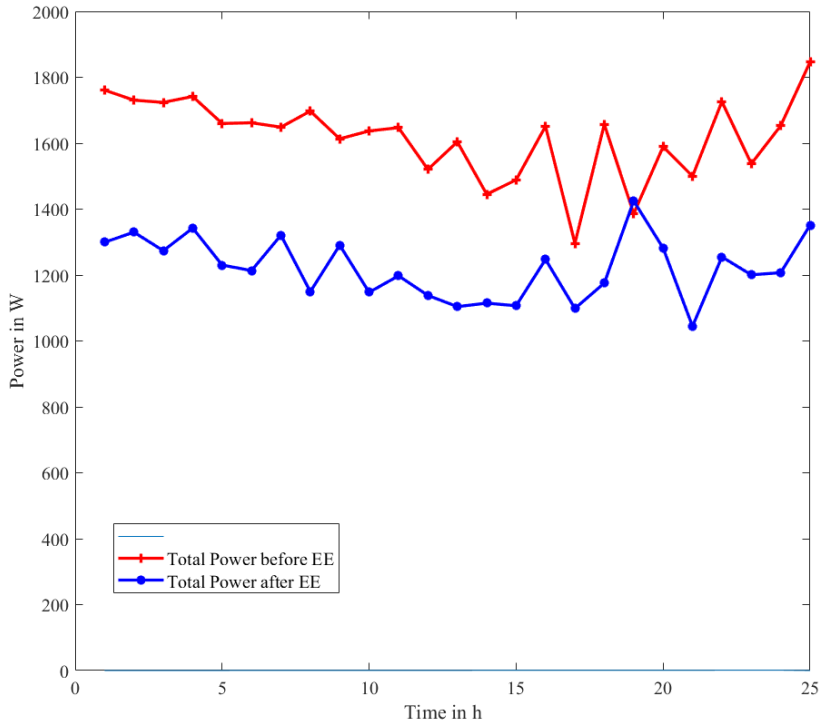

Figure 4-26: *Plot of total power consumption before and after energy efficiency for all the refrigeration appliances.*

Table 4-7: *Overall annual energy and cost savings after energy-efficient DSM*

	Before EE	**After EE**	**Savings**	**Percentage Saving (%)**
Energy (kWh/year)	14754.92	12518.99	2235.92	15.15
Cost (USD/year)	2655.88	2253.42	402.47	15.15

Figure 4-27 shows a projection of cost savings in a span of five years. An initial negative saving of about 284USD is observed in the first year which is primarily due to the upfront investment required for the purchase new energy-efficient appliances. However, as the in the long run, a steady increase in cost savings is observed reflecting the cumulative effect

of reduced energy consumption and lower operating costs over time. Over the five-year period, the total cost savings are substantial (1325USD), demonstrating that while there is an initial financial outlay, the long-term gains from energy efficiency far outweigh the initial costs. This reinforces the value of making energy-efficient upgrades, not just for immediate benefits, but for sustainable cost savings in the long run.

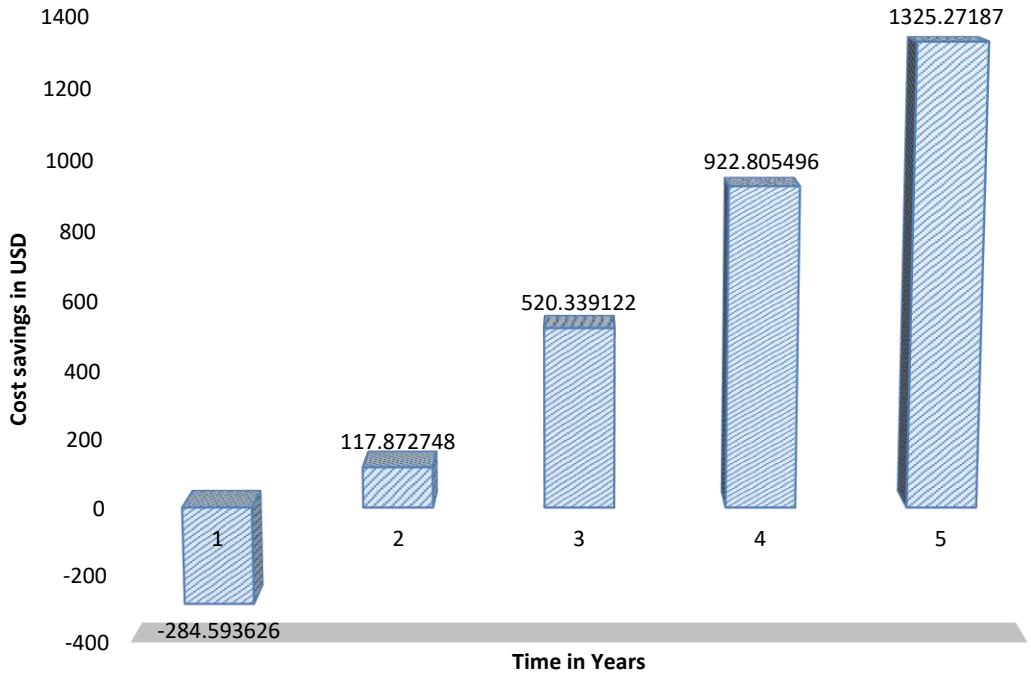

Figure 4-27: *Cost savings before and after energy efficiency DSM for a span of five years*

The setup was first made before the control to see the overview of power consumption and temperature changes in the appliances. The figures below show measurements taken before fridge control starts; a one-day range was taken on 25th September 2023 from 0849 hrs to 26th September 2023 at 1000 hrs. A control was then initiated, and a range of day effects was taken to assess the impact. However, the control is still ongoing on the Lwak site after the control range was taken from 26th September 2023 at 1002 hrs to 27th September 2023 at 1952 hrs.

Figure 4-28, Figure 4-29, Figure 4-30, Figure 4-31, Figure 4-32, Figure 4-33, Figure 4-34 and Figure 4-35 shows the daily demand plots before and after temperature-based control for all the studied appliances. The results show that freezers 1, 3, 6, 7, and 8 have less energy-consuming profiles after load control. That means we can save energy by switching them off while preserving food as before. Fridge 4 and freezer 5 show the worst results after temperature-based control. They tend to consume more energy instead of saving, and

from the users' experience, they tend to have poor cooling capabilities, and food is not adequately stored as before. The results can best be explained by the previous analysis on finding inefficient fridges and freezers using the rebound effect described in

Table **4-5**, where fridge 4 and freezer 5 were the most inefficient appliances. This incident can explain why their temperature control yielded negative results since the two appliances might have struggled to maintain the temperatures, consuming more energy with more temperature fluctuations. So, for inefficient fridges or freezers, temperature-based control can be challenging or less effective since they suffer from limited temperature stability and hence struggle to maintain stable temperatures, which might compromise food safety and quality. The struggle to maintain temperature leads to more power consumption, and since inefficient fridges/freezers have ageing cooling systems, attempting to do rigorous temperature control could strain the system more. Therefore, it is crucial to assess and recognize the limitations of inefficient appliances before doing temperature control to exploit the benefit of temperature-based control sustainably.

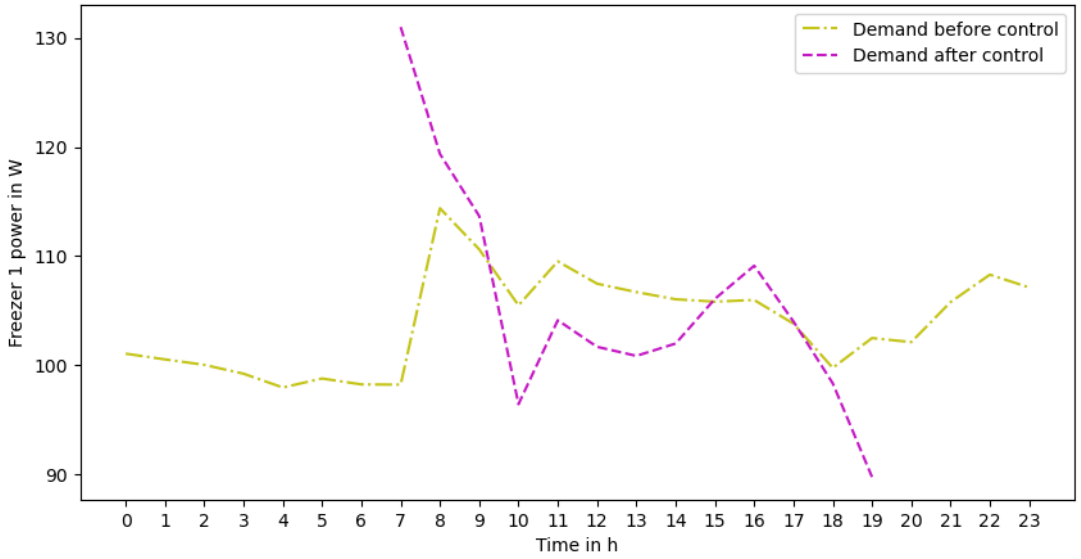

Figure 4-28: *Daily profile before and after temperature-based control for Freezer 1*

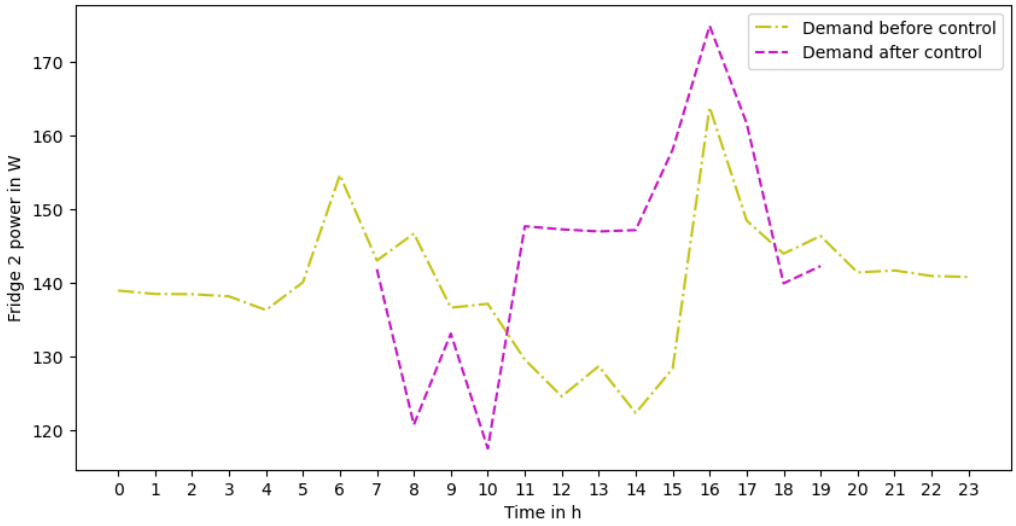

Figure 4-29: *Daily profile before and after temperature-based control for Fridge 2*

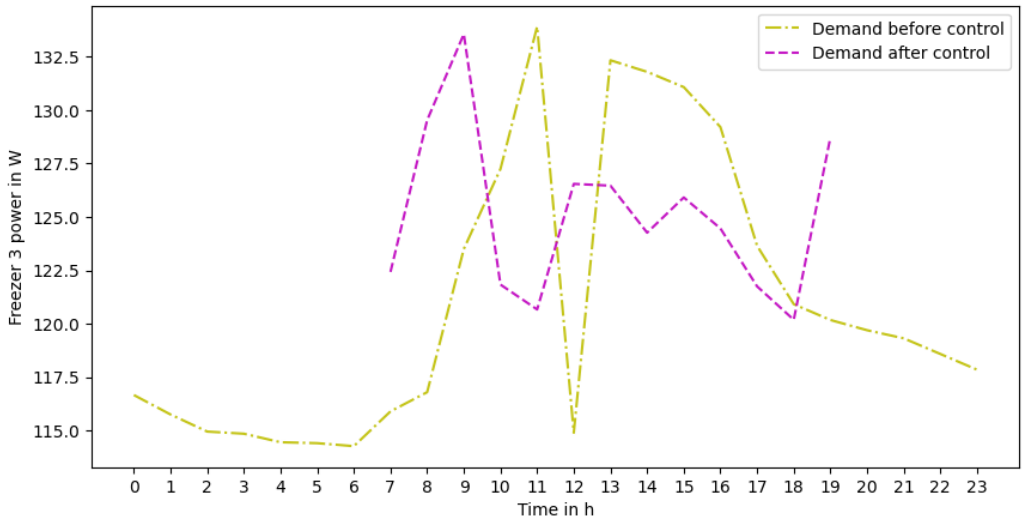

Figure 4-30: *Daily profile before and after temperature-based control for Freezer 3*

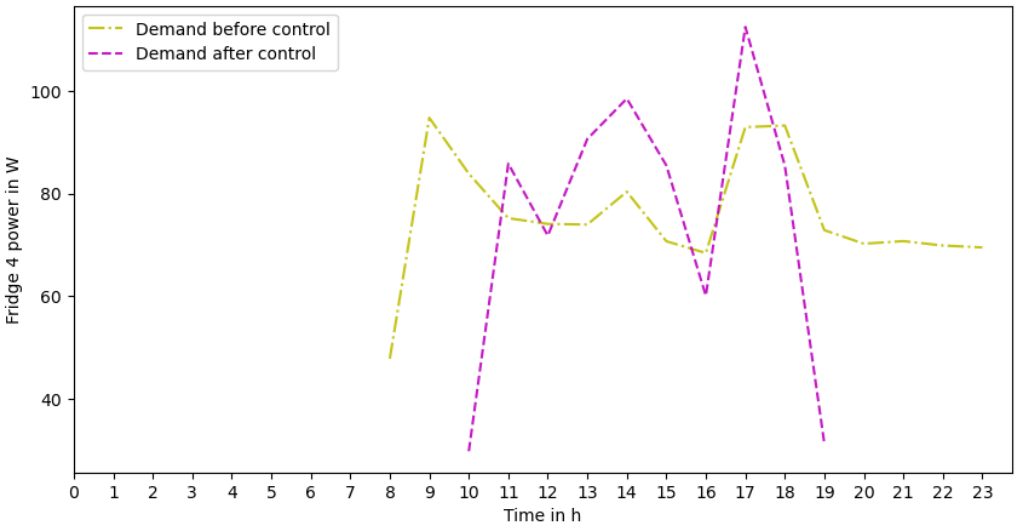

Figure 4-31: *Daily profile before and after temperature-based control for Fridge 4*

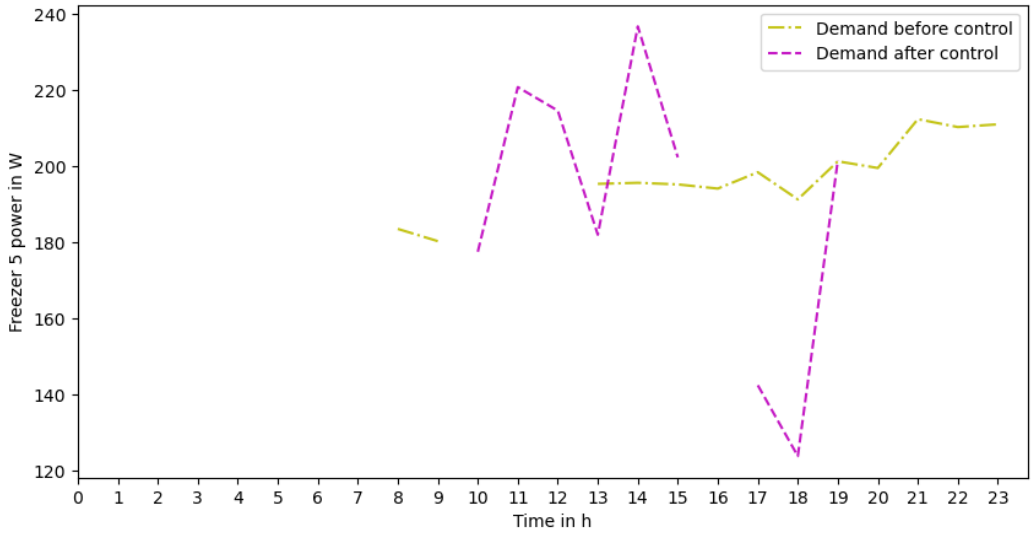

Figure 4-32: *Daily profile before and after temperature-based control for Freezer 5*

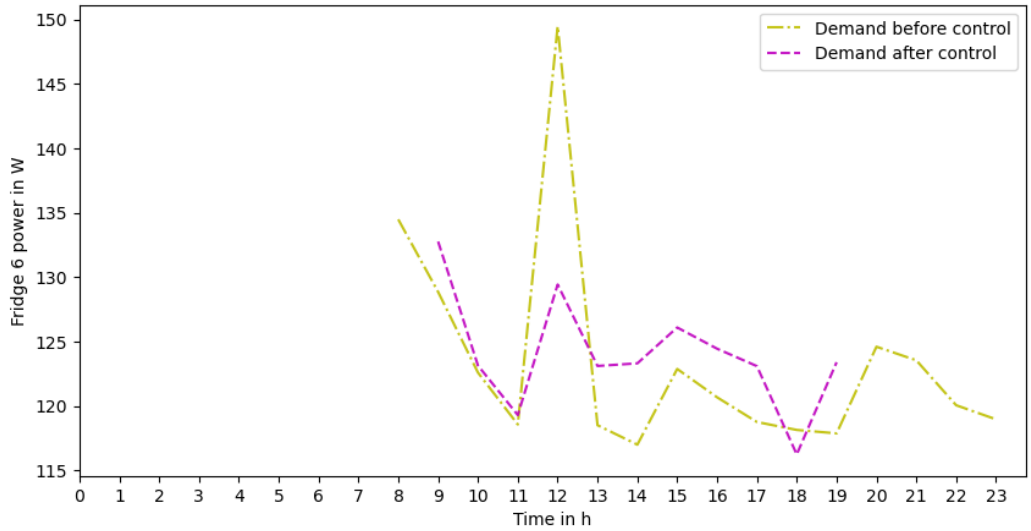

Figure 4-33: *Daily profile before and after temperature-based control for Fridge 6*

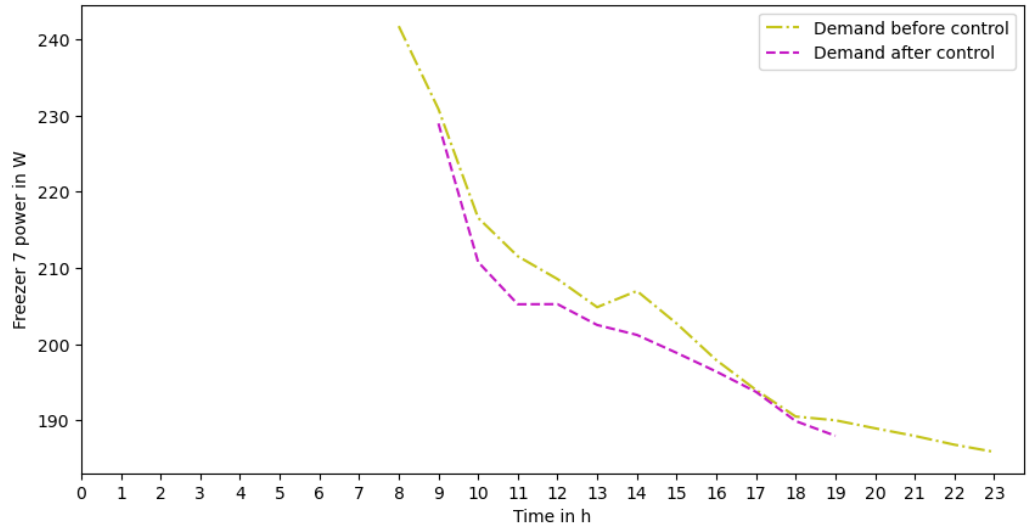

Figure 4-34: *Daily profile before and after temperature-based control for Freezer 7*

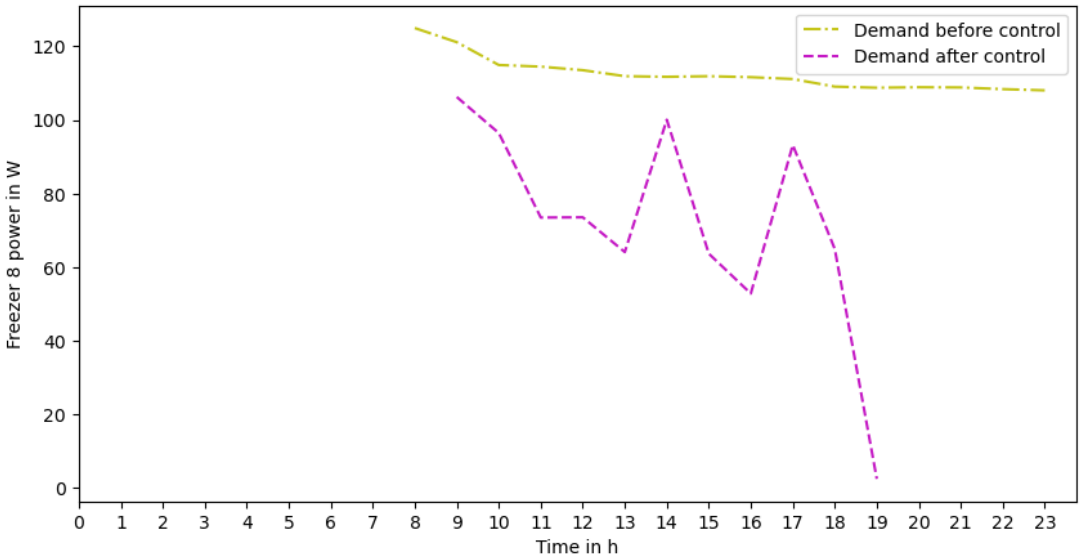

Figure 4-35: *Daily profile before and after temperature-based control for Freezer 8*

CHAPTER FIVE

5. Conclusion and Recommendations

5.1. Conclusions

This work analysed data from three microgrids: Mpale, Bunjako, and Lwak. Possible DSM measures were modelled and analysed based on the data analysis results and the location context of the microgrids. The following specific conclusions can be drawn from the results analysed and discussed in Chapter 4.

5.1.1. Assessing and analysing customer demand and other power quality parameters to establish a baseline for demand-side management measures.

The results of technical data analysis implied that most East African microgrids have similar characteristics regarding electricity consumption, nature of appliances, and location context. Most microgrids are found in rural areas, and the inhabitants have identical economic activities, thus affecting electricity usage patterns. Electricity consumption spikes during evening hours when there is insufficient sunlight as most inhabitants are available at home. Furthermore, the nature of appliances is similar, consisting of medium appliances with fridges and freezers, as the heavy loads affect electricity consumption.

There is a trend of frequent power outages due to unreliable electricity, negatively impacting daily life, businesses, and essential services. The unreliable power led to reliance on diesel generators as a backup power source in off-grid or weak-grid areas. Diesel generators have the economic and environmental implications of relying on non-renewable and often costly energy sources.

Most microgrids face challenges in meeting the energy demand during peak periods due to similar energy pattern usage. In addition, there are inefficiencies in the dispatch and scheduling of energy generation sources, such as when generators are underutilized.

Lack of appliance control mechanisms as no initiatives of load control mechanisms or appliance scheduling based on their internal conditions to facilitate shifting usage to more energy production hours. Furthermore, inefficient appliances are used: Substantial energy wastage or suboptimal performance in many connected appliances is due to a lack of knowledge of the importance of efficiency measures.

5.1.2. Optimisation of microgrid operations through proper demand-side management schemes using modelling and simulation.

The study considered two cases in the Mpale microgrid and one in the Bunjako microgrid. Firstly, a multi-objective optimisation strategy was applied to the Mpale microgrid system through incentive provision. The optimisation model determined the optimal power generation schedule for diesel and PV generators, optimal power curtailed, and incentive received in a scheduled 24-hour period. Sensitivity analysis was conducted on the impact of preference weights on objectives and their effect on microgrid solutions. Results indicated that including a demand response program in the optimisation problem provides a demand-supply match and optimal operation of the microgrid. Due to the improved matching of load to generation, the storage necessities can be reduced.

Furthermore, a power reduction of 14% was achieved through the provision of incentives for equal weights of objective functions. Sensitivity analysis showed that higher costs are achieved when minimising generator fuel cost at the expense of maximising utility benefit. Therefore, the proposed method efficiently reduces energy consumption during the unavailability of the sun.

Secondly, the study also considered utilising different generator arrangements and two metaheuristic optimisation algorithms, i.e., PSO and GA, for optimal dispatching of a microgrid to improve the performance of diesel generators. The result showed that the multiple generators dependent on demand time promoted optimal performance and peak demand reduction costs. Three generator configurations resulted in the lowest cost with GA compared to PSO. The three diesel generators are the most prioritised to allow the optimum performance of the diesel generators, minimising fuel consumption and emissions. The proposed study optimised five generators considering morning and evening peaks. GA gives the lowest cost of around 28.06 $/day. On the other hand, only one diesel generator is required for the minimum cost of all the algorithms. This observation aligns with Rangel et al., (2023), who simulated different hybrid configurations and observed that one generator system promises minimum costs if a battery is included.

In the Bunjako microgrid, the study proposed scheduling household appliances based on load shifting and peak clipping DSM simulated in MATLAB/ Simulink environment. The concept of shiftable and non-shiftable appliances was modelled considering their operating time and the possibility of rescheduling. The proposed method was tested using real-time data for a 24-hour period. After applying the proposed DSM strategies, it was observed that

the proposed algorithm reduces the peak demand, smoothing the load profile to the desired level, and improves the system's peak-to-average ratio (PAR). The presence of deferrable loads has been considered to bring more flexible demand-side management. Results promise decreases in peak demand and peak-to-average ratio of about 31.2% and 7.5% through peak clipping. In addition, load shifting promises more flexibility to customers.

5.1.3. Promoting energy efficiency of microgrids through practical load control and appliance demand data analysis.

Finally, the experimental setup was done at the Lwak microgrid to assess the effectiveness of load control, mainly for fridges and freezers, considering their actual temperatures. In addition, energy efficiency was analysed by using real data measured at the Lwak microgrid.

For load control, less energy-consuming profiles were observed after load control for some of the refrigeration appliances since some parts of the cooling were without electricity consumption. In contrast, the worst results were observed for other refrigeration appliances, which tend to consume more after temperature-based control due to inefficiencies, leading to a struggle to maintain their temperatures. These results tell us that we can save energy by switching off refrigeration appliances and preserving food as before; however, it is crucial to assess and recognize the limitations of inefficient appliances before doing temperature control to exploit the benefit of temperature-based control sustainably. Also, there is a significant promise of cost savings when moving to more energy-efficient appliances.

5.1.4. Summary

Generally, this study will benefit most East African microgrids when considering design solutions to address environmental and Climate change targets, accelerating the achievement of African countries' targets in the Paris Climate Agreement. It also efficiently reduces energy consumption during the unavailability of the sun. Due to the improved matching of load to generation, the storage necessities have been reduced. Future work will include calculating all microgrid energy sources' capital, operation, and maintenance costs and finding the best configurations.

5.2. Recommendations

The study assessed the effectiveness of microgrids in the East African context through modelling, simulation, and practical load control to propose methods to save energy and

improve the microgrids' operation and sustainability. Following the results and discussion, the following are the recommendations proposed by this study:

a) Utility companies should employ incentives to promote the shifting of loads during peak hours through dynamic tariffs, smart meters, etcetera.
b) Microgrid operators should consider using multiple generators instead of a single generator during designing and redesigning processes to avoid underutilisation of the generator and promote cost effectiveness through fuel cost savings and emission reduction.
c) Utility companies can liaise with customers with high load demands, such as industries and businesses, to register shiftable loads operating during non-peak hours, e.g., when PV generation is at its maximum, to maximise solar utilisation.
d) Utility companies, in conjunction with customers, can control appliances based on their condition, such as temperature, which can improve energy savings, especially during peak hours, to avoid deep discharge of the batteries.
e) Energy efficiency is vital in everyday appliances, and increased energy consumption due to inefficiency can lead to energy cost implications as well as environmental impact.
f) Individuals and entities should find ways to improve their energy efficiency in appliances by optimising operational practices and improving or changing to a proper appliance design or technology that saves energy.
g) As shifting to energy-efficient appliance usage requires long-lasting policy and behaviour changes, the government or responsible organisation should promote the reduction of barriers to the penetration of energy-efficient appliances and set thresholds for energy consumption limits.
h) Furthermore, the government should promote phasing out non-efficient appliances by utilising incentives and loans with low interest rates, especially for low-income families that cannot afford the complete or quick transformation.
i) Customer awareness regarding the importance of energy-efficient habits should be promoted.
j) Further research can explore load shifting by utilising the thermal capacities of refrigeration units to achieve a meaningful temporal load shift.

References

Abdi, H. (2008). Kendall Rank Correlation Coefficient. *The Concise Encyclopedia of Statistics*, 278–281. https://doi.org/10.1007/978-0-387-32833-1_211

Aboul-Magd, M. A., & Ahmed, E. E. D. E. S. (2001). An artificial neural network model for electrical daily peak load forecasting with an adjustment for holidays. *LESCOPE 2001 - 2001 Large Engineering Systems Conference on Power Engineering: Powering Beyond 2001, Conference Proceedings*, 105–113. https://doi.org/10.1109/LESCPE.2001.941635

Abriendomundo. (2023). *IEA (2024), Renewables 2023, IEA, Paris https://www.iea.org/reports/renewables-2023, Licence: CC BY 4.0*. 141. www.iea.org

Ahmad, J., Tahir, M., & Mazumder, S. K. (2019). Dynamic economic dispatch and transient control of distributed generators in a microgrid. *IEEE Systems Journal*, *13*(1), 802–812. https://doi.org/10.1109/JSYST.2018.2859755

Akmam Naamandadin, N., Jian Ming, C., & Azani Mustafa, W. (2018). Relationship between Solar Irradiance and Power Generated by Photovoltaic Panel: Case Study at UniCITI Alam Campus, Padang Besar, Malaysia. *Journal of Advanced Research in Engineering Knowledge*, *5*(1), 16–20. www.akademiabaru.com/arek.html

Alvarado, F. L., & Fahriog, M. (2000). Designing Incentive Compatible Contracts for Effective Demand Management. *Power*, *15*(4), 1255–1260.

Azurza, O., Arranbide, I., & Zubia, I. (2012). Rural electrification based on renewable energies. A review. *Renewable Energy and Power Quality Journal*, *1*(10), 497–502. https://doi.org/10.24084/repqj10.361

Babayomi, O., & Okharedia, T. (2019). Challenges to Sub-Saharan Africa's Renewable Microgrid Expansion-A CETEP Solution Model. *IEEE PES/IAS PowerAfrica Conference: Power Economics and Energy Innovation in Africa, PowerAfrica 2019*, 617–621. https://doi.org/10.1109/PowerAfrica.2019.8928865

Bakare, M. S., Abdulkarim, A., Zeeshan, M., & Shuaibu, A. N. (2023). A comprehensive overview on demand side energy management towards smart grids: challenges, solutions, and future direction. *Energy Informatics*, *6*(1). https://doi.org/10.1186/s42162-023-00262-7

Balat, M., & Ayar, G. (2005). Biomass energy in the world, use of biomass and potential

trends. *Energy Sources*, *27*(10), 931–940. https://doi.org/10.1080/00908310490449045

Barton, J. P., & Infield, D. G. (2004). Energy Storage and Its Use With Intermittent Renewable Energy. *IEEE TRANSACTIONS ON ENERGY CONVERSION*, *19*(2), 441–448.

Barupal, D. K., & Fiehn, O. (2019). Generating the blood exposome database using a comprehensive text mining and database fusion approach. *Environmental Health Perspectives*, *127*(9), 2825–2830. https://doi.org/10.1289/EHP4713

Biglia, A., Gemmell, A. J., Foster, H. J., & Evans, J. A. (2018). Temperature and energy performance of domestic cold appliances in households in England. *International Journal of Refrigeration*, *87*, 172–184. https://doi.org/10.1016/j.ijrefrig.2017.10.022

Blimpo, M. P., & Cosgrove-davies, M. (2020). *Accès à l ' électricité en Afrique subsaharienne*.

Bouvet, A., Mermoz, S., Le Toan, T., Villard, L., Mathieu, R., Naidoo, L., & Asner, G. P. (2018). An above-ground biomass map of African savannahs and woodlands at 25 m resolution derived from ALOS PALSAR. *Remote Sensing of Environment*, *206*(December 2017), 156–173. https://doi.org/10.1016/j.rse.2017.12.030

Bui, V. H., Hussain, A., & Kim, H. M. (2018). A multiagent-based hierarchical energy management strategy for multi-microgrids considering adjustable power and demand response. *IEEE Transactions on Smart Grid*, *9*(2), 1323–1333. https://doi.org/10.1109/TSG.2016.2585671

Cecati, C., Citro, C., & Siano, P. (2011). Combined operations of renewable energy systems and responsive demand in a smart grid. *IEEE Transactions on Sustainable Energy*, *2*(4), 468–476. https://doi.org/10.1109/TSTE.2011.2161624

Chauhan, R. K., & Chauhan, K. (2018). Management of renewable energy source and battery bank for power losses optimization. In *Smart Power Distribution Systems: Control, Communication, and Optimization*. Elsevier Inc. https://doi.org/10.1016/B978-0-12-812154-2.00015-8

Chirambo, D. (2018). Towards the achievement of SDG 7 in sub-Saharan Africa: Creating synergies between Power Africa, Sustainable Energy for All and climate finance in-order to achieve universal energy access before 2030. *Renewable and Sustainable Energy Reviews*, *94*(May), 600–608. https://doi.org/10.1016/j.rser.2018.06.025

Cross, J., & Neumark, T. (2021). Solar Power and its Discontents: Critiquing Off-grid Infrastructures of Inclusion in East Africa. *Development and Change*, *0*(0), 1–25. https://doi.org/10.1111/dech.12668

Degefa, M. Z., Sale, H., Petersen, I., & Ahcin, P. (2018). Data-driven Household Load Flexibility Modelling: Shiftable Atomic Load. *Proceedings - 2018 IEEE PES Innovative Smart Grid Technologies Conference Europe, ISGT-Europe 2018*, 5–10. https://doi.org/10.1109/ISGTEurope.2018.8571836

Denholm, P., Ong, S., & Booten, C. (2012). *Using Utility Load Data to Estimate Demand for Space Cooling and Potential for Shiftable Loads*. *May*, 23.

Devi, S., & Ayswarya, N. (2015). Artificial Neural Network Approach for Load Forecasting in Demand Side Management. *International Journal of Advanced Research in Electrical, Electronics and Instrumentation Engineering*, *04*(02), 581–586. https://doi.org/10.15662/ijareeie.2015.0402011

Diyan, M., Silva, B. N., & Han, K. (2020). A multi-objective approach for optimal energy management in smart home using the reinforcement learning. *Sensors (Switzerland)*, *20*(12), 1–20. https://doi.org/10.3390/s20123450

Duby, S., Engelmeier, T., & TFE Consulting. (2017). *The World's Microgrid Lab*. http://www.tfeconsulting.com/_website/wp-content/uploads/2017/09/TFE_Report-Kenya-new.pdf

Elattar, E. E. (2018). Modified harmony search algorithm for combined economic emission dispatch of microgrid incorporating renewable sources. *Energy*, *159*, 496–507. https://doi.org/10.1016/j.energy.2018.06.137

Erdoğan, S., Onifade, S. T., Altuntaş, M., & Bekun, F. V. (2022a). Synthesizing urbanization and carbon emissions in Africa: how viable is environmental sustainability amid the quest for economic growth in a globalized world? *Environmental Science and Pollution Research*, *29*(16), 24348–24361. https://doi.org/10.1007/s11356-022-18829-4

Erdoğan, S., Onifade, S. T., Altuntaş, M., & Bekun, F. V. (2022b). Synthesizing urbanization and carbon emissions in Africa: how viable is environmental sustainability amid the quest for economic growth in a globalized world? *Environmental Science and Pollution Research*, *29*(16), 24348–24361. https://doi.org/10.1007/s11356-022-18829-4

ERPA. (2021). *the Kenya Electricity Grid Code Part 2: Kenya National Grid Distribution Code (Kndgc)*. *April*.

Eskom, & Nersa. (2003). Electricity Supply - Quality of Supply (Part 2 : Voltage characteristics , compatibility levels , limits and assessment methods). In *Technology Standardization Department*. www.stansa.co.za

Evans, J. A., Foster, H. J., & Gemmell, A. J. (2018). Evaluation of suitability of recycled domestic appliances for RE-USE. *Refrigeration Science and Technology*, *2018-April*, 393–401. https://doi.org/10.18462/iir.iccc.2018.0051

Gebreslassie, K. G., & Khellaf, A. (2021). A Review on Energy Access: A Case Study in Africa. *International Conference on Electrical, Computer, and Energy Technologies, ICECET 2021*, *December*, 1–6. https://doi.org/10.1109/ICECET52533.2021.9698488

Gellings, C. W. (1985). The Concept of Demand-Side Management for Electric Utilities. *Proceedings of the IEEE*, *73*(10), 1468–1470. https://doi.org/10.1109/PROC.1985.13318

Google Earth. (2023). *Microgrids locations*. https://earth.google.com/web/search/Mpale,+Tanga,+Tanzania/@-4.9998624,38.45497125,1064.46526292a,18528.87970284d,35y,0h,0t,0r/data=CoEBGlcSUQolMHgxODQ2YTY1MmU5ZDVhY2JiOjB4NWMzYjU5MDJkYjE3NzcxNxlcYhun1_wTwCE49BYP7ztDQCoWTXBhbGUsIFRhbmdhLCBUYW56YW5pYRgCIAE

Greg Adams, Aloulou, F., Aniti, L., Boedecker, E., Brown, W., Chase, N., Cole, M., Cook, T., Daniels, D., Farber-DeAnda, M., Federhen, C., Ford, M., Geagla, A., Hutchins, P., Jell, S., Johnson, S., Jones, J., Kahan, A., Kearney, D., … Wells, P. (2016). *International Energy Outlook 2016* (Vol. 0484, Issue May). www.eia.gov

Gyamfi, S., Diawuo, F. A., Asuamah, E. Y., & Effah, E. (2022). The role of demand-side management in sustainable energy sector development. In *Renewable Energy and Sustainability: Prospects in the Developing Economies* (First Edit). Elsevier Ltd. https://doi.org/10.1016/B978-0-323-88668-0.00010-3

Hartvigsson, E., Ehnberg, J., Ahlgren, E., & Molander, S. (2015). Assessment of load profiles in minigrids: A case in Tanzania. *Proceedings of the Universities Power Engineering Conference*, *2015-Novem*. https://doi.org/10.1109/UPEC.2015.7339818

He, J., Chen, J., He, X., Gao, J., Li, L., Deng, L., & Ostendorf, M. (2017). Deep

Reinforcement Learning And Model Predictive Control Approaches For The Scheduled Operation Of Domestic Refrigerators. *Iclr*, *1999*, 1–17.

Huang, Z., & Zhu, T. (2016). Real-Time Data and Energy Management in Microgrids. *Proceedings - Real-Time Systems Symposium*, *0*, 79–88. https://doi.org/10.1109/RTSS.2016.017

Iljazi, T. (2021). the Impact of Professor'S Personality on Teaching Mathematics. *Journal of Educational Research*, *36*, 51–58. https://www.ceeol.com/search/article-detail?id=985139

IRENA. (2003). *Estimating the Renewable Energy Potential in Africa: A GIS-based approach*. *18*(2), 29–31.

Jakhrani, A. Q., Rigit, A. R. H., Othman, A. K., Samo, S. R., & Kamboh, S. A. (2012). Estimation of carbon footprints from diesel generator emissions. *Proceedings of the 2012 International Conference in Green and Ubiquitous Technology, GUT 2012*, 78–81. https://doi.org/10.1109/GUT.2012.6344193

Jasim, A. M., Jasim, B. H., Mohseni, S., & Brent, A. (2022). *Consensus-based dispatch optimization of a microgrid considering meta-heuristic-based demand response scheduling and network packet loss characterization*.

Kakande, J. N., Philipo, G. H., & Krauter, S. (2023). Demand Side Management Potential of Refrigeration Appliances. *2023 IEEE PES/IAS PowerAfrica*, 1–5. https://doi.org/10.1109/powerafrica57932.2023.10363161

Kempener, R., D'Ortigue, O. L., Saygin, D., Skeer, J., Vinci, S., & Gielen, D. (2015). *Off-grid renewabe energy systems - Status and methodology.pdf*.

Kent, R. (2018). Renewables. In *Plastics Engineering* (Vol. 74, Issue 9). https://doi.org/10.1002/peng.20026

Khalid, A. M., Mitra, I., Warmuth, W., & Schacht, V. (2016). Performance ratio – Crucial parameter for grid connected PV plants. *Renewable and Sustainable Energy Reviews*, *65*, 1139–1158. https://doi.org/10.1016/j.rser.2016.07.066

Krishnamurthy, S, & Tzoneva, R. (2012). *Multi Objective Dispatch Problem with Valve Point Effect Loading of Fuel Cost and Emission Criterion*. *4*(5), 775–784.

Krishnamurthy, Senthil, & Tzoneva, R. (2011). *Comparative Analyses of Min-Max and Max-Max Price Penalty Factor Approaches for Multi Criteria Power System Dispatch*

Problem Using Lagrange ' s Method. 36–43.

Kruyt, B., van Vuuren, D. P., de Vries, H. J. M., & Groenenberg, H. (2009). Indicators for energy security. *Energy Policy*, *37*(6), 2166–2181. https://doi.org/10.1016/j.enpol.2009.02.006

Kwac, J., Member, S., Flora, J., & Rajagopal, R. (2014). *Household Energy Consumption Segmentation Using Hourly Data*. *5*(1), 420–430.

Lampropoulos, I. (2014). Energy Management of Distributed Resources in Power System Operations. In *Ph.D. Thesis, Eindhoven University of Technology* (Issue 2014). Technische Universiteit Eindhoven. https://doi.org/10.6100/IR771935

Lazaroiu, G. C., Dumbrava, V., Balaban, G., Longo, M., & Zaninelli, D. (2016). Stochastic optimization of microgrids with renewable and storage energy systems. *EEEIC 2016 - International Conference on Environment and Electrical Engineering*. https://doi.org/10.1109/EEEIC.2016.7555486

Li, D., Chiu, W., & Sun, H. (2017). *Demand Side Management in Microgrid Control Systems* (pp. 203–230). https://doi.org/10.1016/B978-0-08-101753-1.00007-3

Lu, R., Hong, S. H., & Yu, M. (2019). Demand Response for Home Energy Management Using Reinforcement Learning and Artificial Neural Network. *IEEE Transactions on Smart Grid*, *10*(6), 6629–6639. https://doi.org/10.1109/TSG.2019.2909266

Menos-aikateriniadis, C., Lamprinos, I., & Georgilakis, P. S. (2022). Particle Swarm Optimization in Residential Demand-Side Management: A Review on Scheduling and Control Algorithms for Demand Response Provision. *Energies*, *15*(6). https://doi.org/10.3390/en15062211

Micangeli, A., Del Citto, R., Checchi, F., Viganò, D., Nouboundieu, S., & Cestari, G. (2018). Rural electrification in Central America and East Africa, two case studies of sustainable microgrids. *Iberoamerican Journal of Development Studies*, *7*(2), 82–113. https://doi.org/10.26754/ojs_ried/ijds.254

Mirjalili, S., Song Dong, J., & Lewis, A. (2020). Nature-inspired Optimizers. In *Studies in Computational Intelligence* (Vol. 811).

Moghaddam, M. P., Abdollahi, A., & Rashidinejad, M. (2011). Flexible demand response programs modeling in competitive electricity markets. *Applied Energy*, *88*(9), 3257–3269. https://doi.org/10.1016/j.apenergy.2011.02.039

Muhihi, B., & Paschal, L. L. (2022). Rural electricity system reliability: Do outages exacerbate spending on backup fuel in rural Tanzania? *Journal of Energy in Southern Africa*, *33*(2), 52–64. https://doi.org/10.17159/2413-3051/2022/v33i2a13018

Narula, K. (2014). Is sustainable energy security of India increasing or decreasing? *International Journal of Sustainable Energy*, *33*(6), 1054–1075. https://doi.org/10.1080/14786451.2013.811411

NASA. (2023). *ArcGIS World Geocoding Service*. ArcGIS World Geocoding Service. https://power.larc.nasa.gov/data-access-viewer/

Nawaz, A., Hafeez, G., Khan, I., Jan, K. U., Li, H., Khan, S. A., & Wadud, Z. (2020). An Intelligent Integrated Approach for Efficient Demand Side Management with Forecaster and Advanced Metering Infrastructure Frameworks in Smart Grid. *IEEE Access*, *8*, 132551–132581. https://doi.org/10.1109/ACCESS.2020.3007095

Nwulu, N. I., & Xia, X. (2017). Optimal dispatch for a microgrid incorporating renewables and demand response. *Renewable Energy*, *101*, 16–28. https://doi.org/10.1016/j.renene.2016.08.026

Ogg, F. (2015). Pico, Nano, Micro, Mini and Macrogrids and the role of windturbines in a grid. *6th World Summit for Small Wind 2015*, *March*, 19.

Pachauri, S. (2011). Reaching an international consensus on defining modern energy access. *Current Opinion in Environmental Sustainability*, *3*(4), 235–240. https://doi.org/10.1016/j.cosust.2011.07.005

Pacheco, F. E., & Foreman, J. C. (2017). Microgrid Reference Methodology for Understanding Utility and Customer Interactions in Microgrid Projects. *Electricity Journal*, *30*(3), 44–50. https://doi.org/10.1016/j.tej.2017.03.005

Palanichamy, C., & Babu, N. S. (2008). *Analytical solution for combined economic and emissions dispatch*. *78*, 1129–1137. https://doi.org/10.1016/j.epsr.2007.09.005

Panda, S., Mohanty, S., Rout, P. K., Sahu, B. K., Bajaj, M., Zawbaa, H. M., & Kamel, S. (2022). Residential Demand Side Management model, optimization and future perspective: A review. *Energy Reports*, *8*, 3727–3766. https://doi.org/10.1016/j.egyr.2022.02.300

Paul, J., Lee, K., & Mushfiq, A. (2017). Electricity Reliability and Economic Development in Cities : A Microeconomic Perspective Paul J . Gertler , Kenneth Lee , A . Mushfiq Mobarak EEG State-of-Knowledge Paper Ser ies Oxford Policy Management Center

for Effective Global Action. *Energy and Economic Growth*.

Philipo, G. H., Chande Jande, Y. A., & Kivevele, T. (2020). Demand-Side Management of Solar Microgrid Operation: Effect of Time-of-Use Pricing and Incentives. *Journal of Renewable Energy*, *2020*, 1–12. https://doi.org/10.1155/2020/6956214

Philipo, G. H., Chande Jande, Y. A., & Kivevele, T. (2021). Clustering and Fuzzy Logic-Based Demand-Side Management for Solar Microgrid Operation: Case Study of Ngurudoto Microgrid, Arusha, Tanzania. *Advances in Fuzzy Systems, 2021*. https://doi.org/10.1155/2021/6614129

Philipo, G. H., Kakande, J. N., & Krauter, S. (2022). *Neural Network-Based Demand-Side Management in a Stand-Alone Solar PV-Battery Microgrid Using Load-Shifting and Peak-Clipping*.

Postnikov, A., Albayati, I. M., Pearson, S., Bingham, C., Bickerton, R., & Zolotas, A. (2019). Facilitating static firm frequency response with aggregated networks of commercial food refrigeration systems. *Applied Energy*, *251*(January), 113357. https://doi.org/10.1016/j.apenergy.2019.113357

Rajabi, A., Eskandari, M., Ghadi, M. J., Li, L., Zhang, J., & Siano, P. (2020). A comparative study of clustering techniques for electrical load pattern segmentation. *Renewable and Sustainable Energy Reviews*, *120*(January). https://doi.org/10.1016/j.rser.2019.109628

Rangel, N., Li, H., & Aristidou, P. (2023). An optimisation tool for minimising fuel consumption, costs and emissions from Diesel-PV-Battery hybrid microgrids. *Applied Energy*, *335*(January). https://doi.org/10.1016/j.apenergy.2023.120748

Refrigeration, I. I. of. (2019). *" Refrigeration is of paramount importance for mankind and must become a priority for policy makers ."*

Riahi, K., Bertram, C., Huppmann, D., Rogelj, J., Bosetti, V., Cabardos, A. M., Deppermann, A., Drouet, L., Frank, S., Fricko, O., Fujimori, S., Harmsen, M., Hasegawa, T., Krey, V., Luderer, G., Paroussos, L., Schaeffer, R., Weitzel, M., van der Zwaan, B., … Zakeri, B. (2021). Cost and attainability of meeting stringent climate targets without overshoot. *Nature Climate Change*, *11*(12), 1063–1069. https://doi.org/10.1038/s41558-021-01215-2

Rodgers, J. L., & Nicewander, W. A. (1988). *Thirteen Ways to Look at the Correlation Coefficient Published by : Taylor & Francis , Ltd . on behalf of the American*

Statistical Association Stable URL : http://www.jstor.org/stable/2685263 REFERENCES Linked references are available on JSTOR for this ar. *42*(1), 59–66.

Roosa, S. A. (2021). Fundamentals of Microgrids: Development and Implementation. In *The Economics of Microgrids*. https://doi.org/10.1002/9781394162482.ch1

Roy, C., Das, D. K., & Srivastava, A. (2019). Particle Swarm Optimization based Cost Optimization for Demand Side Management in Smart Grid. *Proceedings - 2019 International Conference on Electrical, Electronics and Computer Engineering, UPCON 2019*, 1–6. https://doi.org/10.1109/UPCON47278.2019.8980149

Sarfi, V., Livani, H., & Yliniemi, L. (2018). A New Multi-Objective Economic Emission Dispatch in Microgrids. *2017 IEEE Power & Energy Society General Meeting*, 5. 10.1109/PESGM.2017.8274401

Schnitzer, D., Shinde, D. L., Carvallo, J. P., Deshmukh, R., Apt, J., & Kammen, D. M. (2014). *Microgrids for Rural Electrification : A critical review of best practices* (Issue February). https://doi.org/10.13140/RG.2.1.1399.9600

Selami Shaqiri, M., Iljazi, T., Kamberi, L., Shaqiri, M., & Ramani -halili, R. (2023). *Differences between the correlation coefficients pearson, kendall and spearman*. *November*. http://ikm.mk/ojs/index.php/kij/issue/view/154

Slowik, A. (2011). Particle Swarm Optimization. *The Industrial Electronics Handbook - Five Volume Set*, 1942–1948. https://doi.org/10.1007/978-3-319-46173-1_2

Smith, B. A., Wong, J., & Rajagopal, R. (2012). A Simple Way to Use Interval Data to Segment Residential Customers for Energy Efficiency and Demand Response Program Targeting. *ACEEE Sum. Study Ener. Effic. in Buil.*, 374–386.

SolarGIS. (2021). *Solar resource maps of Africa*. SolarGIS. https://solargis.com/maps-and-gis-data/download/africa

Song, J., Lee, J., Kim, T., & Yoon, Y. (2017). Study of peak load demand estimation methodology by pearson correlation analysis with macro-economic indices and power generation considering power supply interruption. *Journal of Electrical Engineering and Technology*, *12*(4), 1427–1434. https://doi.org/10.5370/JEET.2017.12.4.1427

Stevanato, N., Lombardi, F., Colmbo, E., Balderrama, S., & Quoilin, S. (2019). Two-stage stochastic sizing of a rural micro-grid based on stochastic load generation. *2019 IEEE Milan PowerTech, PowerTech 2019*, 1–6. https://doi.org/10.1109/PTC.2019.8810571

Steyer, S., Hughes, S., & Whitney, N. (2014). *Predicting Low Voltage Events on Rural Micro-Grids in Tanzania*. 1–6. https://www.semanticscholar.org/paper/d493122e774ea6daf775e8deb7833154eb7d6aca

SunEarthTools. (2023). *Tools for consumers and designers of solar*. https://www.sunearthtools.com/

Takalani, R., & Bekker, B. (2020). Load and load growth models for rural microgrids, and how to future-proof designs. *2020 International SAUPEC/RobMech/PRASA Conference*, 10–15. https://doi.org/10.1109/SAUPEC/RobMech/PRASA48453.2020.9041001

Tanzania Bureau of Standards (TBS). (2011). *COMPLEMENTARY COPY - EWURA © TBS Power quality – Quality of supply* (1st ed.). Tanzania Bureau of Standards (TBS).

Tazvinga, H., Zhu, B., & Xia, X. (2014). Energy dispatch strategy for a photovoltaic-wind-diesel-battery hybrid power system. *Solar Energy*, *108*, 412–420. https://doi.org/10.1016/j.solener.2014.07.025

Thakur, T., Sem, K., Saini, S., & Sharma, S. (2006). *Emissions for Environmentally Constrained Economic Dispatch Problem*. *00*.

Thirunavukkarasu, G. S., Seyedmahmoudian, M., Jamei, E., Horan, B., Mekhilef, S., & Stojcevski, A. (2022). Role of optimization techniques in microgrid energy management systems—A review. *Energy Strategy Reviews*, *43*(June), 100899. https://doi.org/10.1016/j.esr.2022.100899

Tiffany Sue Burgess. (2015). *the Effects of External Temperature on the Energy Consumption of Household Refrigerator- Freezers and Freezers*. *August*.

Torriti, J. (2012). Price-based demand side management: Assessing the impacts of time-of-use tariffs on residential electricity demand and peak shifting in Northern Italy. *Energy*, *44*(1), 576–583. https://doi.org/10.1016/j.energy.2012.05.043

Tran, J., Gilles, J., Mann, R., & Murthy, V. (2015). Automated Demand Response Refrigerator Project. *Tran2015AutomatedDR*, *186*(October), 1–7. https://ecal.berkeley.edu/files/ce186/projects/mannryancasey_4883549_63830968_CE 186 Final Paper.pdf

Traoré, A., Elgothamy, H., & Zohdy, M. A. (2018). Optimal Sizing of Solar/Wind Hybrid Off-Grid Microgrids Using an Enhanced Genetic Algorithm. *Journal of Power and*

Energy Engineering, *06*(05), 64–77. https://doi.org/10.4236/jpee.2018.65004

Trivedi, I. N., Jangir, P., Bhoye, M., & Jangir, N. (2018). An economic load dispatch and multiple environmental dispatch problem solution with microgrids using interior search algorithm. *Neural Computing and Applications*, *30*(7), 2173–2189. https://doi.org/10.1007/s00521-016-2795-5

Turiel, I. (1997). Present status of residential appliance energy efficiency standards - An international review. *Energy and Buildings*, *26*(1), 5–15. https://doi.org/10.1016/s0378-7788(96)01011-0

Walczak, S., & Cerpa, N. (2003). Artificial Neural Networks. In *Encyclopedia of Physical Science and Technology* (Third, pp. 631–645). Academic Press. https://doi.org/10.1016/B0-12-227410-5/00837-1.

Wang, Y., Chen, Q., Kang, C., Zhang, M., Wang, K., & Zhao, Y. (2015). Load profiling and its application to demand response: A review. *Tsinghua Science and Technology*, *20*(2), 117–129. https://doi.org/10.1109/tst.2015.7085625

Warren, P. (2014). A review of demand-side management policy in the UK. *Renewable and Sustainable Energy Reviews*, *29*, 941–951. https://doi.org/10.1016/j.rser.2013.09.009

Weetch, B. (2021). *Winch Energy completes funding for African solar projects*. Energy Global. https://www.energyglobal.com/special-reports/17022021/winch-energy-completes-funding-for-african-solar-projects/

Williams, N. J., Jaramillo, P., Cornell, B., Lyons-Galante, I., & Wynn, E. (2017). Load characteristics of East African microgrids. *Proceedings - 2017 IEEE PES-IAS PowerAfrica Conference: Harnessing Energy, Information and Communications Technology (ICT) for Affordable Electrification of Africa, PowerAfrica 2017*, 236–241. https://doi.org/10.1109/PowerAfrica.2017.7991230

Xu, H., Meng, Z., & Wang, Y. (2020). Economic dispatching of microgrid considering renewable energy uncertainty and demand side response. *Energy Reports*, *6*, 196–204. https://doi.org/10.1016/j.egyr.2020.11.261

Yang, X.-S. (2021). Genetic algorithms. In *Nature-Inspired Optimization Algorithms* (Second Edi, pp. 91–100). Academic Press. https://doi.org/10.1016/B978-0-12-821986-7.00013-5

Yazdkhasti, P., & Diduch, C. P. (2020). Demand side management using model-free fuzzy

controller in a direct load control program. *2020 IEEE Electric Power and Energy Conference, EPEC 2020*, *3*, 9–13. https://doi.org/10.1109/EPEC48502.2020.9320090

Yoder, E., & Williams, N. J. (2020). Load Profile Prediction Using Customer Characteristics. *2020 IEEE PES/IAS PowerAfrica, PowerAfrica 2020*. https://doi.org/10.1109/PowerAfrica49420.2020.9219811

Zar, J. H. (1972). Significance testing of the spearman rank correlation coefficient. *Journal of the American Statistical Association*, *67*(339), 578–580. https://doi.org/10.1080/01621459.1972.10481251

Research Outputs

A. Publications

Philipo, G. H., Kakande, J. N., & Krauter, S. (2022). Neural Network-Based Demand-Side Management in a Stand-Alone Solar PV-Battery Microgrid Using Load-Shifting and Peak-Clipping. *Energies*, *15*(14), 5215. https://doi.org/10.3390/en15145215

Philipo, G. H., Kakande, J. N., & Krauter, S. (2023, September). Demand-Side-Management for Optimal Dispatch of an Isolated Solar Microgrid. In 2023 IEEE AFRICON (pp. 1-6). IEEE. https://doi.org/10.1109/AFRICON55910.2023.10293343

Philipo, G. H., Kakande, J. N., & Krauter, S. (2023, November). Combined Economic and Emission Dispatch of a Microgrid Considering Multiple Generators. In 2023 IEEE PES/IAS PowerAfrica (pp. 1-5). IEEE. https://doi.org/10.1109/PowerAfrica57932.2023.10363325

Kakande, J. N., Philipo, G. H., & Krauter, S. (2021). Load Data Acquisition in Rural East Africa for the Layout of Microgrids and Demand–Side–Management Measures. In Proceedings of the 38th European Photovoltaic Solar Energy Conference and Exhibition (EUPVSEC 2021). https://doi.org/10.4229/EUPVSEC20212021-6BV.5.38

Kakande, J. N., Philipo, G. H., & Krauter, S. (2023, November). Demand Side Management Potential of Refrigeration Appliances. In *2023 IEEE PES/IAS PowerAfrica* (pp. 1-5). IEEE. https://doi.org/10.1109/PowerAfrica57932.2023.10363161

Kakande, J. N., Philipo, G. H., & Krauter, S. (2022). Optimal Design of a Semi Grid-Connected PV System for a Site in Lwak, Kenya, Using HOMER. *Proceedings of the 8th World Conference on Photovoltaik Energy Conversion*. 8th World Conference on Photovoltaik Energy Conversion, Milano / Italy.

B. Master's Thesis Supervision

Analyse und Auslegung eines Stromversorgungssystems für das Mädcheninternat am Standort Lwak in Kenia zur Minimierung des CO2-Fußabdrucks und der Kosten: **Omid Malki, 28.08.2023, Paderborn.**

Development of an energy management system to control a Load system Through IoT platform: **Waddah Alturk, 09.04.2024, Paderborn.**

C. Practical Output

Demand side management practical set up in Lwak Convent in Kenya.

Appendices

Appendix A: Mavowatt Power Quality Reports

Appendix A-1: MAVOWATT Manual website link

MAVOWATT 270 | GOSSEN METRAWATT | CAMILLE BAUER

Mpale Mavowatt power quality data obtained from MAVOWATT quick report

Appendix A-2: Voltage Timeplots

Site: MPALEDATATUESDAY

Measured from 10/05/2022 13:31:04 to 11/05/2022 11:25:00

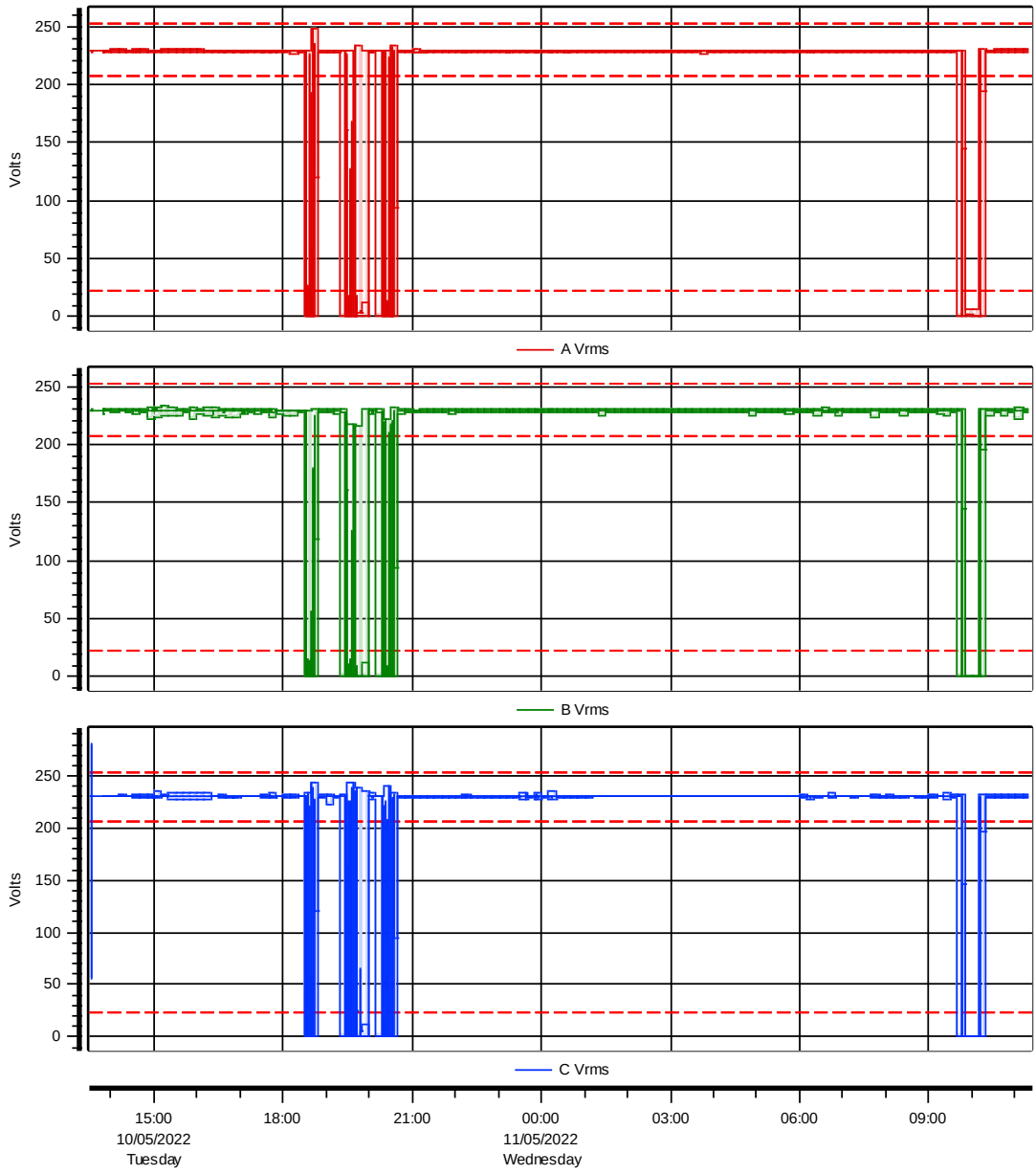

Appendix A-3: Activity Plots

Site: MPALEDATATUESDAY

Measured from 10/05/2022 13:31:04 to 11/05/2022 11:25:00

VOLTAGE DIPS

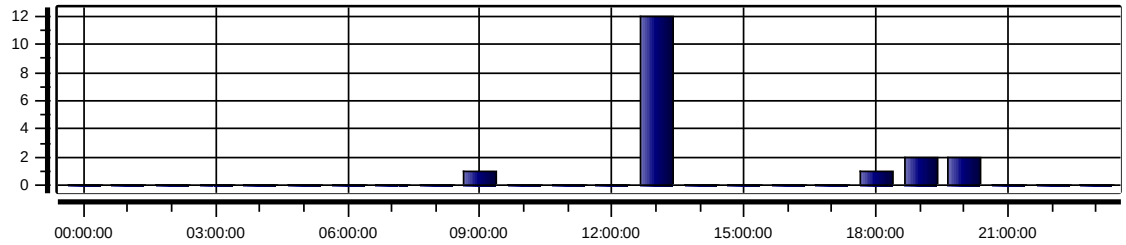

VOLTAGE SWELLS

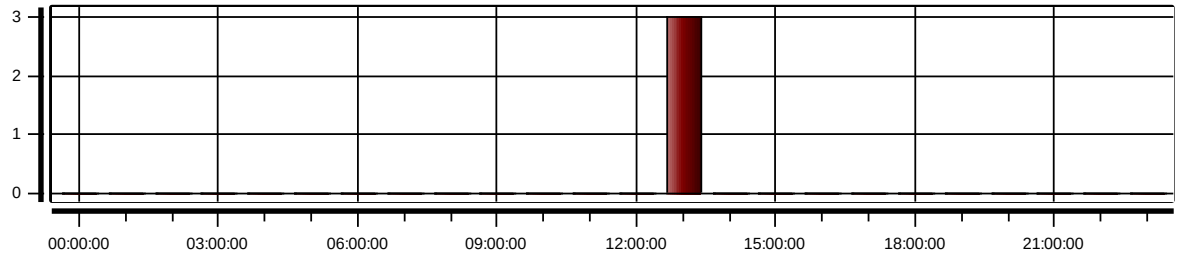

VOLTAGE INTERRUPTIONS

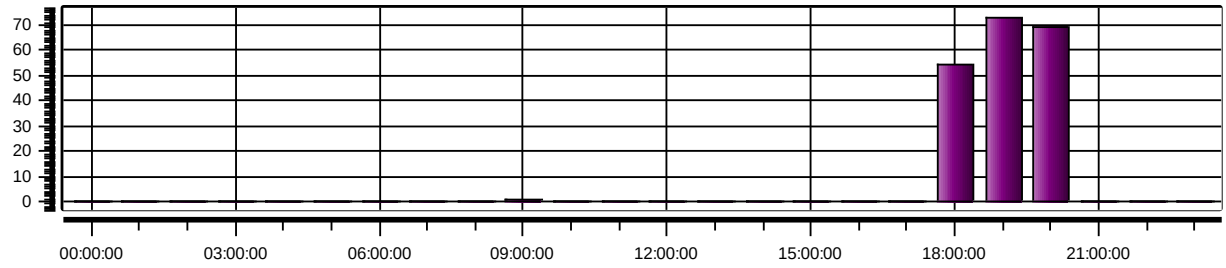

VOLTAGE TRANSIENTS

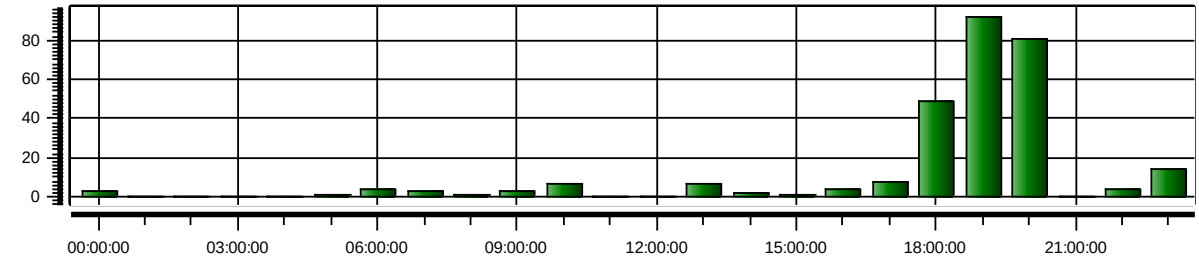

Appendix A-4: Worst Case Summary Waveforms

Site: MPALE DATA TUESDAY

Measured from 10/05/2022 13:31:04 to 11/05/2022 11:25:00

Lowest Magnitude Voltage Dip: Phase C

Sustained 0.1V,1947.619 Sec., on 10/05/2022 19:27:02.64 13:32:55.71

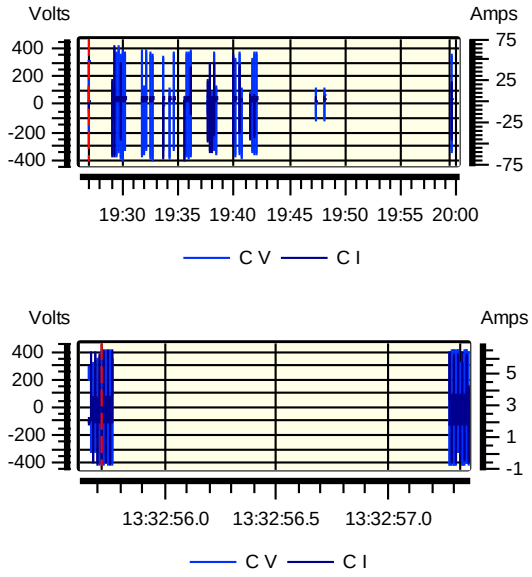

Highest Magnitude Voltage Swell: Phase C

Momentary 281.4V,1.615 Sec., on 10/05/2022

Longest Duration Voltage Dip: Phase A

Sustained 0.1V,1947.619 Sec., on 10/05/2022 19:27:02.64 13:32:57.35

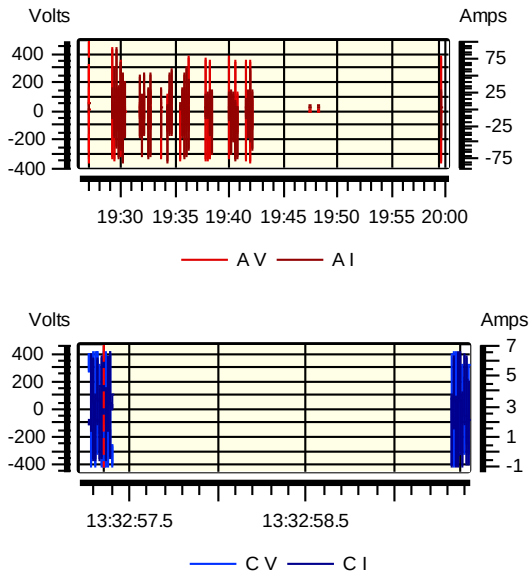

Longest Duration Voltage Swell: Phase C

Momentary 281.2V,2.027 Sec., on 10/05/2022

Most Energy Missing Voltage Dip: Phase C

Instantaneous 55.4V,0.423 Sec., on 10/05/2022 13:32:47.43 13:32:57.35

Most Energy Added Voltage Swell: Phase C

Momentary 281.2V,2.027 Sec., on 10/05/2022

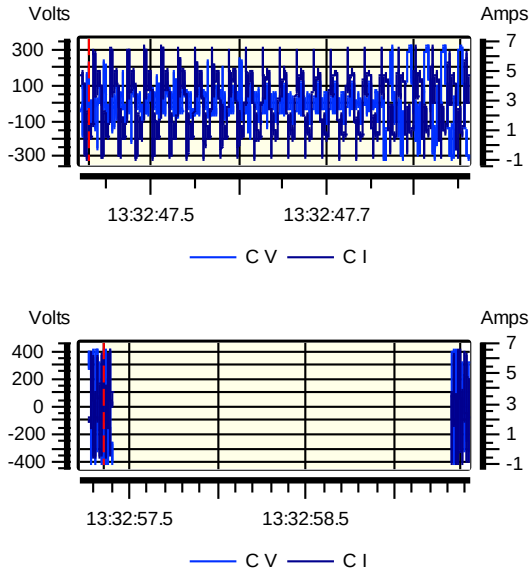

Longest Duration Voltage Interruption: Phase A

Momentary 0.1V,1511.455 Sec., on 11/05/2022 09:46:19.44

Largest Magnitude Voltage Transients: Phase A

1261.0V,0.003 Sec., on 10/05/2022 18:41:55.18

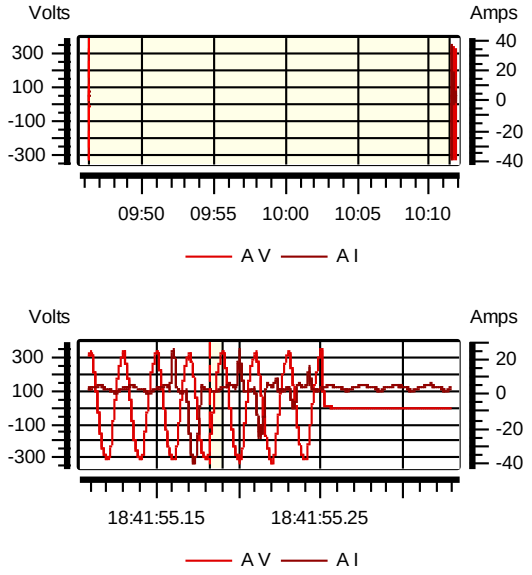

Appendix A-5: Phase A Harmonic Timeplot

Site: MPALE DATA TUESDAY

Measured from 10/05/2022 13:31:04 to 11/05/2022 11:25:00

VOLTAGE

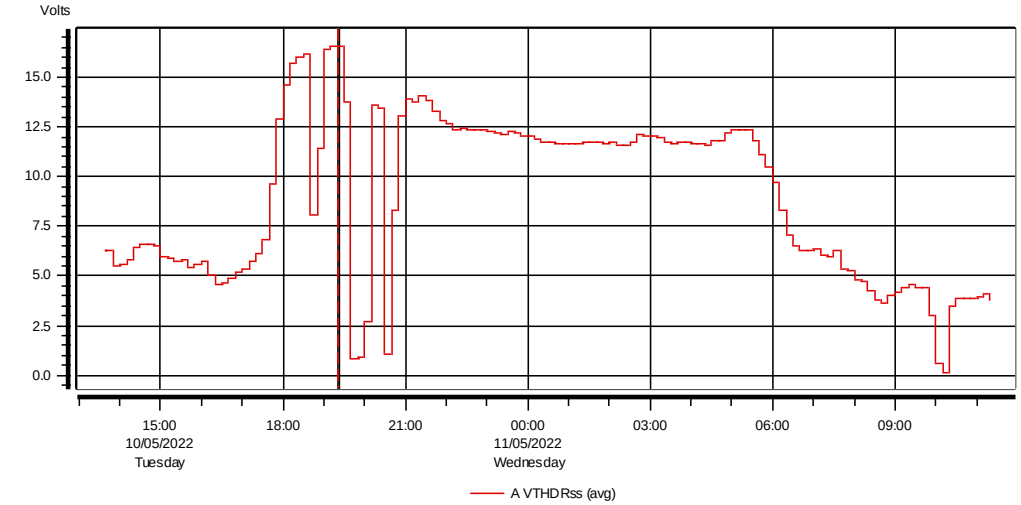

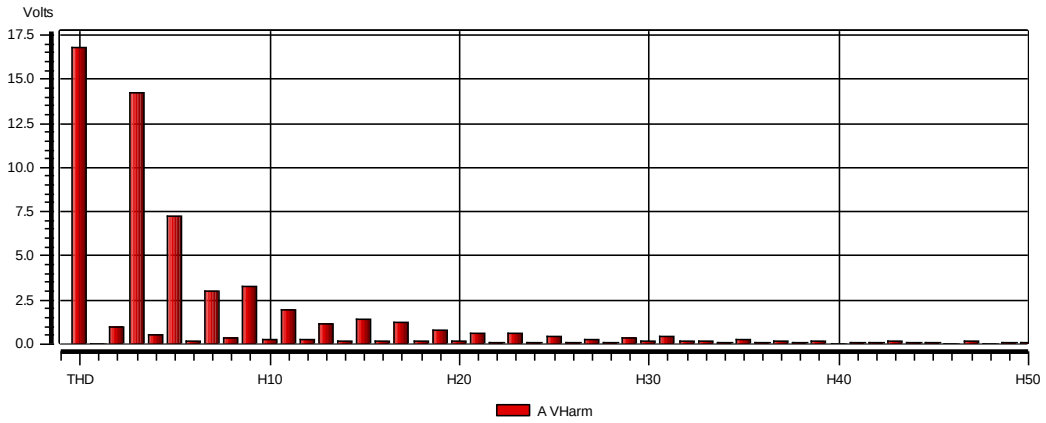

Total RMS:	228.91 V
DC Level:	0.02 V
Fundamental(H1) RMS:	227.91 V
Total Harmonic Distortion THD:	16.83 V (Even: 1.37 V, Odd: 16.91 V)

CURRENT

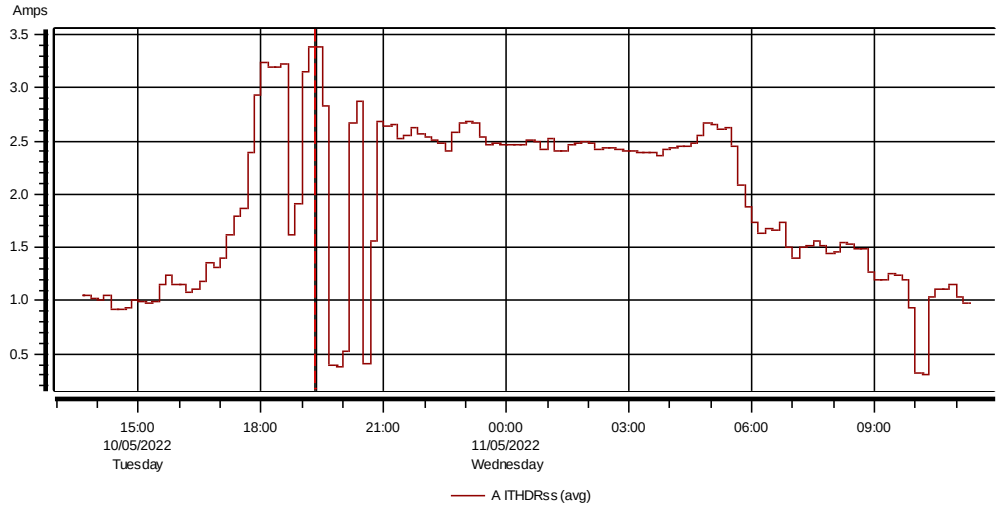

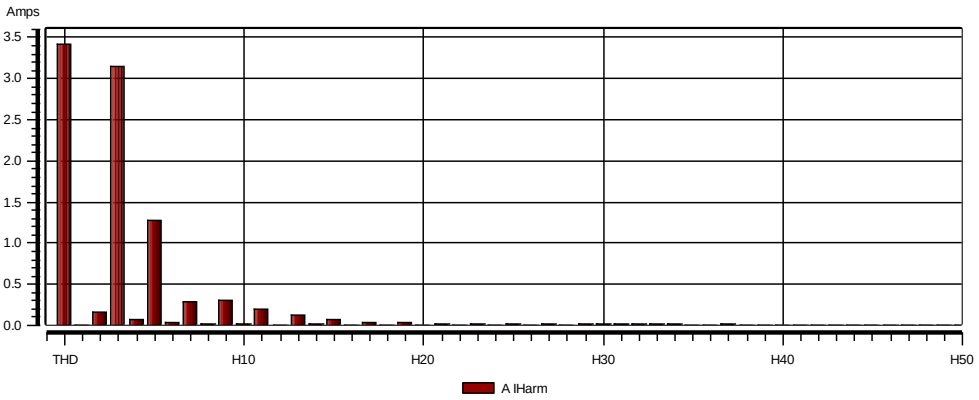

Total RMS:	6.52 A
DC Level:	2.87 A
Fundamental(H1) RMS:	4.23 A
Total Harmonic Distortion THD:	3.43 A (Even: 0.18 A, Odd: 3.43 A)

Appendix A- 6: Phase B Harmonic Timeplot

Site: MPALE DATA TUESDAY

Measured from 10/05/2022 13:31:04 to 11/05/2022 11:25:00

VOLTAGE

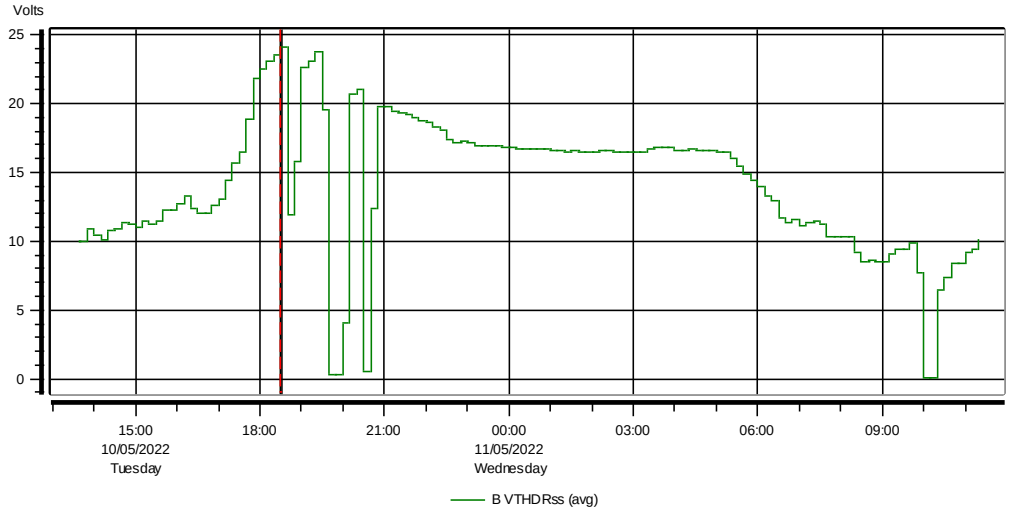

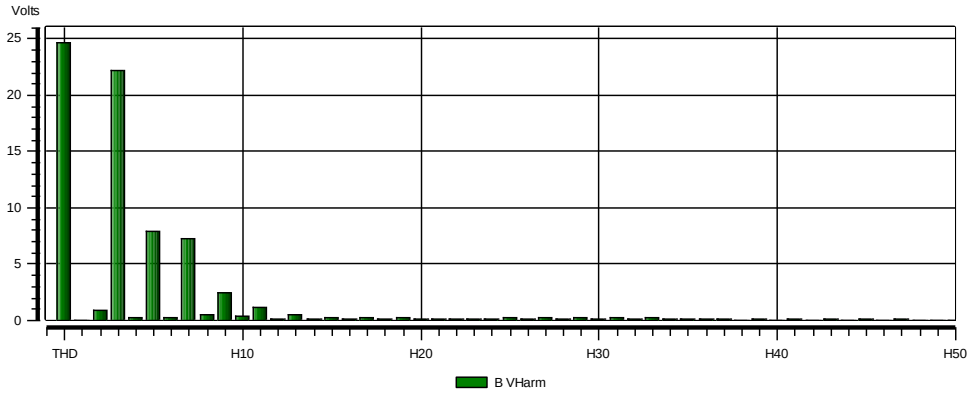

Total RMS:	229.83 V
DC Level:	0.09 V
Fundamental(H1) RMS:	227.78 V
Total Harmonic Distortion THD:	24.73 V (Even: 1.22 V, Odd: 24.86 V)

CURRENT

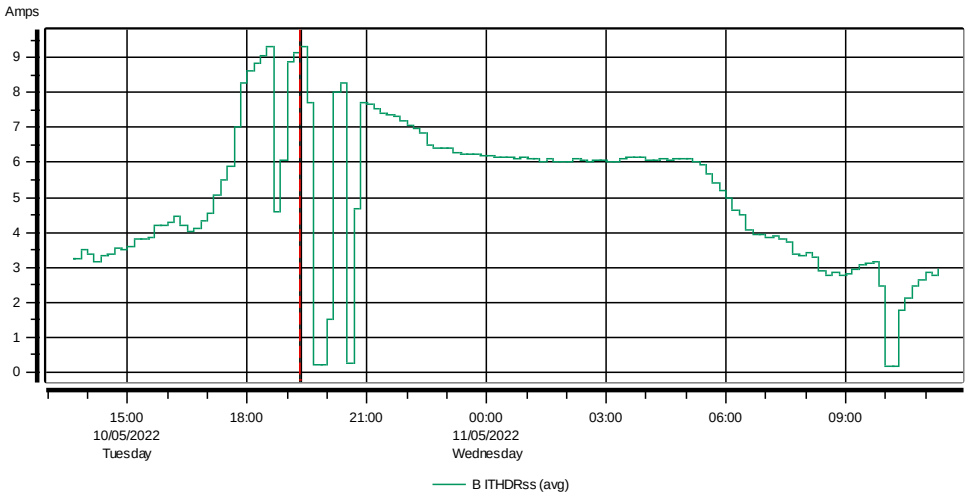

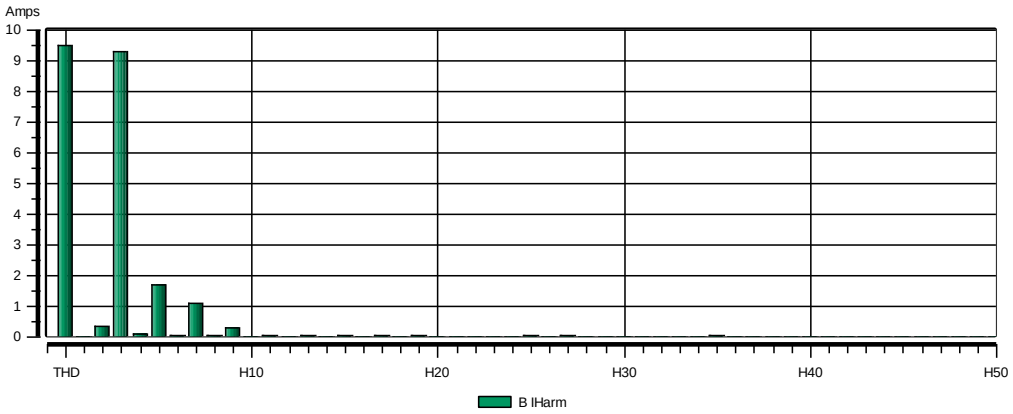

Total RMS:	23.34 A
DC Level:	3.03 A
Fundamental(H1) RMS:	19.74 A
Total Harmonic Distortion THD:	9.51 A (Even: 0.36 A, Odd: 9.52 A)

Appendix A- 7: Phase C Harmonic Timeplot

Site: MPALE DATA TUESDAY

Measured from 10/05/2022 13:31:04 to 11/05/2022 11:25:00

VOLTAGE

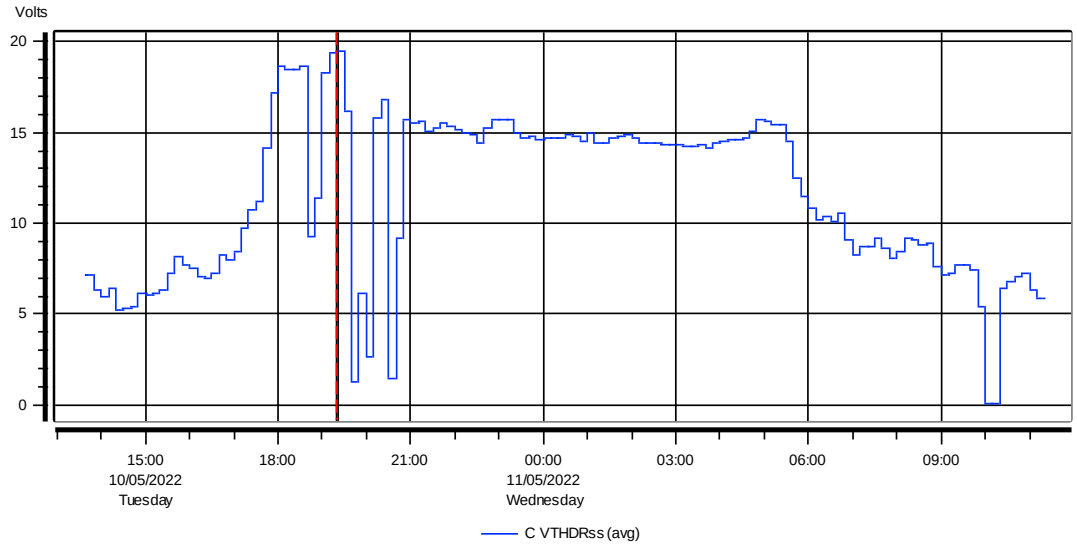

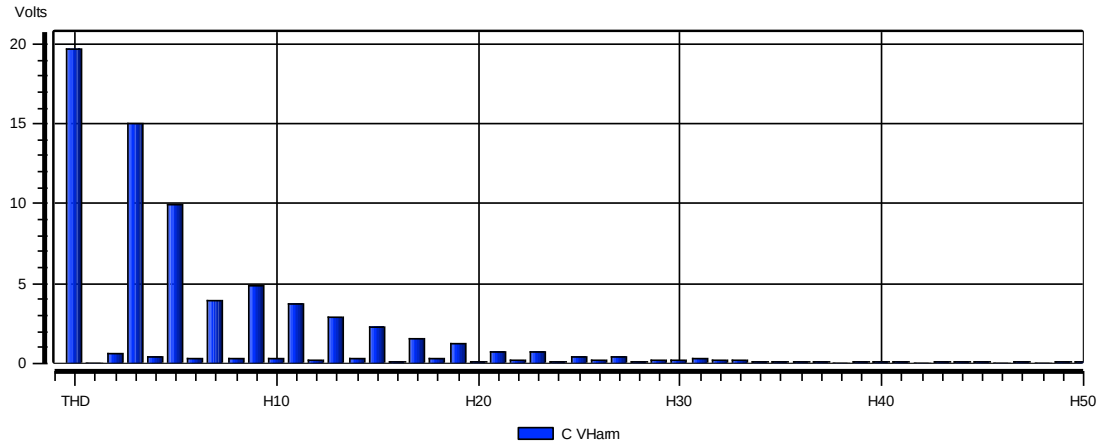

Total RMS:	230.80 V
DC Level:	0.10 V
Fundamental(H1) RMS:	229.75 V
Total Harmonic Distortion THD:	19.73 V (Even: 1.18 V, Odd: 19.90 V)

CURRENT

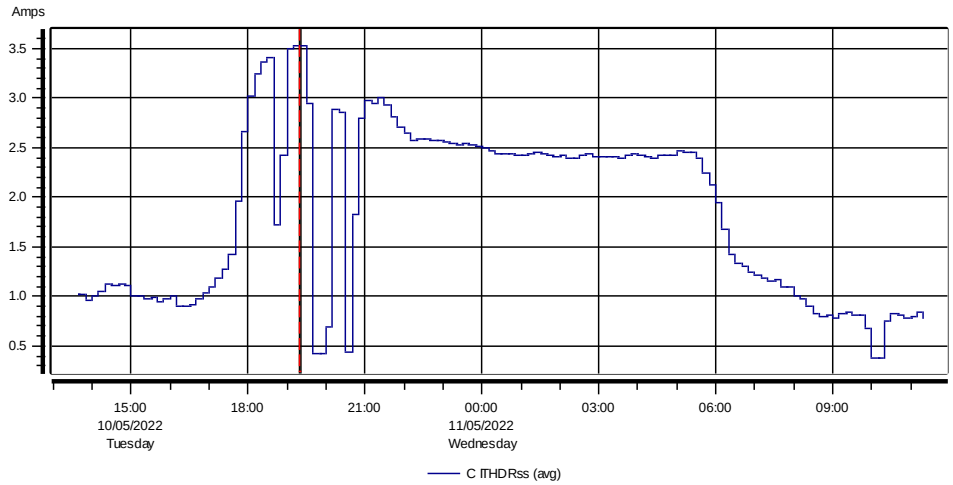

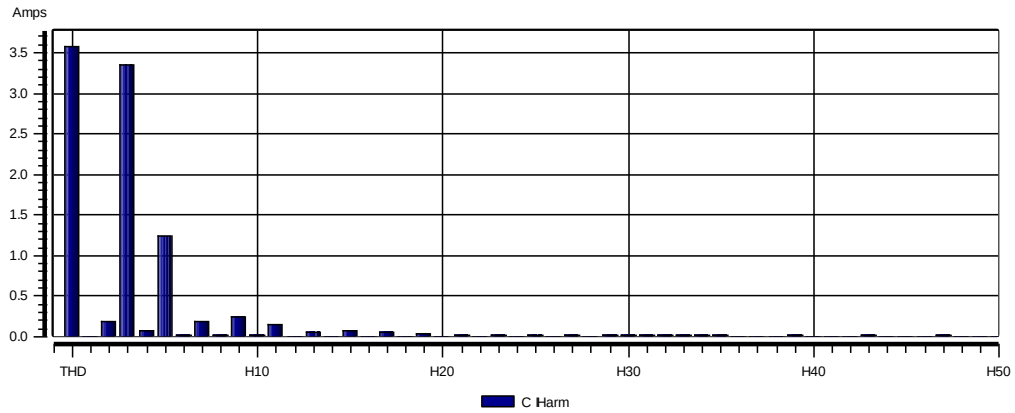

Total RMS:	8.01 A
DC Level:	2.92 A
Fundamental(H1) RMS:	5.91 A
Total Harmonic Distortion THD:	3.58 A (Even: 0.22 A, Odd: 3.58 A)

Appendix A- 8: Voltage Timeplots

Site: Bunjako
Measured from 24/02/2022 12:43:14 to 04/03/2022 10:05:00

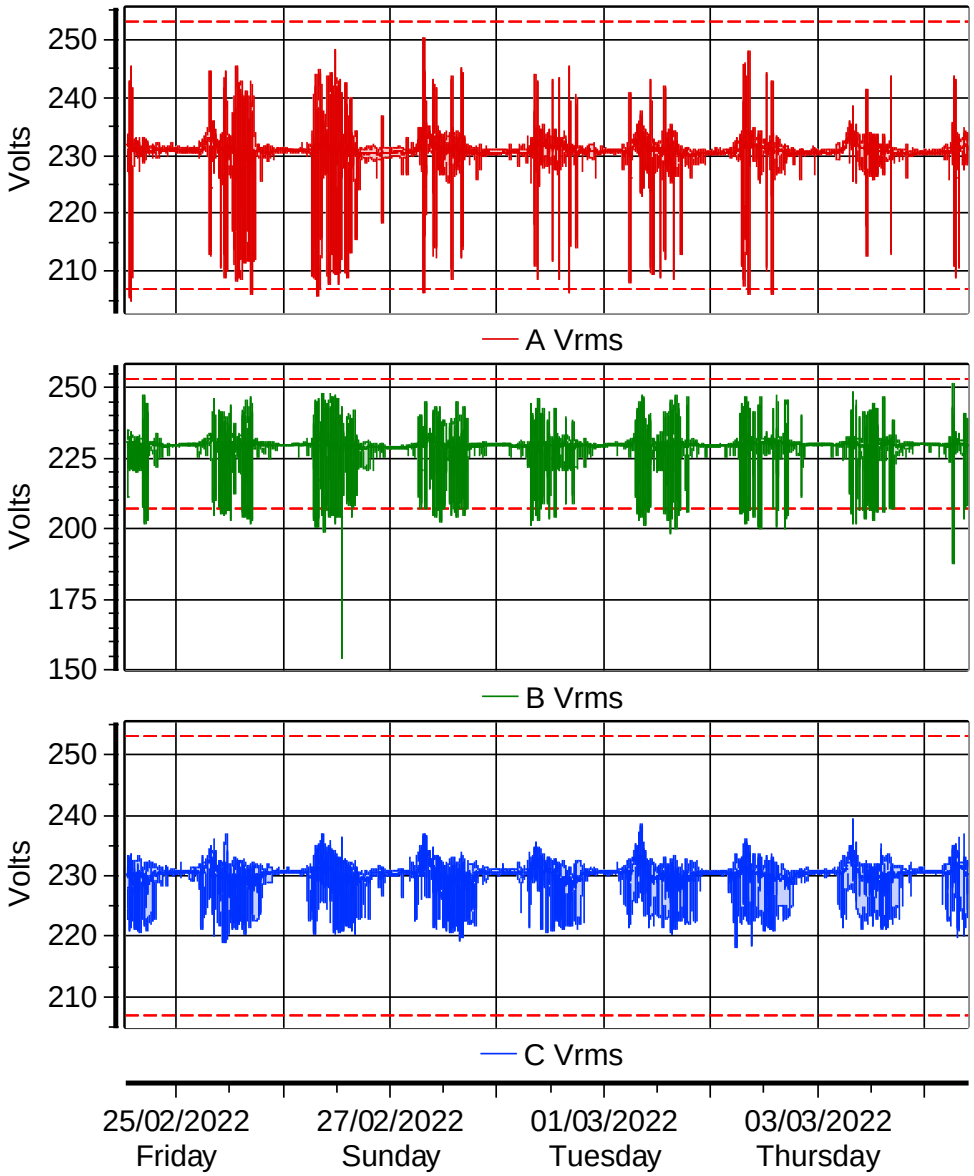

Appendix A- 9: Current Timeplots

Site: Bunjako
Measured from 24/02/2022 12:43:14 to 04/03/2022 10:05:00

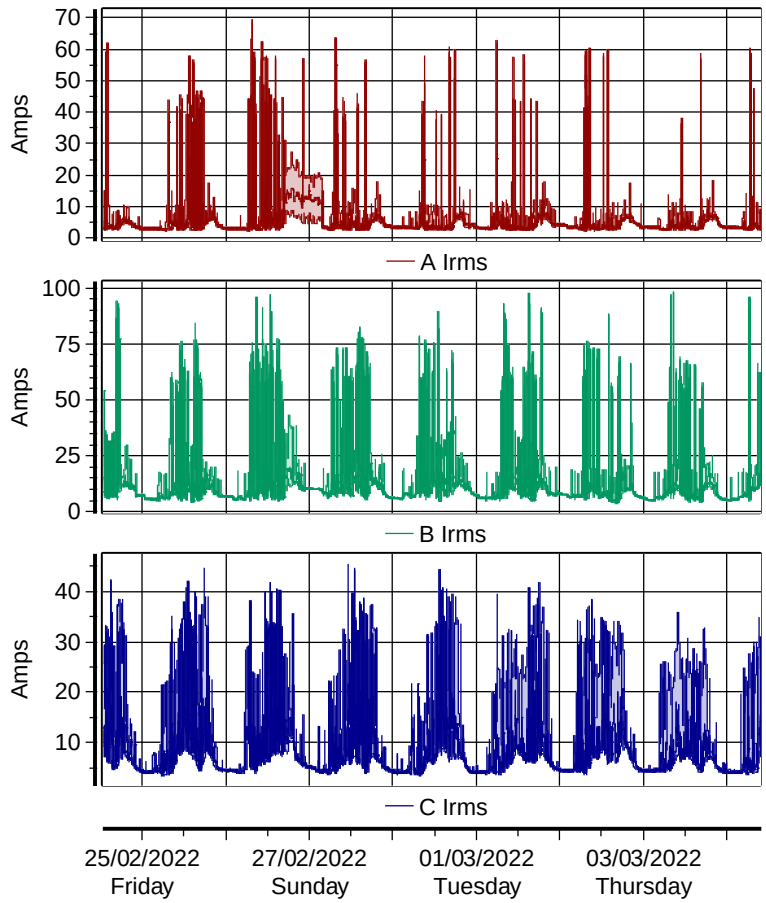

Appendix A-10: VTHD TIMEPLOTS

Site: Bunjjako
Measured from 24/02/2022 12:43:14 to 04/03/2022 10:05:00

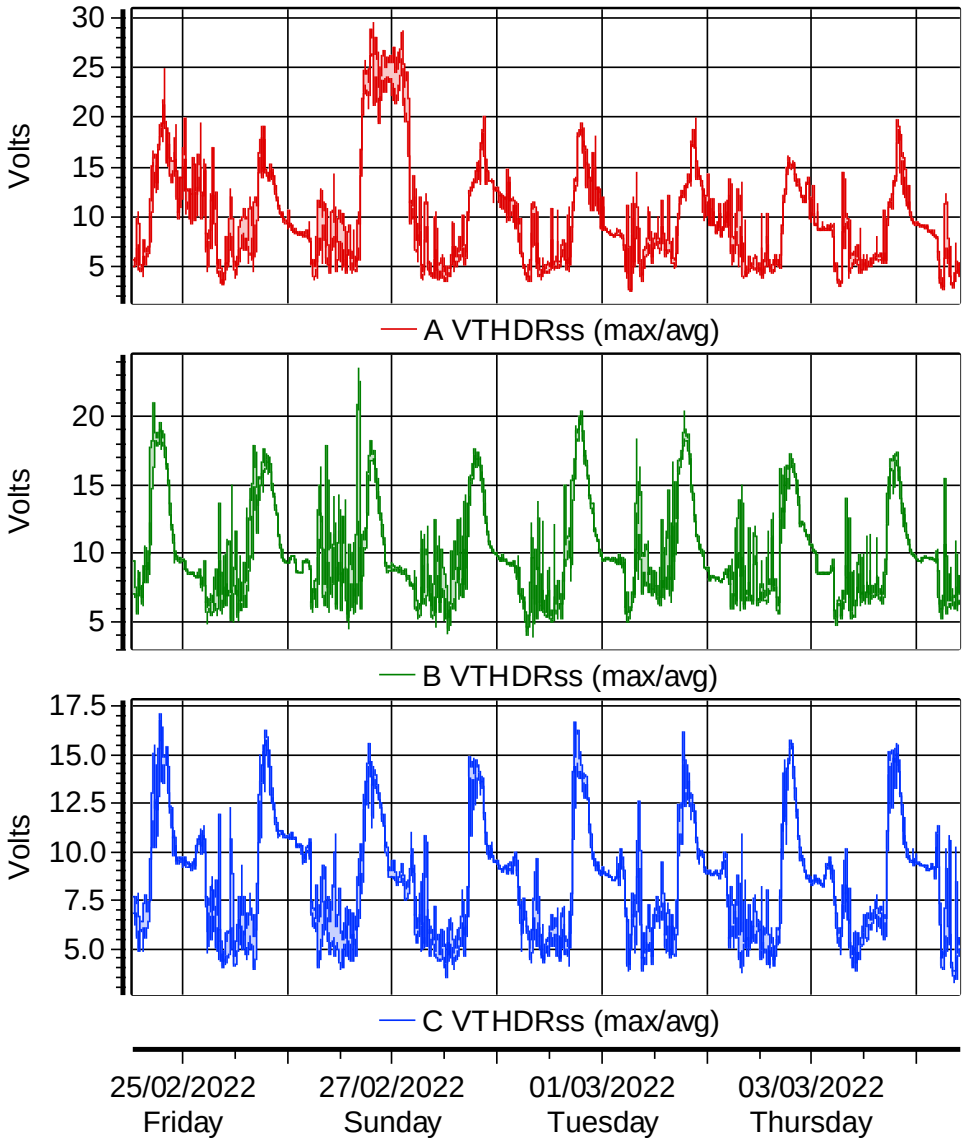

Appendix A-11: VOLTAGE UNBALANCE TIMEPLOTS

Site: Bunjako
Measured from 24/02/2022 12:43:14 to 04/03/2022 10:05:00

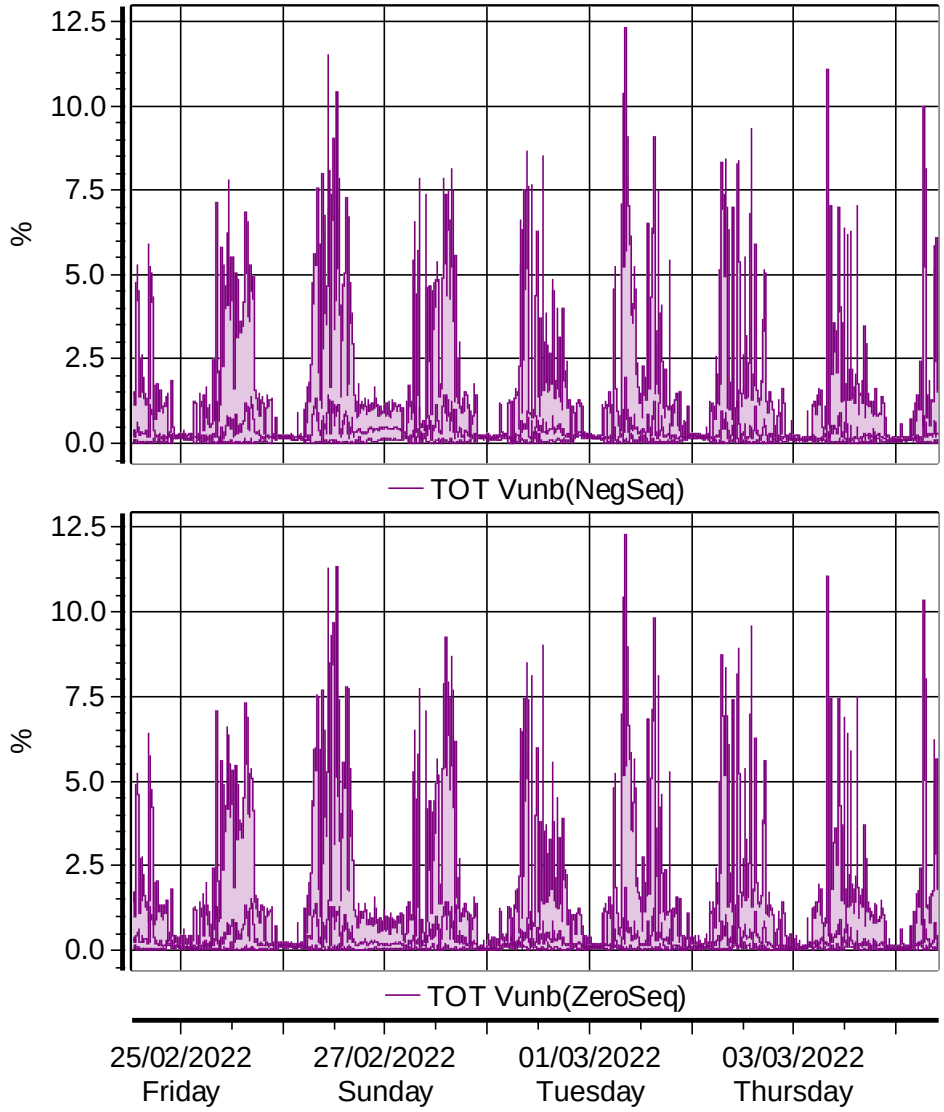

Appendix A-12: FLICKER (PLT) TIMEPLOTS

Site: Bunjako
Measured from 24/02/2022 12:43:14 to 04/03/2022 10:05:00

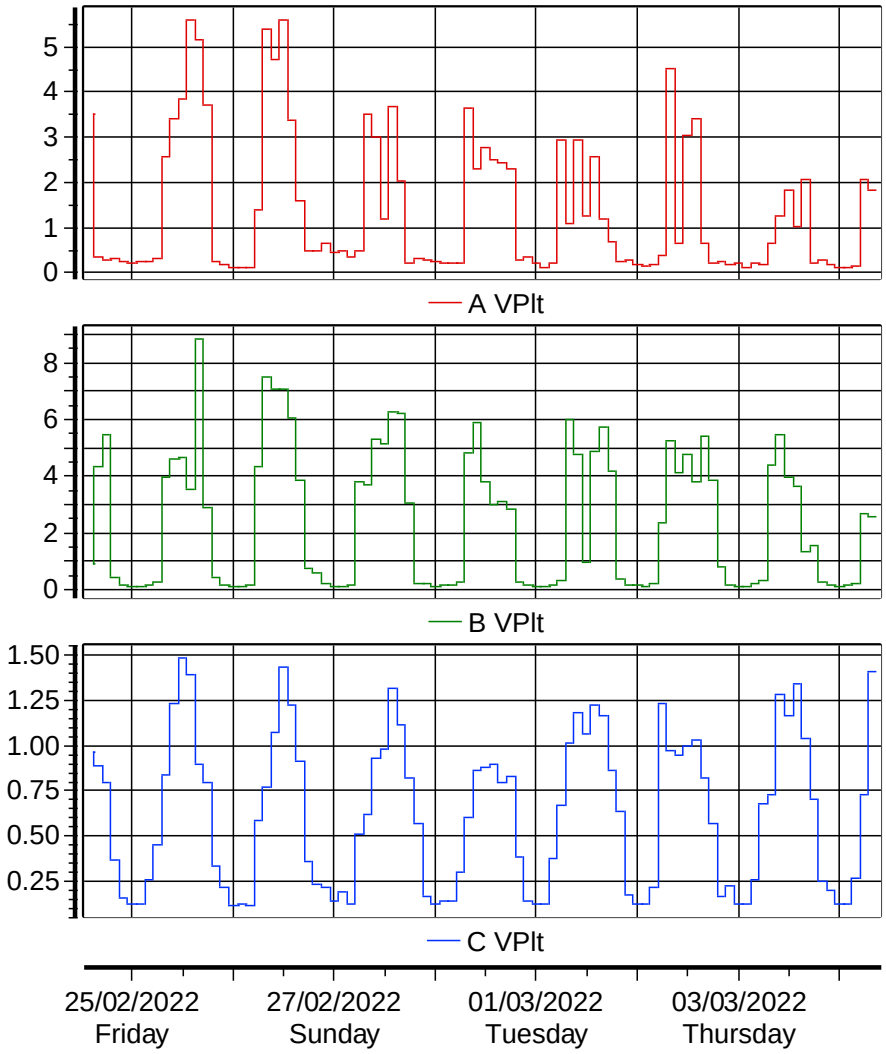

Appendix A-13: VOLTAGE FREQUENCY TIMEPLOTS

Site: Bunjako
Measured from 24/02/2022 12:43:14 to 04/03/2022 10:05:00

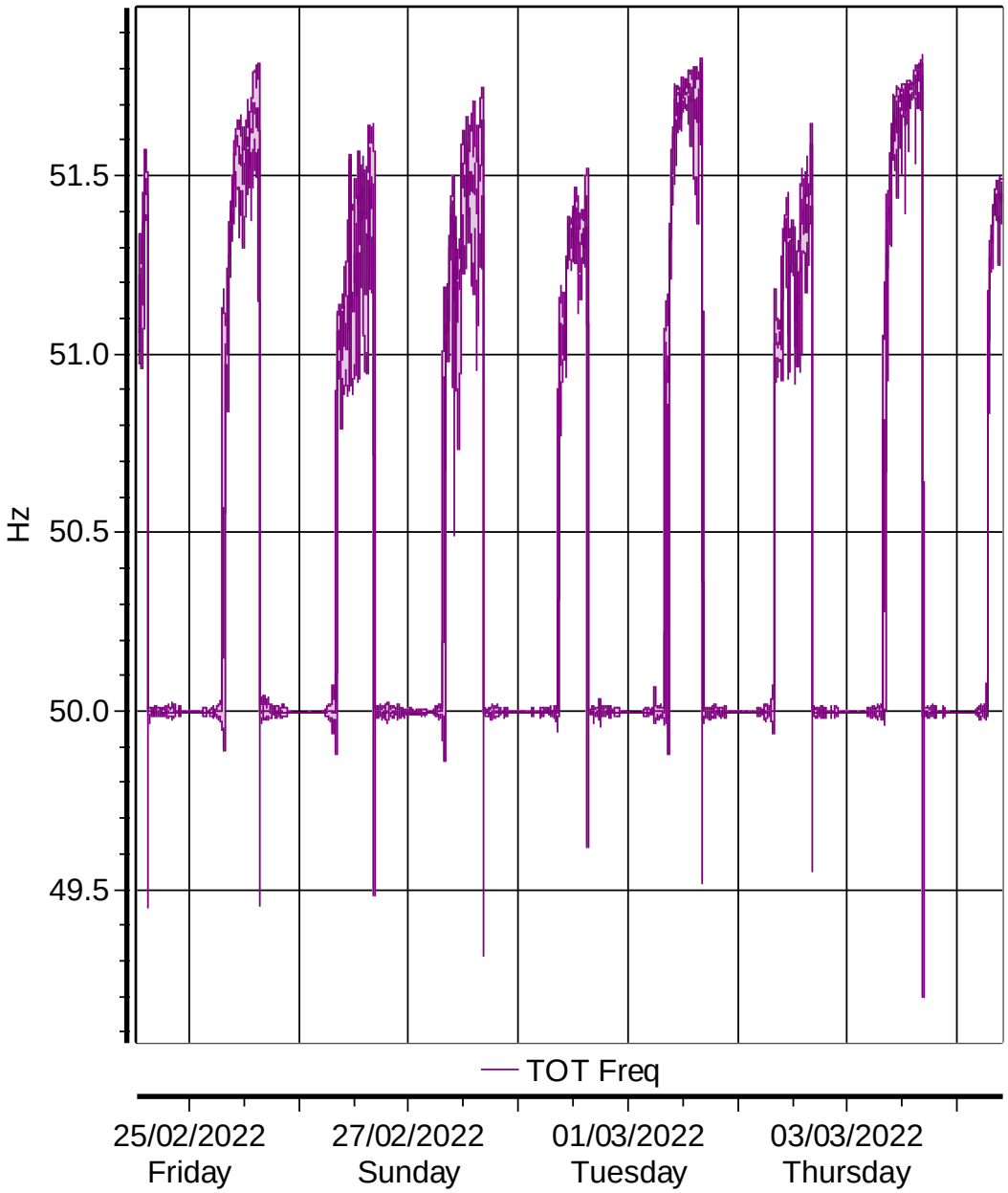

Appendix A- 14: Quality of Supply

Site: Bunjako
Measured from 24/02/2022 12:43:14 to 04/03/2022 10:05:00

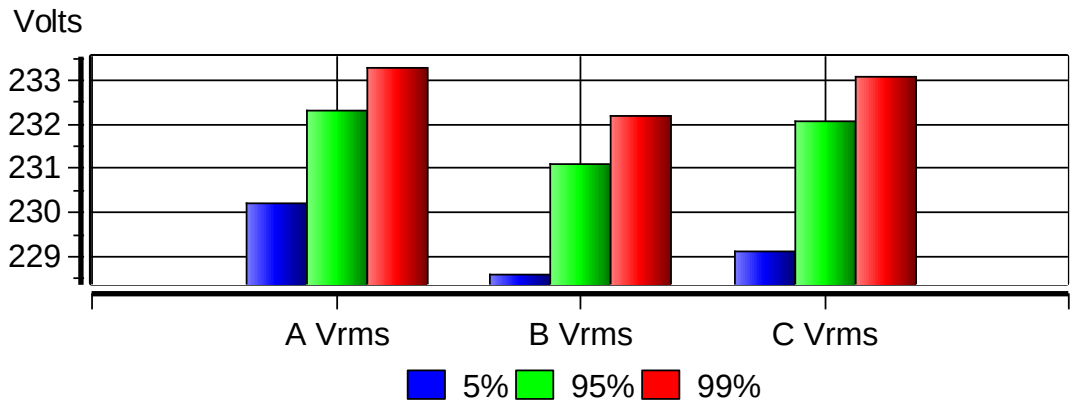

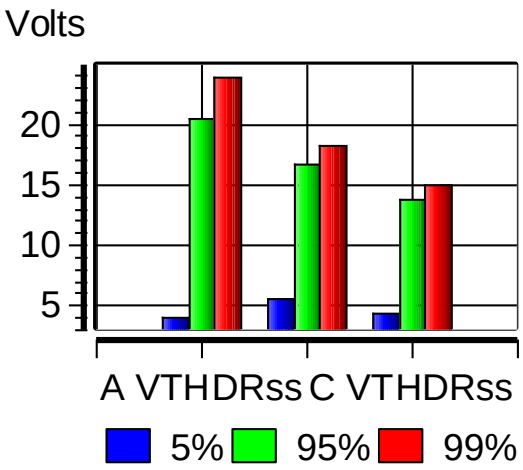

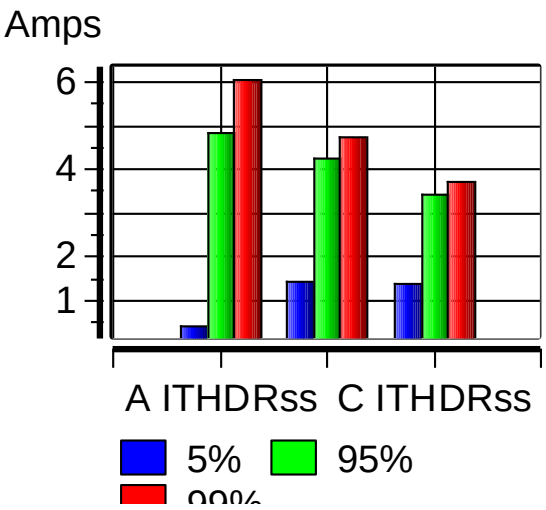

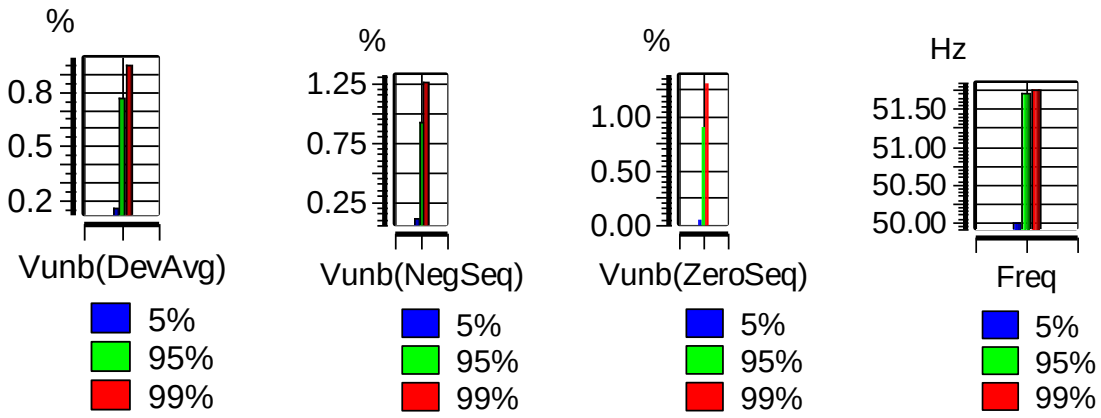

Appendix A- 15:ACTIVITY PLOTS

Site: Bunjako
Measured from 24/02/2022 12:43:14 to 04/03/2022 10:05:00

VOLTAGE DIPS

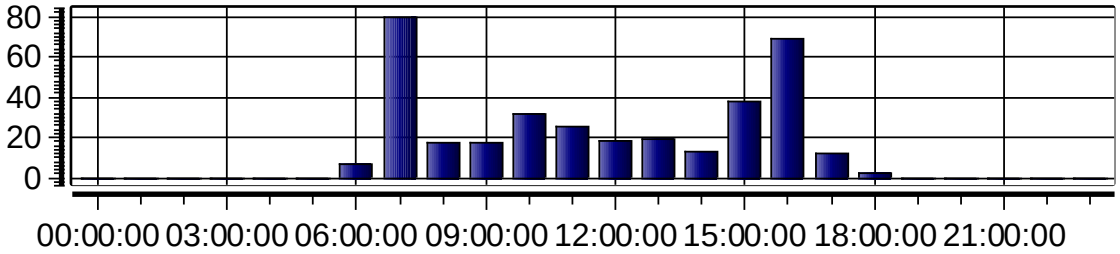

VOLTAGE SWELLS

NO EVENTS WERE FOUND IN THIS CATEGORY

VOLTAGE INTERRUPTIONS

NO EVENTS WERE FOUND IN THIS CATEGORY

VOLTAGE TRANSIENTS

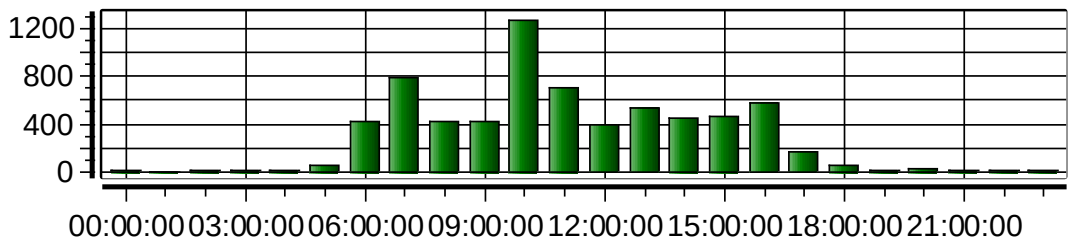

Appendix A- 16: Worst Case Summary

Site: Bunjako
Measured from 24/02/2022 12:43:14 to 04/03/2022 10:05:00

Of 349 total VOLTAGE DIPS

CRITERIA	PHASE	CATEGORY	DATA	DATE/TIME
Lowest Magnitude	B	INSTANTANEOUS	154.5V, 0.519 Sec.	26/02/2022 13:10:42.80
	B	INSTANTANEOUS	188.0V, 0.350 Sec.	04/03/2022 06:36:03.29
	B	INSTANTANEOUS	198.4V, 0.029 Sec.	01/03/2022 15:07:10.30
	B	INSTANTANEOUS	199.1V, 0.029 Sec.	26/02/2022 09:13:19.31
Longest Duration	B	INSTANTANEOUS	154.5V, 0.519 Sec.	26/02/2022 13:10:42.80
	B	INSTANTANEOUS	188.0V, 0.350 Sec.	04/03/2022 06:36:03.29
	B	INSTANTANEOUS	203.3V, 0.040 Sec.	01/03/2022 07:57:34.07
	B	INSTANTANEOUS	205.5V, 0.040 Sec.	02/03/2022 07:02:40.32
Most Energy Missing	B	INSTANTANEOUS	154.5V, 0.519 Sec.	26/02/2022 13:10:42.80
	B	INSTANTANEOUS	188.0V, 0.350 Sec.	04/03/2022 06:36:03.29
	B	INSTANTANEOUS	205.5V, 0.040 Sec.	02/03/2022 07:02:40.32
	B	INSTANTANEOUS	206.2V, 0.039 Sec.	01/03/2022 08:19:46.69

Of 0 total VOLTAGE SWELLS

CRITERIA	PHASE	CATEGORY	DATA	DATE/TIME

Of 0 total VOLTAGE INTERRUPTIONS

CRITERIA	PHASE	CATEGORY	DATA	DATE/TIME

Of 6782 total VOLTAGE TRANSIENTS

CRITERIA	PHASE	DATA	DATE/TIME
Largest Magnitude	B	720.8V, 0.002 Sec.	01/03/2022 16:17:59.73
	B	716.0V, 0.000 Sec.	04/03/2022 06:31:14.03
	A	711.6V, 0.001 Sec.	25/02/2022 10:52:18.82
	B	711.0V, 0.000 Sec.	04/03/2022 08:56:46.88

Appendix A- 17: Worst Case Summary Waveforms

Site: Bunjako
Measured from 24/02/2022 12:43:14 to 04/03/2022 10:05:00

Lowest Magnitude Voltage Dip: Phase B
Instantaneous 154.5V,0.519 Sec., on 26/02/2022 13:10:42.80

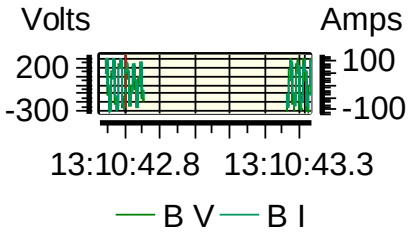

NO WAVEFORM AVAILABLE

Highest Magnitude Voltage Swell: No event

Longest Duration Voltage Dip: Phase B
Instantaneous 154.5V,0.519 Sec., on 26/02/2022 13:10:42.80

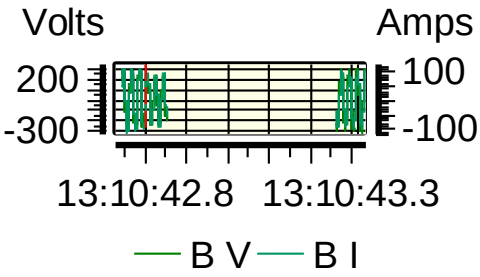

NO WAVEFORM AVAILABLE

Longest Duration Voltage Swell: No event

Most Energy Missing Voltage Dip: Phase B
Instantaneous 154.5V,0.519 Sec., on 26/02/2022 13:10:42.80

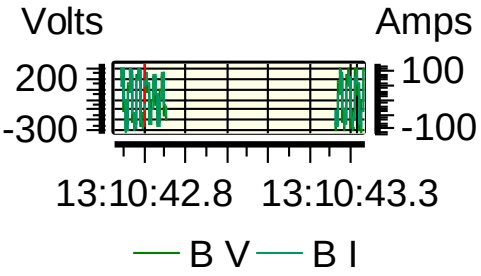

NO WAVEFORM AVAILABLE

Most Energy Added Voltage Swell: No event

Longest Duration Voltage Interruption: No event

Largest Magnitude Voltage Transients: Phase B
720.8V,0.002 Sec., on 01/03/2022 16:17:59.73

NO WAVEFORM AVAILABLE

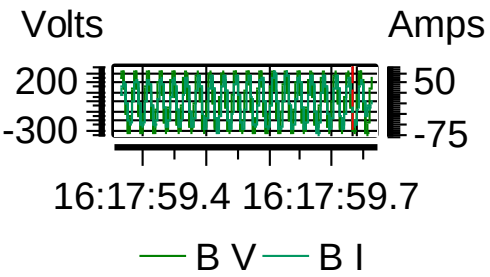

Appendix A- 18: Min/Max/Avg Summary Report

Site: Bunjako
Measured from 24/02/2022 12:43:14 to 04/03/2022 10:05:00

VOLTAGE

	Channel A	**Channel B**
Min Volts	205.02 on 24/02/2022 13:50:00	154.47 on 26/02/2022 13:20:00
Max Volts	250.30 on 27/02/2022 07:40:00	251.55 on 04/03/2022 06:40:00
Median Volts	230.77	229.77
Average Volts	230.94	229.78
	Channel C	**Channel A-B**
Min Volts	218.16 on 02/03/2022 06:00:00	308.6 on 26/02/2022 10:50:00
Max Volts	239.47 on 03/03/2022 08:00:00	454.0 on 03/03/2022 08:00:00
Median Volts	230.50	400.4
Average Volts	230.39	400.5
	Channel B-C	**Channel C-A**
Min Volts	296.5 on 26/02/2022 13:20:00	343.0 on 26/02/2022 12:50:00
Max Volts	447.9 on 04/03/2022 06:40:00	447.4 on 26/02/2022 10:10:00
Median Volts	397.2	398.5
Average Volts	397.3	398.6

CURRENT

	Channel A	**Channel B**
Min Amps	2.22 on 25/02/2022 06:50:00	3.77 on 02/03/2022 16:40:00
Max Amps	69.31 on 26/02/2022 07:40:00	97.93 on 03/03/2022 08:50:00
Median Amps	3.71	9.38
Average Amps	4.73	10.14
	Channel C	
Min Amps	3.45 on 25/02/2022 06:00:00	
Max Amps	45.28 on 27/02/2022 11:20:00	
Median Amps	6.99	
Average Amps	7.94	

Appendix A- 19: Demand and Energy Timeplots

Site: Bunjako
Measured from 24/02/2022 12:43:14 to 04/03/2022 10:05:00

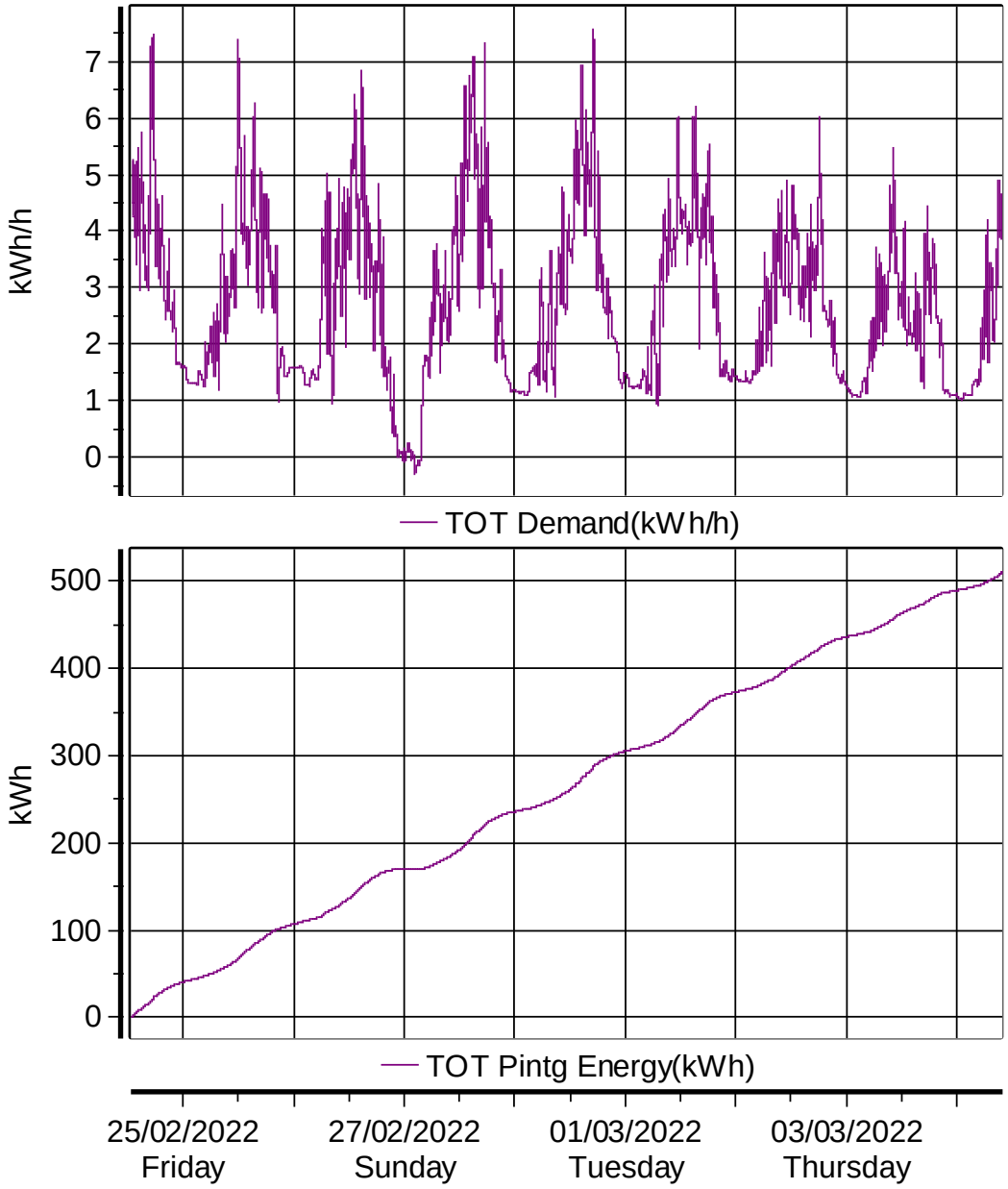

Appendix A- 20: Min/Max/Avg Power Report

Site: Bunjako
Measured from 24/02/2022 12:43:14.0 to 04/03/2022 10:05:00.0

POWER

ACTIVE POWER, P (W)

	A	B	C	TOTAL
Min kW	-10.559	0.475	0.316	-7.308 on 27/02/2022 16:10:00
Max kW	0.290	17.350	7.829	20.286 on 26/02/2022 12:50:00
Median kW	-0.391	1.719	1.197	2.504
Average kW	-0.597	1.894	1.398	2.695

APPARENT POWER,S (VA)

	A	B	C	TOTAL
Min kVA	0.604	0.905	0.848	2.793 on 03/03/2022 16:50:00
Max kVA	13.366	18.999	8.003	25.571 on 26/02/2022 10:50:00
Median kVA	0.857	2.171	1.613	5.172
Average kVA	1.109	2.372	1.827	5.307

REACTIVE POWER Q, AT FUND. FREQ. (VAR)

	A	B	C	TOTAL
Min kVAR	-8.126	-0.236	0.097	-5.445 on 25/02/2022 17:10:00
Max kVAR	0.070	8.839	2.737	9.764 on 25/02/2022 15:30:00
Median kVAR	-0.232	0.803	0.420	0.981
Average kVAR	-0.297	0.905	0.558	1.165

POWER FACTOR, PF

	A	B	C	TOTAL
Min	-0.886	-0.982	0.366	-1.000 on 25/02/2022 06:40:00
Max	0.961	0.976	0.985	1.000 on 25/02/2022 06:40:00
Median	0.424	0.777	0.721	0.646
Average	0.439	0.769	0.692	0.603

DEMAND

REAL POWER DEMAND

	A	B	C	TOTAL
Min kWh/h				-0.296 on 27/02/2022 02:20:00
Max kWh/h				7.567 on 28/02/2022 17:10:00
Median kWh/h				2.502
Average kWh/h				2.695

ENERGY

ENERGY - INTEGRATED ACTIVE POWER (W-HRS)

	A	B	C	TOTAL
kWh	113.01	358.3	264.47	509.8 on 04/03/2022 10:05:00

Appendix B: NodeRED Flow of Temperature-Based Control and Data Collection for Cooling Appliances in Lwak

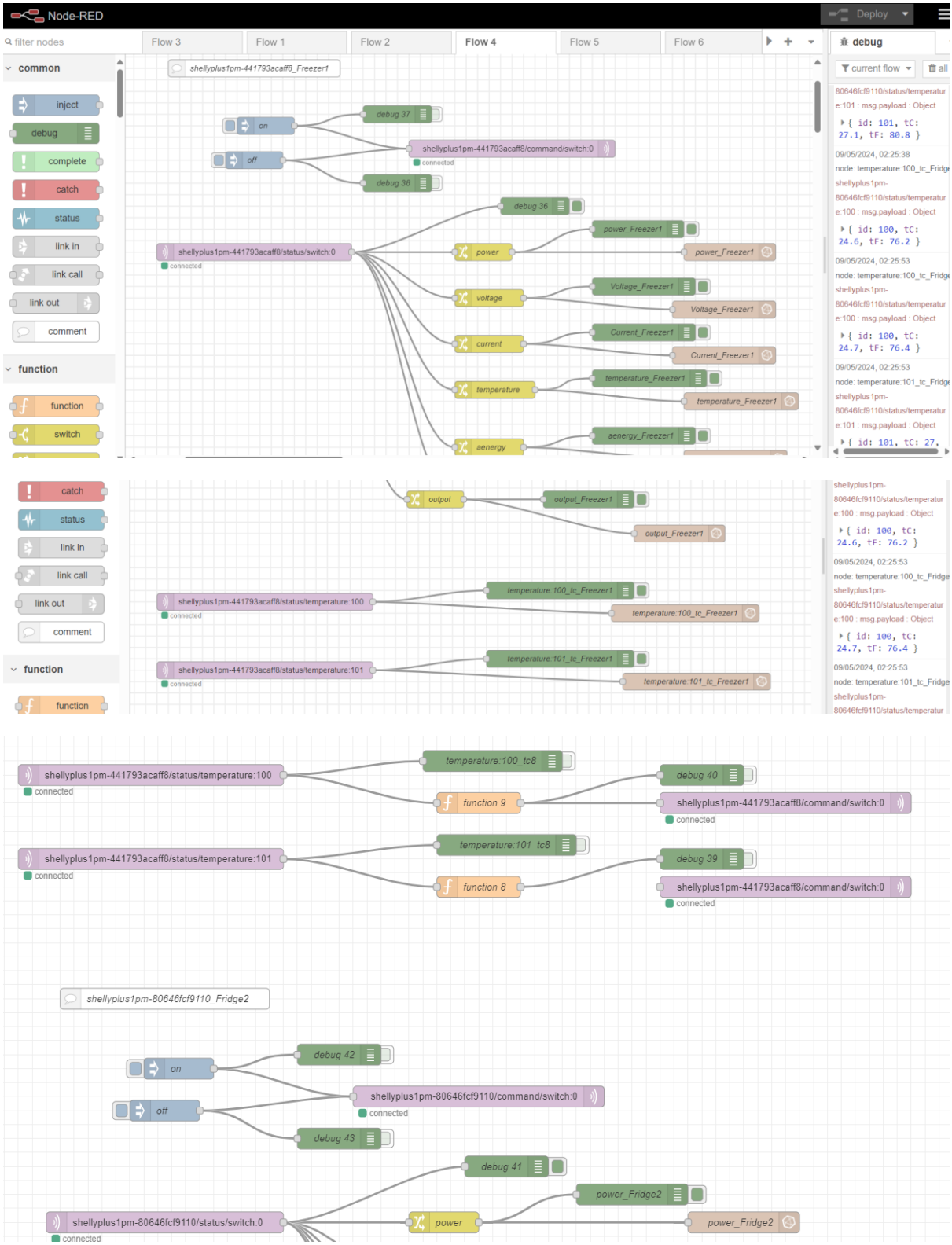

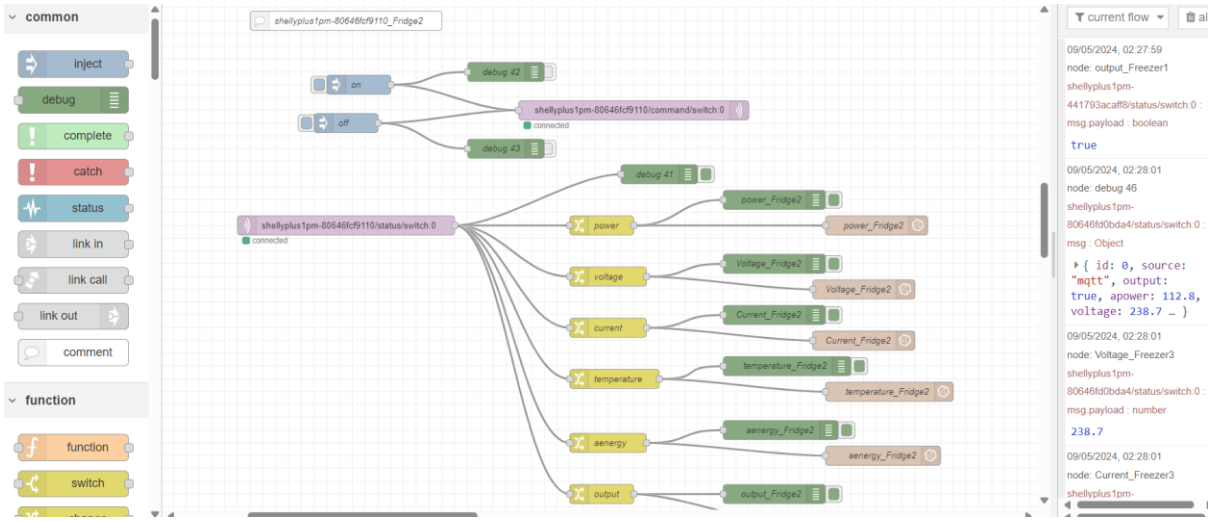

EM 3 CONNECTIONS

Appendix C: Electronic Devices Datasheet

Appendix C- 1: Datasheet for the Temperature data logger

EXTECH INSTRUMENTS
A FLIR COMPANY

Experience the Extech Advantage

PRODUCT DATASHEET

Light Meter/Datalogger

Records data on an SD card in Excel® format
For easy transfer to a PC for analysis

PRELIMINARY DATASHEET

Features:

- Wide range to 10,000Fc or 100kLux
- Cosine and color-corrected measurements
- Utilizes precision silicon photo diode and spectral response filter
- Datalogger date/time stamps and stores readings on an SD card in Excel® format for easy transfer to a PC
- Selectable data sampling rate: 1 to 3600 seconds
- Manually store/recall up to 99 readings
- Type K/J Thermocouple input for high temperature measurements
- Large backlit LCD
- Record/Recall MIN, MAX readings
- Data Hold plus Auto power off with disable function
- Zero function
- Built-in RS-232 interface
- Complete with 6 x AA batteries, SD card, hard carrying case and light sensor with protective cover

Specifications	Range	Resolution	Basic Accuracy
Fc Range	200, 2000, 10kFc	0.1Fc	±4%rdg
Lux Range	2000, 20k, 100kLux	1Lux	±4%rdg
Type K Temperature	-148 to 2372°F (-100 to 1300°C)	0.1°	±(0.4% + 1.8°F/1°C)
Type J Temperature	-148 to 2192°F (-100 to 1200°C)	0.1°	±(0.4% + 1.8°F/1°C)
Memory	20M data records using 2G SD card		
Dimensions	7.2 x 2.9 x 1.9" (182 x 73 x 47.5mm)		
Weight	16.2oz (475g)		

Ordering Information:

SDL400 .....Light Meter/Datalogger **$299.99**
SDL400-NIST .....SDL400 with NIST Certificate .....**$**

c UL us LISTED CE

www.extech.com

5/25/11 - R1

Appendix C- 2: SP2Lite Pyranometer/ Irradiance Sensor Data sheet